Research

ProLBB - A Probabilistic Approach to Leak Before Break Demonstration

Peter Dillström
Weilin Zang

November 2007

SKi

SKI Perspective

Background

The SKI regulation SKIFS 2004:2 allows for the use of Leak Before Break (LBB) as one way to provide assurance that adequate protection exists against the local dynamic consequences of a pipe break. The way to demonstrate that LBB prevails relies on a deterministic procedure for which a leakage crack is postulated in certain sections of the pipe based on the leak detection capability of the plant. It shall then be demonstrated that certain margins exist against the critical crack length at which a pipe break can be expected. In certain situations, probabilistic methods can strengthen the conclusion that LBB prevails. Then it is necessary to demonstrate that the likelihood of a pipe failure is sufficiently low and that there is a sufficient margin between a detectable leak and pipe rupture. The research project presented in this report provides information on failure probabilities for both leak and rupture for pipes of different sizes in Swedish BWR- as well as PWR-plants. No active degradation mechanisms are assumed to exist. Defects are assumed only to originate from welding defects from the manufacture.

Purpose

The purpose of the project is to evaluate leak- and rupture probabilities for pipes of different sizes in Swedish BWR- and PWR-plants. The project will also give information on which failure probability corresponds to a precise fulfilment of the deterministic LBB-criteria.

Results

- The probabilistic approach developed in this study was applied to different piping systems in both Boiler Water Reactors (BWR) and Pressurised Water Reactors (PWR). Pipe sizes were selected so that small, medium and large pipes were included in the analysis. The present study shows that the conditional probability of fracture (given the existence of a leaking crack) is in general small for the larger diameter pipes when evaluated as function of leak flow rate. However, when evaluated as function of fraction of crack length around the circumference, then the larger diameter pipes will belong to the ones with the highest conditional fracture probabilities.

- The total failure probability, corresponding to the product between the leak probability and the conditional fracture probability, will be very small for all pipe geometries when evaluated as function of fraction of crack length around the circumference. This is mainly due to a small leak probability which is consistent with expectations since no active damage mechanism has been assumed.

- The weld residual stresses have quite an impact on the resulting fracture probabilities, especially for smaller cracks (this is relevant both for small and large pipes). The influence from the weld residual stresses on the calculation of leakage flow rate is largest for a thin-walled pipe.

- The conditional fracture probabilities are relatively sensitive to the crack morphology. The conditional fracture probability as function of leak flow rate will be higher for a crack morphology corresponding to a stress corrosion crack compared to a fatigue crack.

- This study has given an indication of the relation between the deterministic LBB-criteria and the corresponding conditional fracture probability. As expected, it is easier to fulfil the deterministic LBB-margins for a large diameter pipe compared to a small diameter pipe.

Effect on SKI supervisory and regulatory task

The results of this project will be of use to SKI in the reviews of applications from Swedish Nuclear Plants to use the LBB concept.

Project information

Responsible at SKI for this project has been Björn Brickstad (bjorn.brickstad@ski.se)

SKI reference: SKI 2005/457
Project number: 200542005

ProLBB - A Probabilistic Approach to Leak Before Break Demonstration

Peter Dillström
Weilin Zang

Inspecta Technology AB
P.O. Box 30100
SE-104 25 STOCKHOLM

Table of Content **Page**

SUMMARY

Recently, the Swedish Nuclear Power Inspectorate has developed guidelines on how to demonstrate the existence of Leak Before Break (LBB). The guidelines, mainly based on NUREG/CR-6765, define the steps that must be fulfilled to get a conservative assessment of LBB acceptability. In this report, a probabilistic LBB approach is defined and implemented into the software ProLBB. The main conclusions, from the study presented in this report, are summarized below.

- The probabilistic approach developed in this study was applied to different piping systems in both Boiler Water Reactors (BWR) and Pressurised Water Reactors (PWR). Pipe sizes were selected so that small, medium and large pipes were included in the analysis. The present study shows that the conditional probability of fracture is in general small for the larger diameter pipes when evaluated as function of leak flow rate. However, when evaluated as function of fraction of crack length around the circumference, then the larger diameter pipes will belong to the ones with the highest conditional fracture probabilities.

- The total failure probability, corresponding to the product between the leak probability and the conditional fracture probability, will be very small for all pipe geometries when evaluated as function of fraction of crack length around the circumference. This is mainly due to a small leak probability which is consistent with expectations since no active damage mechanism has been assumed.

- One of the objectives of the approach was to be able to check the influence of off-centre cracks (i.e. the possibility that cracks occur randomly around the pipe circumference). To satisfy this objective, new stress intensity factor solutions for off-centre cracks were developed. Also to check how off-centre cracks influence crack opening areas, new form factors solutions for COA were developed taking plastic deformation into account.

- The influence from an off-center crack position on the conditional probability of fracture is not important when assuming a uniform distribution. This is because the result is dominated totally by the center crack position. However, if the crack position is treated as a deterministic parameter, the conditional probability of fracture is strongly dependent on the position of the crack, especially for large off-center cracks.

- The weld residual stresses have quite an impact on the resulting fracture probabilities, especially for smaller cracks (this is relevant both for small and large pipes). The influence from the weld residual stresses on the calculation of leakage flow rate is largest for a thin-walled pipe. The influence from the weld residual stresses on the calculation of fracture probability is largest for one of the thick-walled pipes.

- The conditional fracture probabilities are relatively sensitive to the crack morphology. The conditional fracture probability as function of leak flow rate will be higher for stress corrosion cracks compared to fatigue cracks.

- In the formal sensitivity analyses, it is shown that the standard deviation of the yield strength has the strongest influence on the conditional fracture probability.

- This study has given an indication of the relation between the deterministic LBB-criteria and the corresponding conditional fracture probability. As expected, it is easier to fulfil the deterministic LBB-margins for a large diameter pipe compared to a small diameter pipe.

1 INTRODUCTION

The view on pipe fractures and how one can prevent it and also how one should protect against the consequences of pipe fracture has varied during the years [1]. In the beginning pipe fracture of large pipes was a purely hypothetic event, defined to calculate the loss of coolant that must be replaced with the emergency cooling systems. Fractures on these pipes became a design limiting event in the design of the containment and the emergency cooling systems. However, the possibility was noticed that a sudden pipe fracture actual could occur which meant that requirements on limiting the consequence on these event were needed. The main concern was pipe whips, and therefore a large number of pipe whip restraints were installed (to withstand these types of guillotine breaks).

Later, certain disadvantages with pipe whip restraints were noticed [1]. These where mainly related to an increased risk for lockups of the piping system in certain load situations, but also difficulties to perform the non-destructive testing (hard or impossible to test certain welds etc) and an increased dosage rate for the people performing the inspection. Of the above reasons, new analyses and pipe fracture experiments were performed. These indicated that the probability for a sudden pipe fracture on a large pipe, without any damage mechanism, was very small. These type of analyses, introduced the so-called LBB (Leak Before Break) concept that was formalised in the American design criteria GDC-4 in 10CFR50 [2] and also the introduction of one deterministic LBB procedure in SRP 3.6.3 [3]. With Leak Before Break, it is meant that the piping system has a design, operational conditions etc. that the probability of failure is sufficiently small and that measures have been taken so that damage (if it occurs) with a large probability leads to a detectable leak with a sufficient margin before rupture.

Also the regulatory view on LBB has varied internationally during this time. In USA and many European countries, LBB is now accepted to be used as one way to account for local dynamic effects following a pipe rupture. In Sweden SKI has issued new regulations, SKIFS 2004:2, [4] where one allow for the use of LBB as a way to demonstrate a sufficient protection against the consequences of a guillotine break and not having to install pipe whip restraints.

With the new regulations on LBB there was a need to develop guidelines on how to demonstrate the existence of Leak Before Break [1]. As a complement to these guidelines and also to help identify the key parameters that influence the resulting leakage and failure probabilities, a probabilistic LBB approach has been developed. The purpose of this report is to present the new probabilistic LBB approach.

2 DETERMINISTIC GUIDELINES FOR LEAK BEFORE BREAK

SKI has issued new regulations where one allow for the use of LBB as a way to demonstrate a sufficient protection against the consequences of a guillotine break and not having to install pipe whip restraints. With the new regulations on LBB there was a need to develop guidelines on how to demonstrate the existence of Leak Before Break. These new guidelines are presented in [1] and the most important points are given below.

The new guidelines [1], partly based on NUREG/CR-6765 [5], define the steps that should be fulfilled to get a conservative assessment of LBB acceptability.

- LBB should be applied to an entire piping segment (within class 1 or 2). Locations with both high and low stresses should be included in the analysis.
- No active damage mechanism (or water hammer loading events) should be present in the piping segment.
- A leakage detection system should be present (that among other requirements fulfill RG 1.45 [6]).
- The piping segment should have been inspected using a qualified NDE procedure. Preferably a qualified NDE procedure should also be used in all future inspections.
- Postulate a leaking through-wall crack (leakage crack size) at the chosen assessment location.
    - The leakage crack size is chosen to get a leakage which is 10 times larger than the detection limit.
    - The leakage flow should be calculated using loads from the normal operation of the plant (including weld residual stresses, if a weld is present at the chosen assessment location).
    - The leakage crack should be postulated at locations with both high and low stresses along the chosen piping segment.
    - In the calculation, one should include the contribution from the flexibility of the piping system, the crack morphology on the leakage flow and the dependence of the crack opening (COD).
- Calculate the critical crack size using the normal operating conditions and also one of the worst loading case/transient according to the design specification.
- Check the safety margins:
    - The margin between the calculated critical crack size and the postulated leakage crack size should be at least 2.
    - The leakage crack should be stable using a load which is 1.4 times larger then the load used to calculate the critical crack size.

During the development of these guidelines, it was decided that a probabilistic LBB approach should be developed. The main objective of this probabilistic approach was to act as a complement in the LBB decision process, but also to help identify the key parameters that influence the resulting leakage and failure probabilities. This approach is presented in the next section of the present report.

3 PROBABILISTIC APPROACH FOR LEAK BEFORE BREAK

To be consistent with the new guidelines developed by the regulator [1], the probabilistic LBB approach should be able to calculate the following:

- Probability of leakage (given the existence of a surface crack). The results should be presented as a function of crack size.
- Probability of fracture (given the existence of a leaking through-thickness crack). The results should be presented as a function of crack size or leakage flow rate.

Within the new probabilistic LBB approach two different limit state functions, $g(X)$ ($g_{FAD}(X)$ and $g_{L_r^{max}}(X)$) are used [7].

$$g_{FAD}(X) = f_{FAD}(X) - K_r(X) \quad , \tag{3.0.1}$$

$$g_{L_r^{max}}(X) = L_r^{max}(X) - L_r(X) \quad . \tag{3.0.2}$$

These limit state functions are based on a simplified R6 failure assessment curve. To calculate the probability of leakage/fracture, a multi-dimensional integral has to be evaluated:

$$P_l \text{ or } P_f = \Pr[g(X) < 0] = \int_{g(X)<0} f_X(x)dx \quad . \tag{3.0.3}$$

The set where the above analysed event is fulfilled, is formulated as $g(X) < 0$, and is called the failure set. The set where $g(X) > 0$ is called the safe set. $f_X(x)$ is a known joint probability density function of the random vector X. This integral is very hard (impossible) to evaluate, by numerical integration, if there are many random parameters. In the calculations, all the random parameters are treated as not being correlated with one another. The parameters can follow almost any distribution.

As mentioned above, the failure probability integral is very hard to solve using numerical integration. Instead, the following numerical algorithms are used [7]:

- Simple Monte Carlo Simulation (MCS), only used to check the results using the other methods.
- First-Order Reliability Method (FORM)
- Monte Carlo Simulation with Importance Sampling (MCS-IS)

3.1 Probability calculation using Simple Monte Carlo Simulation (MCS)

MCS is a simple method that uses the fact that the failure probability integral can be interpreted as a mean value in a stochastic experiment. An estimate is therefore given by averaging a suitably large number of independent outcomes (simulations) of this experiment.

The basic building block of this sampling is the generation of random numbers from a uniform distribution (between 0 and 1). Once a random number u, between 0 and 1, has been generated, it can be used to generate a value of the desired random variable with a given distribution. A common method is the inverse transform method. Using the cumulative distribution function $F_X(x)$, the random variable would then be given as:

$$x = F_X^{-1}(u) \quad . \tag{3.1.1}$$

To calculate the failure probability, one performs N deterministic simulations and for every simulation checks if the component analysed has failed (i. e. if $g(X) < 0$). The number of failures is N_F, and an estimate of the mean probability of failure is:

$$P_{F,MCS} = \frac{N_F}{N} \quad . \tag{3.1.2}$$

An advantage with MCS, is that it is robust and easy to implement into a computer program, and for a sample size $N \to \infty$, the estimated probability converges to the exact result. Another advantage is that MCS works with any distribution of the random variables and there is no restriction on the limit state functions.

However, MCS is inefficient when calculating failure probabilities, since most of the contribution to P_F is in a limited part of the integration interval. Within this project, Simple Monte Carlo Simulation was only used to check the results using the other methods.

3.2 Probability calculation using Monte Carlo Simulation with Importance Sampling (MCS-IS)

MCS-IS is an algorithm that concentrates the samples in the most important part of the integration interval. Instead of sampling around the mean values (MCS), one samples around the most probable point of failure (MCS-IS). This point, called MPP, is generally evaluated using information from a FORM / SORM analysis (see section 3.3 below).

3.3 Probability calculation using the First-Order Reliability Method (FORM)

FORM / SORM uses a combination of both analytical and approximate methods, when estimating the probability of failure [7].

First, one transforms all the variables into equivalent normal variables in standard normal space (i. e. with mean = 0 and standard deviation = 1). This means that the original limit state surface $g(x) = 0$ then becomes mapped onto the new limit state surface $g_U(u) = 0$.

Secondly, one calculates the shortest distance between the origin and the limit state surface (in a transformed standard normal space U). The answer is a point on this surface, and it is called the most probable point of failure (MPP), design point or β-point. The distance between the origin and the MPP is called the reliability index β_{HL} (see figure 3.3.1).
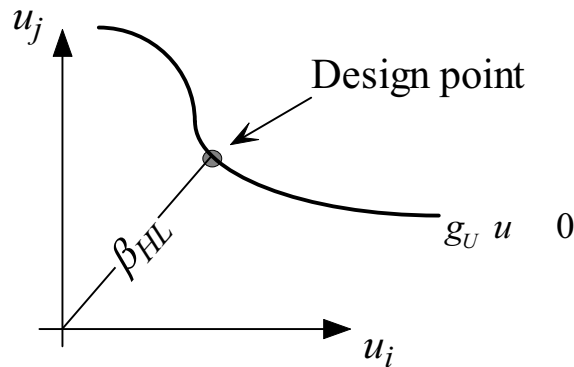

Figure 3.3.1. The definition of design point / MPP and reliability index β_{HL}.

In [7, 8] a linearization of the limit state function is used to calculate the MPP.

$$y_{i+1} = \frac{1}{\left|\nabla g_U(y_i)\right|^2} \cdot \left[\nabla g_U(y_i) \cdot y_i - g_U(y_i)\right] \cdot \nabla g_U(y_i)^T \quad , \tag{3.3.1}$$

where y_i is the current approximation to the MPP and $\nabla g_U(y_i)$ is the gradient of the limit state function. This algorithm, generally called the Rackwitz & Fiessler (R & F) algorithm [9], is commonly used when evaluating P_F, mainly because it is very easy to implement and it converges fast in many cases. However, the R & F algorithm converges extremely slowly in some cases or oscillates about the solution without any convergence at all. Therefore, the R & F algorithm was not chosen in this case.

In [8], a modified Rackwitz & Fiessler algorithm was chosen. It works by "damping" the gradient contribution of the limit state function and this algorithm is very robust and converges quite fast for most cases. In this algorithm one defines a search direction vector d_i:

$$d_i = \frac{1}{|\nabla g_U(y_i)|^2} \cdot [\nabla g_U(y_i) \cdot y_i - g_U(y_i)] \cdot \nabla g_U(y_i)^T - y_i \quad . \tag{3.3.2}$$

A new approximation to the MPP can then be calculated:

$$y_{i+1} = y_i + s_i \cdot d_i \quad . \tag{3.3.3}$$

The step size s_i was selected as given in [10] such that the inequality $m(y_i + s_i d_i) < m(y_i)$ holds, where $m(y_i)$ is the merit function:

$$m(y_i) = \frac{1}{2} \cdot |y_i|^2 + c \cdot |g_U(y_i)| \quad , \tag{3.3.4}$$

in which c is a parameter satisfying the condition $c > |y_i|/|\nabla g_U(y_i)|$ at each step i. This algorithm is globally convergent, i. e., the sequence is guaranteed to converge to a minimum-distance point on the limit state surface, provided $g_U(u)$ is continuous and differentiable [10].

Finally, one calculates the failure probability using an approximation of the limit state surface at the most probable point of failure. Using FORM, the surface is approximated to a hyperplane (a first order / linear approximation). SORM uses a second order / quadratic approximation to a hyperparaboloid (see figure 3.3.2).
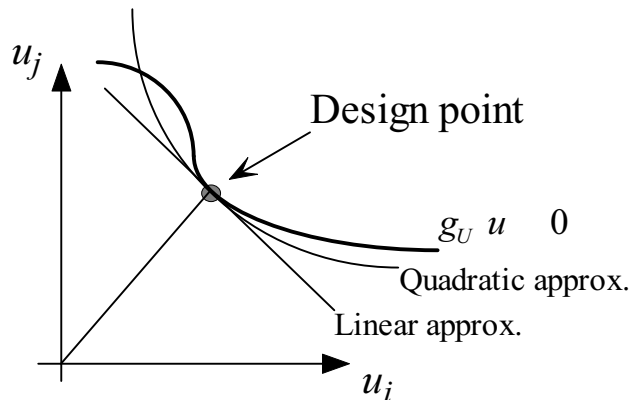

Figure 3.3.2   Schematic difference between a linear and a quadratic approximation of the limit state surface.

The probability of failure is given as [7]:

$$P_{F,FORM} = \Pr\left[g_{Linear}(u) < 0\right] = \Phi(-\beta_{HL}) \quad , \tag{3.3.5}$$

$$P_{F,SORM} = \Pr\left[g_{Quadratic}(u) < 0\right] \approx \Phi(-\beta_{HL}) \cdot \prod_{i=1}^{N-1}\left(1 - \kappa_i \cdot \beta_{HL}\right)^{-1/2} \quad , \tag{3.3.6}$$

where $\Phi(u)$ is the cumulative distribution function in standard normal space and κ_i are the principal curvatures of the limit state surface at the most probable point of failure (MPP).

FORM / SORM are, as regards CPU-time, extremely efficient as compared to MCS. Using the FORM implementation within [8], you get quite accurate results for failure probabilities between 10^{-1} to 10^{-15}. A disadvantage is that the random parameters must be continuous, and every limit state function must also be continuous.

4   NEW STRESS INTENSITY FACTORS SOLUTIONS FOR OFF-CENTRE CRACKS

To predict the probability of fracture under external loads (e.g. bending or combined bending and tension loads), the crack-driving force, is typically evaluated by assuming that these cracks are symmetrically placed with respect to the bending plane of the pipe. This is usually justified by reasoning that the tensile stress due to bending is largest at the center of this symmetric crack.

In reality, defects occur randomly around the pipe circumference, at least in the absence of any active damage mechanism (which is assumed in this study). Additionally, during the normal operating condition of a nuclear power plant, the stress component due to pressure is often more significant than that due to bending [11]. As such, the postulated crack in LBB analysis may be off-centered (see Fig. 4.1) and can thus be located anywhere around the pipe circumference.
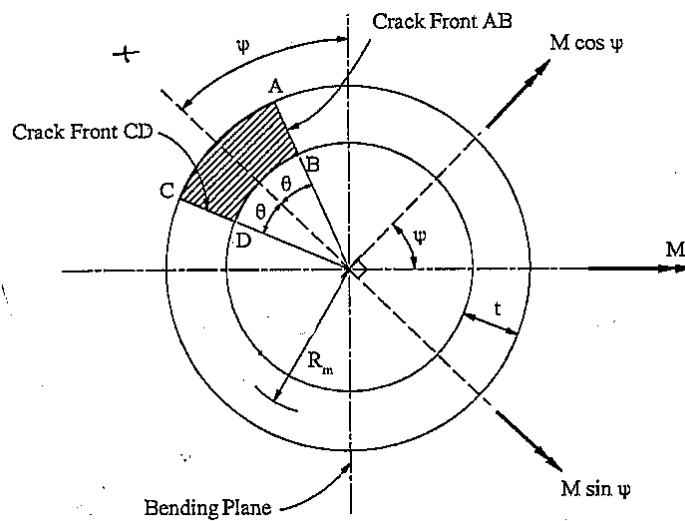

Figure 4.1. Illustration of the geometry and load application for an off-centre crack.

The influence from off-centre cracks on the calculation of stress intensity factors and the probability of failure has been investigated [11, 12]. However, these studies are somewhat limited and also shown to be not so accurate. A comparison was made between the results presented in [11, 12] and the results given in this report. For the case with an off-centre angle $\psi = 60°$, the results from [11] under-estimates the resulting J-values both for an elastic and an elastic-plastic analysis. In [11], the calculations shows that crack closure occurs at crack front CD (see Fig. 4.1). In the present study, no closure occurs at $\psi = 60°$. However, using the elastic results for $0°$ and $90°$, the results for $\psi = 60°$ can be calculated by superposition. Such a comparison gives almost identical results using data from the present analysis and the one presented in [11]. Therefore, it can be concluded that the results for off-centre cracks given in this report are more accurate than the results presented in [11].

New stress intensity factors solutions for off-centre cracks are therefore given in this report using different pipe geometries (SKI recommended pipe sizes with an outer diameter between ~100 mm and ~700 mm) and material properties. The results are presented in Appendix A and also summarized below.

The stress intensity factors are calculated using the finite element program ABAQUS [13], with a sufficiently accurate finite element mesh. The stress intensity factors are given via the *J*-integral as,

$$K = \sqrt{J} \cdot \sqrt{\frac{E}{1 - \upsilon^2}} \ .$$

(4.1)

In the presentation of the results, the R6 method option 1 is used. The stress intensity factor by the R6 method is calculated as,

$$K_{R6} = \frac{K_{EL}}{f_{R6}(L_r)} \ ,$$

(4.2)

where

$$f_{R6}(L_r) = (1 - 0.14L_r^2)\left[0.3 + 0.7\exp(-0.65L_r^6)\right] \ ,$$

(4.3)

and

$$K_{EL} = \left[K^0 * \cos(\psi) + K^{90} * \sin(\psi)\right] \ .$$

(4.4)

In Eqn (4.4), K^0 is the stress intensity factor of a centre crack ($\psi = 0°$) in a pipe subjected to a bending moment *M* and K^{90} is the stress intensity factor at crack front AB (defined in Fig. A1.1) for an off centre crack ($\psi = 90°$) subjected to a bending moment *M*. The use of Eqn. (4.4) is a simplification, using the projected moment only, but the agreement with the ABAQUS results is satisfactory.

The geometry function, f, of the stress intensity factor is defined as,

$$K = \sigma_b \sqrt{\pi a_m} \cdot f(2\theta, R_i / t) \ .$$

(4.5)

In Eqn (4.5), σ_b is the maximum global bending stress and a_m is one half the average crack length ($l_m / 2 = R_m \theta$). The new geometry functions for the different cases are listed in Table 4.1.

Table 4.1. Geometry functions for off-centre cracks.

Case	R_i / t	2θ	f^0	f^{90}
1	5.63	45	1.134	0.191
2		90	1.461	0.406
3		135	1.863	0.644
4		180	2.602	0.944
5	4.08	45	1.088	0.185
6		90	1.375	0.389
7		135	1.744	0.607
8		180	2.435	0.881
9	8.88	45	1.226	0.200
10		90	1.693	0.459
11		135	2.090	0.716
12		180	3.019	1.097

How the resulting probabilities depend on different assumptions regarding off-centre cracks are presented in a sensitivity study below. The main results and conclusions can be found in section 8.10.

5 NEW CRACK OPENING AREAS SOLUTIONS FOR OFF-CENTRE CRACKS

Crack opening area (COA) is an important parameter in a LBB analysis. It is commonly known that COA is strongly influenced by plastic deformation. Therefore the use of a correction factor which takes into account the effect of the plastic deformation is necessary.

In this report, new crack opening area (COA) form factor solutions for off-centre cracks are developed using different pipe geometries and material properties. These form factors can be used to define new plastic correction factor solutions for off-centre cracks. The results from this study are presented in Appendix B and also summarized below.

The crack opening areas (COA) are calculated using the finite element program ABAQUS, with a sufficiently accurate finite element mesh. In the presentation of the results in Appendix B, a comparison is also made between two different approximate methods.

- Method 1: The crack opening areas are calculated using elastic form factors (COA_{EL}).

- Method 2: The crack opening areas are calculated using elastic form factors with a correction factor that takes into account the effect of the plastic deformation (COA_{PL}).

The elastic COA is calculated as,

$$COA_{EL} = COA_{EL}^0 \cdot \cos(\psi) + COA_{EL}^{90} \cdot \sin(\psi) \ . \tag{5.1}$$

In Eqn. (5.1), COA_{EL}^0 is the crack opening area of a centre crack ($\psi = 0°$) in a pipe subjected to a bending moment M and COA_{EL}^{90} is the crack opening area for an off centre crack ($\psi = 90°$) subjected to a bending moment M.

The form factor (COA) is defined as,

$$COA_k = \frac{\sigma_b \cdot l_k^2}{E} \left(\frac{1}{l_k^2} \int_0^l COD_k(x) dx \right) = \frac{\sigma_b \cdot l_k^2}{E} D_k \ . \tag{5.2}$$

In Eqn. (5.2), k is either the inside surface or the outside surface of the pipe. It is obvious that D_k is the average COD (taken from the finite element analysis) divided by l_k under the action of the global bending stress $\sigma_b = E$. The new COA form factors are listed in Table 5.1.

Table 5.1. COA form factors for off-centre cracks.

Case	R_i/t	2θ	D_{in}^0	D_{in}^{90}	D_{out}^0	D_{out}^{90}
1	5.63	45	1.557	0.057	1.896	0.067
2		90	2.348	0.113	2.604	0.155
3		135	3.844	0.202	3.843	0.273
4		180	7.050	0.339	6.661	0.425
5	4.08	45	1.487	0.055	1.795	0.066
6		90	2.155	0.108	2.377	0.145
7		135	3.469	0.183	3.423	0.250
8		180	6.108	0.309	5.585	0.391
9	8.88	45	1.679	0.058	2.069	0.070
10		90	2.720	0.123	3.004	0.172
11		135	2.044	0.107	2.306	0.158
12		180	8.061	0.427	7.731	0.513

The plastic COA is calculated as,

$$\mathrm{COA_{PL}} = g \cdot \mathrm{COA_{EL}} \ , \tag{5.3}$$

where g is a correction factor that takes into account the effect of the plastic deformation. g is essentially a curve fit to the elastic ($\mathrm{COA_{EL}}$) and elastic-plastic ($\mathrm{COA_{PL}}$) results from the finite element analysis. New $\mathrm{COA_{PL}}$ can then be calculated using g and $\mathrm{COA_{EL}}$.

The new plastic correction factors are summarised in Fig. 5.1, using different L_r-values (from the applied primary global bending moment M).
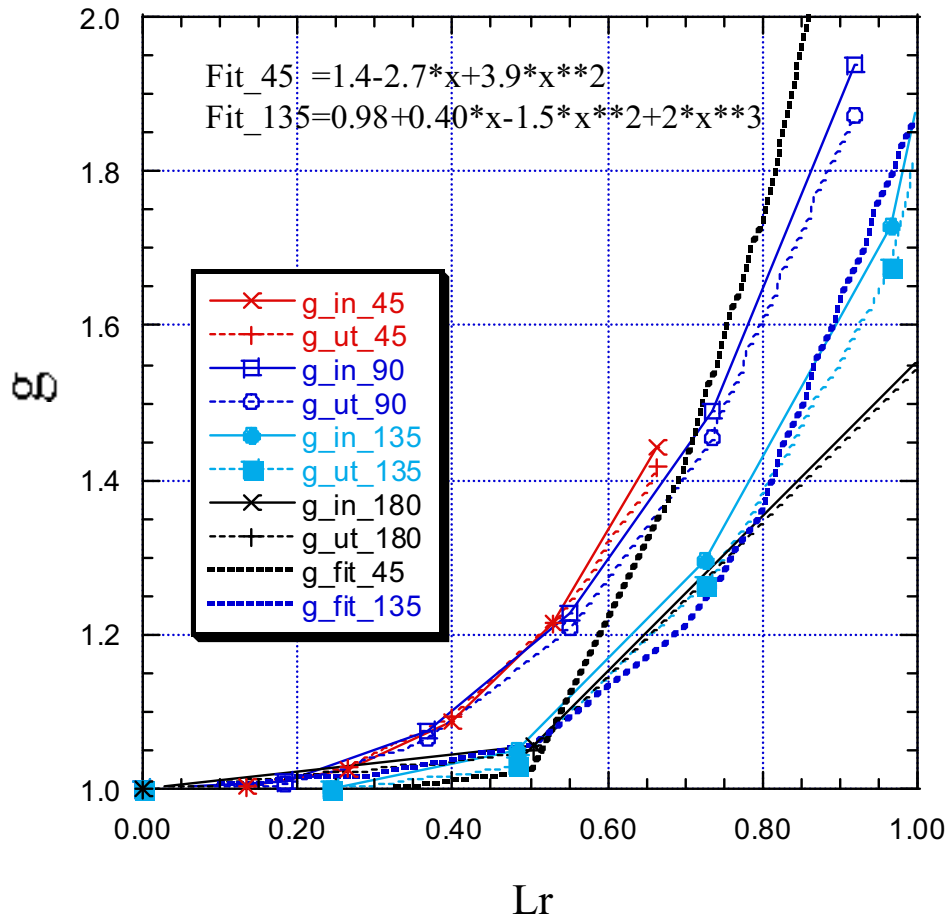
Figure 5.1. COA plastic correction factor.

The results in appendix B shows that using Method 1 (when the crack opening areas are calculated using elastic form factors only) gives a maximum error of ~20 % compared to the elastic-plastic finite element analysis when the applied L_r is below ~0.5. For larger L_r-values the error becomes quite large and Method 1 should not be used for these cases.

The results in appendix B also shows that using Method 2 (when the crack opening areas are calculated using elastic form factors with a correction factor that takes into account the effect of the plastic deformation) gives an excellent agreement with the elastic-plastic finite element analysis (independent of the applied L_r-value).

6 IMPLEMENTATION OF THE NEW PROBABILISTIC LBB APPROACH

The probabilistic LBB approach was implemented using the calculation engine from the software ProSACC [8]. The reason for not using the original version of the ProSACC program was that a more general application was needed that could have an arbitrary parameter as a random variable and also that new distribution functions were needed to implement the probabilistic LBB approach. Finally a new stress intensity factor solution for off-centre cracks was included in the calculation engine.

Two different probabilities was calculated using this implementation of the probabilistic LBB approach (ProLBB approach):
- Probability of leakage (given the existence of a surface crack).
- Probability of fracture (given the existence of a leaking through-thickness crack).

The influence from the quality of the NDE procedure (by using the information from different POD curves) is not taken into account when calculating the different probabilities. Also, the influence from the leakage detection system is not included in the current implementation. However, the information regarding detection of cracks and leakage could be included in an expanded probabilistic LBB approach.

Results using Simple Monte Carlo Simulation (MCS), was only used to check the results using the other methods.

The results for the baseline cases were generated using FORM to get the most probable point of failure and then using Monte Carlo Simulation with Importance Sampling to get a better estimate of the very small probabilities generated in most cases.

The major part of the sensitivity study consists of checking how the probability of fracture changes when varying a number of parameters one by one, keeping all other parameters fixed at their baseline values (the baseline cases correspond to the "best estimate" values of all parameters, reflecting actual plant conditions for each case). However, a more formal sensitivity analysis is presented in sections 8.12-8.13. This analysis tries to answer the following questions: i) What parameter contributes the most to the calculated fracture probability? ii) What parameter change has the most influence on the calculated fracture probability? This formal sensitivity analysis is generated using information from an expanded FORM analysis.

In the probabilistic approach, the following parameters are considered as being deterministic:
- Pipe diameter
- Pipe wall thickness
- Internal pressure
- Temperature
- Leakage flow rate
- Crack morphology variables

In the probabilistic approach, the following parameters are considered as being random:

- Crack length (both for surface cracks and through-thickness cracks)
- Crack depth (surface cracks only)
- Off-centred position of crack
- Fracture toughness
- Yield strength
- Ultimate tensile strength
- Primary membrane stress
- Primary global bending stress
- Secondary global bending stress (expansion stress)

The interface to the calculation engine is written so that more parameters could easily be considered as being random (if needed). It is also possible to consider that some (or all) of the random parameters are treated as being correlated with one another.

7 ANALYSIS OF THE BASELINE CASES

7.1 Definition of the baseline cases

The probabilistic approach developed in this study was applied to different piping systems in both Boiler Water Reactors (BWR) and Pressurised Water Reactors (PWR). Pipe sizes were selected so that small, medium and large pipes were included in the analysis (and also to cover actual differences in the loading conditions). Three BWR and three PWR pipes from Swedish Nuclear Power Plants were selected and their geometry can be found in Table 7.1.1 (the relative pipe sizes are compared in Fig. 7.1.1). Both surface and through-thickness crack are included/ postulated in the analysis (needed to be able to calculate the different probabilities in the approach).

Table 7.1.1. Geometry for the baseline cases.

Case	Piping system	Outer diameter D_y [mm]	Thickness t [mm]
BWR1	System 313	114	8
BWR2	System 312	266	15.5
BWR3	System 313	670	35
PWR1	Accumulator line	323.8	8.3
PWR2	Main steam line	762	26.1
PWR3	Primary loop	871.5	64.85
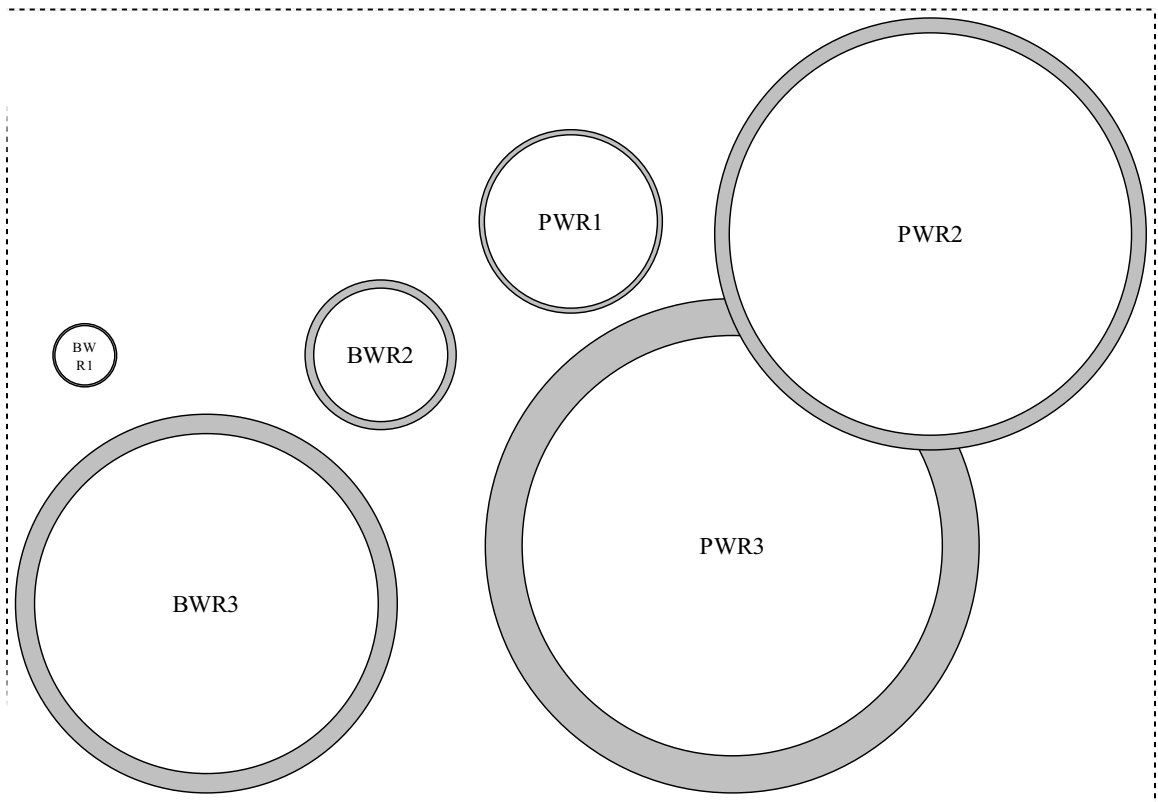
Figure 7.1.1. Relative pipe sizes for the baseline cases.

The material data and the pipe loadings (quite a large difference regarding the pipe loadings between the six cases) are from the actual pipe welds considered and are summarised in Table 7.1.2-7.1.4 (PWR2 is a ferritic weld; the other five cases are austenitic stainless steel welds).

Table 7.1.2. Material data for the baseline cases.

Case	Fracture toughness K_{Ic} [MPa$\sqrt{m}$]	Yield strength σ_y [MPa]	Ultimate tensile strength σ_u [MPa]
BWR1	182	150	450
BWR2	182	150	450
BWR3	182	150	450
PWR1	182	137	495
PWR2	150	260	500
PWR3	182	150	450

Table 7.1.3. Pipe loading for the BWR baseline cases.

Case	P_m [MPa]	P_b [MPa]	P_e [MPa]	Note
BWR1	20	11	18	Normal operation
	20	40	18	Worst Level A-D
BWR2	25	42	105	Normal operation
	25	87	105	Worst Level A-D
BWR3	28	60	15	Normal operation
	28	82	15	Worst Level A-D

Table 7.1.4. Pipe loading for the PWR baseline cases.

Case	P_m [MPa]	$P_b + P_e$ [MPa]	Note
PWR1	43.2	47.2	Normal operation
	42.1	56.2	Level C/D
PWR2	40.3	7.2	Normal operation
	60.9	68.1	Level C/D
PWR3	40.4	51.1	Normal operation
	44.8	89.6	Level C/D

In Table 7.1.3-7.1.4, P_m is the primary membrane stress, P_b is the primary global bending stress and P_e is the expansion bending stress. In Table 7.1.4, no distinction is made between the two global bending stresses (P_b and P_e). This has to do with the background data, which only gives the sum of these stresses (only for the PWR cases). To be conservative, the assumption in the analysis is to consider this sum to be a primary stress only.

Weld residual stresses are included in the probabilistic analysis and also considered in the calculation of leakage flow rate. The assumptions, taken from [7, 14], are summarised in Table 7.1.5.

Table 7.1.5. Assumptions regarding the weld residual stresses for the baseline cases.

Case	Note
BWR1	Local bending stress = ±233 MPa (given that $7 < t \leq 25$ mm, see [7]).
BWR2	Local bending stress = ±154 MPa (given that $7 < t \leq 25$ mm, see [7]).
BWR3	Nonlinear stress distribution (given that $t > 30$ mm, see [7]).
PWR1	Local bending stress = ±230 MPa (given that $7 < t \leq 25$ mm, see [7]).
PWR2	Local bending stress = ±80 MPa (given that $25 < t \leq 30$ mm, see [7]).
PWR3	Nonlinear stress distribution, from a simulation of weld residual stresses [14].

7.2 Acceptable and critical crack lengths for through-thickness cracks

Before starting with the probabilistic analysis it is important to get a deterministic understanding of the chosen baseline cases. Acceptable and critical crack lengths for through-thickness cracks are therefore given in Table 7.2.1 (the results are presented both as a crack length and as a percentage of the circumference). The calculations have been made using the software ProSACC [8] with input data as given in section 7.1. The safety factors in the calculation of acceptable crack lengths have been chosen to retain the safety margins expressed in ASME 1995, Sect. III and XI.

Table 7.2.1. Acceptable and critical crack lengths for through-thickness cracks.

Case	l_{acc} [mm]	l_{acc} [%]	l_{crit} [mm]	l_{crit} [%]	Note
BWR1	87.2	28.3	151.0	49.0	Normal operation
BWR2	23.1	3.1	167.6	22.7	Normal operation
BWR3	110.3	5.9	420.6	22.3	Normal operation
PWR1	28.7	3.0	205.2	21.3	Normal operation
PWR2	168.2	7.5	690.1	30.9	Normal operation
PWR3	68.7	2.9	509.3	21.9	Normal operation

As show in Table 7.2.1 the results regarding the acceptable and critical crack lengths (as a percentage of the circumference) is quite similar for BWR2, BWR3, PWR1 and PWR3; all with a critical crack length of ~22 % of the circumference of the pipe. The largest difference is for the smallest pipe (BWR1) which has a critical crack length of almost 50 % of the circumference of the pipe and the ferritic weld (PWR2) with a critical crack length of ~30 % of the circumference of the pipe. The larger critical crack length for BWR1 is due to the low nominal loading for this pipe.

In Table 7.2.1, the loading conditions are for the baseline cases using loads from the normal operating conditions. According to the deterministic guidelines, the critical crack sizes should be calculated using the normal operating conditions and also one of the worst loading case/transient according to the design specification. These loads are considered in section 7.4.9 but are not included in the sensitivity analysis presented in section 8.

7.3 Leakage flow rate

In simple terms, LBB is the demonstration that a postulated defect will leak and be detected, before a catastrophic failure. This means that a leakage detection system should exist with sufficient leak flow rate detection capabilities and also connected to clear conditions to bring the reactor to a cold shutdown if leak rate limits are exceeded. This indicates the important link between the calculated fracture probabilities and the corresponding leakage flow rate.

In this section, the calculated leakage flow rate for the baseline cases is given as a function of the length of a postulated through-thickness crack. The calculations have been done using the software SQUIRT [15], which is based the so-called Henry-Fauske model for two-phase flow through long channels [16].

Some of the key parameters contributing to the mass flow equations (in the Henry-Fauske model) are the:
- quality of the fluid
- pipe diameter
- flow path length
- pressure losses due to entrance effects
- pressure losses due to crack flow path losses
- pressure losses due to the acceleration of the fluid
- pressure losses due to the crack cross section area changes.

In the Henry-Fauske model used, some of the factors that affect these pressure losses are the:
- hydraulic diameter, which is a function of the crack opening displacement (COD)
- surface roughness
- number of turns that the fluid has to take as it transverses along the flow path.

In the SQUIRT calculations, default values are used for most the parameters not related to the geometry of the baseline cases. The main input data are the pipe geometry, postulated crack length, COD (using loads from the normal operation of the plant and the new COA-solutions with a correction factor that takes into account the effect of the plastic deformation) and type of cracking mechanism. For the baseline cases we assume that data for fatigue growth is most relevant (note that no active damage mechanism should be present in the piping segment, if LBB should be considered). This assumption will be investigated in a sensitivity analysis in section 8. This means that we have used the following values in the SQUIRT calculations:
- Global surface roughness, $\mu_G = 0.0405$
- Local surface roughness, $\mu_L = 0.0088$
- Global PLC (Vel. Heads/mm) = 0.673
- Local PLC (Vel. Heads/mm), $\eta_L = 6.730$
- Global thickness parameter, $K_G = 1.02$
- Local thickness parameter, $K_L = 1.06$

Finally, the calculations have been made using the improved model for crack morphology parameters (which is dependent of the given COD-values, as given by Eqn. 7.3.1-7.3.3).

$$\mu = \begin{cases} \mu_L & , 0.0 \le COD/\mu_G < 0.1 \\ \mu_L + \dfrac{\mu_G - \mu_L}{9.9}(COD/\mu_G - 0.1), & 0.1 \le COD/\mu_G < 10. \\ \mu_G & , COD/\mu_G > 10. \end{cases} \quad , \tag{7.3.1}$$

$$\eta = \begin{cases} \eta_L & , 0.0 \le COD/\mu_G < 0.1 \\ \eta_L - \dfrac{0.9 * \eta_L}{9.9}(COD/\mu_G - 0.1) & , 0.1 \le COD/\mu_G < 10. \\ \eta_L * 0.1 & , COD/\mu_G > 10. \end{cases} \quad , \tag{7.3.2}$$

$$\frac{t_e}{t} = \begin{cases} K_L & , 0.0 \le COD/\mu_G < 0.1 \\ K_L + \dfrac{K_G - K_L}{9.9}(COD/\mu_G - 0.1) & , 0.1 \le COD/\mu_G < 10. \\ K_G & , COD/\mu_G > 10. \end{cases} \quad . \tag{7.3.3}$$

The resulting leakage flow rates are presented in Fig. 7.3.1-7.3.6.

Leakage flow rate [kg/s]
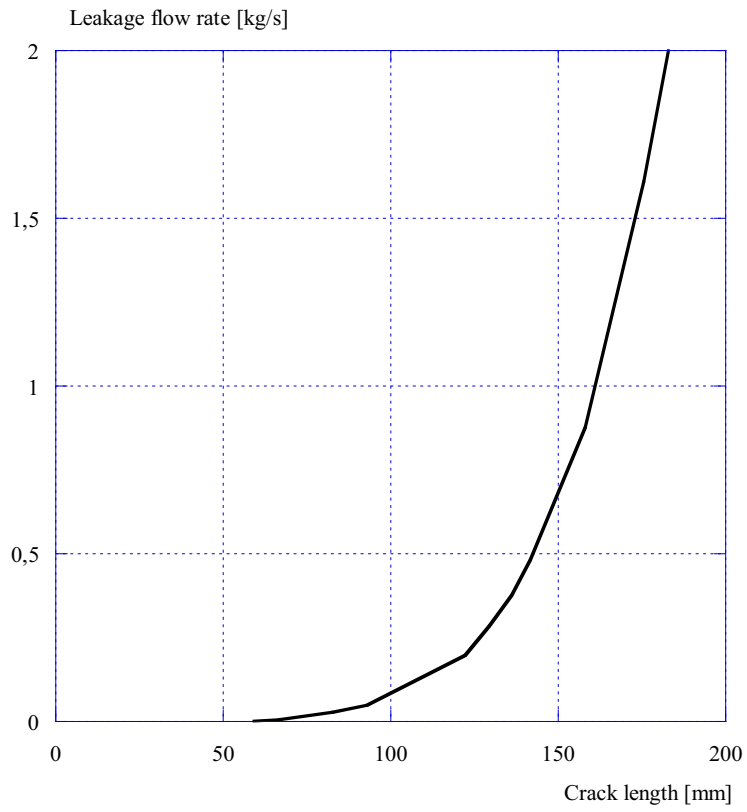
Figure 7.3.1. Leakage flow rate for the case BWR1.

Leakage flow rate [kg/s]
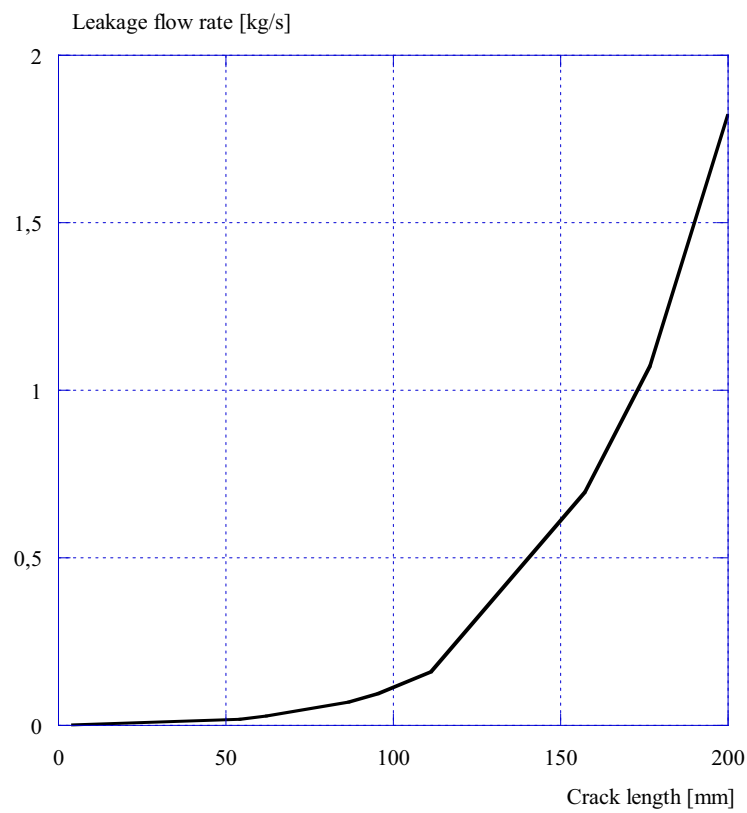
Figure 7.3.2. Leakage flow rate for the case BWR2.
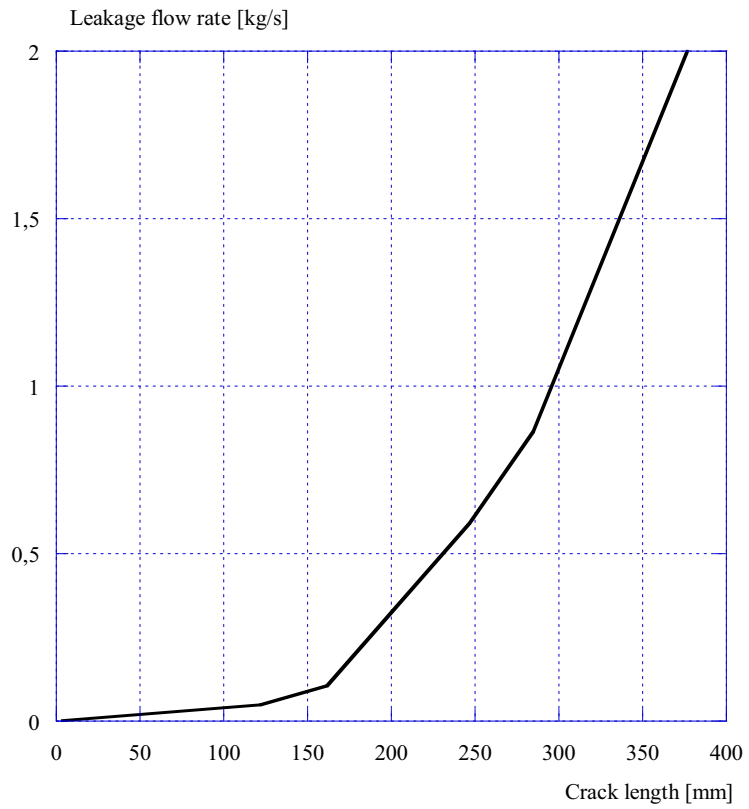
Figure 7.3.3. Leakage flow rate for the case BWR3.
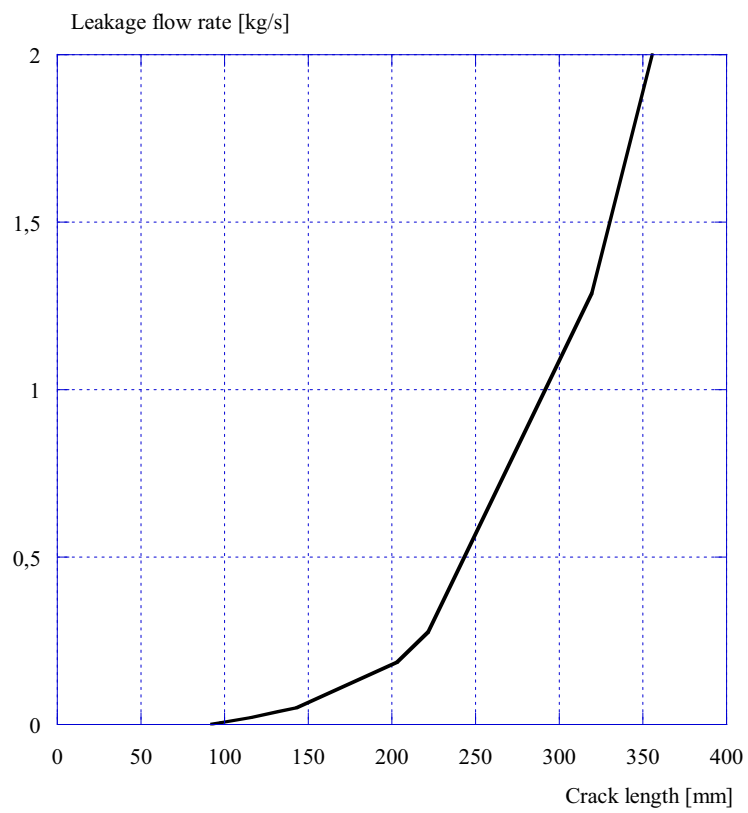
Figure 7.3.4. Leakage flow rate for the case PWR1.
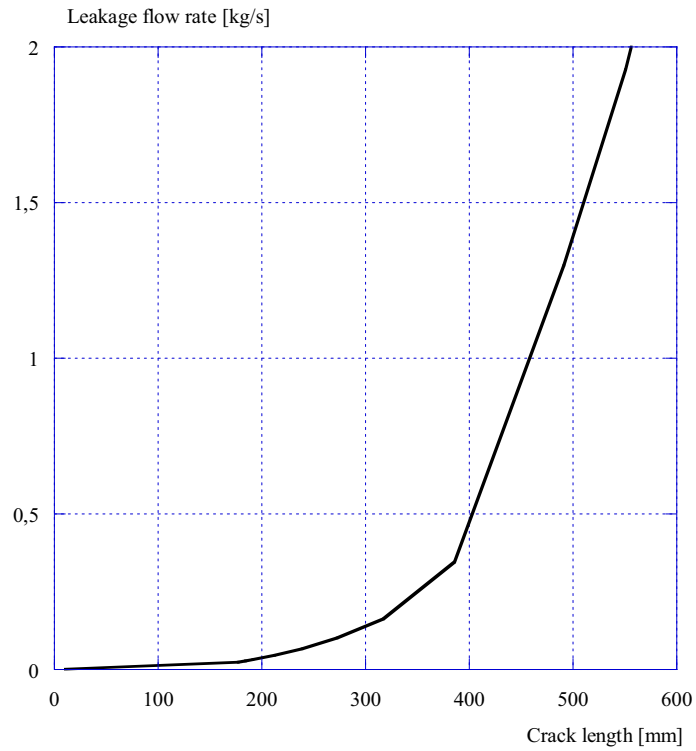
Figure 7.3.5. Leakage flow rate for the case PWR2. In this case, the leakage flow rate is quite low, even for very long cracks. This has to do with the fact that the applied global bending stress ($P_b + P_e$) is very small compared to the other baseline cases.
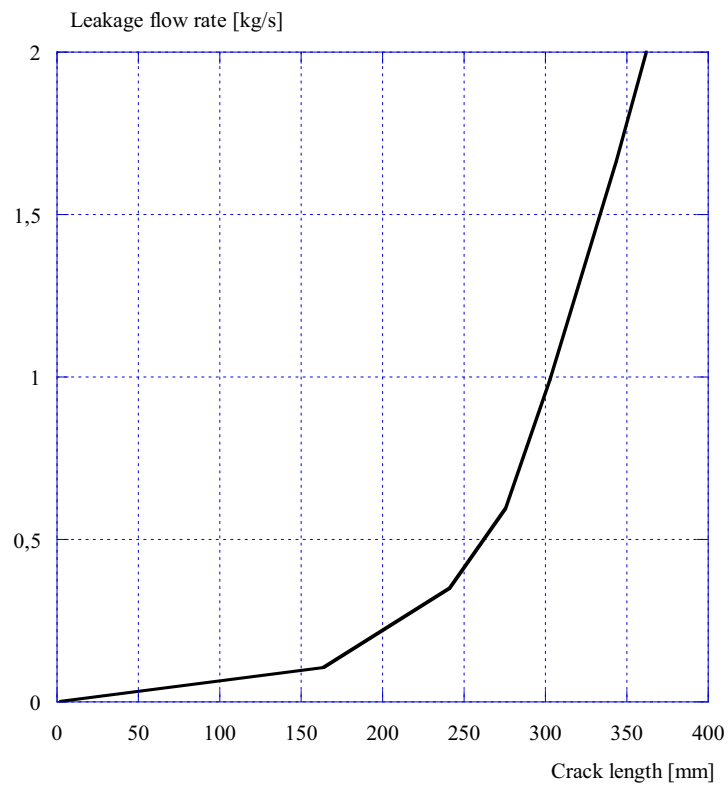
Figure 7.3.6. Leakage flow rate for the case PWR3.

26

7.4 Probability of fracture

In this section, the results for the conditional probability of fracture (given the existence of a leaking through-thickness crack) are given for the baseline cases.

7.4.1 Input data for the probabilistic analysis

Following the recommendations in [7], the input data given in Table 7.4.1-7.4.8 is used in the probabilistic analysis.

Table 7.4.1. Input data – geometry – crack length (l).

Case	Distribution	Mean value, μ_l [mm]	Standard deviation, σ_l [mm]
BWR1	Normal	15, 31, 46, 62, 92, 123, 154	5% of μ_l
BWR2	Normal	37, 74, 111, 148, 185, 221	5% of μ_l
BWR3	Normal	94, 188, 283, 377, 471, 565, 754	5% of μ_l
PWR1	Normal	24, 48, 96, 145, 193, 241, 289	5% of μ_l
PWR2	Normal	56, 111, 223, 334, 446, 557, 669	5% of μ_l
PWR3	Normal	58, 117, 233, 350, 466, 583, 699	5% of μ_l

Table 7.4.2. Input data – geometry – off-centered position of crack (ψ).

Case	Distribution	Mean value, μ_ψ	Min/Max value
BWR1	Uniform	0º	±90º
BWR2	Uniform	0º	±90º
BWR3	Uniform	0º	±90º
PWR1	Uniform	0º	±90º
PWR2	Uniform	0º	±90º
PWR3	Uniform	0º	±90º

Note: Using a uniform distribution between -90º and +90º, is equivalent to assuming that the off-centered crack position is random and equally likely to take on an angle anywhere between -90º and +90º.

Table 7.4.3. Input data – material data – fracture toughness (K_{Ic}).

Case	Distribution	Mean value, $\mu_{K_{Ic}}$ [MPa$\sqrt{m}$]	Standard dev., $\sigma_{K_{Ic}}$ [MPa$\sqrt{m}$]
BWR1	Normal	182	14
BWR2	Normal	182	14
BWR3	Normal	182	14
PWR1	Normal	182	14
PWR2	Normal	150	11.25
PWR3	Normal	182	14

Note: The standard deviation is ~7.5% of the mean value.

Table 7.4.4. Input data – material data – yield strength (σ_y).

Case	Distribution	Mean value, μ_{σ_y} [MPa]	Standard deviation, σ_{σ_y} [MPa]
BWR1	Normal	150	15
BWR2	Normal	150	15
BWR3	Normal	150	15
PWR1	Normal	137	13.7
PWR2	Normal	260	26
PWR3	Normal	150	15

Note: The standard deviation is 10% of the mean value.

Table 7.4.5. Input data – material data – ultimate tensile strength (σ_u).

Case	Distribution	Mean value, μ_{σ_u} [MPa]	Standard deviation, σ_{σ_u} [MPa]
BWR1	Normal	450	30
BWR2	Normal	450	30
BWR3	Normal	450	30
PWR1	Normal	495	30
PWR2	Normal	500	30
PWR3	Normal	450	30

Note: The standard deviation is 30 MPa (independent of the mean value).

Table 7.4.6. Input data – loading (stresses) – primary membrane stress (P_m).

Case	Distribution	Mean value, μ_{P_m} [MPa]	Standard deviation, σ_{P_m} [MPa]
BWR1	Normal	20.0	2.0
BWR2	Normal	25.0	2.0
BWR3	Normal	28.0	2.0
PWR1	Normal	43.2	2.0
PWR2	Normal	40.3	2.0
PWR3	Normal	40.4	2.0

Note: The standard deviation is 2 MPa (independent of the mean value).

Table 7.4.7. Input data – loading (stresses) – primary global bending stress (P_b).

Case	Distribution	Mean value, μ_{P_b} [MPa]	Standard deviation, σ_{P_b} [MPa]
BWR1	Normal	11.0	2.0
BWR2	Normal	42.0	2.0
BWR3	Normal	60.0	2.0
PWR1	Normal	47.2	2.0
PWR2	Normal	7.2	2.0
PWR3	Normal	51.1	2.0

Note 1: The standard deviation is 2 MPa (independent of the mean value).

Note 2. In the case of PWR1, PWR2 and PWR3, the applied stress is taken as $P_b + P_e$. This has to do with the background data, which only gives the sum of these stresses (only for the PWR cases). To be conservative, the assumption in the analysis is to consider this sum to be a primary stress only.

Table 7.4.8. Input data – loading (stresses) – secondary global bending stress (P_e).

Case	Distribution	Mean value, μ_{P_e} [MPa]	Standard deviation, σ_{P_e} [MPa]
BWR1	Normal	18.0	2.0
BWR2	Normal	105.0	2.0
BWR3	Normal	15.0	2.0
PWR1	Normal	0.0	2.0
PWR2	Normal	0.0	2.0
PWR3	Normal	0.0	2.0

Note 1: The standard deviation is 2 MPa (independent of the mean value).

Note 2. In the case of PWR1, PWR2 and PWR3, the applied stress is taken as zero (since the applied primary global bending stress is taken as $P_b + P_e$, see table 7.4.7).

Below, the results for the conditional probability of fracture (given the existence of a leaking through-thickness crack) are given for the baseline cases. All the probabilistic results are plotted both as a function of crack length and as a function of leakage flow rate. The most important parameter in a LBB application is the leakage flow rate, but to get a better insight into the results it is also plotted versus the through-thickness crack length (given as a percentage of the circumference).

7.4.2 Probability of fracture for the case BWR1
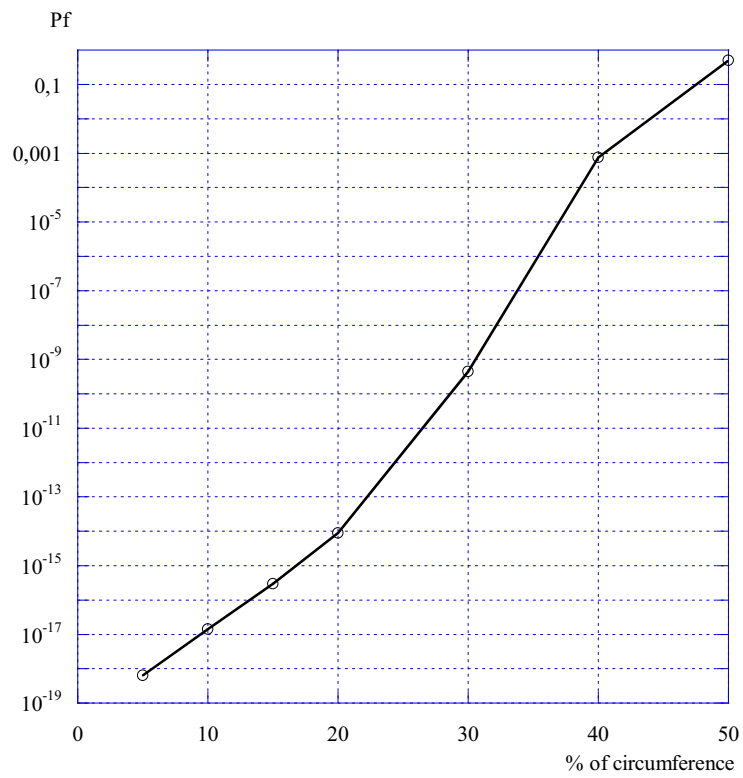
Figure 7.4.1. Conditional probability of fracture as a function of crack length $\left(l/(2 \cdot \pi \cdot R) \right)$ (BWR1).
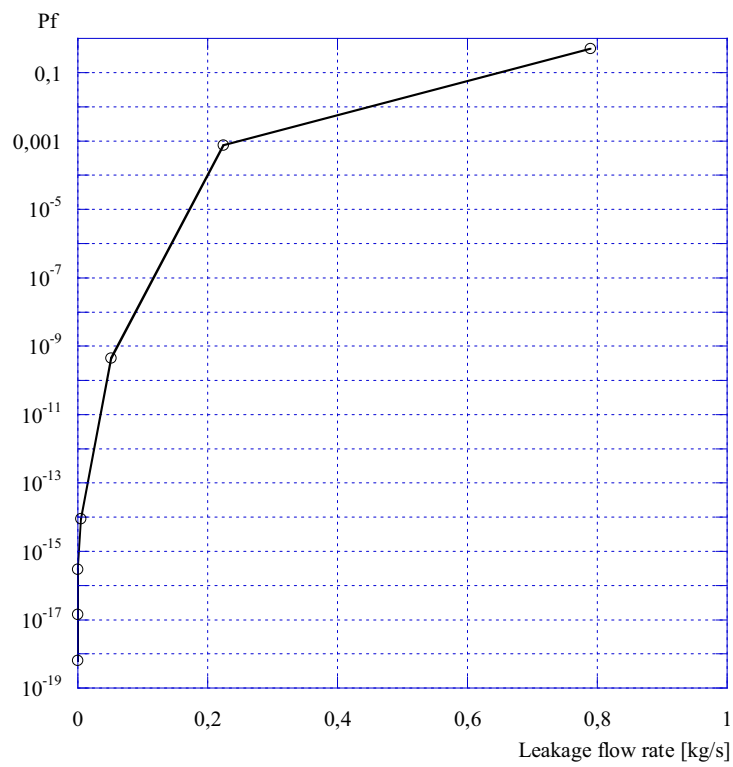
Figure 7.4.2. Conditional probability of fracture as a function of leakage flow rate (BWR1).

7.4.3 Probability of fracture for the case BWR2
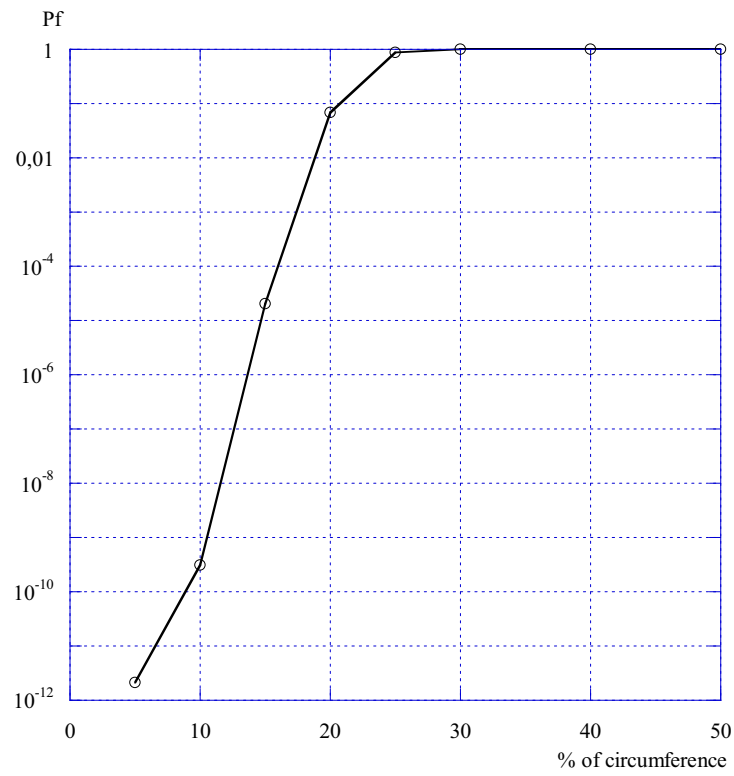
Figure 7.4.3. Conditional probability of fracture as a function of crack length $\left(l/(2 \cdot \pi \cdot R) \right)$ (BWR2).
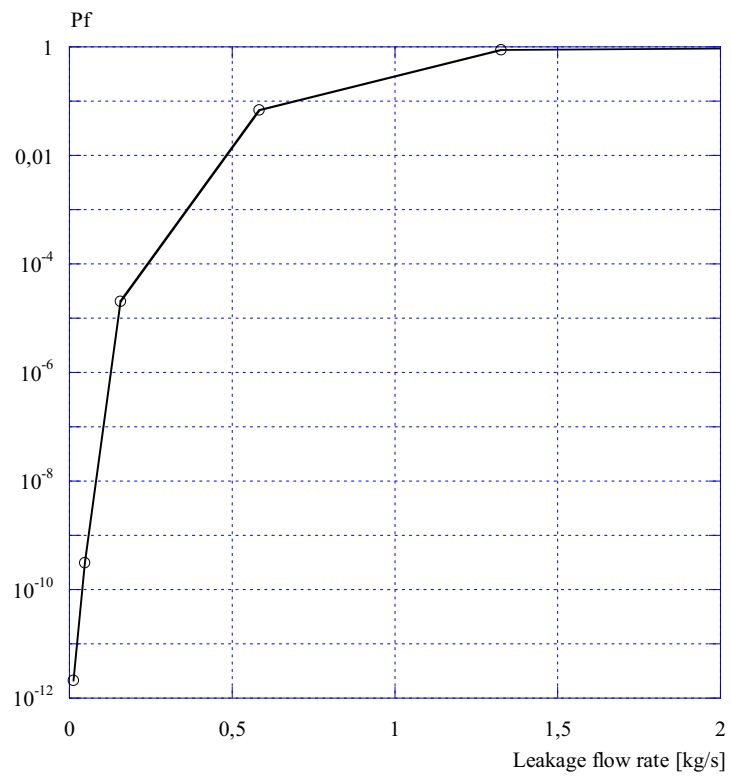
Figure 7.4.4. Conditional probability of fracture as a function of leakage flow rate (BWR2).

7.4.4   Probability of fracture for the case BWR3
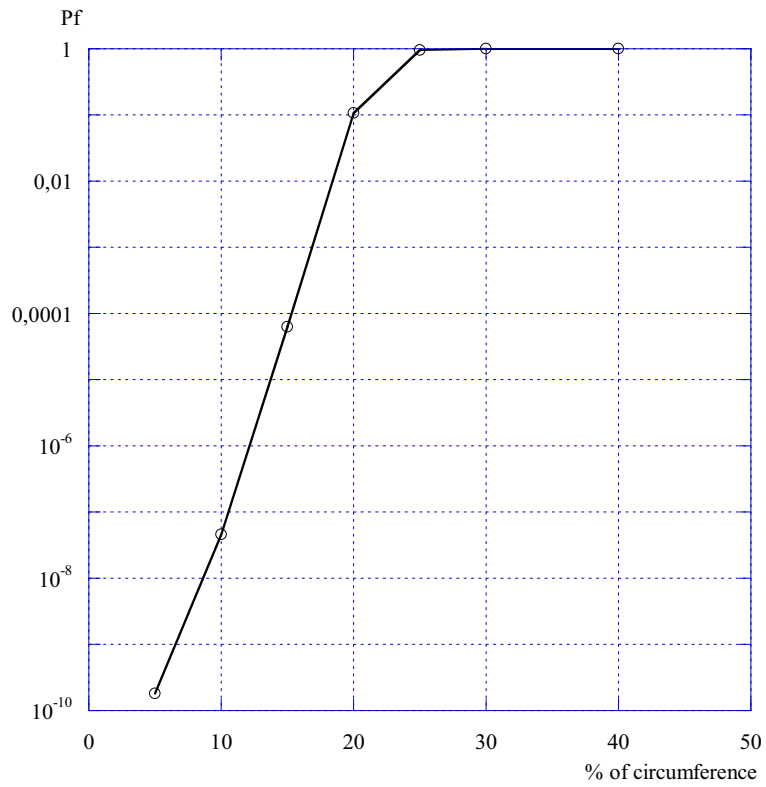
Figure 7.4.5. Conditional probability of fracture as a function of crack length $\left(l/(2\cdot\pi\cdot R)\right)$ (BWR3).
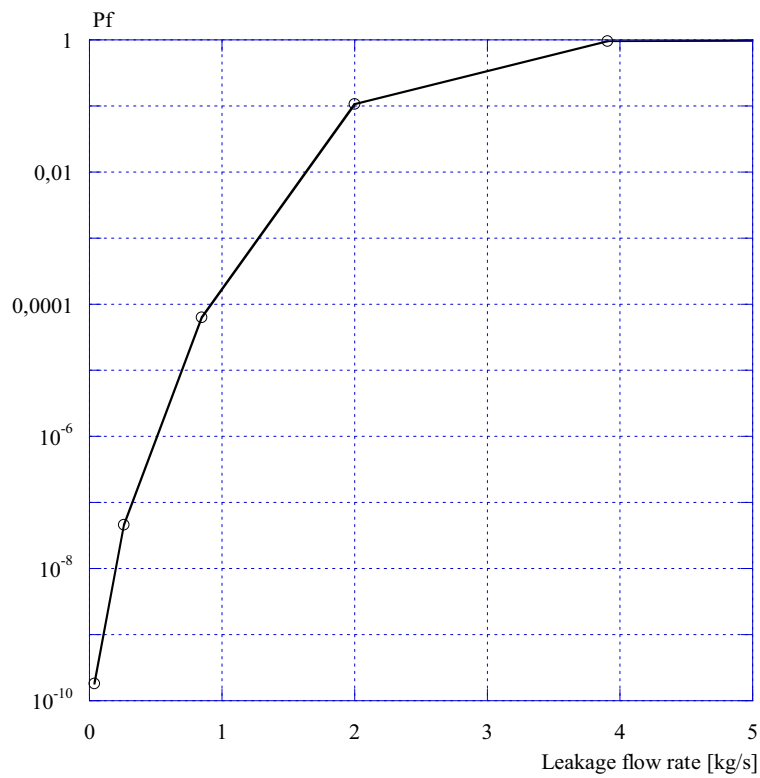
Figure 7.4.6. Conditional probability of fracture as a function of leakage flow rate (BWR3).

7.4.5   Probability of fracture for the case PWR1
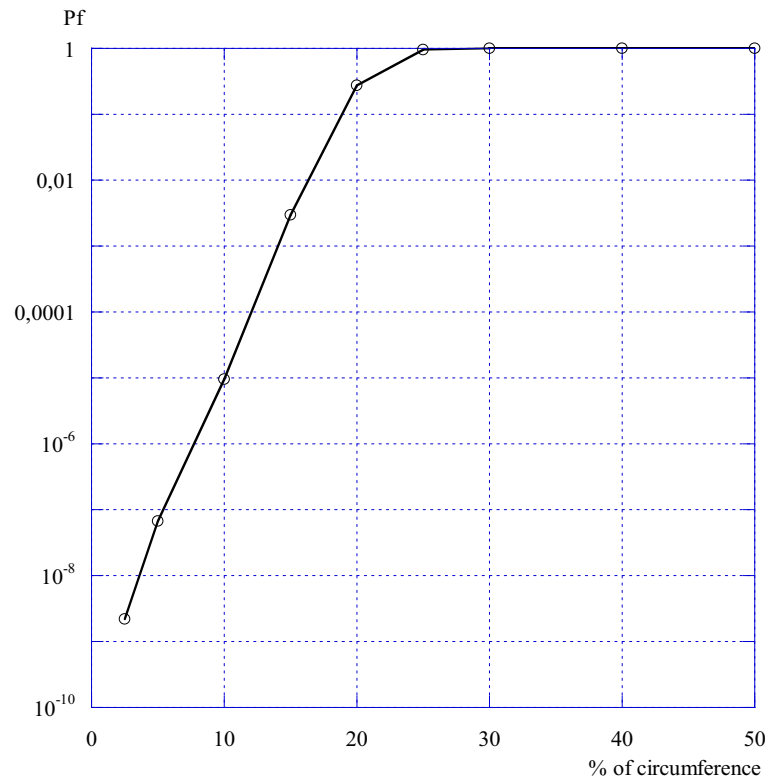
Figure 7.4.7. Conditional probability of fracture as a function of crack length $\left(l/\left(2\cdot\pi\cdot R\right)\right)$ (PWR1).
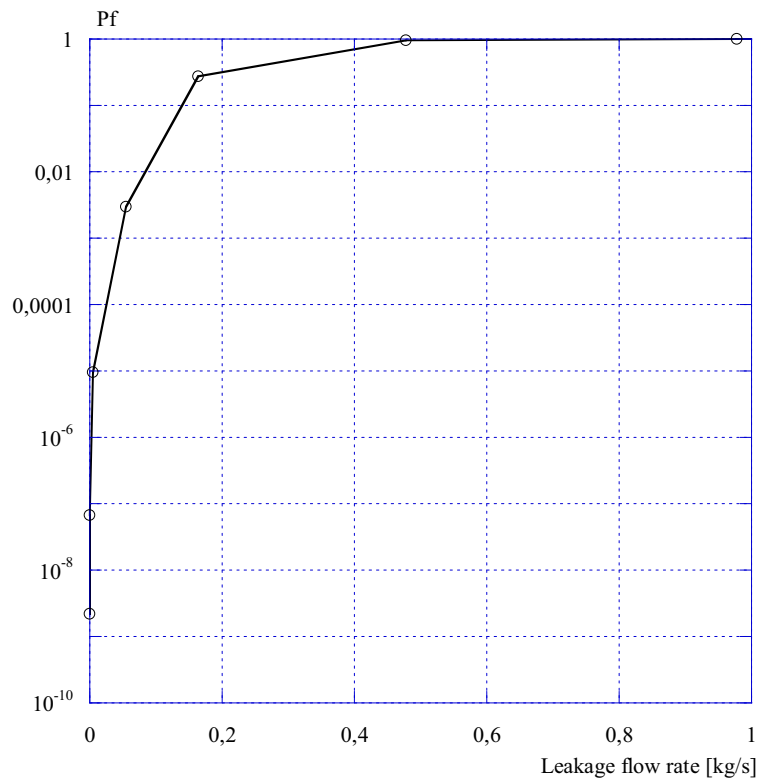
Figure 7.4.8. Conditional probability of fracture as a function of leakage flow rate (PWR1).

7.4.6   Probability of fracture for the case PWR2
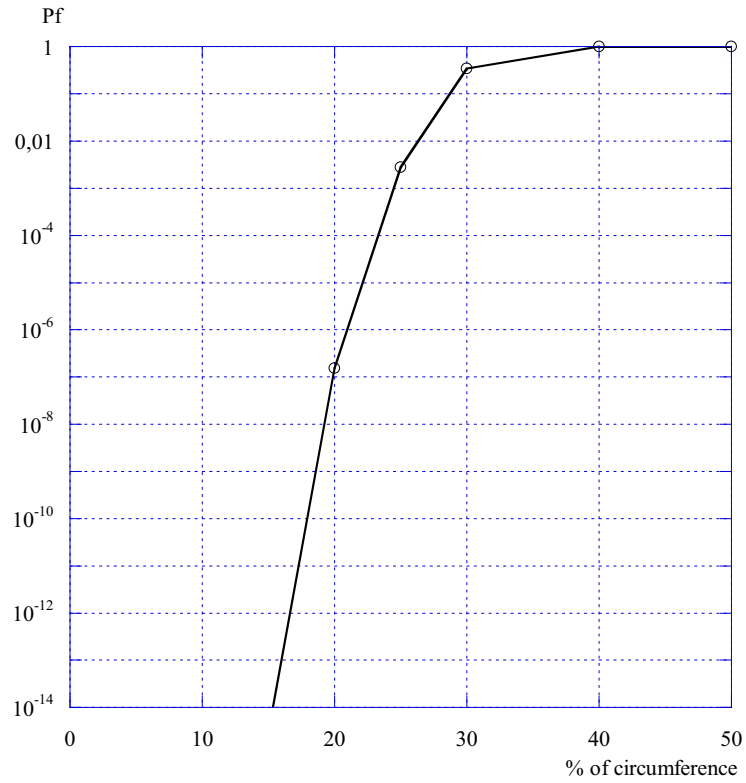
Figure 7.4.9. Conditional probability of fracture as a function of crack length $\left(l/\left(2\cdot\pi\cdot R\right)\right)$ (PWR2).
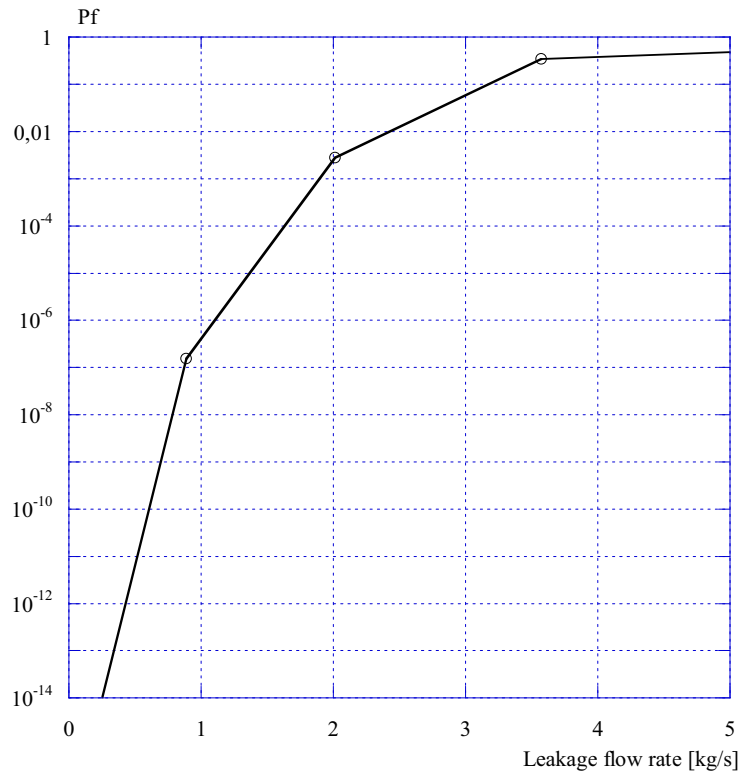
Figure 7.4.10. Conditional probability of fracture as a function of leakage flow rate (PWR2).

7.4.7   Probability of fracture for the case PWR3
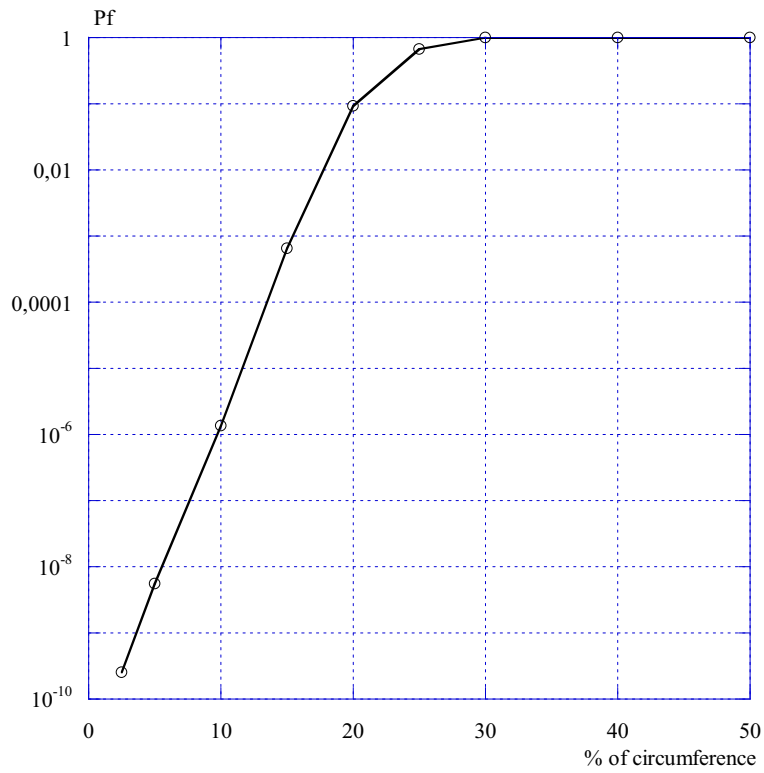
Figure 7.4.11. Conditional probability of fracture as a function of crack length $\left(l/\left(2\cdot\pi\cdot R\right)\right)$ (PWR3).
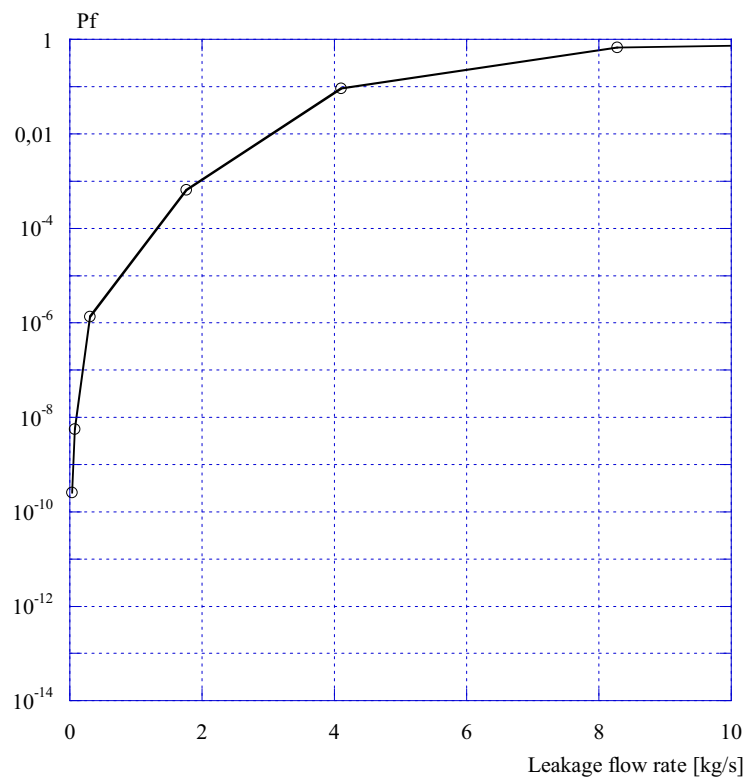
Figure 7.4.12. Conditional probability of fracture as a function of leakage flow rate (PWR3).

7.4.8   Probability of fracture for all the baseline cases

In Figs. 7.4.13-7.4.14 below, a comparison is made between the chosen baseline cases.
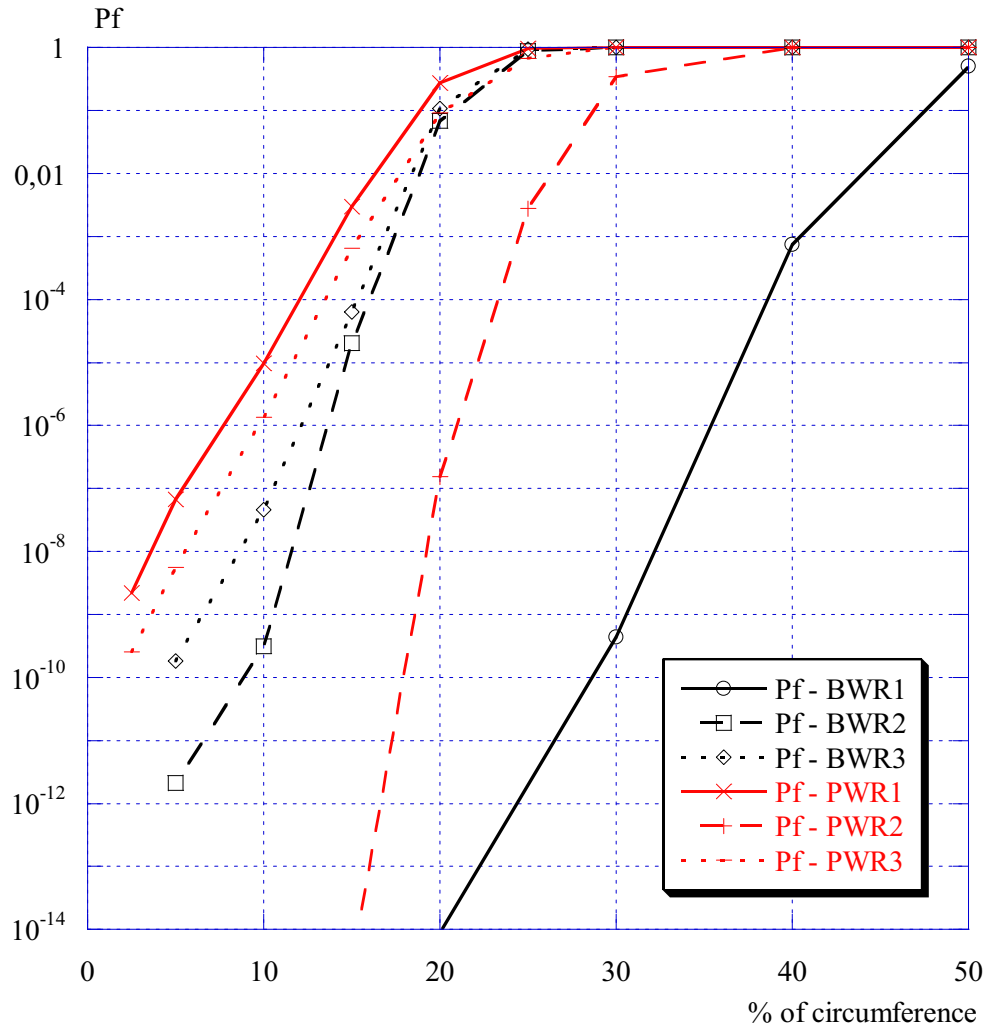
Figure 7.4.13. Conditional probability of fracture as a function of crack length $\left(l/\left(2\cdot\pi\cdot R\right)\right)$.
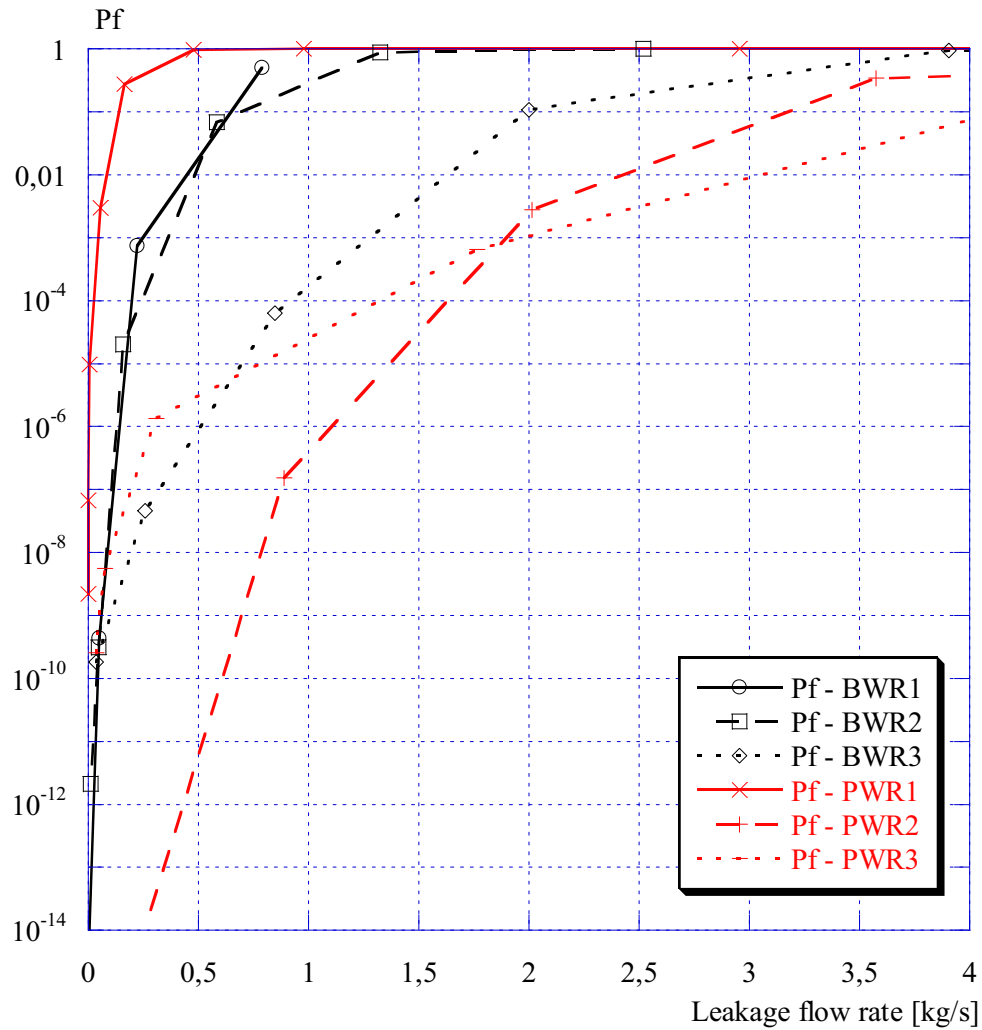
Figure 7.4.14. Conditional probability of fracture as a function of leakage flow rate.

As shown above, PWR1 has the highest probabilities among the baseline cases (both when the results are given as a function of the percentage of the circumference and as a function of the leakage flow rate). This result is reasonable since PWR1 has the lowest yield strength (in this case also combined with a large D_y/t -ratio) and most of the results are dominated by this parameter (see the sensitivity study in section 8).

Also shown above, BWR1 has much lower probabilities for large cracks (given as a percentage of the circumference) than the other baseline cases. If the probability of failure is plotted as a function of leakage flow rate, then BWR1 has much larger probabilities than most of the other baseline cases. This result is reasonable since BWR1 is the smallest pipe among of the baseline cases.

Also shown above, PWR3 has much higher probabilities for all crack lengths (given as a percentage of the circumference) than most of the other baseline cases. If the probability of failure is plotted as a function of leakage flow rate, then PWR3 has much smaller probabilities than most of the other baseline cases. This result is reasonable since PWR3 is the largest pipe among of the baseline cases.

Because of this contradictory behavior, BWR1 and PWR3 were chosen for the sensitivity study in section 8 below and also when presenting the difference between leakage and fracture probabilities in section 7.5.

Finally, a general comment regarding the relation between the resulting probabilities and the sizes of the pipes. It is obvious that the fracture probabilities for large diameter pipes (PWR2, PWR3 and BWR3 in Fig. 7.4.14) are much lower than the small diameter pipes, when looking at an equivalent leakage flow rate. Among the large diameter pipes, PWR2 has the lowest fracture probability, since the applied bending stress is quite low for this case. Also, these results give an explanation on why the small diameter pipes generally have more difficulty to fulfill the deterministic acceptance criteria.

7.4.9 Probability of fracture for the worst loading conditions

In the baseline case above, the analysis is conducted using loads from the normal operating conditions. But according to the deterministic guidelines [1] one should also check the worst loading case/transient according to the design specification. In Figs. 7.4.15-7.4.20 below, the results for the conditional probability of fracture (given the existence of a leaking through-thickness crack) are given as a comparison between the baseline case and the worst loading condition found for the cases considered (different Service Level C/D events).
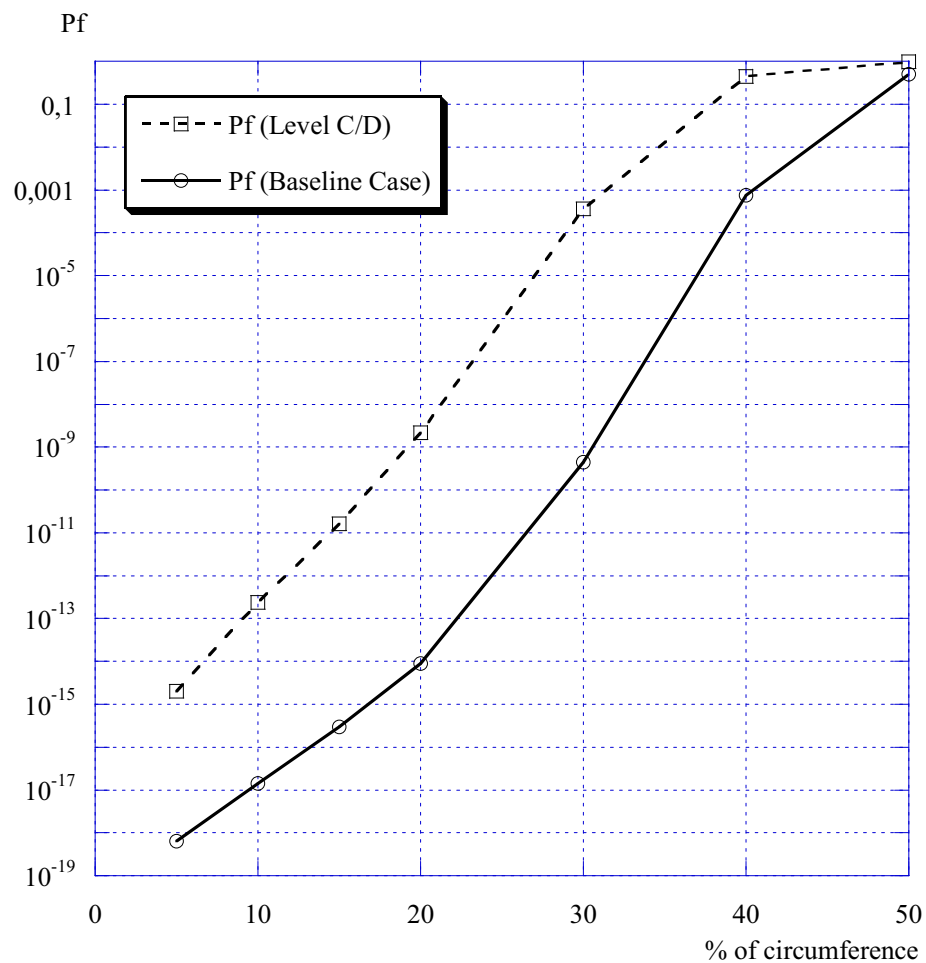
Figure 7.4.15. Conditional probability of fracture as a function of crack length $\left(l/(2\cdot\pi\cdot R)\right)$ (BWR1, comparison between the baseline case and the worst loading conditions).
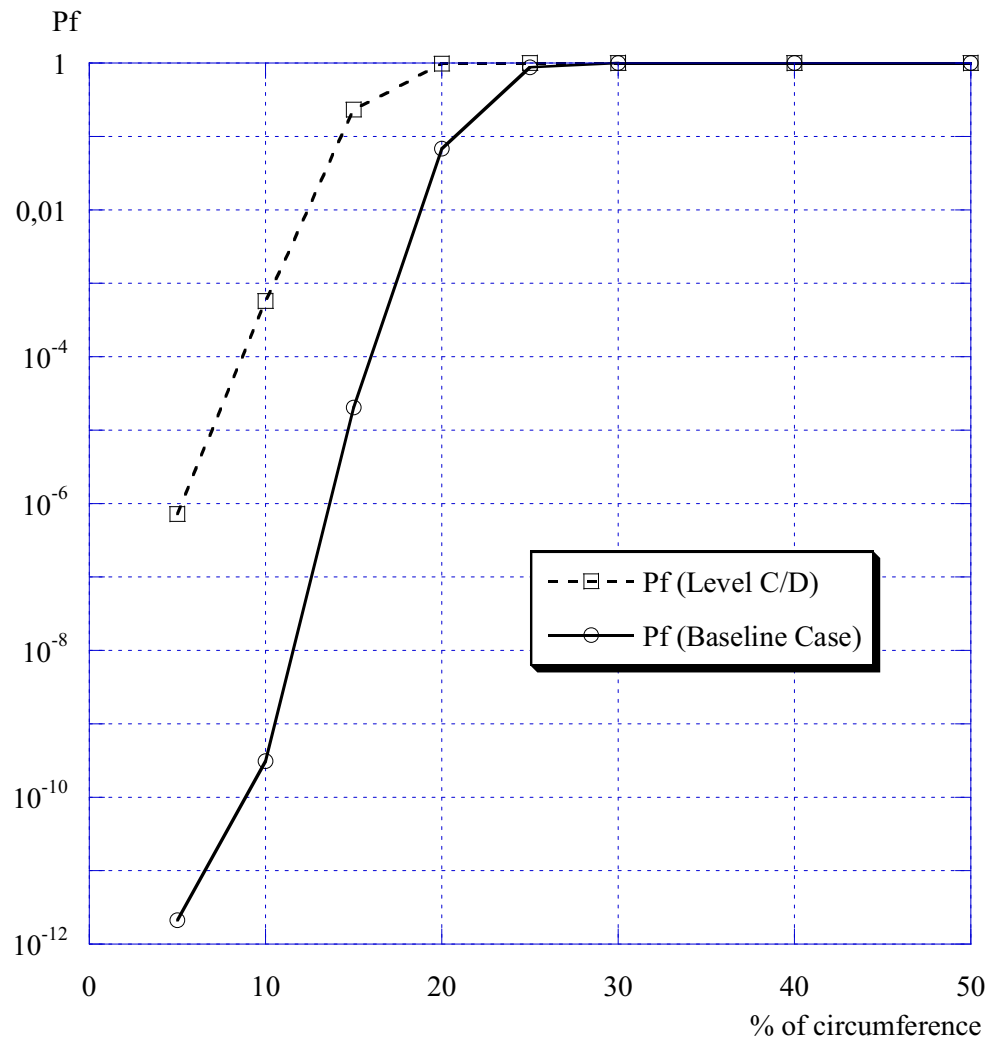
Figure 7.4.16. Conditional probability of fracture as a function of crack length $\left(l/(2\cdot\pi\cdot R)\right)$ (BWR2, comparison between the baseline case and the worst loading conditions).
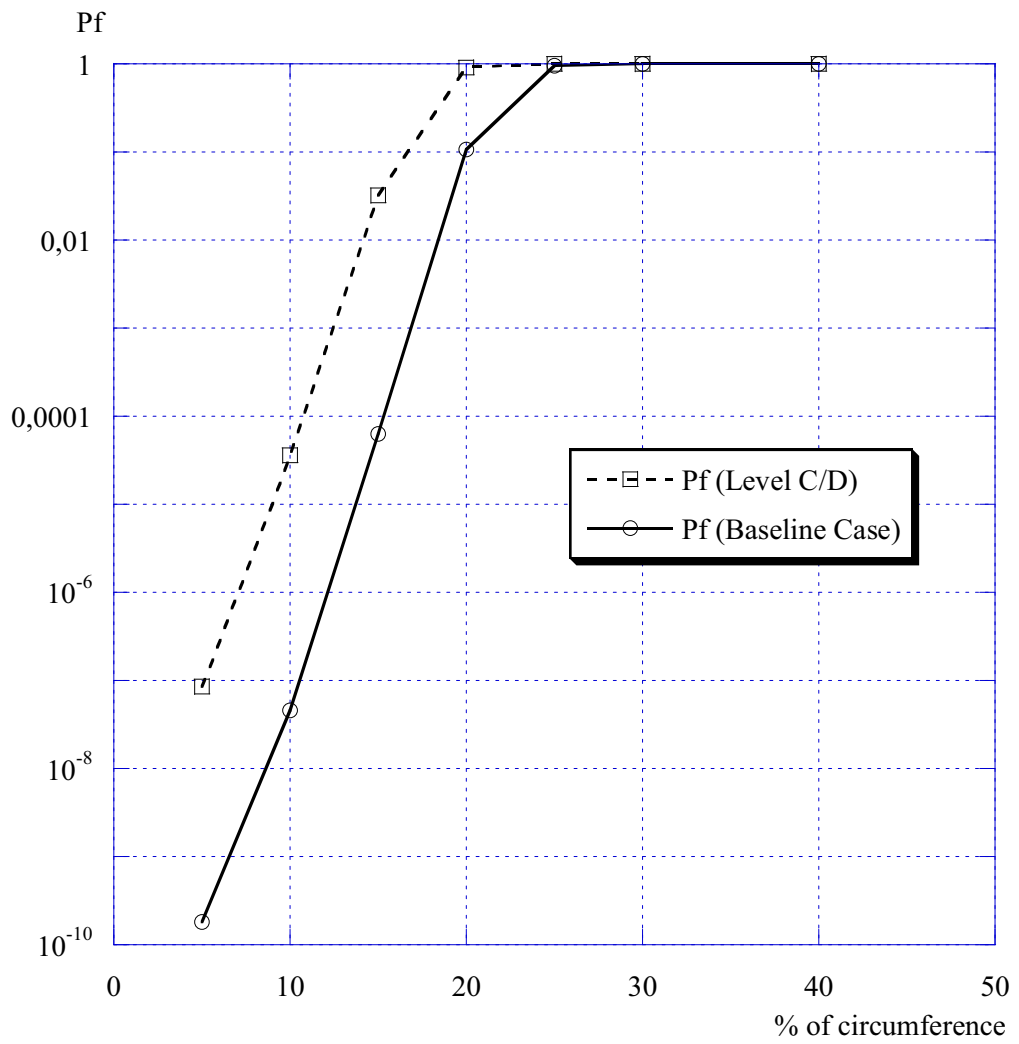
Figure 7.4.17. Conditional probability of fracture as a function of crack length $\left(l/(2\cdot\pi\cdot R)\right)$ (BWR3, comparison between the baseline case and the worst loading conditions).
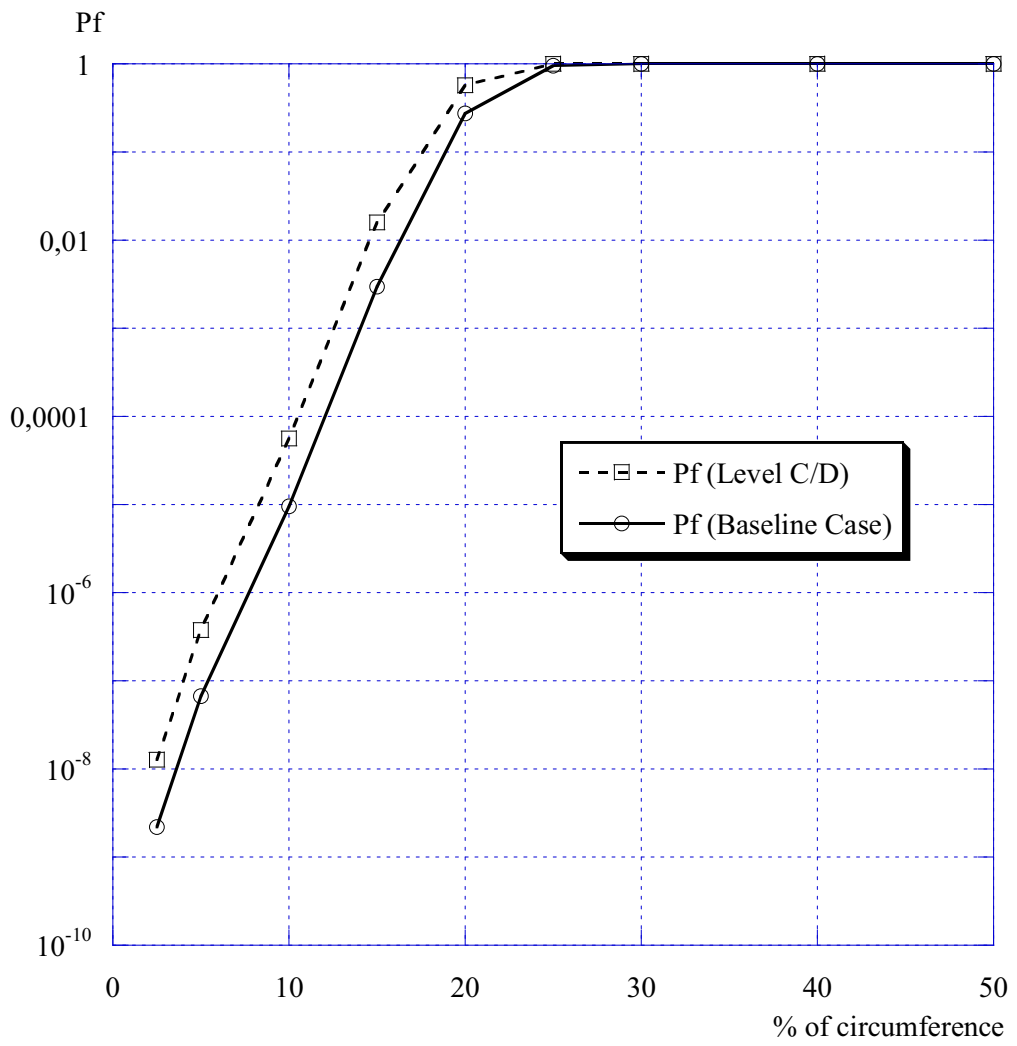
Figure 7.4.18. Conditional probability of fracture as a function of crack length $\left(l/\left(2\cdot\pi\cdot R\right)\right)$ (PWR1, comparison between the baseline case and the worst loading conditions).
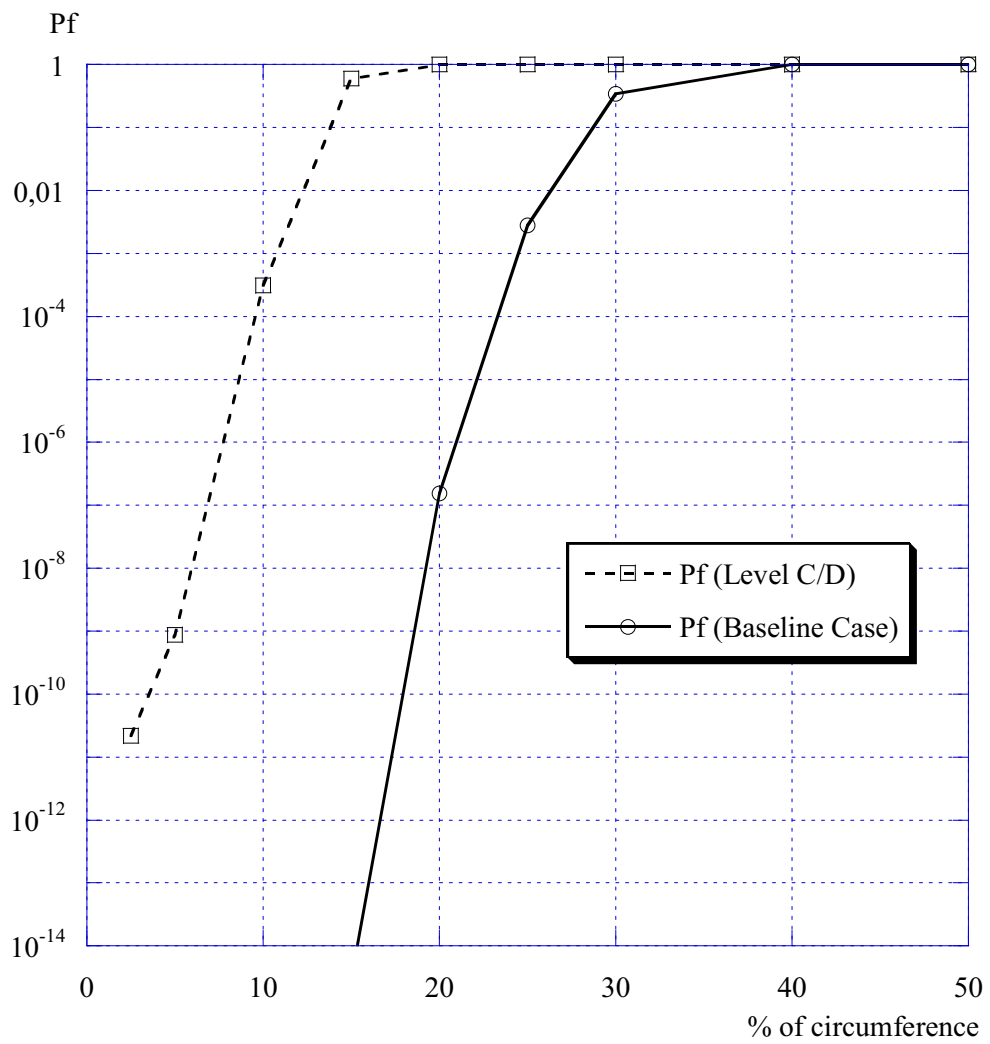
Figure 7.4.19. Conditional probability of fracture as a function of crack length $\left(l/(2 \cdot \pi \cdot R) \right)$ (PWR2, comparison between the baseline case and the worst loading conditions).
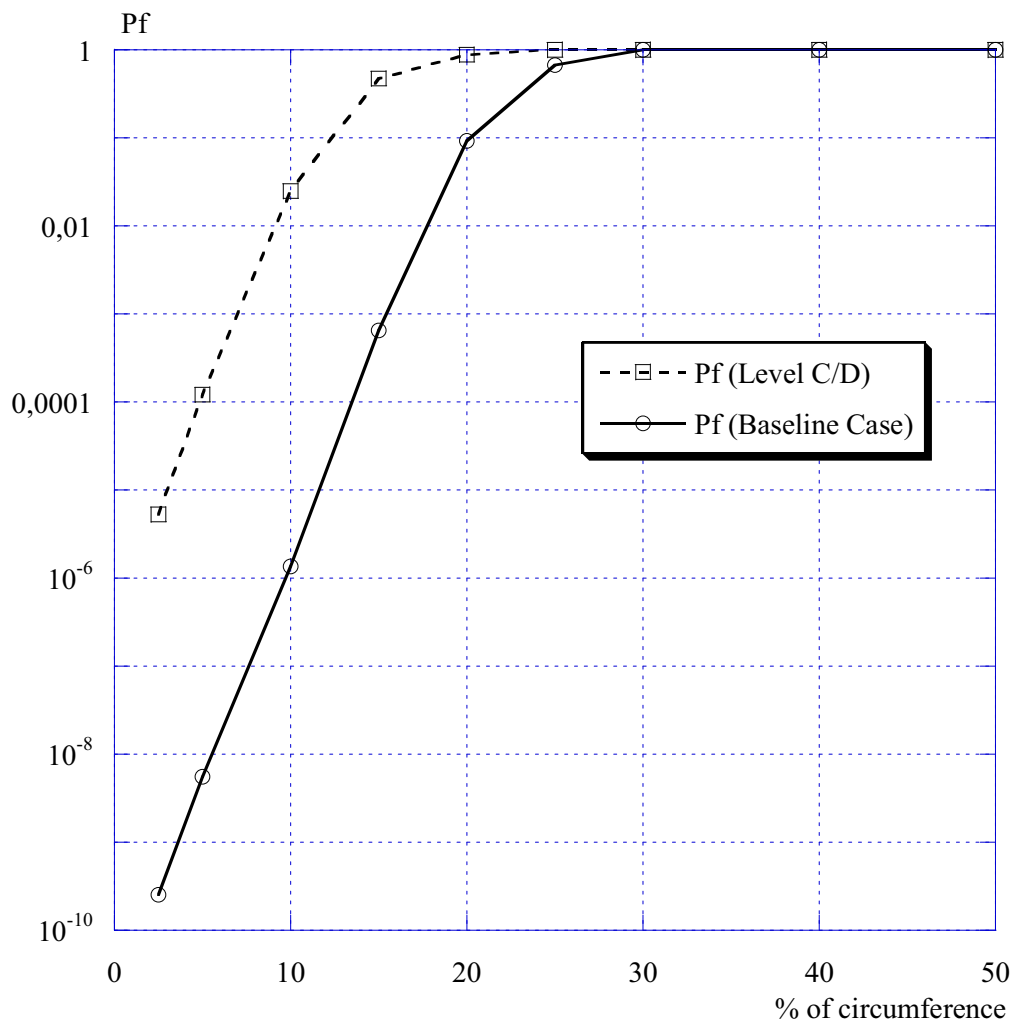
Figure 7.4.20. Conditional probability of fracture as a function of crack length $\left(l / (2 \cdot \pi \cdot R)\right)$ (PWR3, comparison between the baseline case and the worst loading conditions).

As can be seen in Figs. 7.4.15-7.4.20, including the worst loading conditions increases the conditional probability of fracture as compared to the baseline case. This difference is summarised in Fig. 7.4.21, where the P_f-ratio between the worst loading conditions and baseline case is given for all the baseline cases.
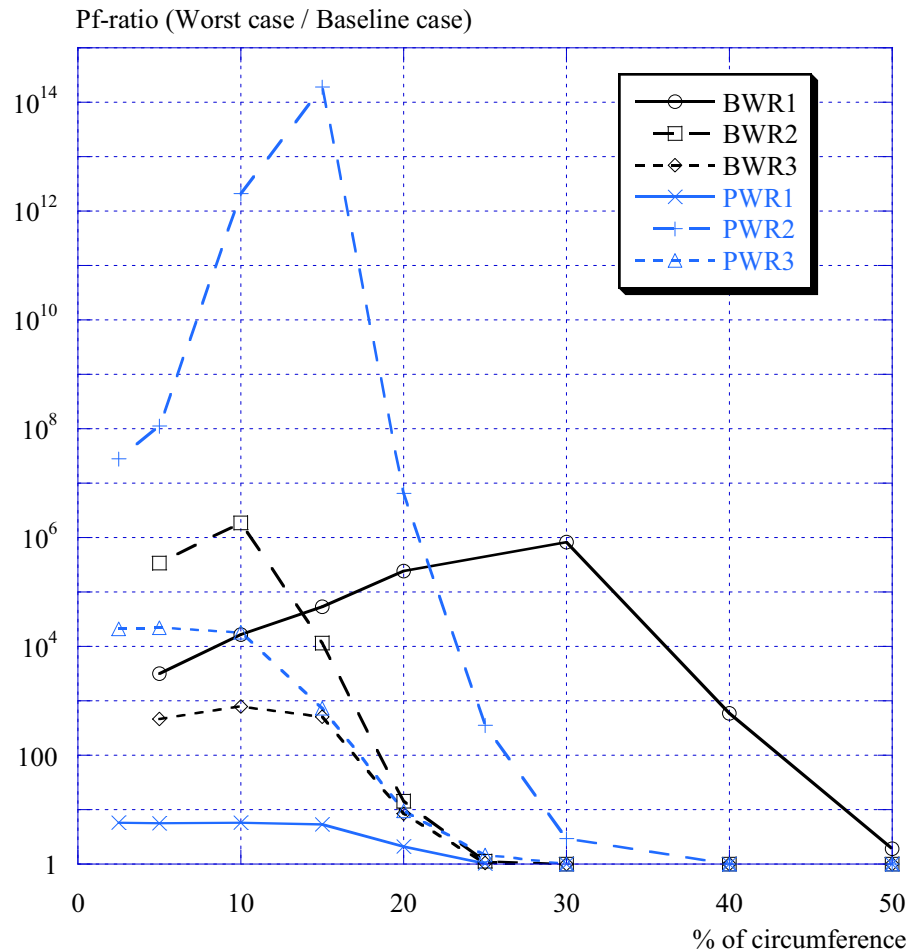
Figure 7.4.21. Conditional probability of fracture ratio between the worst loading conditions and the baseline case as a function of crack length $\left(l/\left(2 \cdot \pi \cdot R\right)\right)$.

As shown in Fig. 7.4.21, there could be a small P_f-difference in some cases which could be related to a small difference in the baseline loading and the worst loading condition (as for the case PWR1). There is also the possibility that there is a very large P_f-difference which could be related to a large difference in the loading conditions (as for the case PWR2). A large P_f-difference could also be related to the fact that if the baseline case has quite small P_f-values then a small increase in load may generate a quite large increase in P_f (also relevant for the case PWR2).

However, a direct comparison between the baseline case and a case with a more severe loading condition could be incorrect. To be consistent, one should multiply the conditional probability of fracture with the probability that the worst loading condition will actually occur (P_{load}^{occur}). For many Service Level C/D events P_{load}^{occur} is between 10^{-5} and 10^{-4}. Using diagrams similar to Fig. 7.4.21 (for the actual case to be analysed) will therefore give an indication into whether a more severe loading condition will contribute to the conditional probability of fracture. In the sensitivity analysis, presented in section 8, the contribution from the worst loading conditions is not included in the calculation (to simplify the analysis).

7.5 Probability of leakage

In this section, the results for the probability of leakage (given the existence of a surface crack) are given for the baseline cases BWR1 and PWR3.

7.5.1 Input data for the probabilistic analysis

The crack length distribution given in Table 7.4.1 (defined for a leaking through-thickness crack) is also used for surface cracks.

The crack depth distribution is taken from the NURBIM benchmark exercise [17] using data for pipes with a similar weld configuration. The software PRODIGAL was used in NURBIM to generate the crack depth distributions of each pipe [17]. PRODIGAL is a form of expert system that generates a defect distribution and density for welds (the objective is to simulate the number and size of defects generated during the welding process). Its output is a histogram or frequency plot of the defects that may occur during the normal build of a weld. For the BWR1 case, data for a small pipe is used and for the PWR3 case, data for a large pipe is used (the original NURBIM data is summarised in Fig. 7.5.1).
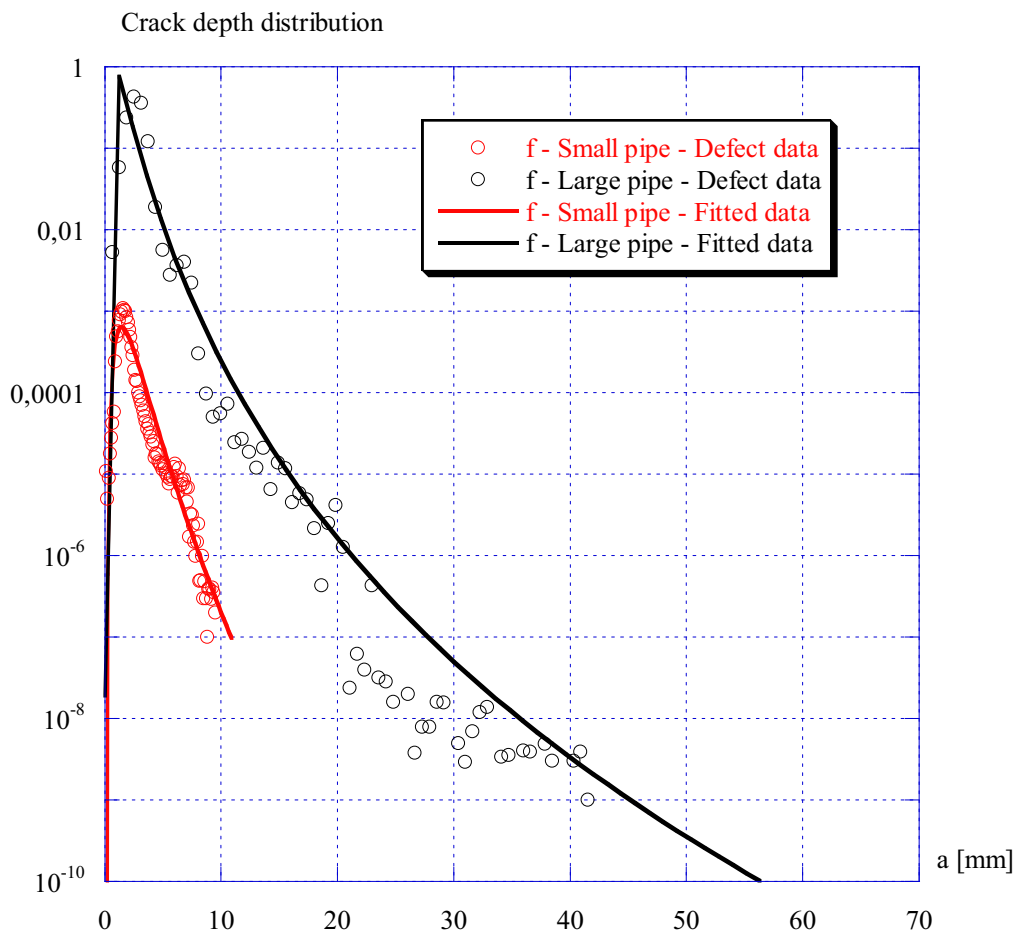
Figure 7.5.1. The original NURBIM crack depth distributions [17].

A lognormal distribution is used in both cases [17]. The data is summarised in Table 7.5.1 (a deterministic defect density factor is applied to get the correct crack existence frequency from the NURBIM benchmark data).

Table 7.5.1. Input data – geometry – crack depth (a).

Case	Distribution	Mean value, μ_l [mm]	Standard deviation, σ_l [mm]	Defect density factor, $C_{density}$
BWR1	Lognormal	2.025	1.043	$1.25 \cdot 10^{-3}$
PWR3	Lognormal	1.35	0.9605	1.5

Material and loading data is given in Table 7.4.3-7.4.8.

Below, the results for the probability of leakage (given the existence of a surface crack) are given for the two baseline cases considered.

7.5.2 Probability of leakage for the case BWR1
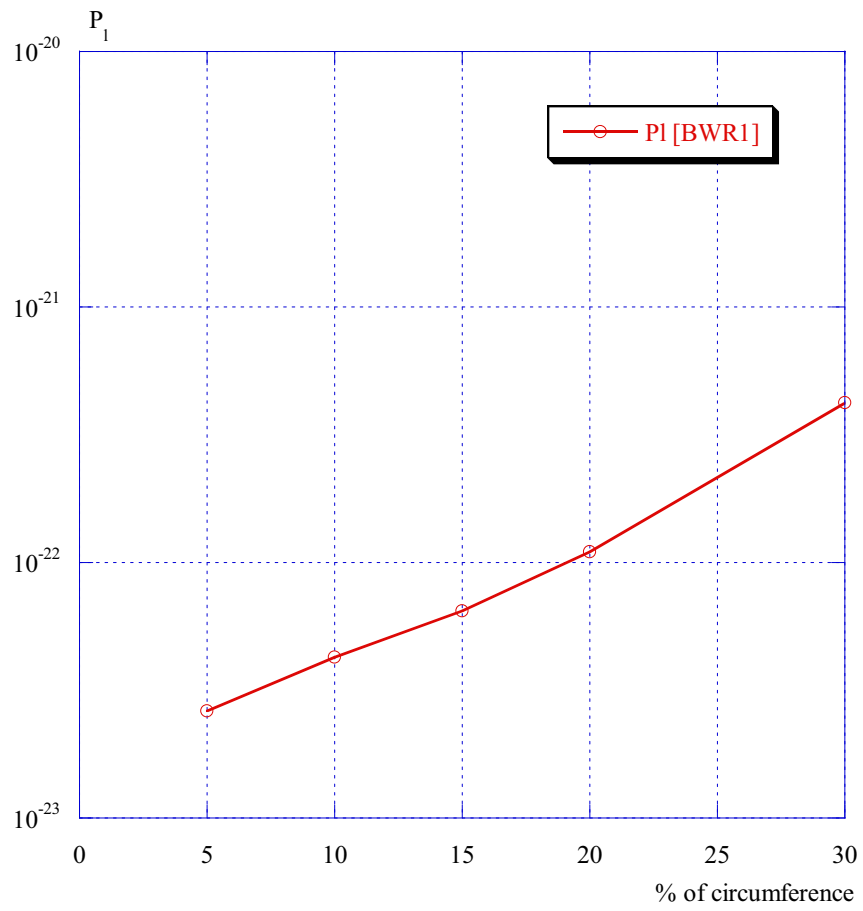
Figure 7.5.2. Probability of leakage as a function of crack length $\left(l/\left(2\cdot\pi\cdot R\right)\right)$ (BWR1).

7.5.3 Probability of leakage for the case PWR3
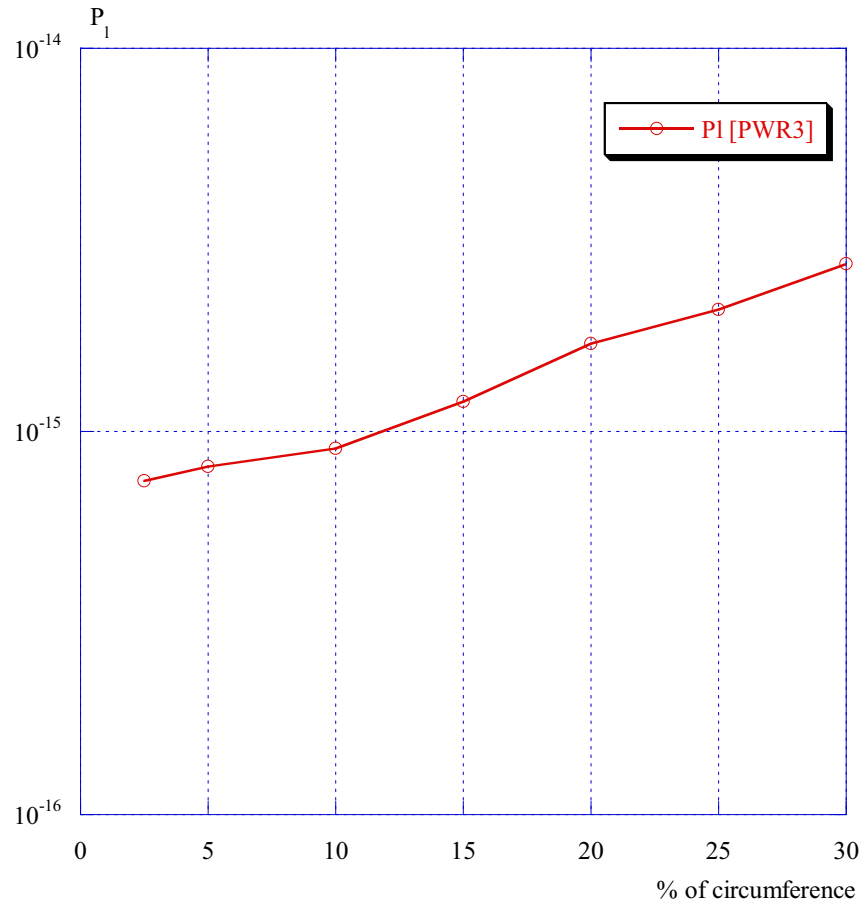
Figure 7.5.3. Probability of leakage as a function of crack length $\left(l/\left(2\cdot\pi\cdot R\right)\right)$ (PWR3).

7.5.4 Comparison between BWR1 and PWR3

The leakage probabilities, as given in figures 7.5.2-7.5.3, are very small compared to the baseline conditional fracture probabilities in section 7.4. However, the calculated leakage probabilities are reasonable, when compared with results from the NURBIM benchmark exercise [17] (using input data from NURBIM). The main difference is that the assumed primary stresses used in NURBIM are much larger than the stresses used in this study (which uses pipe stresses from the actual pipe welds considered).

A consistency check can be made by comparing the calculated leakage and conditional fracture probabilities for the two cases considered in this section. Such a comparison is presented in Fig. 7.5.4-7.5.5.
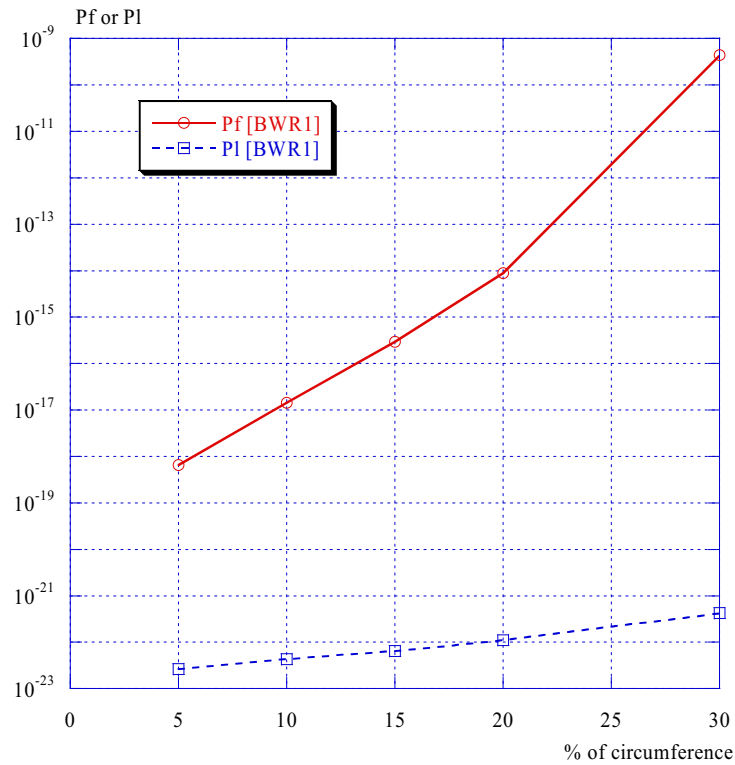
Figure 7.5.4.   Comparison between the calculated leakage and conditional fracture probabilities as a function of crack length $\left(l/(2 \cdot \pi \cdot R)\right)$ (BWR1).
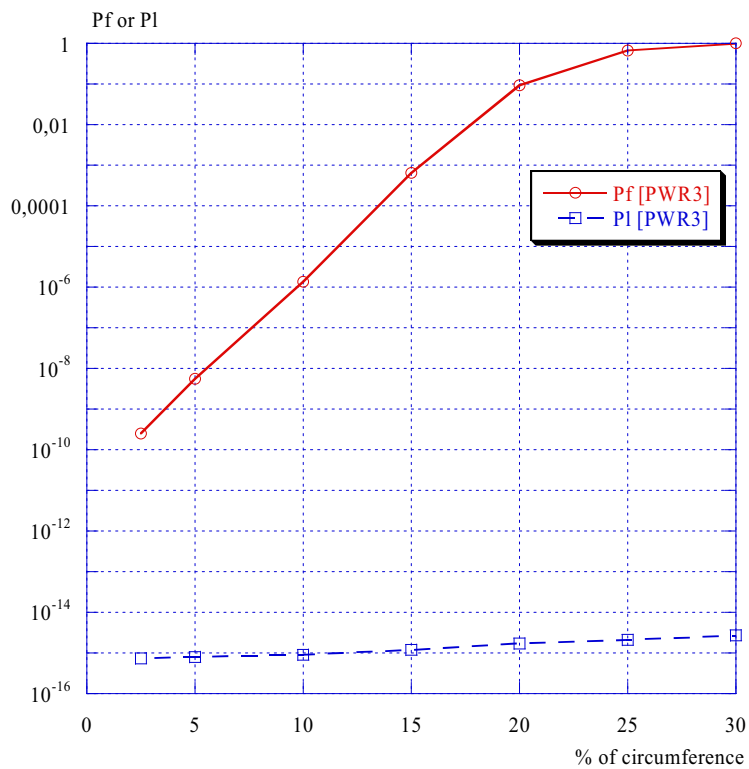
Figure 7.5.5.   Comparison between the calculated leakage and conditional fracture probabilities as a function of crack length $\left(l/(2 \cdot \pi \cdot R)\right)$ (PWR3).

49

The comparison between leakage and conditional fracture probabilities shows that (what is obvious by intuition) a large through-thickness crack is more dangerous than a large surface crack. This comparison gives a quantitative insight on how this difference gets larger for larger cracks.

7.6   Total probability of failure

The total probability of failure may be estimated using the product between the leakage probability and the conditional probability of fracture (given the existence of a leaking through-thickness crack).

$$P_{total} \approx P_l \cdot P_f \ . \tag{7.6.1}$$
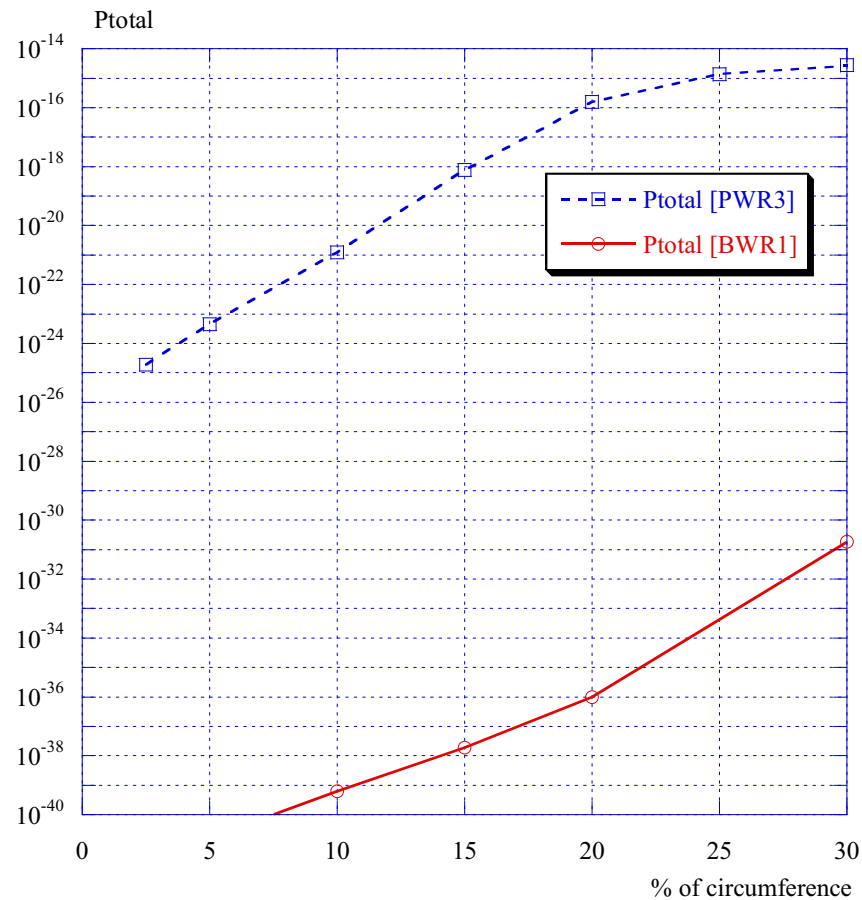
Figure 7.6.1.   The total probability of failure, comparison between the baseline cases BWR1 and PWR3.

The comparison above shows that the total probability of failure for the case PWR3 is much larger than for the case BWR1 (when given as a percentage of the circumference). If the total probability of failure is plotted as a function of leakage flow rate, then the difference would be smaller.

The small probability values are, in general, related to a small leak probability which is consistent with expectations since no active damage mechanism has been assumed. This also means that it can be very conservative to assume the existence of a leaking crack when there is a high confidence of the absence of any active damage mechanism.

8   SENSITIVITY STUDIES

An important aspect of every probabilistic study is to conduct an extensive sensitivity study. The study is performed by first defining a number of baseline cases (see section 7) and then varying a number of parameters one by one, keeping all other parameters fixed at their baseline values. The baseline cases correspond to the "best estimate" values of all parameters, reflecting actual plant conditions for each case.

As shown in section 7.4, the baseline case BWR1 has much lower conditional fracture probabilities for large cracks (given as a percentage of the circumference) than the other baseline cases. If the conditional probability of fracture is plotted as a function of leakage flow rate, then BWR1 has much larger conditional fracture probabilities than most of the other baseline cases. Also shown in section 7.4, the baseline case PWR3 has much higher conditional fracture probabilities for all crack lengths (given as a percentage of the circumference) than most of the other baseline cases. If the conditional probability of fracture is plotted as a function of leakage flow rate, then PWR3 has much smaller conditional fracture probabilities than most of the other baseline cases. Because of this contradictory behavior, BWR1 and PWR3 were chosen for the sensitivity study.

In the sensitivity study, the following cases were investigated (only the conditional probability of fracture, given the existence of a leaking through-wall crack was considered):
- Fracture toughness – Varying the mean value
- Fracture toughness – Varying the standard deviation
- Yield strength – Varying the mean value
- Yield strength – Varying the standard deviation
- Crack length – Varying the standard deviation
- Primary membrane stress – Varying the standard deviation
- Primary global bending stress – Varying the mean value
- Comparing the cases with/without weld residual stresses
- Comparing the cases with/without off-centred cracks
- Leak rate calculation using data for fatigue or stress corrosion cracking

Also a more formal sensitivity analysis is presented in sections 8.12-8.13. This analysis tries to answer the following questions:
- What parameter contributes the most to the calculated conditional fracture probability?
- What parameter change has the most influence on the calculated conditional fracture probability?

51

8.1   Comparison between BWR1 and PWR3

As given above, BWR1 and PWR3 were chosen for the sensitivity study. They represent the smallest and largest pipe sections among the different baseline cases. BWR1 has an external diameter of 114 mm and a wall thickness of 8 mm, PWR3 has an external diameter of 872 mm and a wall thickness of 65 mm (see the comparison in Fig. 8.1.1).
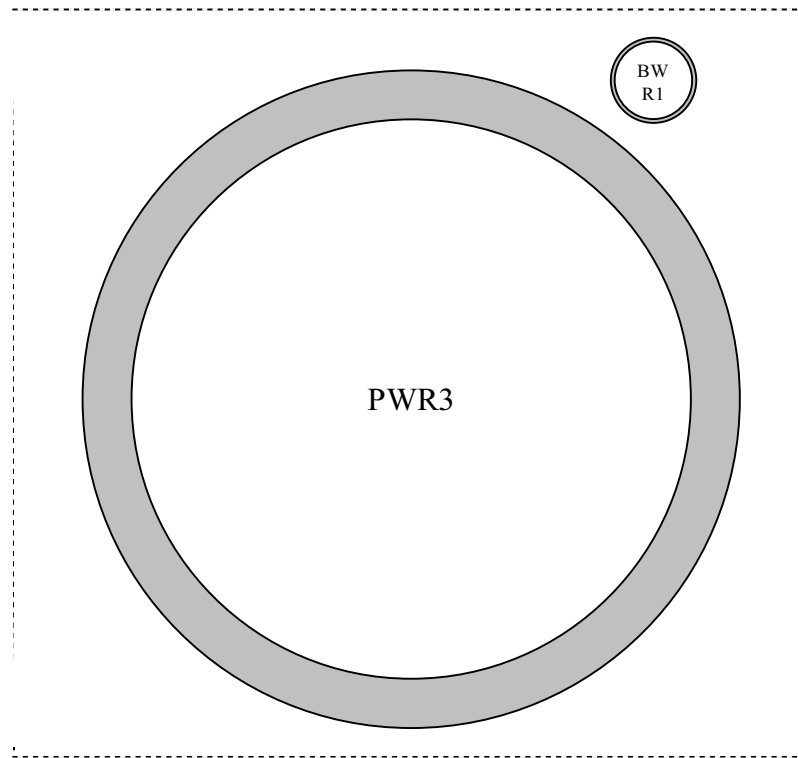
Figure 8.1.1. Relative pipe sizes for two cases considered within the sensitivity study.

Below, the baseline results for the conditional probability of fracture (given the existence of a leaking through-thickness crack) are given as a comparison between BWR1 and PWR3 (details is presented in section 7). The results are plotted both as a function of crack length and as a function of leakage flow rate. This comparison shows the difference between the two cases and emphasize that the conditional probability of fracture for BWR1 is much larger than the conditional probability of fracture for PWR3 (using an equivalent leakage flow rate).
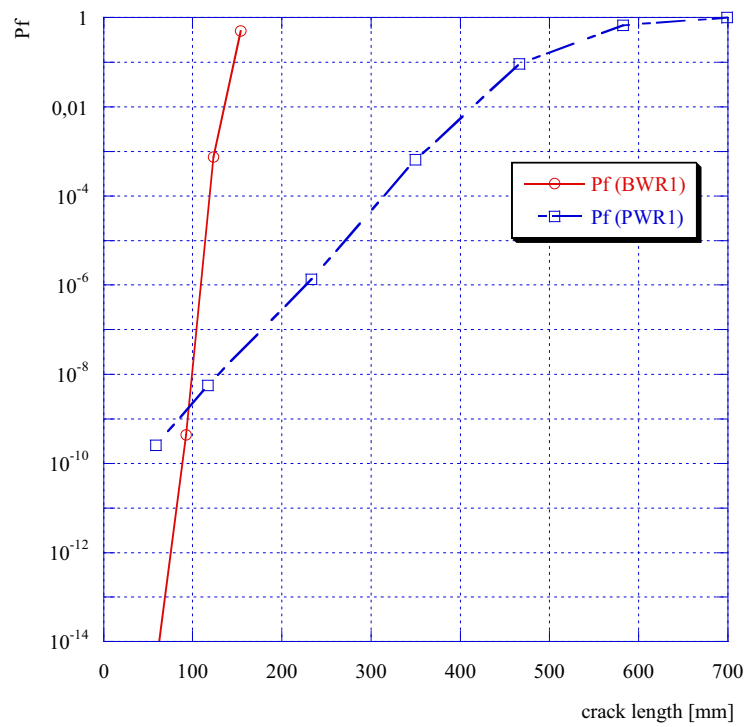
Figure 8.1.2. Conditional probability of fracture as a function of crack length (comparison between BWR1 and PWR3).
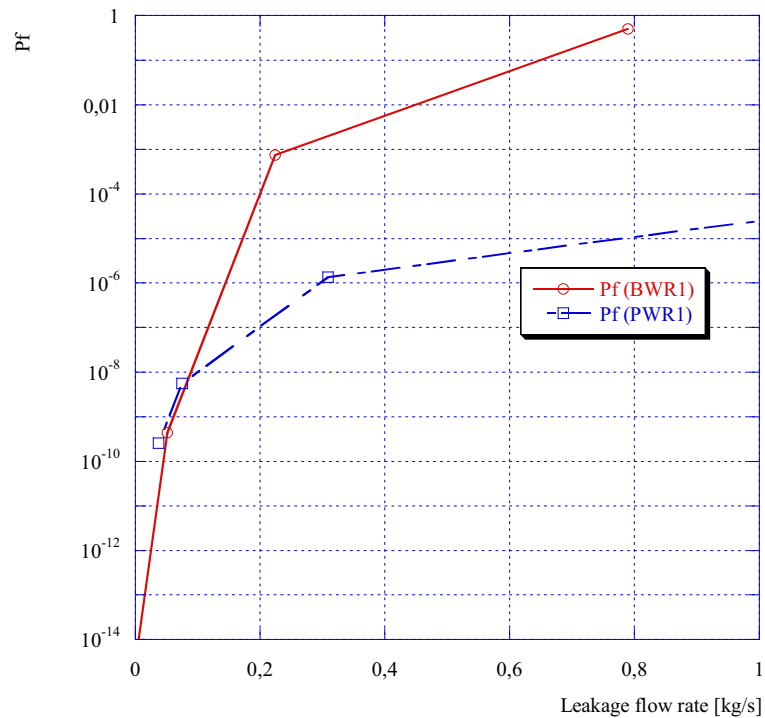
Figure 8.1.3. Conditional probability of fracture as a function of leakage flow rate (comparison between BWR1 and PWR3).

8.2   Sensitivity study – Fracture toughness – Mean value

The mean values of fracture toughness were taken from data for the actual pipe welds considered. For BWR1 and PWR3 (austenitic stainless steel welds) a K_{Ic}-value of 182 MPa$\sqrt{m}$ was used in the analysis. The sensitivity study in this section shows how the resulting fracture probability changes, if different assumptions regarding the fracture toughness data are used.
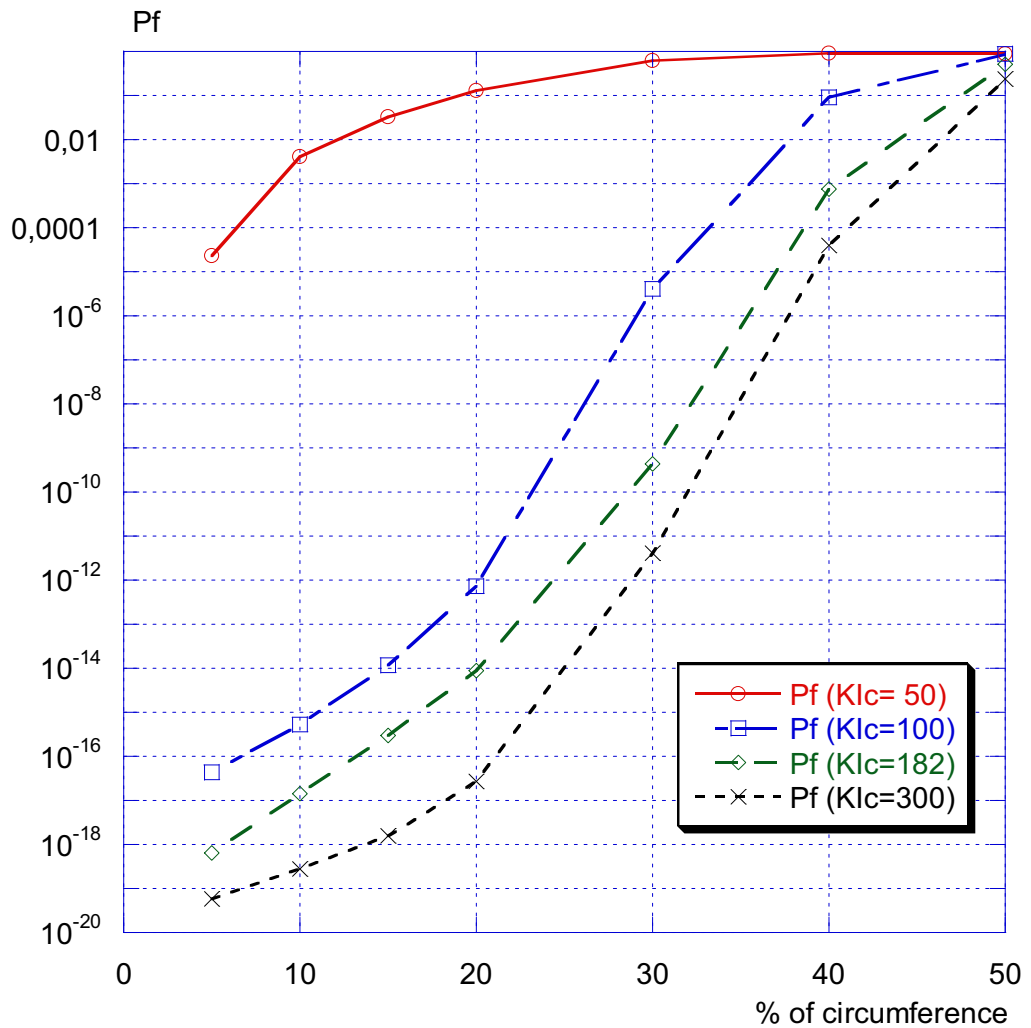
Figure 8.2.1.   Conditional probability of fracture as a function of crack length $\left(l / \left(2 \cdot \pi \cdot R \right) \right)$ (BWR1). Sensitivity analysis using different assumptions regarding the mean value of the fracture toughness.
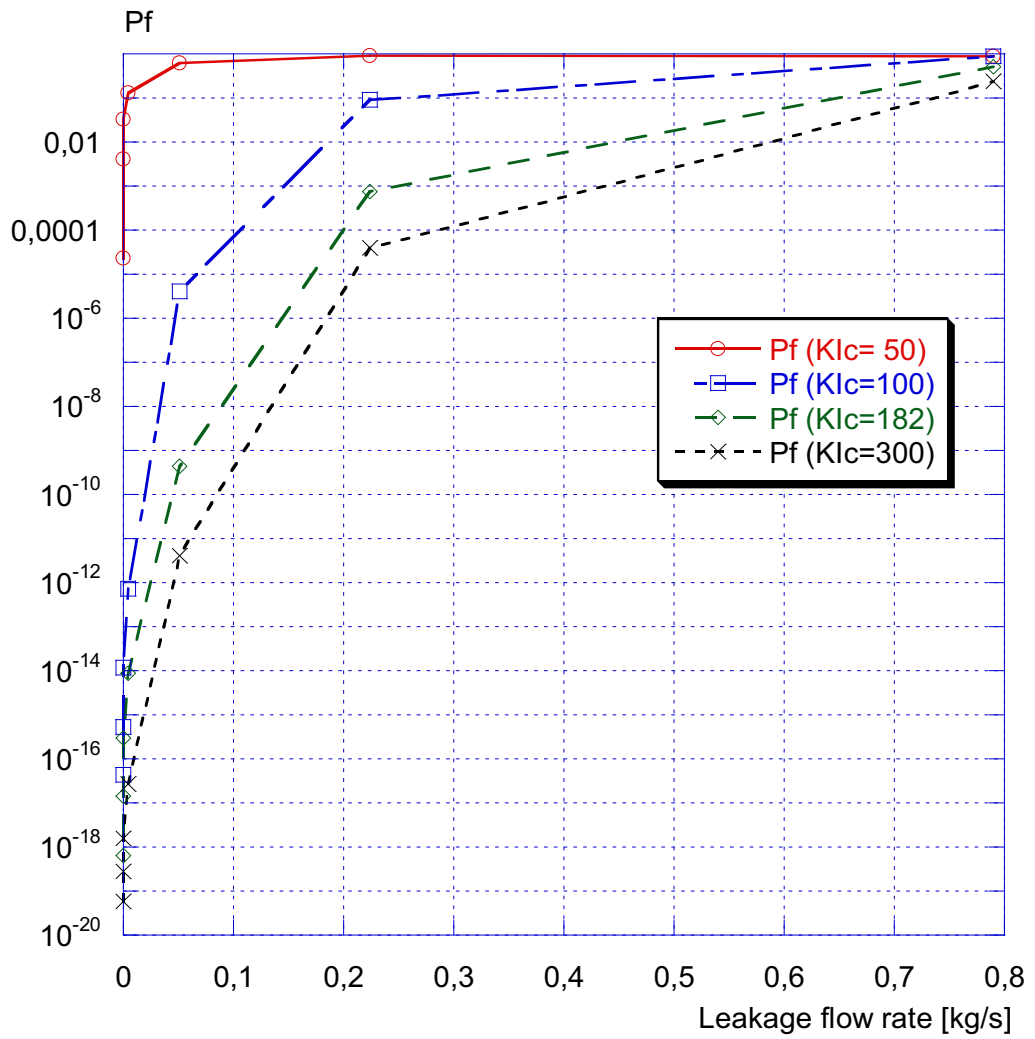
Figure 8.2.2. Conditional probability of fracture as a function of leakage flow rate (BWR1). Sensitivity analysis using different assumptions regarding the mean value of the fracture toughness.
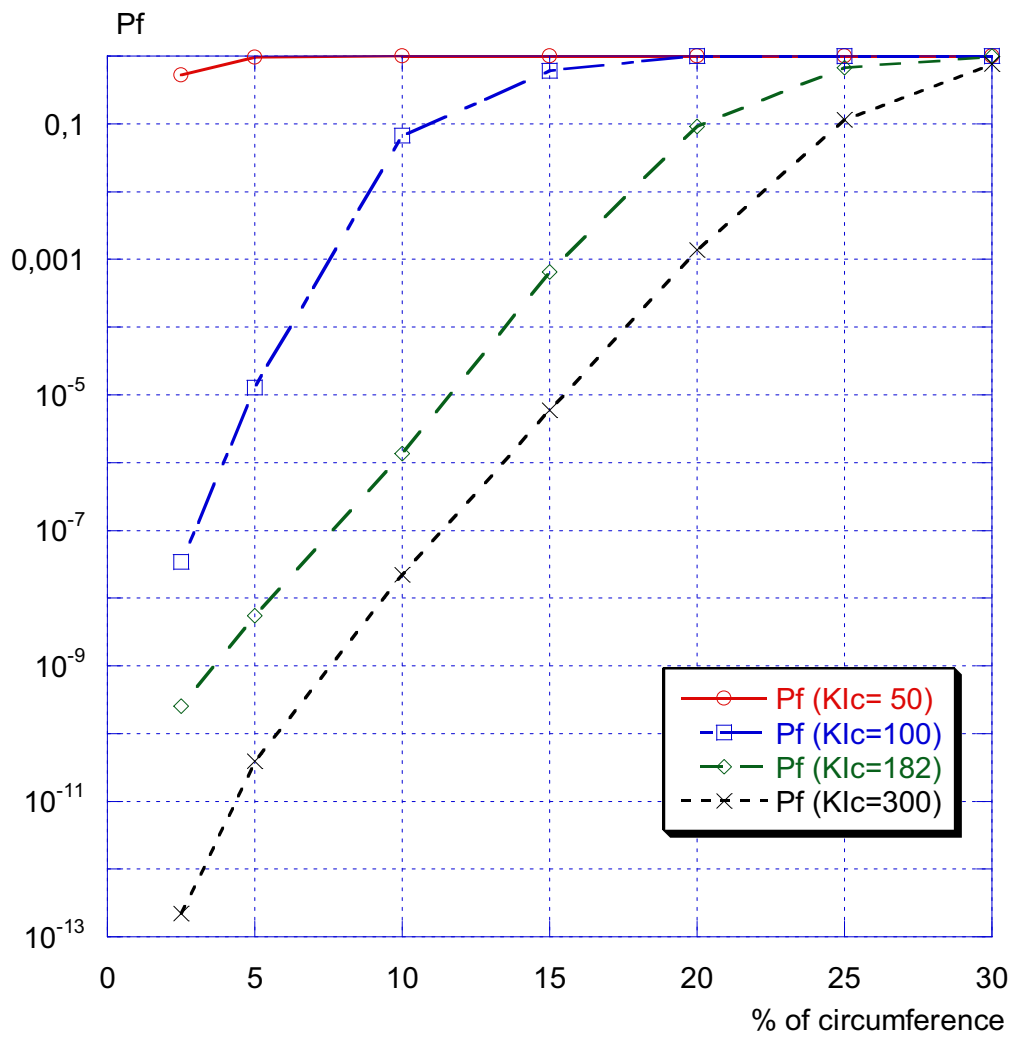
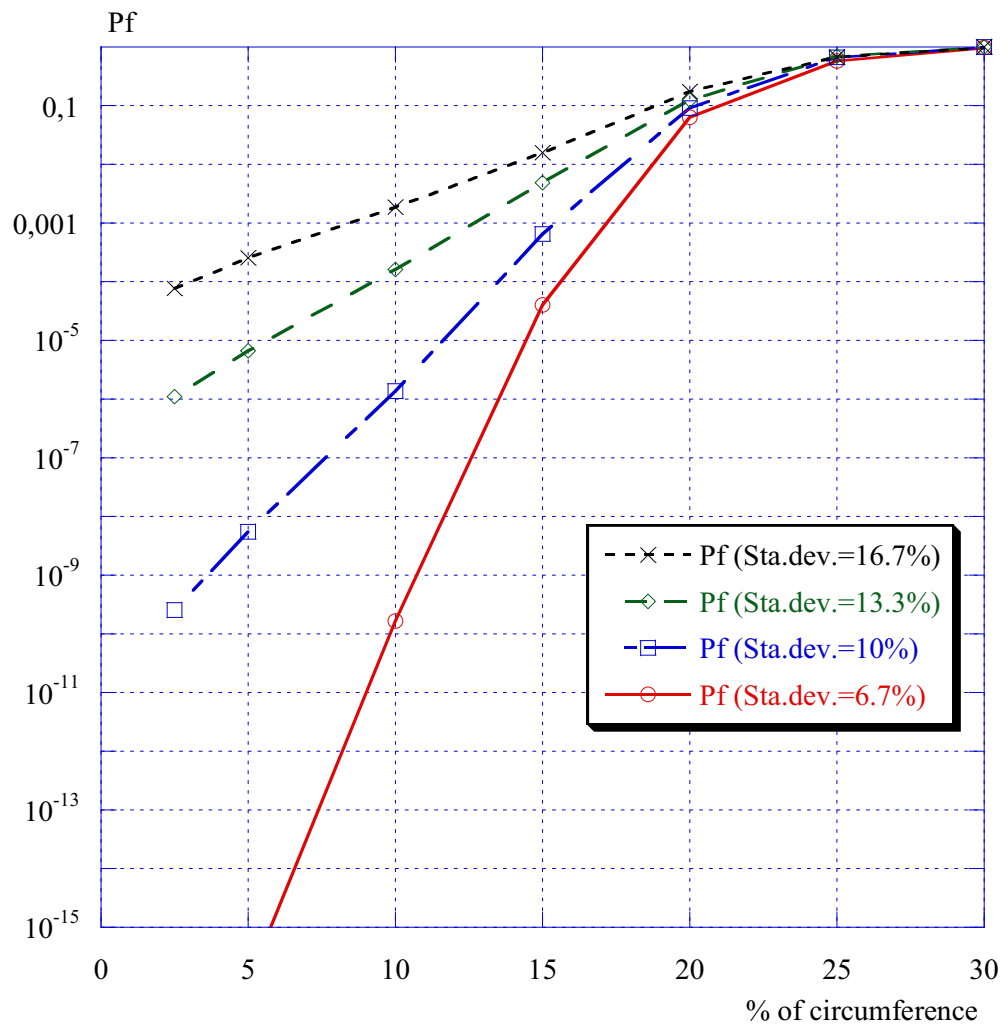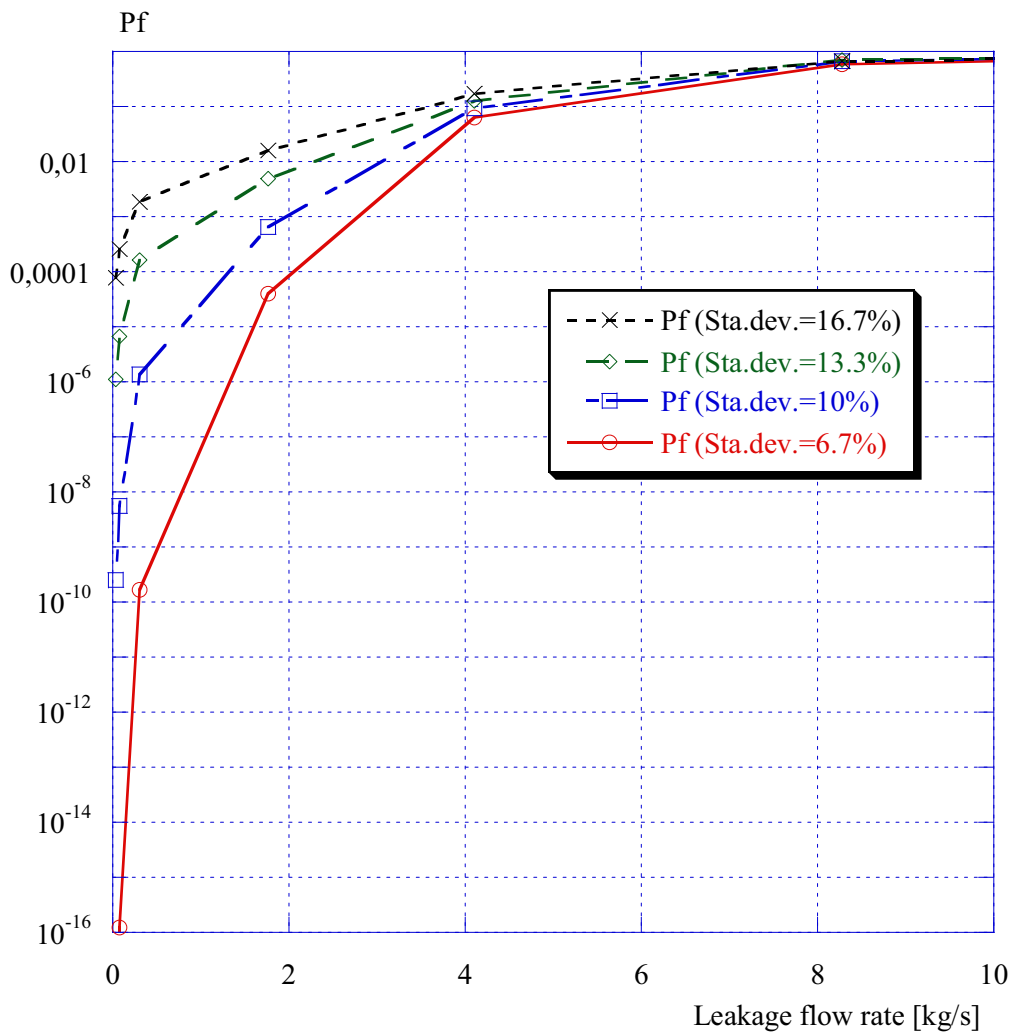Figure 8.2.3. Conditional probability of fracture as a function of crack length $\left(l/\left(2\cdot \pi \cdot R \right) \right)$ (PWR3). Sensitivity analysis using different assumptions regarding the mean value of the fracture toughness.
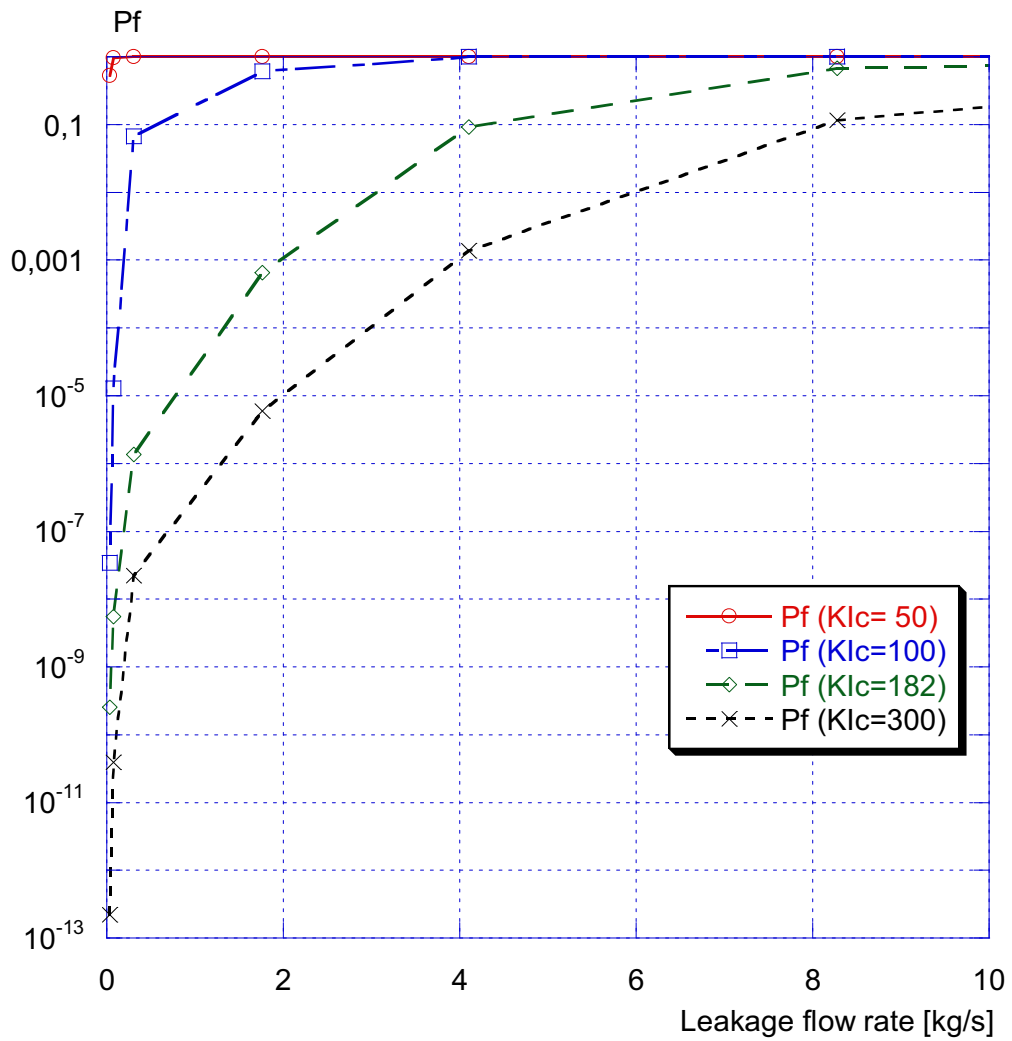
Figure 8.2.4.   Conditional probability of fracture as a function of leakage flow rate (PWR3). Sensitivity analysis using different assumptions regarding the mean value of the fracture toughness.

As shown above, the case PWR3 is more sensitive to the chosen mean value of fracture toughness (than the case BWR1). This is further investigated in section 8.12, where one can see which parameter that contributes the most to the calculated fracture probability.

8.3 Sensitivity study – Fracture toughness – Standard deviation

Following the recommendations in [7], when no experimental data is available on the variation of fracture toughness, one should apply a standard deviation between 5-10% of the mean value (in the wholly ductile temperature region). For BWR1 and PWR3 (austenitic stainless steel welds) a standard deviation value equivalent to 7.5% of the mean value was used in the analysis. The sensitivity study in this section shows how the resulting fracture probability changes, if different assumptions regarding the standard deviation are used.
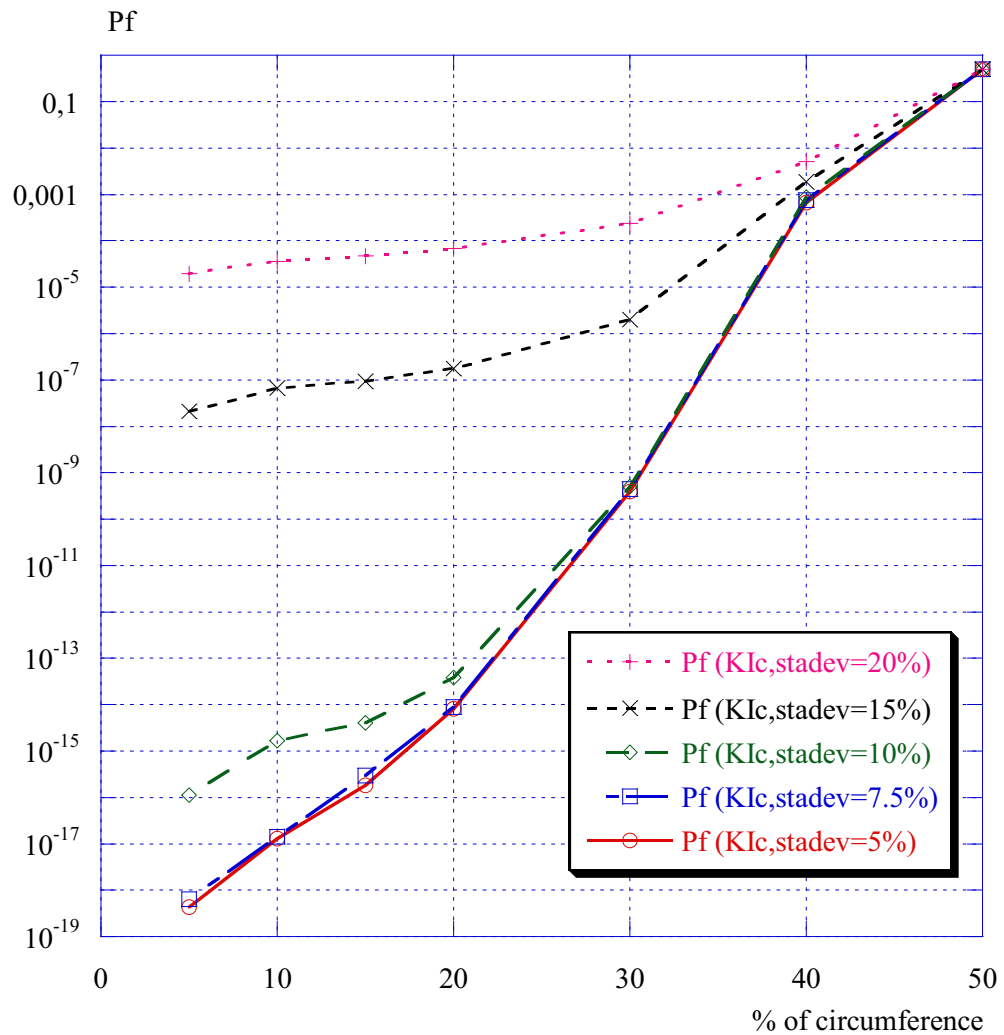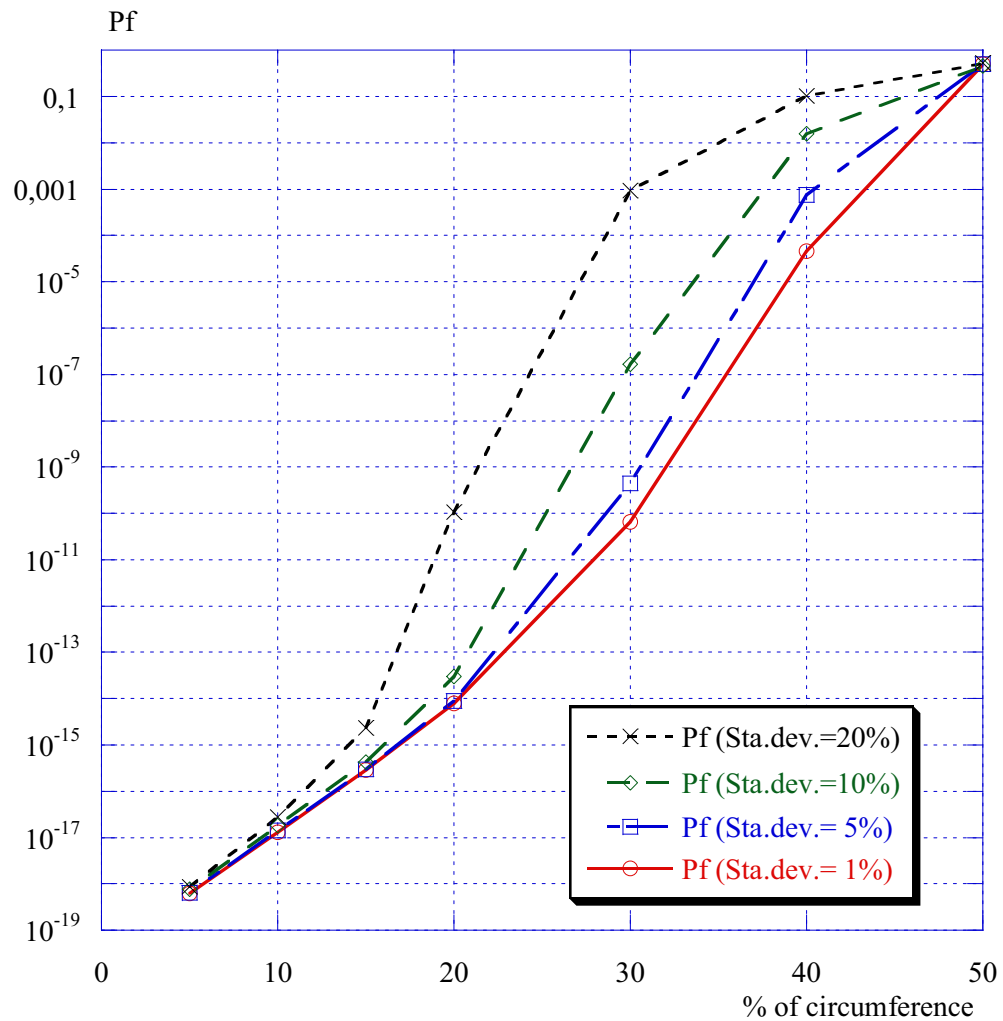

Figure 8.3.1. Conditional probability of fracture as a function of crack length $\left(l / \left(2 \cdot \pi \cdot R \right) \right)$ (BWR1). Sensitivity analysis using different assumptions regarding the standard deviation of the fracture toughness.
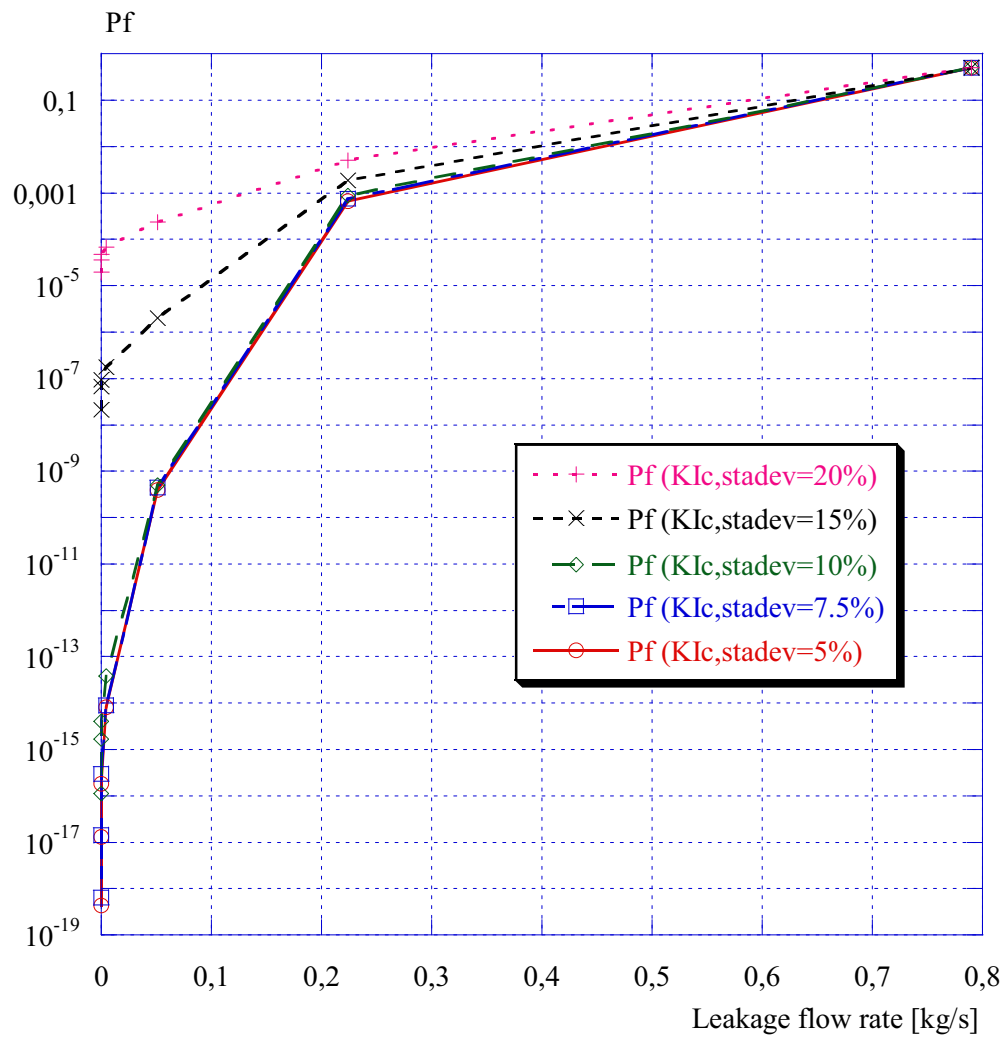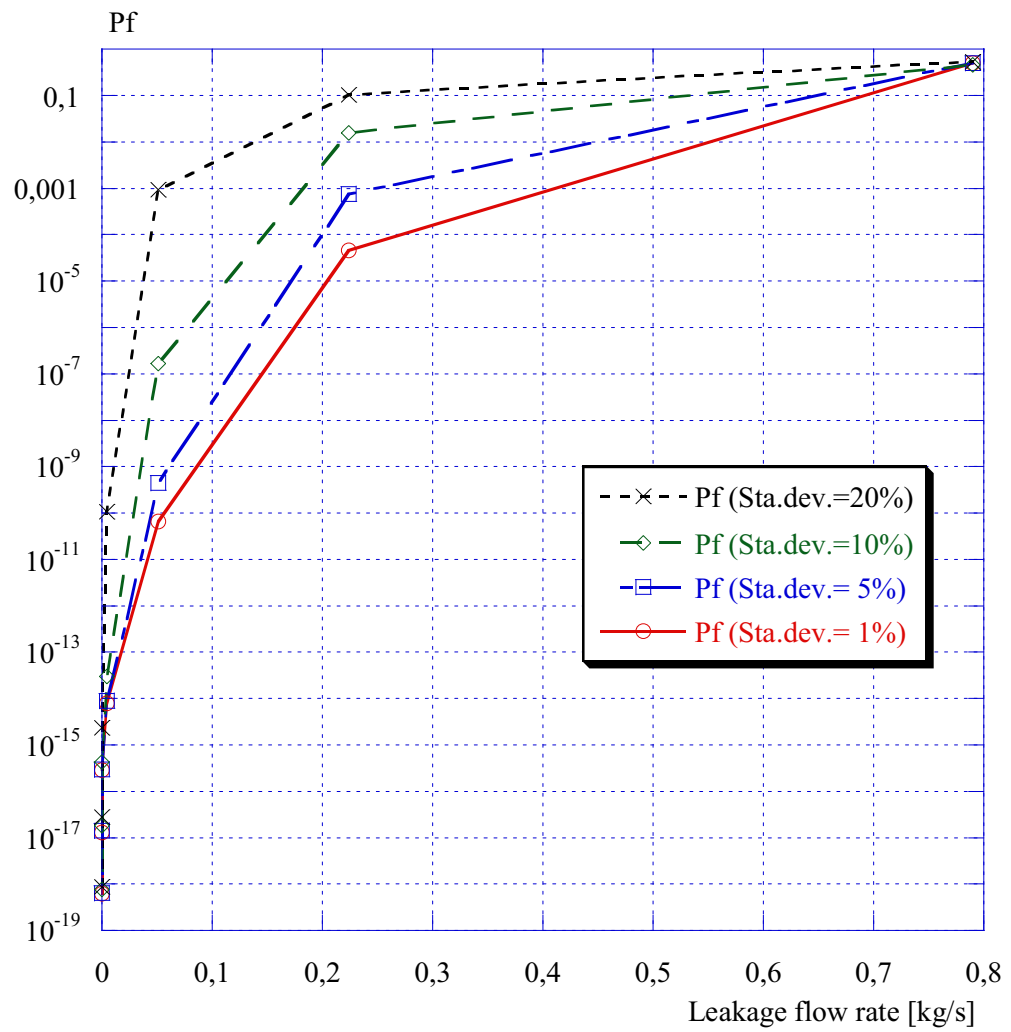
Figure 8.3.2. Conditional probability of fracture as a function of leakage flow rate (BWR1). Sensitivity analysis using different assumptions regarding the standard deviation of the fracture toughness.
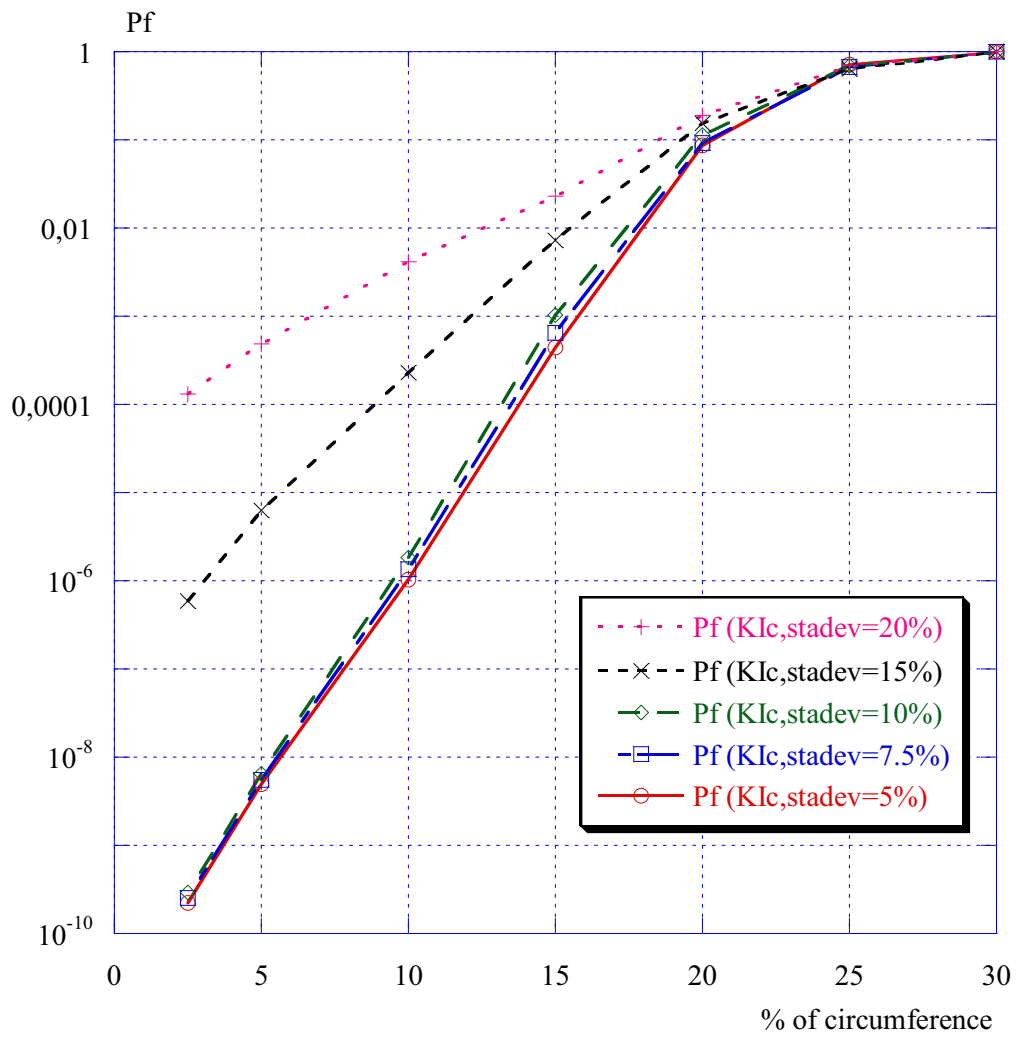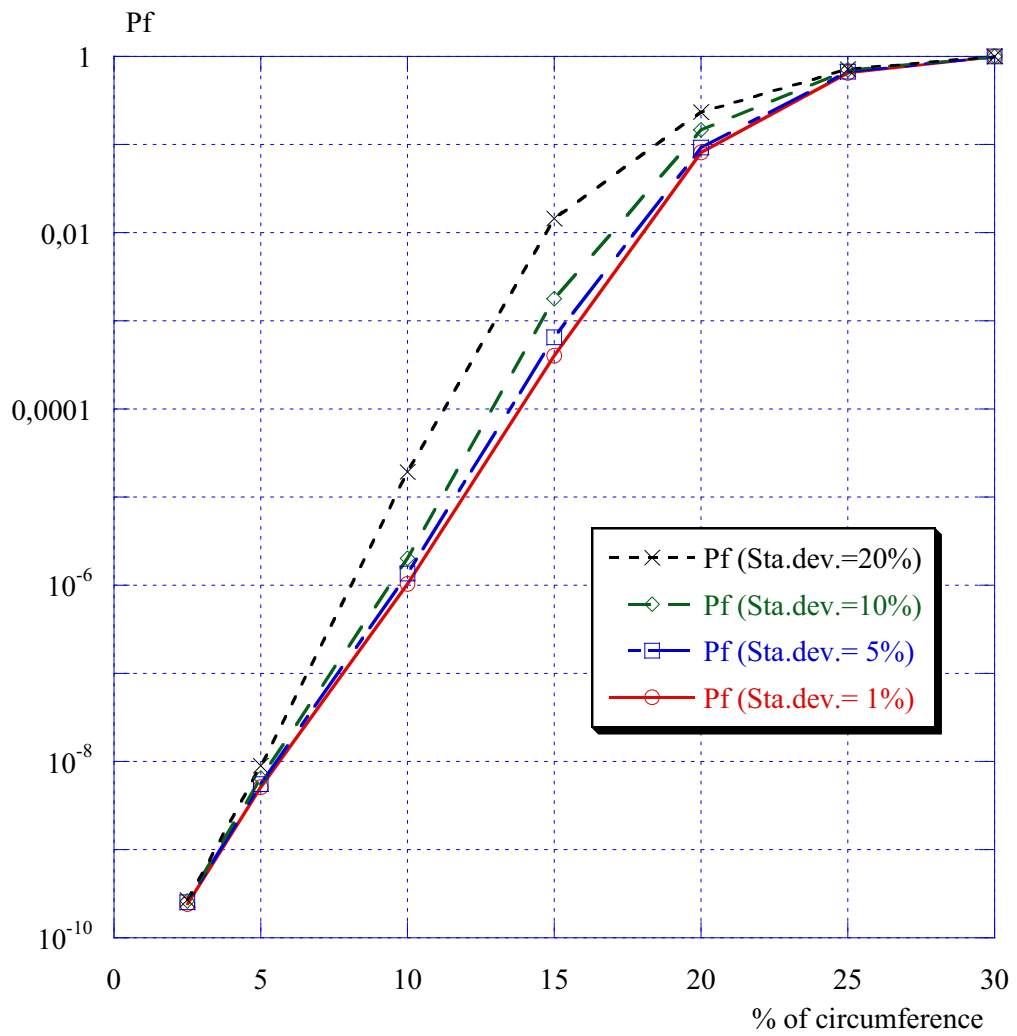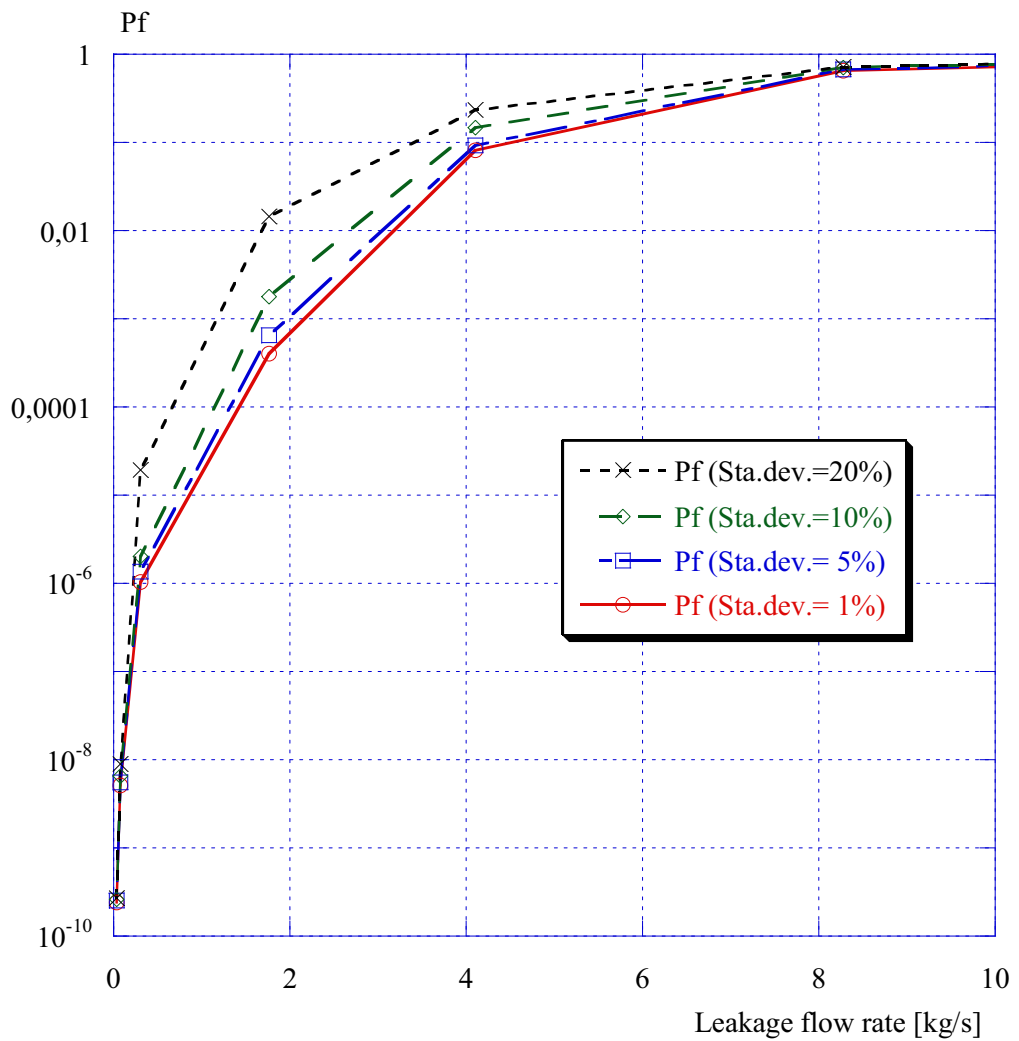
Figure 8.3.3. Conditional probability of fracture as a function of crack length $\left(l/\left(2\cdot\pi\cdot R\right)\right)$ (PWR3). Sensitivity analysis using different assumptions regarding the standard deviation of the fracture toughness.
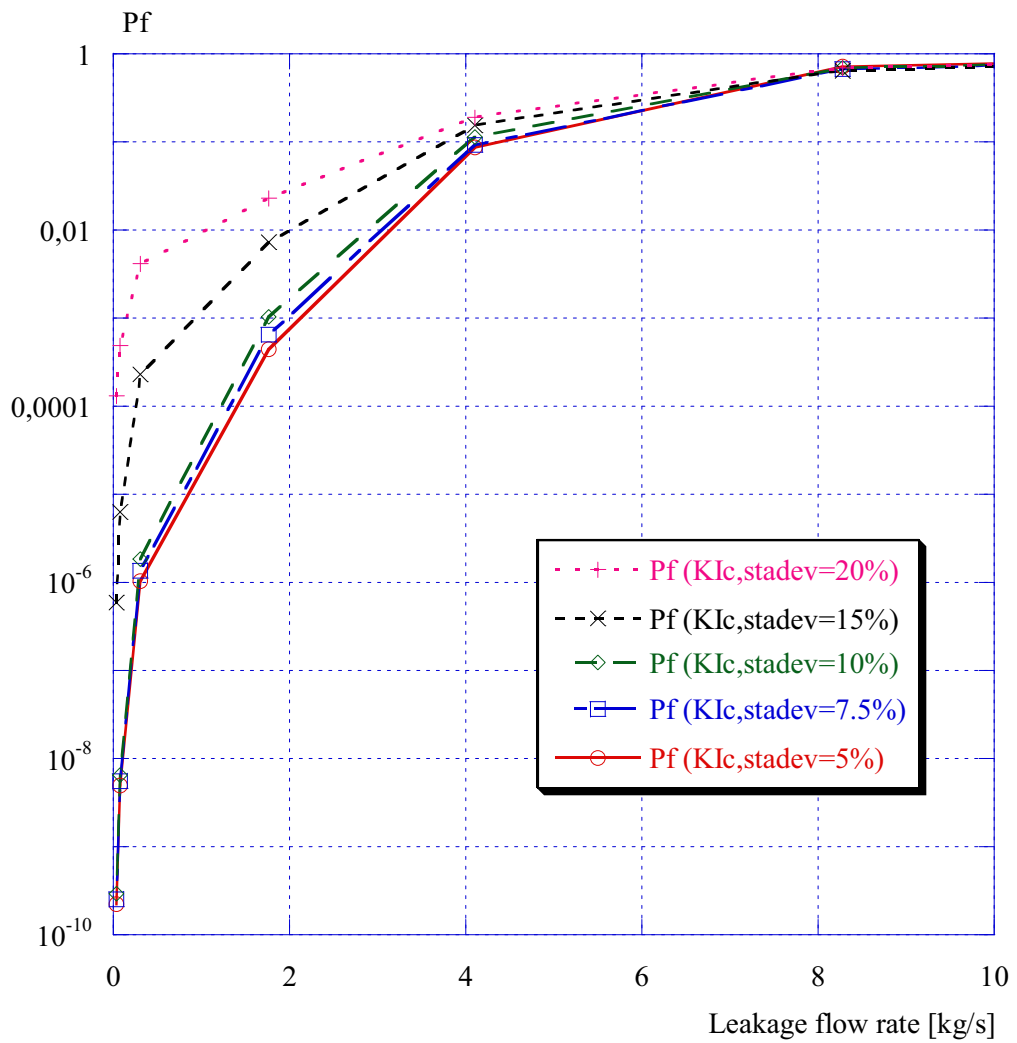
Figure 8.3.4. Conditional probability of fracture as a function of leakage flow rate (PWR3). Sensitivity analysis using different assumptions regarding the standard deviation of the fracture toughness.

As shown above, the assumed value of standard deviation is of minor importance for these cases (if between 5-10% of the mean value of fracture toughness).

8.4 Sensitivity study – Yield strength – Mean value

The mean values of the yield strength were taken using realistic data for the actual pipe welds considered. For BWR1 and PWR3 (austenitic stainless steel welds) a σ_y-value of 150 MPa was used in the analysis. The sensitivity study in this section shows how the resulting fracture probability changes, if different assumptions regarding the yield strength data are used.
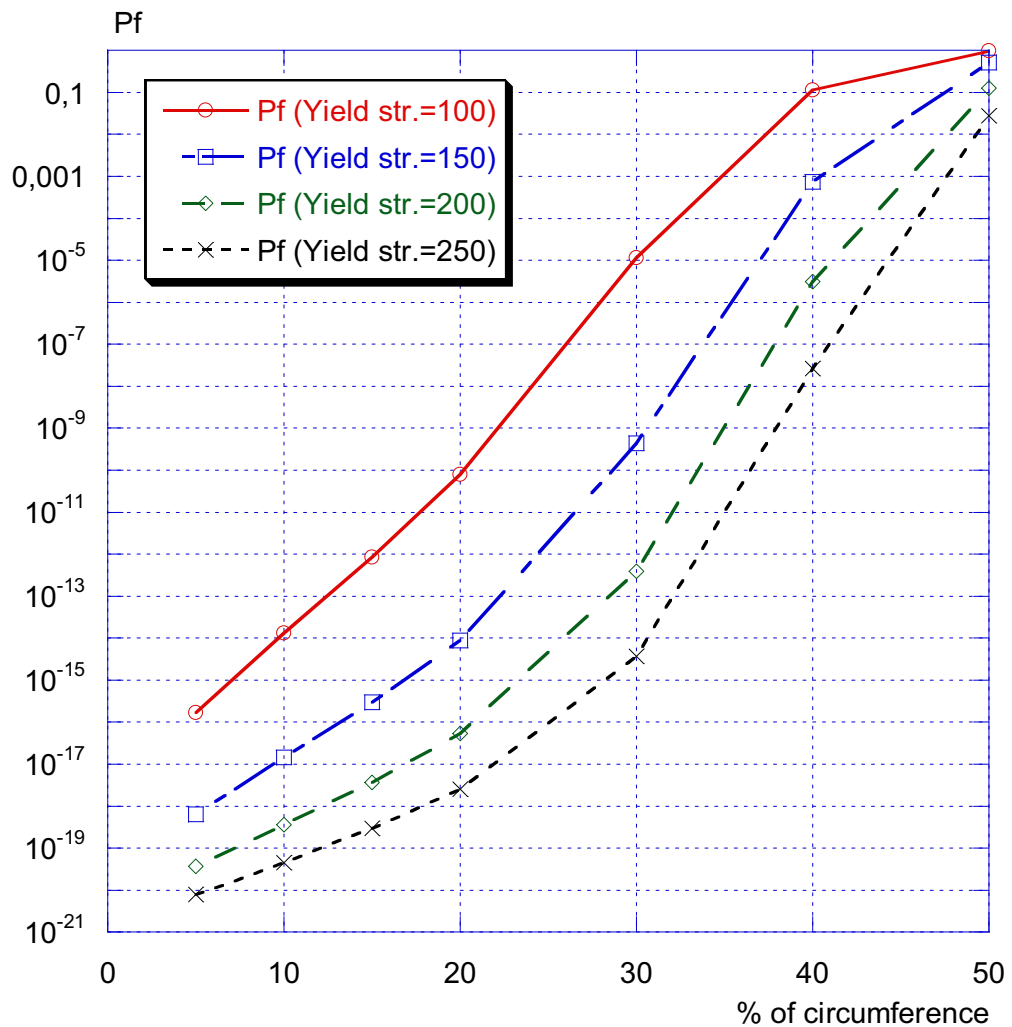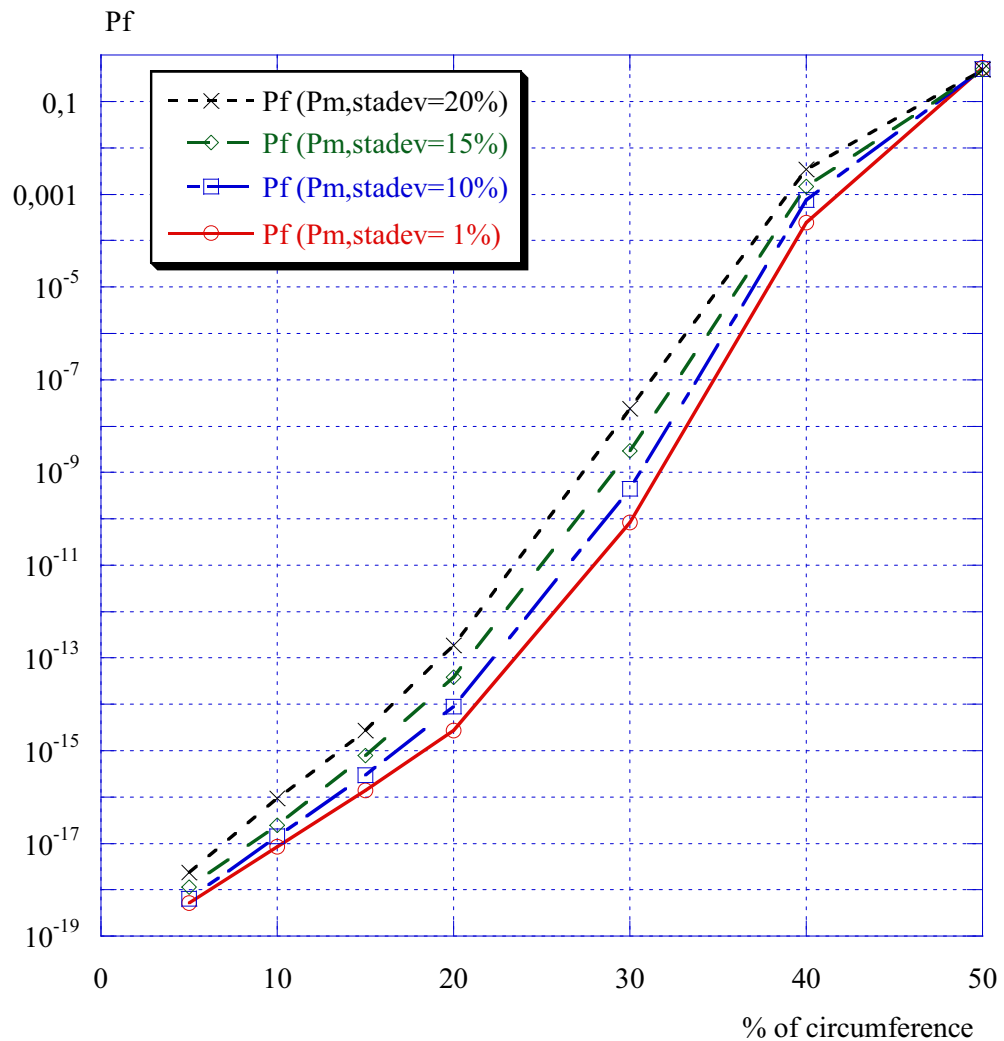

Figure 8.4.1. Conditional probability of fracture as a function of crack length $\left(l/\left(2\cdot\pi\cdot R\right)\right)$ (BWR1). Sensitivity analysis using different assumptions regarding the mean value of the yield strength.
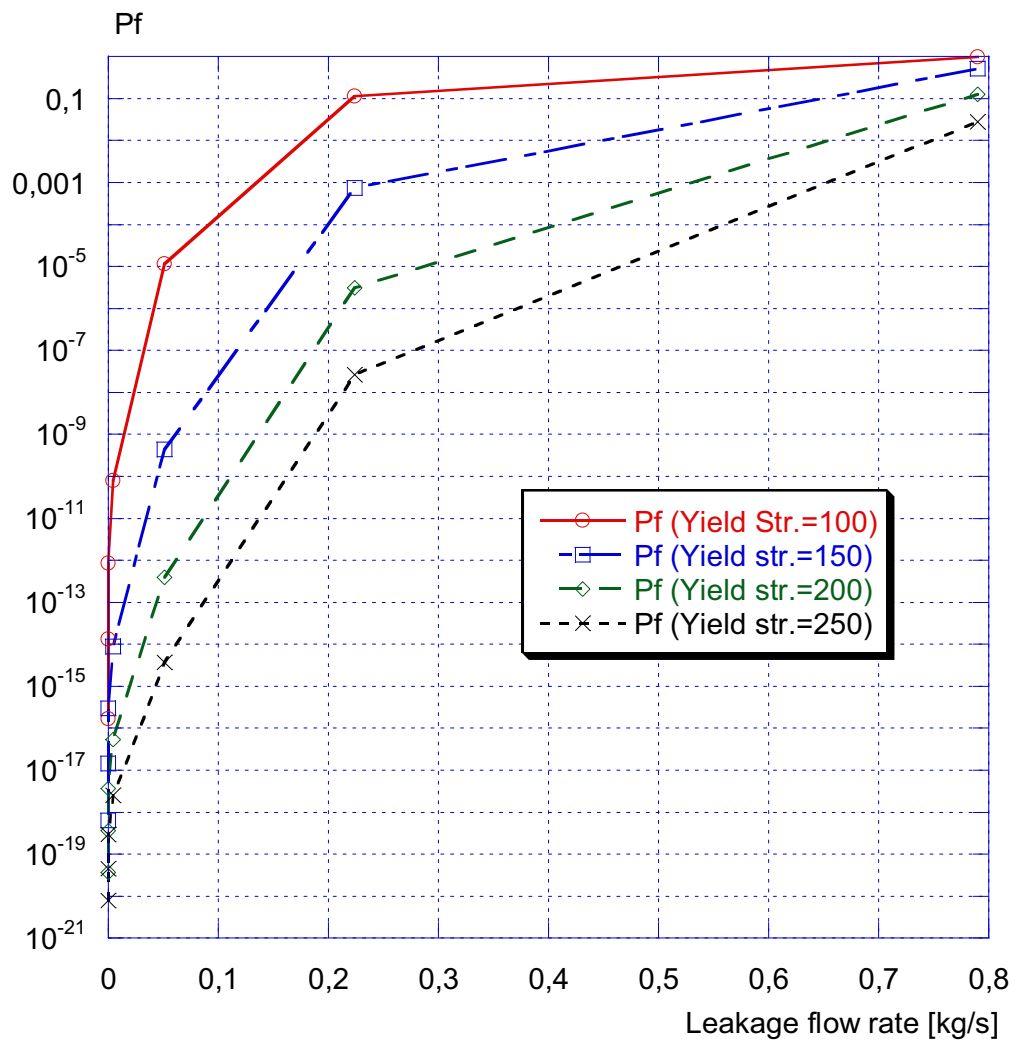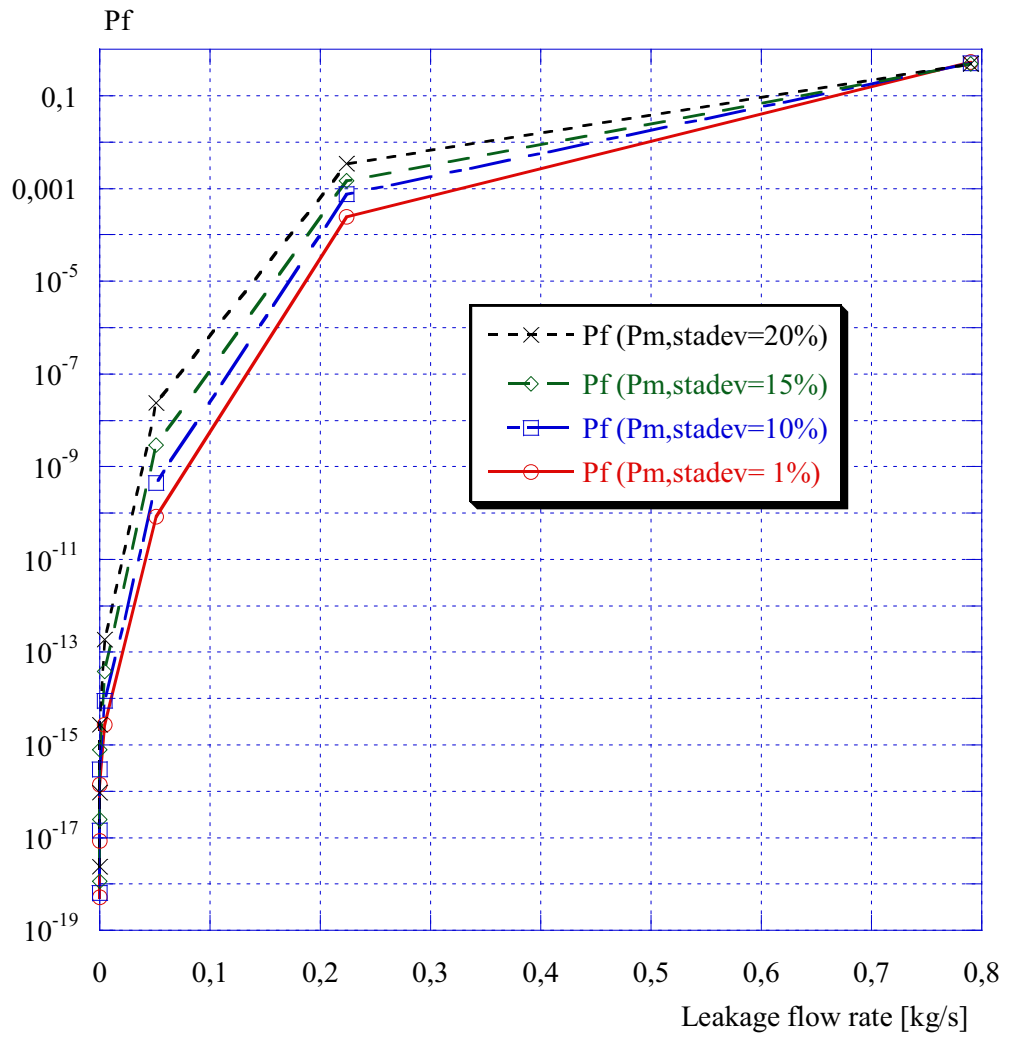
Figure 8.4.2.   Conditional probability of fracture as a function of leakage flow rate (BWR1). Sensitivity analysis using different assumptions regarding the mean value of the yield strength.
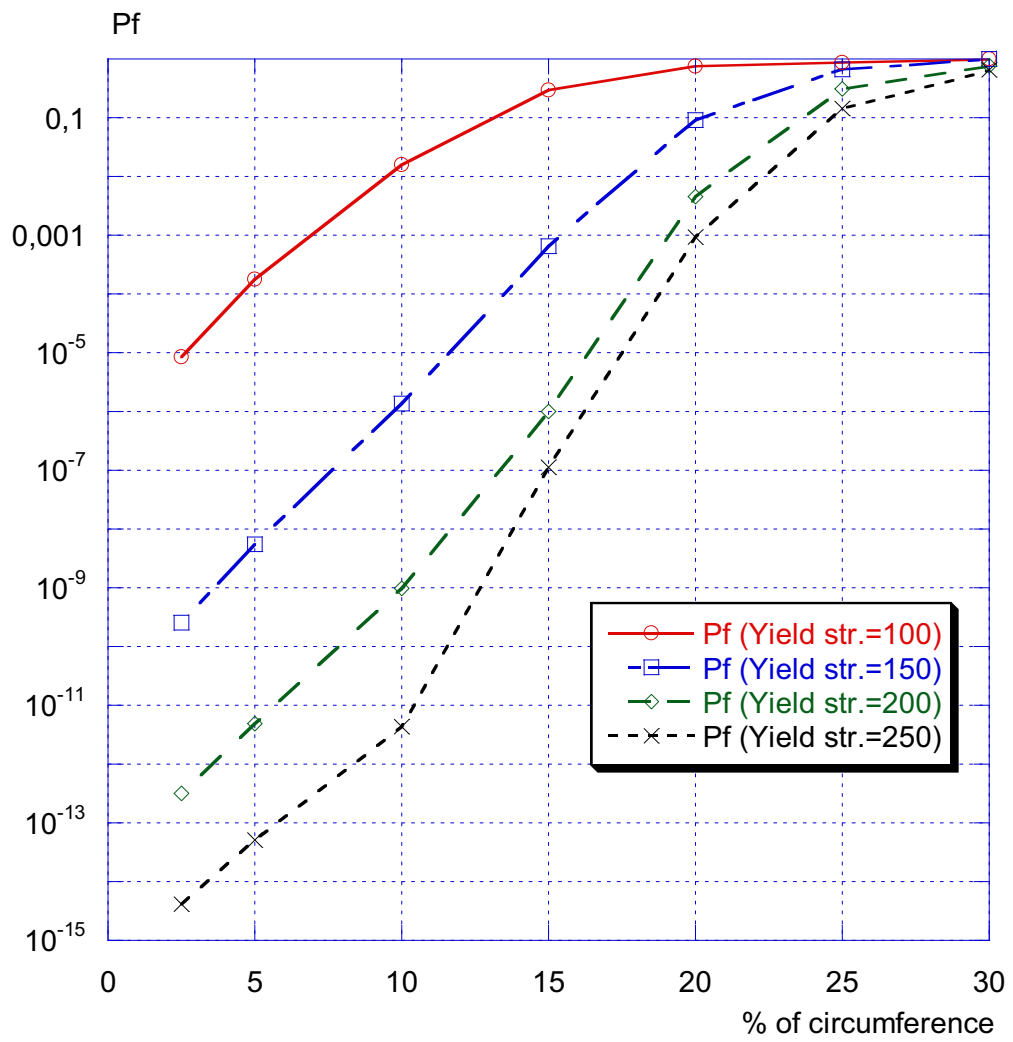
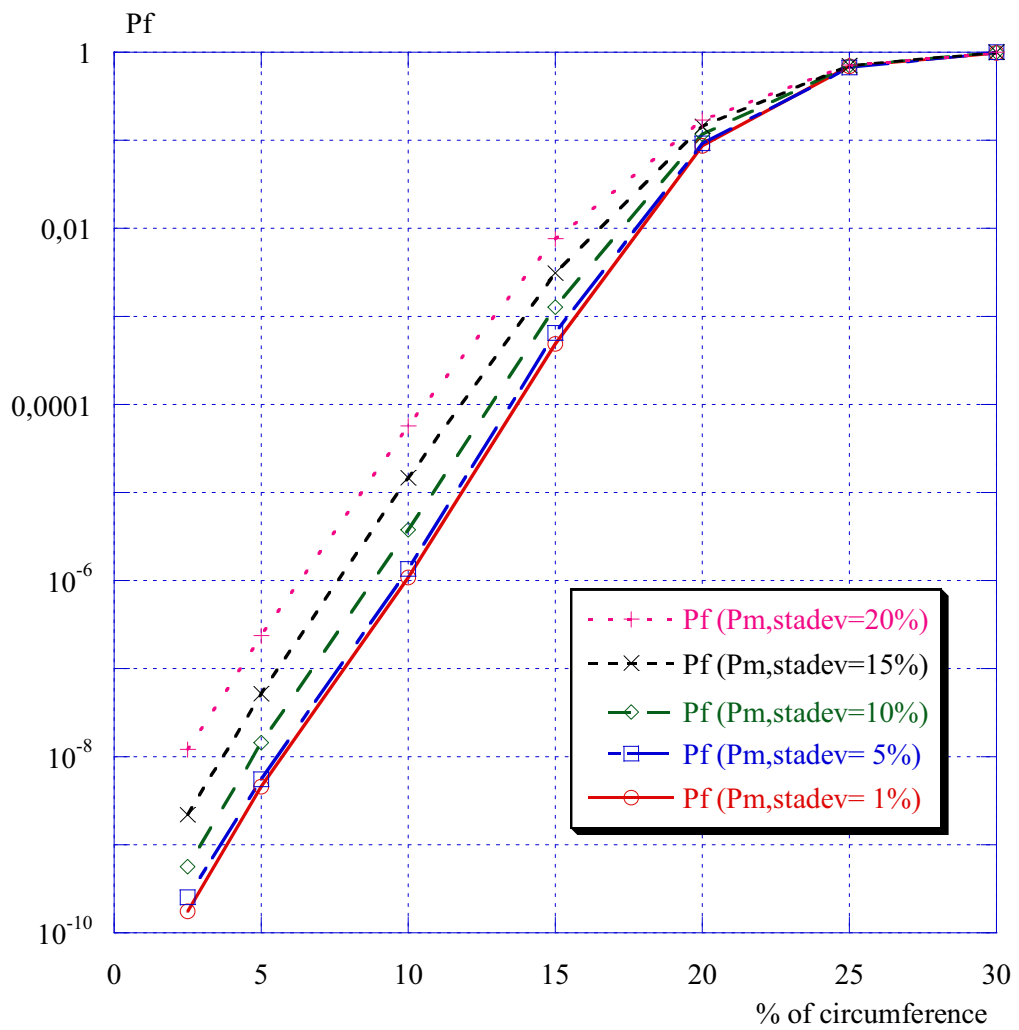Figure 8.4.3. Conditional probability of fracture as a function of crack length $\left(l/\left(2\cdot\pi\cdot R\right)\right)$ (PWR3). Sensitivity analysis using different assumptions regarding the mean value of the yield strength.
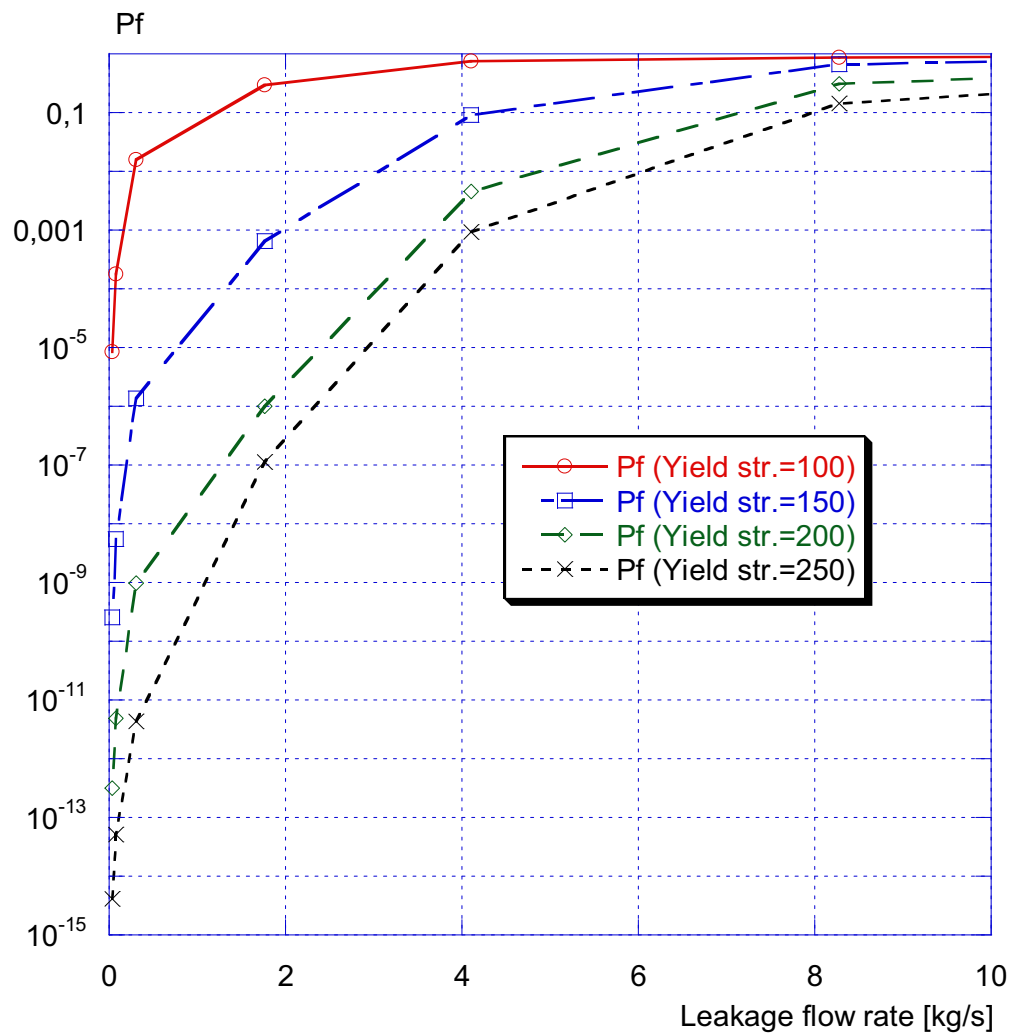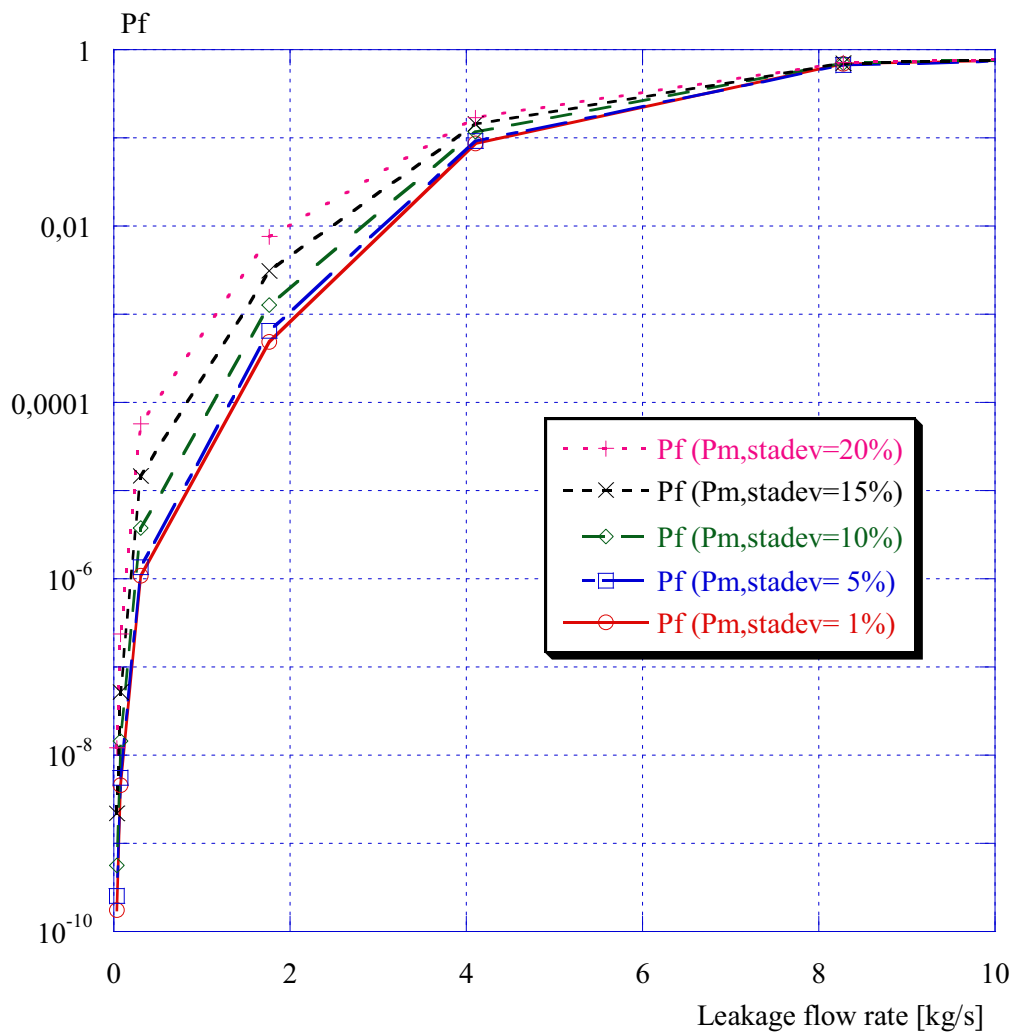
Figure 8.4.4. Conditional probability of fracture as a function of leakage flow rate (PWR3). Sensitivity analysis using different assumptions regarding the mean value of the yield strength.

As shown above, both cases are equally sensitive to the chosen mean value of yield strength. This is further investigated in section 8.12, where one can see which parameter that contributes the most to the calculated fracture probability.

8.5 Sensitivity study – Yield strength – Standard deviation

Following the recommendations in [7], one should apply a standard deviation somewhere between 3-20% of the mean value (dependent on the quality of the data). For BWR1 and PWR3 (austenitic stainless steel welds) a standard deviation value equivalent to 10% of the mean value was used in the analysis. The sensitivity study in this section shows how the resulting fracture probability changes, if different assumptions regarding the standard deviation are used.
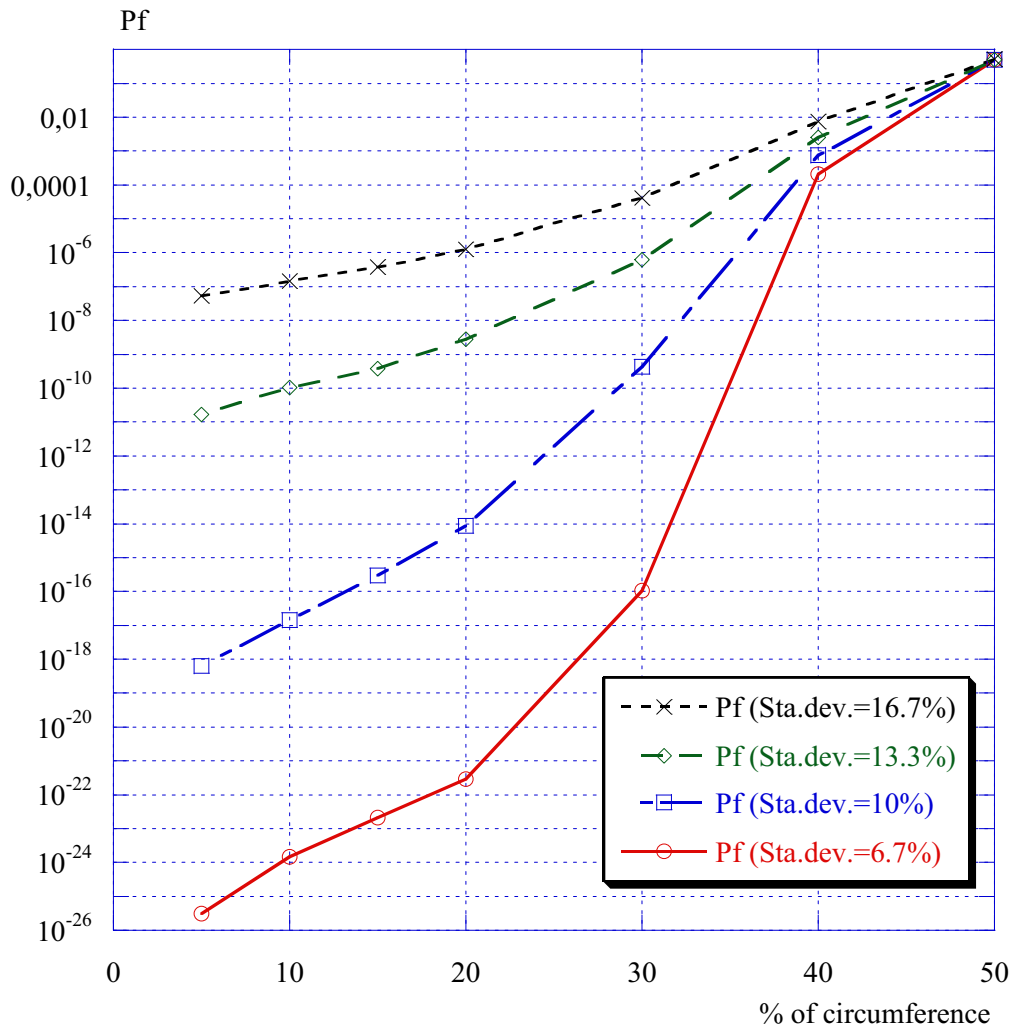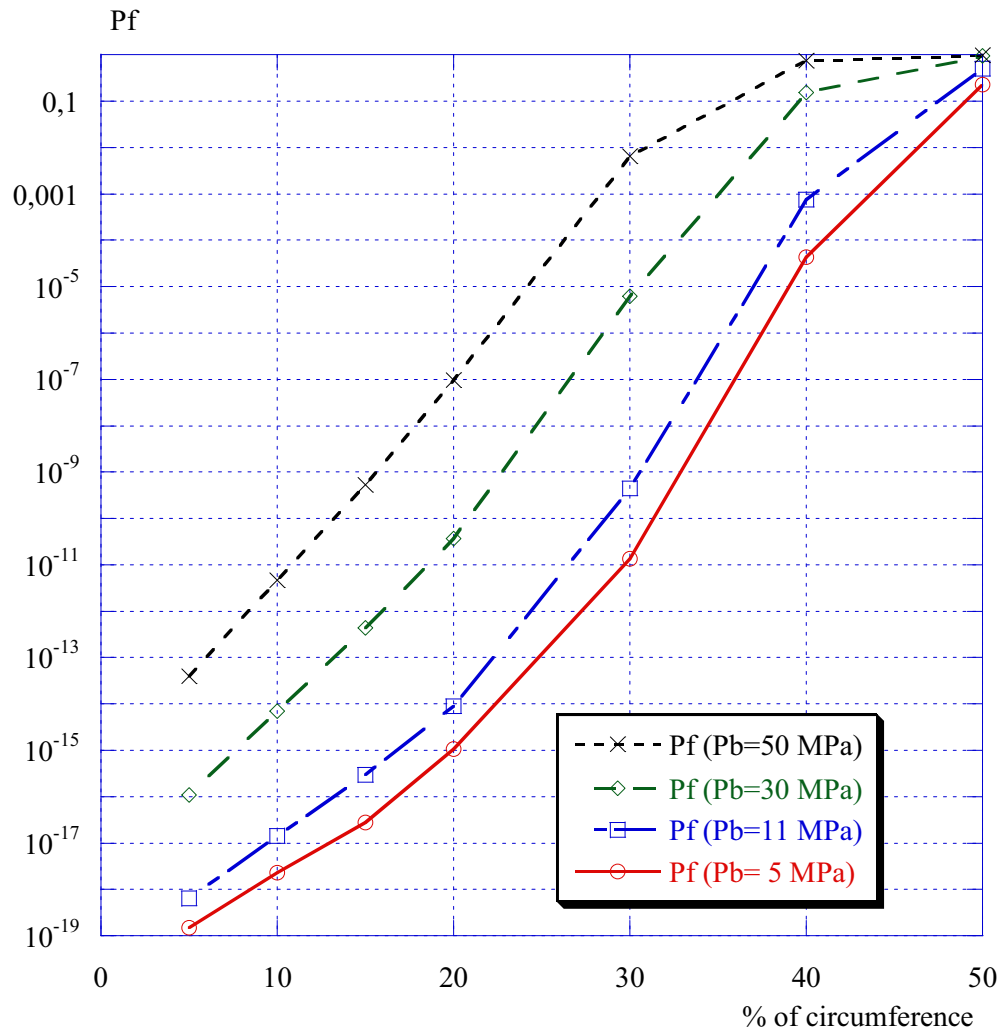

Figure 8.5.1. Conditional probability of fracture as a function of crack length $\left(l/\left(2\cdot\pi\cdot R\right)\right)$ (BWR1). Sensitivity analysis using different assumptions regarding the standard deviation of the yield strength.
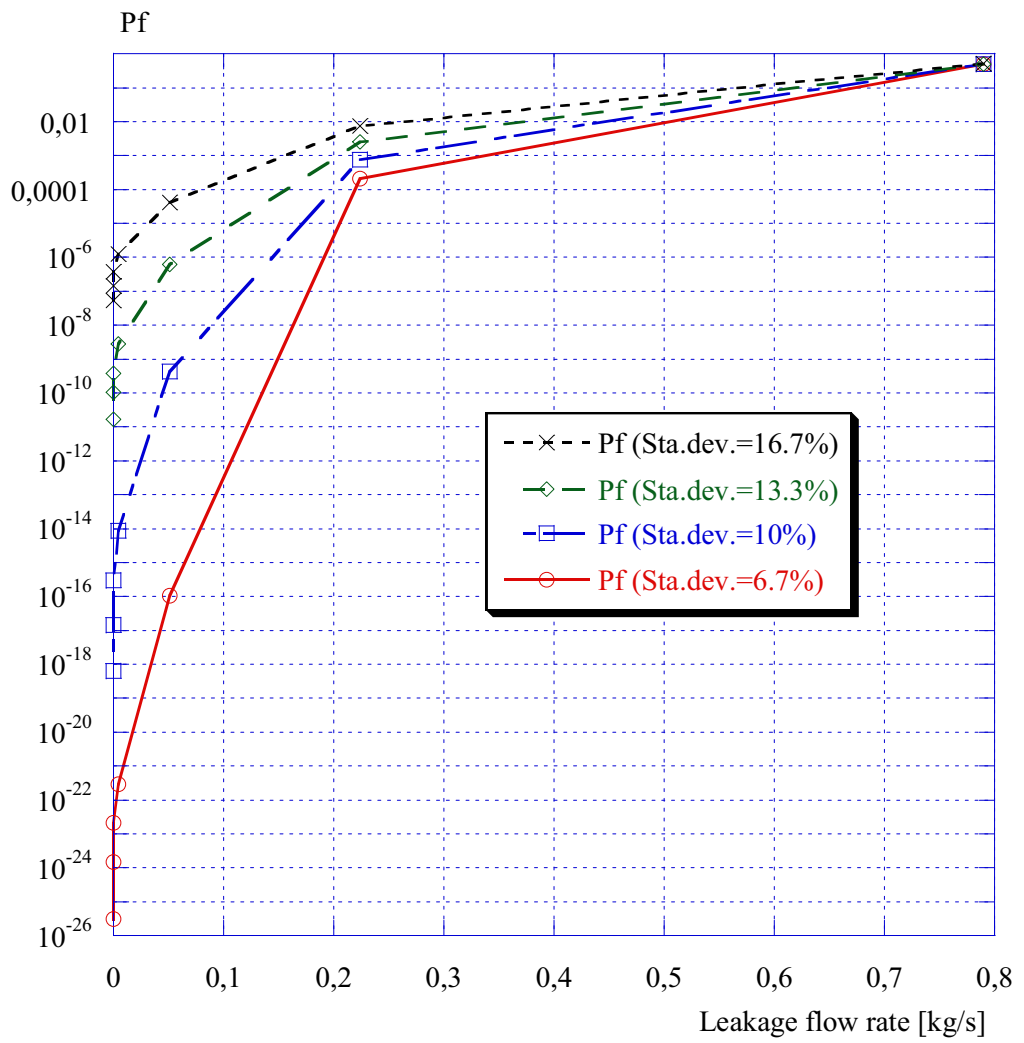
Figure 8.5.2. Conditional probability of fracture as a function of leakage flow rate (BWR1). Sensitivity analysis using different assumptions regarding the standard deviation of the yield strength.

Figure 8.5.3. Conditional probability of fracture as a function of crack length $\left(l/\left(2\cdot\pi\cdot R\right)\right)$ (PWR3). Sensitivity analysis using different assumptions regarding the standard deviation of the yield strength.

Figure 8.5.4. Conditional probability of fracture as a function of leakage flow rate (PWR3). Sensitivity analysis using different assumptions regarding the standard deviation of the yield strength.

As shown above, the assumed value of standard deviation is of minor importance for these cases only if the leakage flow rate is larger than ~0.2 kg/s (BWR1) or larger than ~4 kg/s (PWR3). The reason for this is that the yield strength is the dominating parameter in the probabilistic analysis for all crack lengths up to very long cracks (this is further investigated in sections 8.12-8.13).

8.6   Sensitivity study – Crack length – Standard deviation

All the calculations in this study are presented versus the mean value of crack length. However, the crack length distributions are quite difficult to estimate reliably for any given application (for the baseline cases a standard deviation value equivalent to 5% of the mean value was used in the analysis). Therefore, whenever possible, sensitivity studies should be performed as part of an assessment to investigate the dependency on the assumed crack length distribution [7]. The sensitivity study in this section shows how the resulting fracture probability changes, if different assumptions regarding the standard deviation are used.

Figure 8.6.1. Conditional probability of fracture as a function of crack length $\left(l / \left(2 \cdot \pi \cdot R \right) \right)$ (BWR1). Sensitivity analysis using different assumptions regarding the standard deviation of the crack length.

Figure 8.6.2. Conditional probability of fracture as a function of leakage flow rate (BWR1). Sensitivity analysis using different assumptions regarding the standard deviation of the crack length.
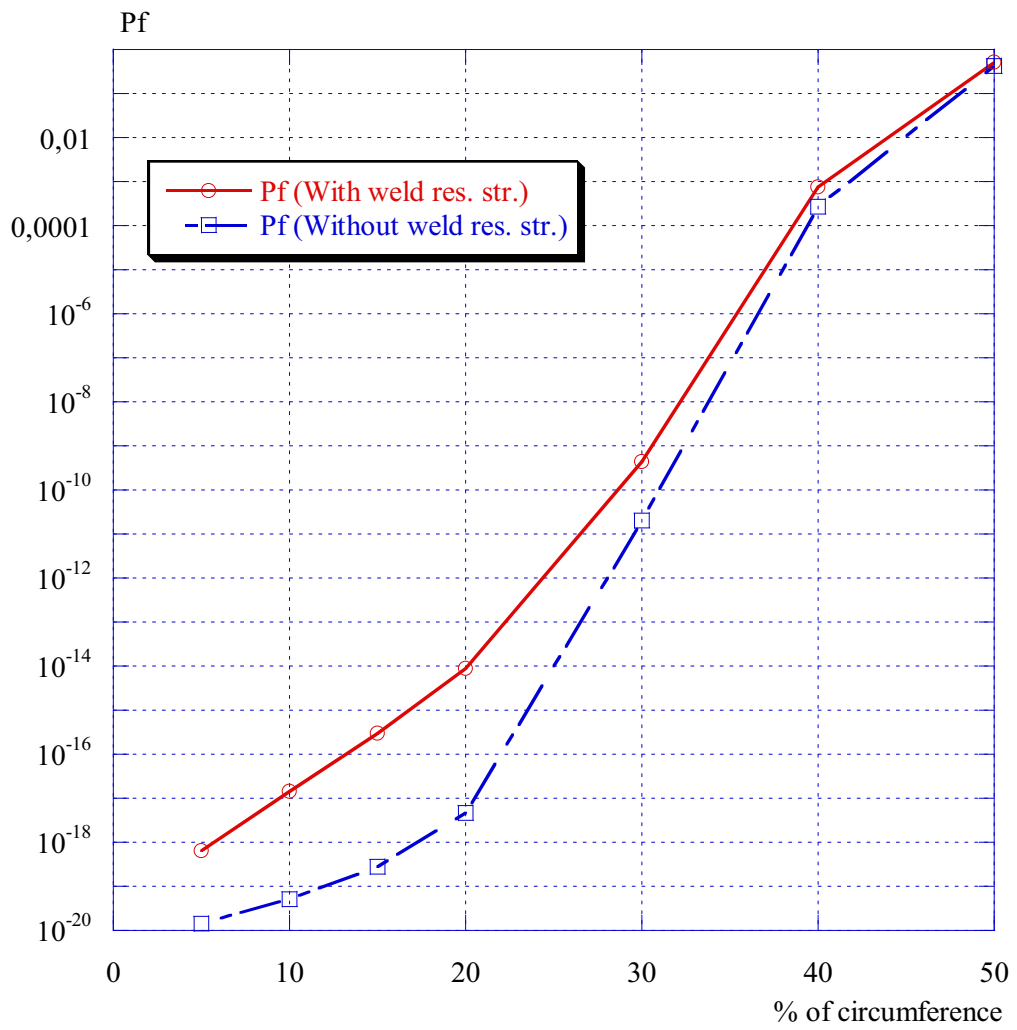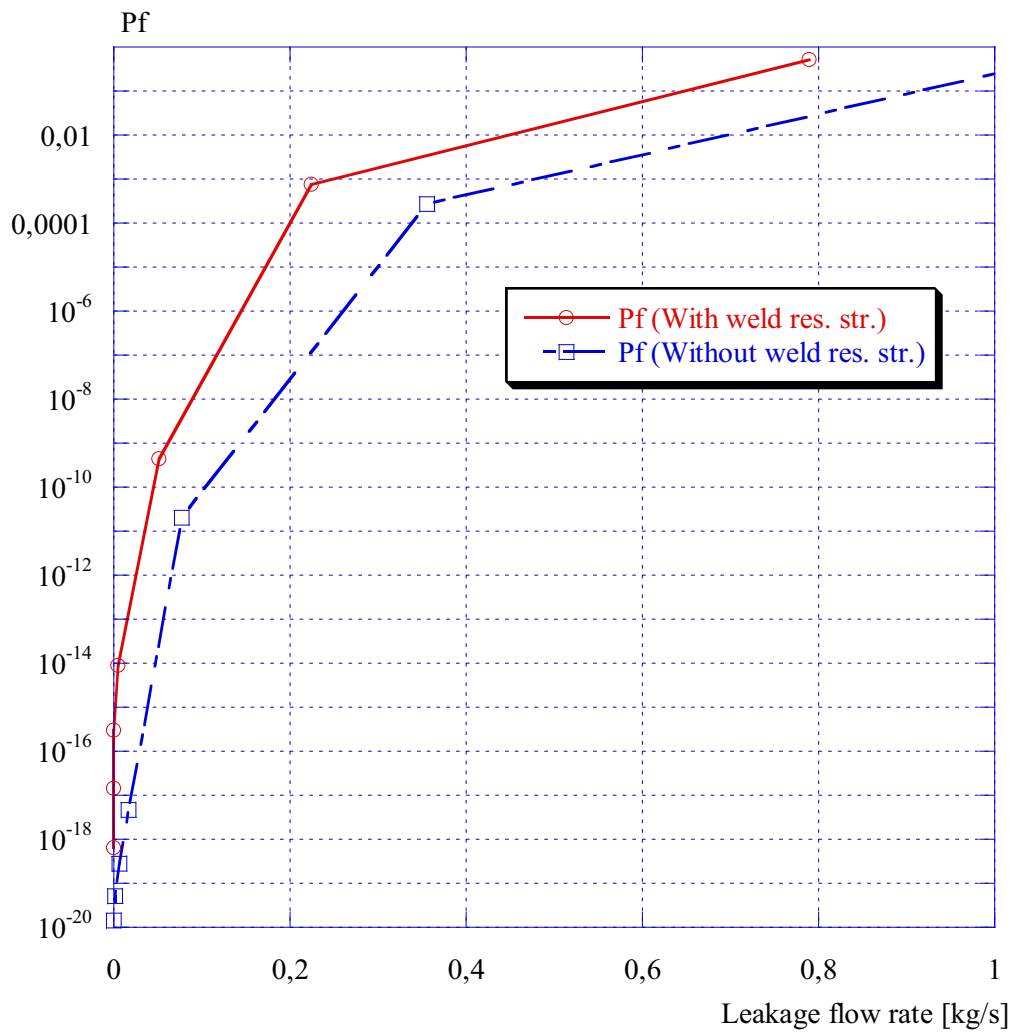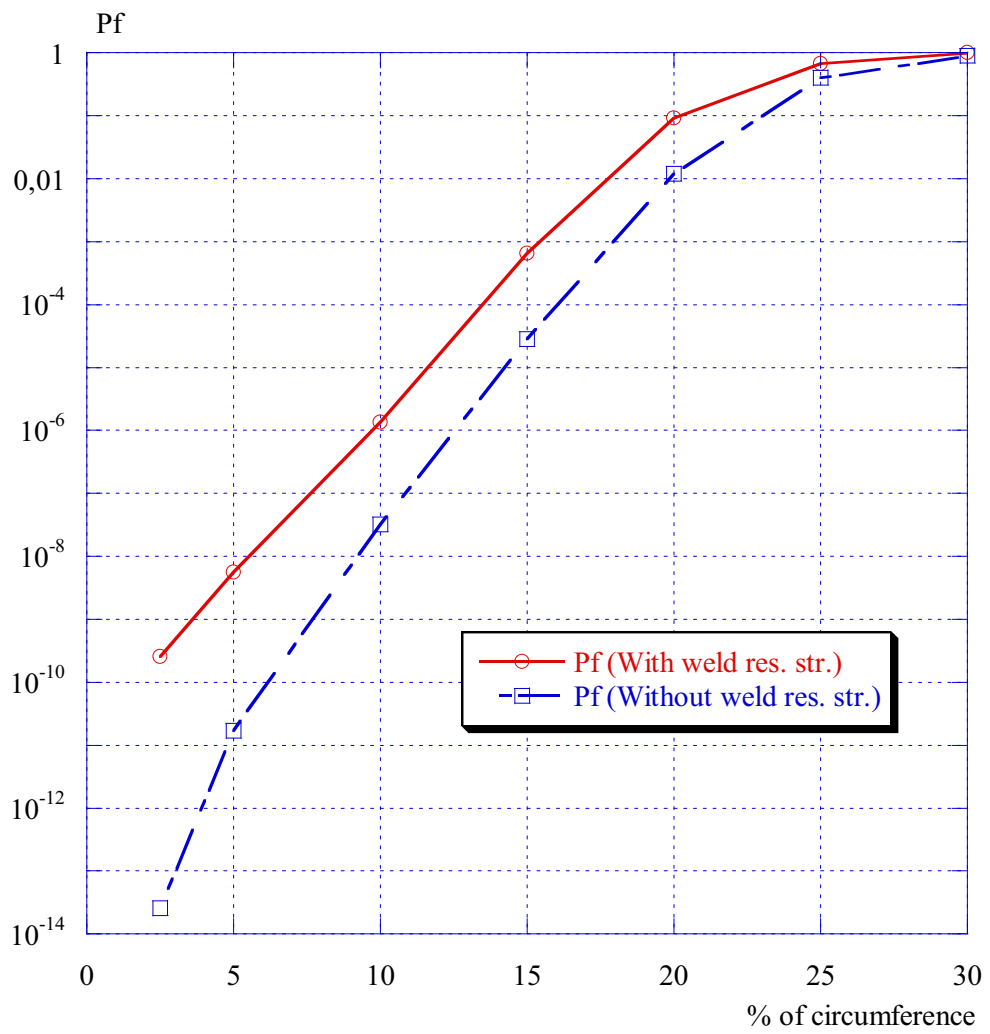
Figure 8.6.3. Conditional probability of fracture as a function of crack length $\left(l/(2 \cdot \pi \cdot R)\right)$ (PWR3). Sensitivity analysis using different assumptions regarding the standard deviation of the crack length.

Figure 8.6.4. Conditional probability of fracture as a function of leakage flow rate (PWR3). Sensitivity analysis using different assumptions regarding the standard deviation of the crack length.

As shown above, the assumed value of standard deviation is of minor importance for these cases (for the leakage flow rates of interest in an LBB application).

8.7 Sensitivity study – Primary membrane stress – Standard deviation

The primary membrane stress is mainly related to the internal pressure of the piping system considered. This stress is therefore well defined and the variation should not be large. For the baseline cases a constant standard deviation value of 2 MPa was used in the analysis (equivalent to 10% of the mean value for BWR1 and 5% of the mean value for PWR3). The sensitivity study in this section shows how the resulting fracture probability changes, if different assumptions regarding the standard deviation are used.

Figure 8.7.1. Conditional probability of fracture as a function of crack length $\left(l/\left(2\cdot\pi\cdot R\right)\right)$ (BWR1). Sensitivity analysis using different assumptions regarding the standard deviation of the primary membrane stress.

Figure 8.7.2. Conditional probability of fracture as a function of leakage flow rate (BWR1). Sensitivity analysis using different assumptions regarding the standard deviation of the primary membrane stress.

Figure 8.7.3. Conditional probability of fracture as a function of crack length $\left(l/\left(2\cdot\pi\cdot R\right)\right)$ (PWR3). Sensitivity analysis using different assumptions regarding the standard deviation of the primary membrane stress.

Figure 8.7.4. Conditional probability of fracture as a function of leakage flow rate (PWR3). Sensitivity analysis using different assumptions regarding the standard deviation of the primary membrane stress.

As shown above, the assumed value of standard deviation is of minor importance for these cases.

8.8 Sensitivity study – Primary global bending stress – Mean value

The primary global bending stress is generally quite well defined (during normal operation). For the baseline cases BWR1 and PWR3 we have used $P_b = 11$ MPa and $P_b = 51.1$ MPa respectively. The sensitivity study in this section shows how the resulting fracture probability changes, if different assumptions regarding the mean value are used.

Figure 8.8.1. Conditional probability of fracture as a function of crack length $\left(l / \left(2 \cdot \pi \cdot R \right) \right)$ (BWR1). Sensitivity analysis using different assumptions regarding the mean value of the primary global bending stress.
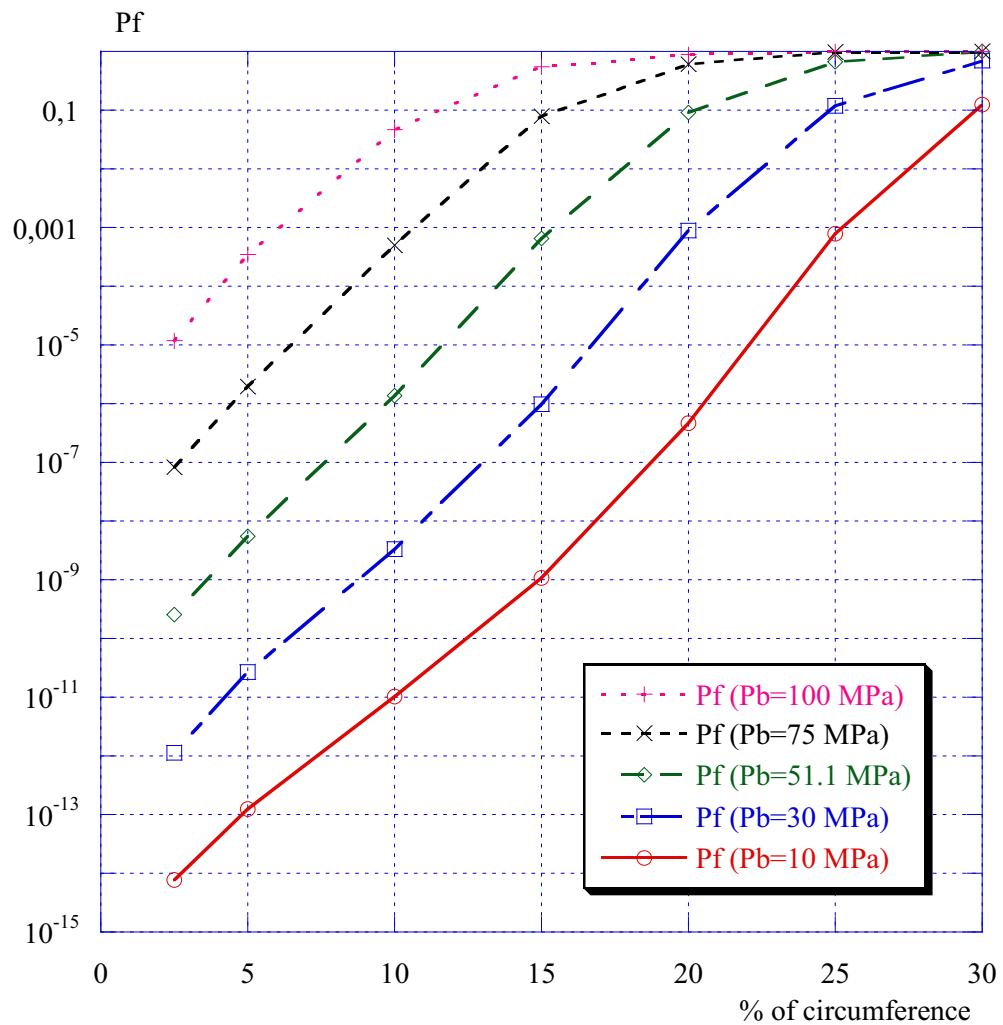
Figure 8.8.2. Conditional probability of fracture as a function of crack length $\left(l / \left(2 \cdot \pi \cdot R\right)\right)$ (PWR3). Sensitivity analysis using different assumptions regarding the mean value of the primary global bending stress.

As shown above, the assumed mean value could have a large impact on the resulting fracture probabilities for the two cases considered. The results above are only presented versus crack length, since no check on the influence on the calculated leakage flow rate was done in this sensitivity analysis.

8.9 Sensitivity study – With/without weld residual stresses

The weld residual stresses have an impact both on the calculation of fracture probability and on the calculation of leakage flow rate. For the baseline cases, weld residual stresses are included in the analysis (see Table 7.1.5). For BWR1 a local bending stress is used (±233 MPa) and for PWR3, a nonlinear stress distribution is used (see Fig. 8.9.0). The sensitivity study in this section shows how the resulting fracture probability changes, if one includes or excludes the weld residual stresses.

Weld residual stresses [Mpa]
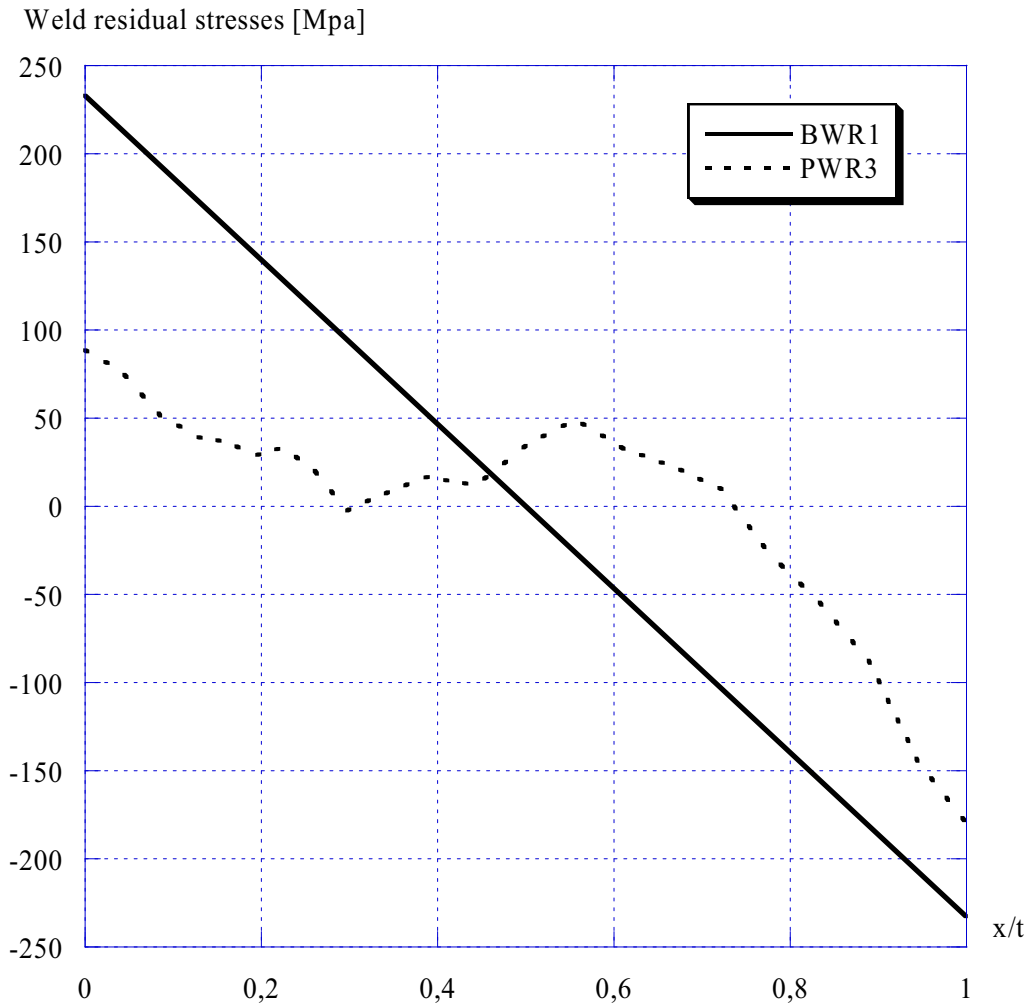
Figure 8.9.0. Assumed weld residual stresses, for the baseline cases BWR1 and PWR3, as a function of a thickness coordinate x ($x = 0$ at the inside of the pipe wall).

Figure 8.9.1. Conditional probability of fracture as a function of crack length $\left(l/\left(2\cdot\pi\cdot R\right)\right)$ (BWR1). Sensitivity analysis with and without weld residual stress.
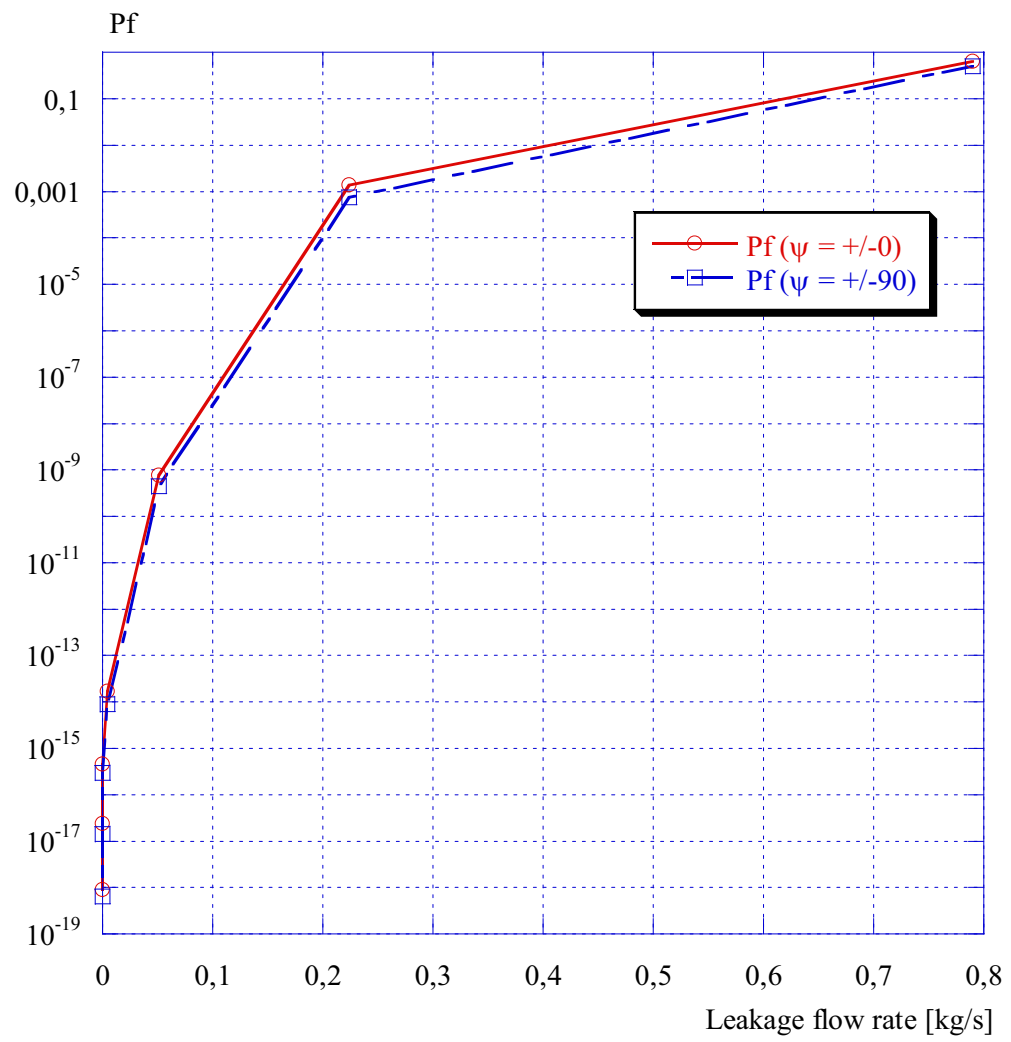
Figure 8.9.2. Conditional probability of fracture as a function of leakage flow rate (BWR1). Sensitivity analysis with and without weld residual stress.
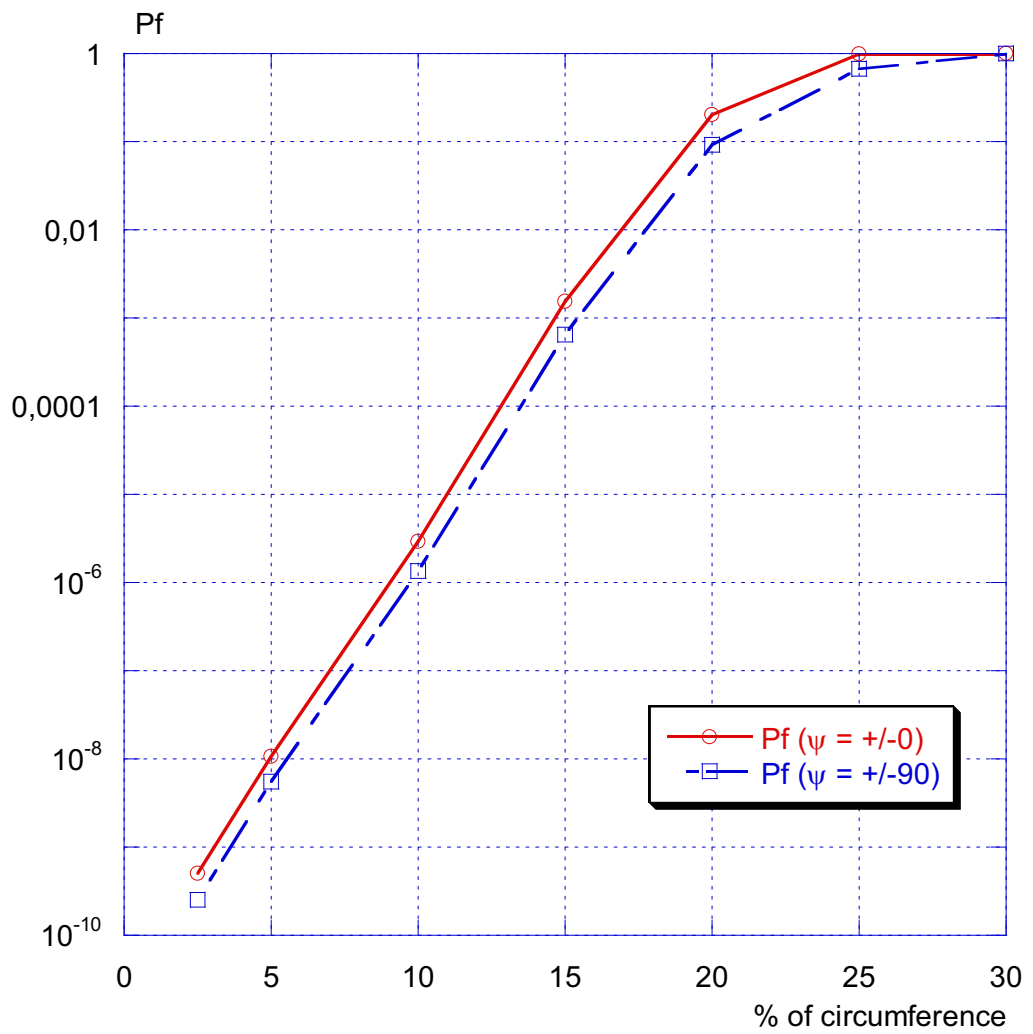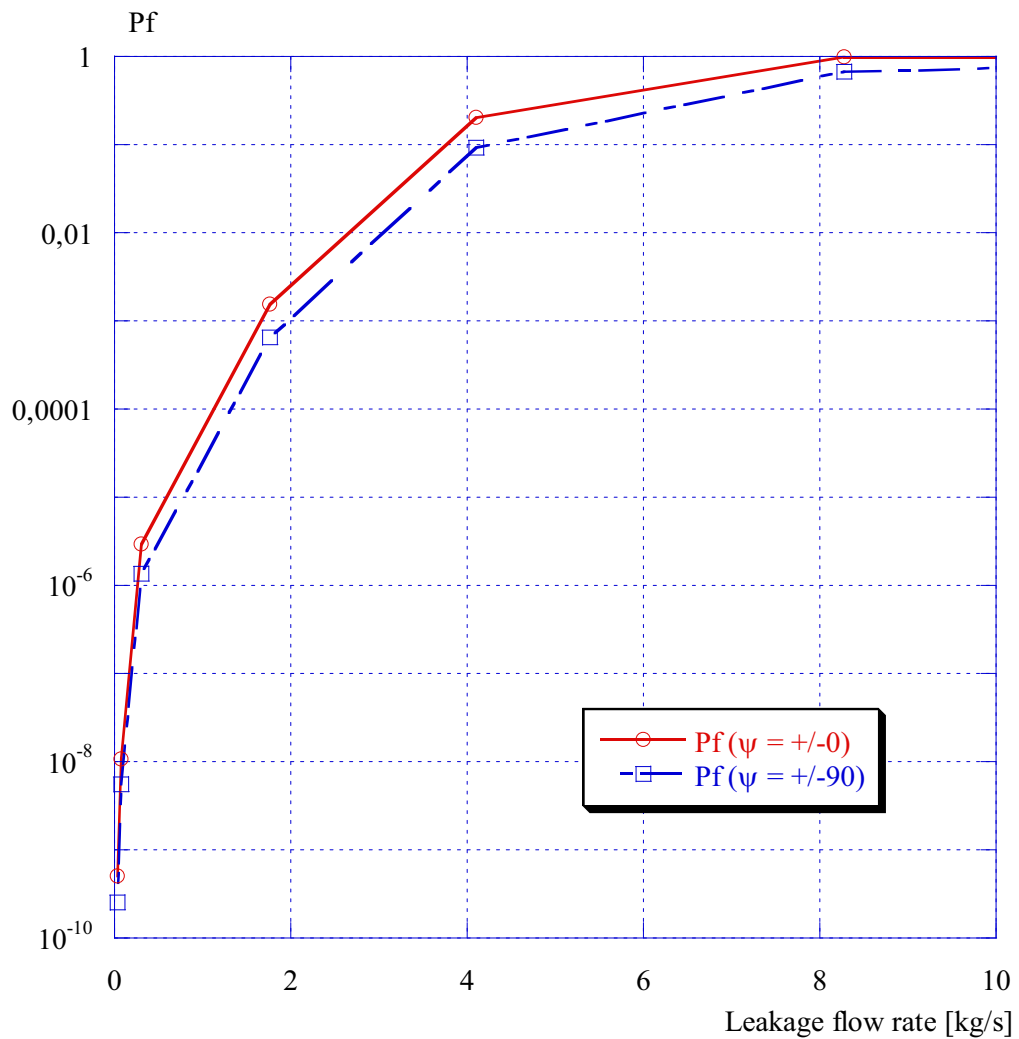
Figure 8.9.3. Conditional probability of fracture as a function of crack length $\left(l/\left(2\cdot\pi\cdot R\right)\right)$ (PWR3). Sensitivity analysis with and without weld residual stress.
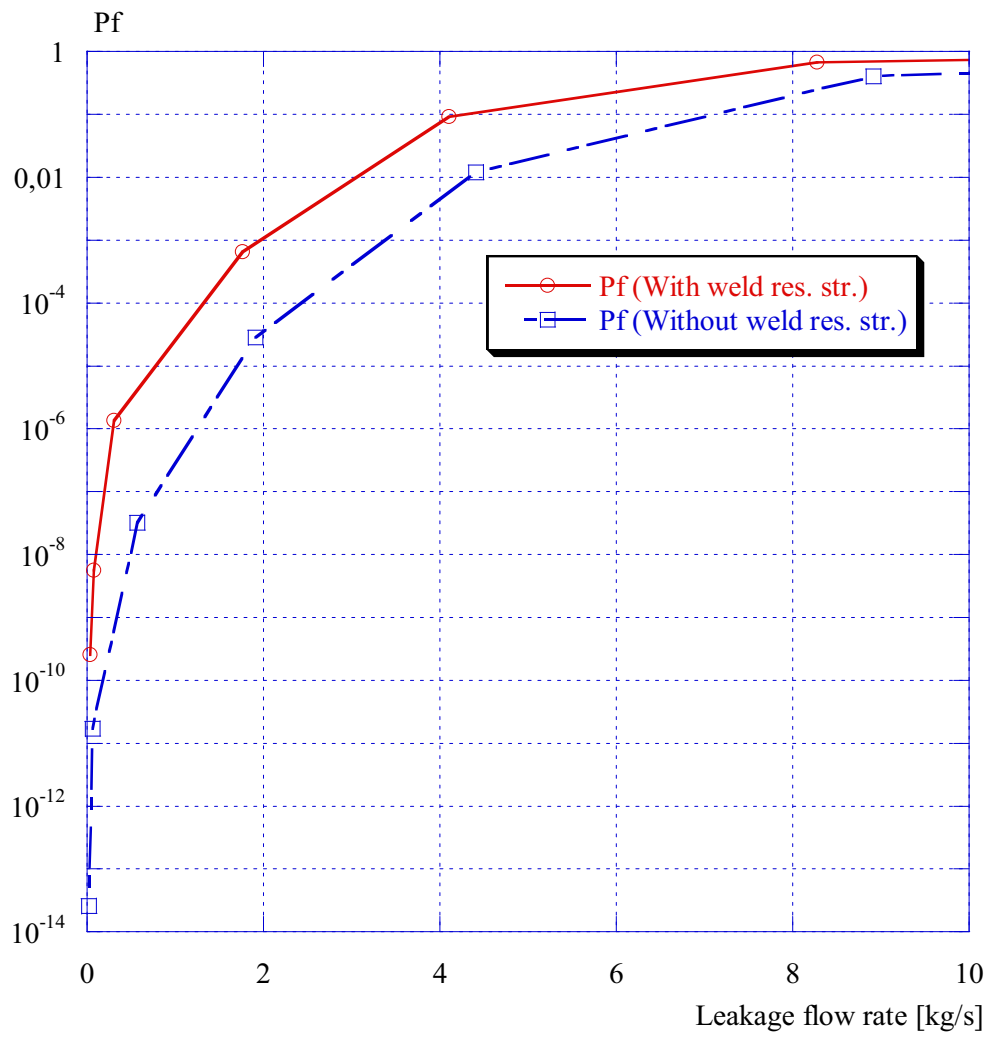
Figure 8.9.4. Conditional probability of fracture as a function of leakage flow rate (PWR3). Sensitivity analysis with and without weld residual stress.

From the calculations presented above, the following conclusions are given:

- The weld residual stresses have quite an impact on the resulting fracture probabilities, especially for smaller cracks. This conclusion is relevant both for small and large pipes.

- The difference (with/without the weld residual stresses) would be smaller if only taking the weld residual stresses into account in the calculation of fracture probability and not in the calculation of leakage flow rate (which is incorrect, since both effects should be included in the analysis).

- The influence from the weld residual stresses on the calculation of leakage flow rate is largest for the case BWR1 (a thin-walled pipe). When comparing Fig. 8.9.2 and 8.9.4 it is obvious that the relative shift along the leakage flow rate axis is approx. 4 times larger for the case BWR1 at $P_f \approx 10^4$ (compared to PWR3). This is reasonable, since a local bending stress is used ($\pm$233 MPa) for the case BWR1 which closes the crack.

- The influence from the weld residual stresses on the calculation of fracture probability is largest for the case PWR3 (a thick-walled pipe). When comparing Fig. 8.9.1 and 8.9.3 it is seen that the relative shift along the conditional probability of fracture axis is larger for the case PWR3 (compared to BWR1). This is related to how the K_I-values vary along the crack front (as a function of crack length) and the fact that PWR3 are more sensitive to the chosen fracture toughness in the calculation of probability of fracture (see section 8.12).

- For a leakage flow rate equal to 10 gpm (equivalent to 0.631 kg/s, which is 10 times larger than the detection limit), the influence on the resulting fracture probabilities are shown in Fig. 8.9.2 (BWR1) and Fig. 8.9.4 (PWR3).

  - For the case BWR1, including the weld residual stresses increases the probability of fracture with a factor of 20. Since this leakage flow rate is related to very large cracks (between 40% and 50% of the circumference for BWR1), then the difference is mainly related to the fact that the weld residual stresses closes the crack and you get a shift in the probability curves given in Fig. 8.9.2.

  - For the case PWR3, including the weld residual stresses increases the probability of fracture with a factor of 100. Since this leakage flow rate is related to quite small cracks (~10% of the circumference for PWR3), then the difference is mainly related to the fact that the weld residual stresses increases the probability of fracture.

8.10 Sensitivity study – With/without off-centred cracks

To predict the probability of fracture under external loads (e.g. bending or combined bending and tension loads), the crack-driving force, is typically evaluated by assuming that these cracks are symmetrically placed with respect to the bending plane of the pipe. This is usually justified by reasoning that the tensile stress due to bending is largest at the center of this symmetric crack.

In reality, defects occur randomly around the pipe circumference. Additionally, during the normal operating condition of a nuclear power plant, the stress component due to pressure is often more significant than that due to bending [11]. As such, the postulated crack in LBB analysis may be off-centered and can thus be located anywhere around the pipe circumference.

For the baseline cases, we assume that the cracks are uniformly distributed with a mean value of $\psi = 0°$ and min/max-value equal to $\pm 90°$ (this is equivalent to assuming that the off-centered crack position is random and equally likely to take on an angle anywhere between -90º and +90º). The sensitivity study in this section shows how the resulting fracture probability changes, if one includes or excludes off-centered cracks.
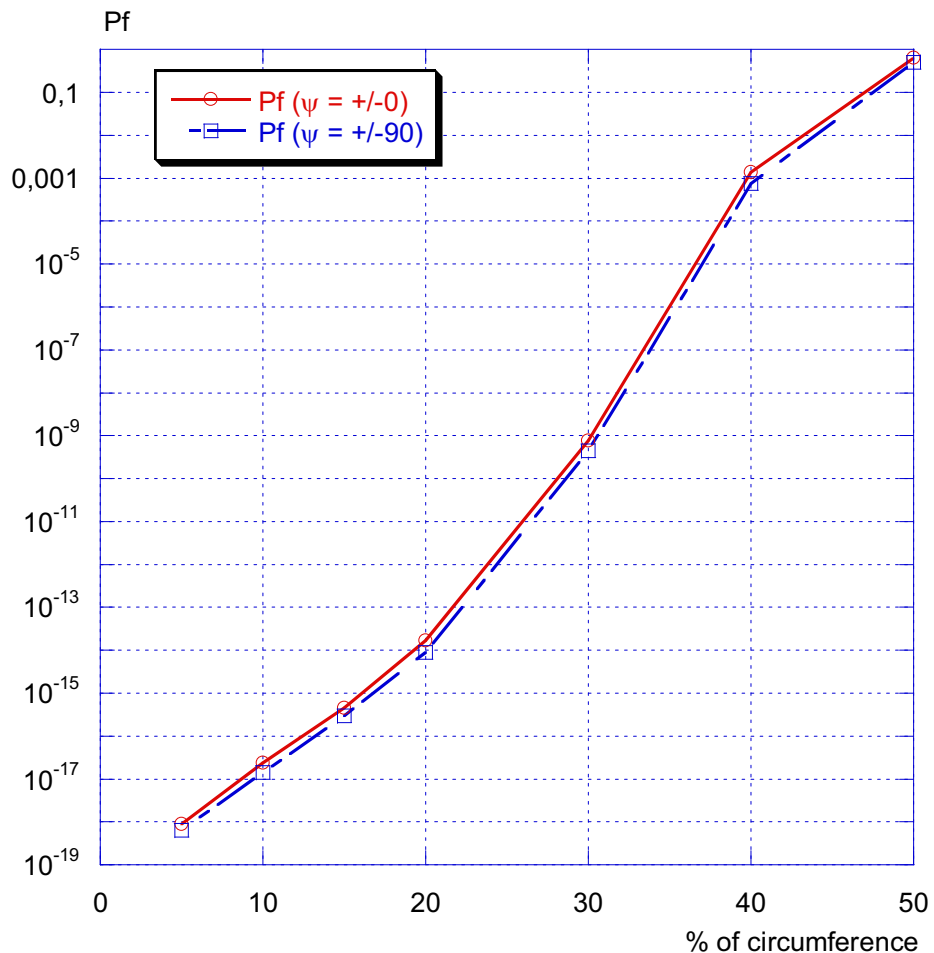
Figure 8.10.1. Conditional probability of fracture as a function of crack length $\left(l/\left(2\cdot\pi\cdot R\right)\right)$ (BWR1). Sensitivity analysis with and without off-centred cracks.

Figure 8.10.2. Conditional probability of fracture as a function of leakage flow rate (BWR1). Sensitivity analysis with and without off-centred cracks.

Figure 8.10.3. Conditional probability of fracture as a function of crack length $\left(l/(2\cdot\pi\cdot R)\right)$ (PWR3). Sensitivity analysis with and without off-centred cracks.

Figure 8.10.4. Conditional probability of fracture as a function of leakage flow rate (PWR3). Sensitivity analysis with and without off-centred cracks.

As shown above, including or excluding off-centered cracks is of minor importance for the considered cases. This is somewhat surprising, and the main reason is that the result is dominated by cracks with an angle around 0º (also investigated in section 8.12).

However, it could be interesting too check under what conditions that an off-centered crack is of importance for the analysis. An obvious choice is to increase the ratio between the applied global bending stress and the applied membrane stress. Also one could exclude the weld residual stresses in the analysis, since this stress is independent of the location of the crack (which is also true for the membrane stress). In Fig. 8.10.5 below, the results is given for a case with a larger bending over membrane ratio and also excluding weld residual stresses.
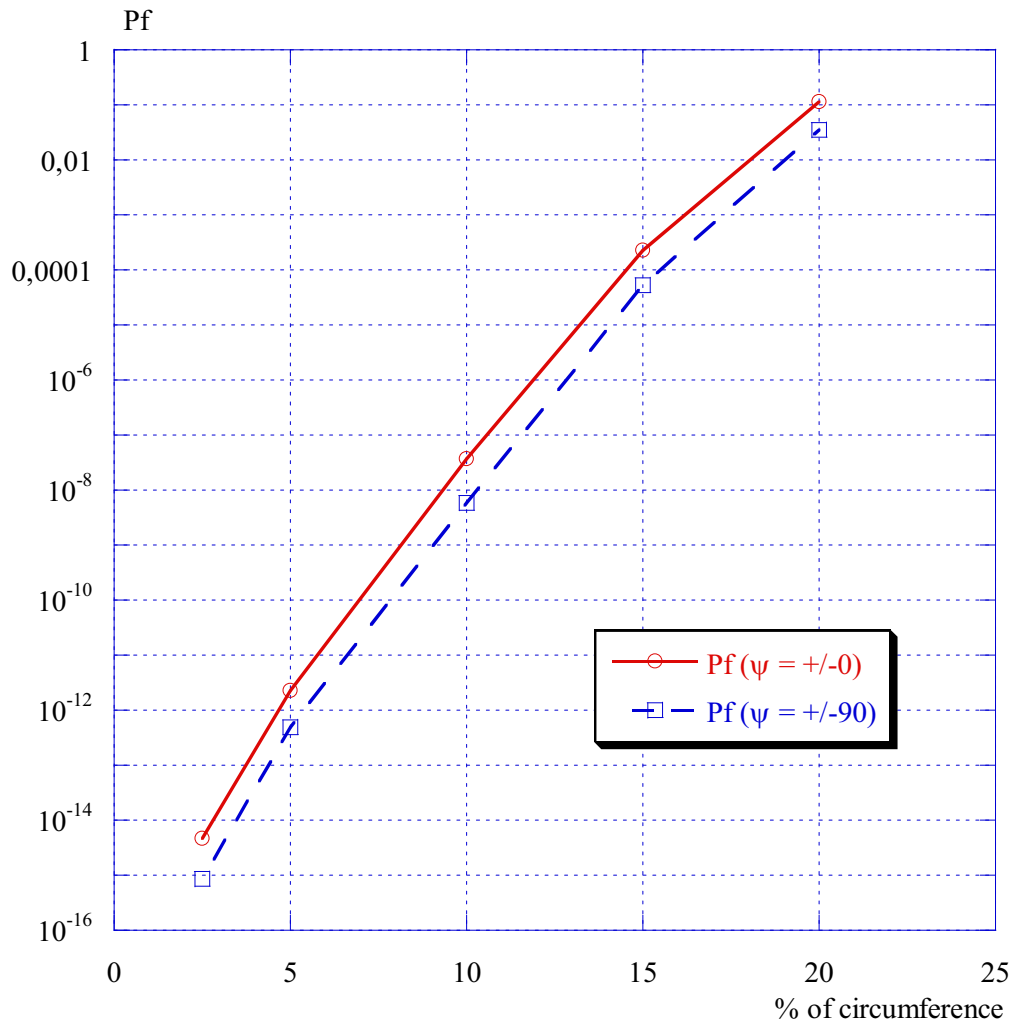
Figure 8.10.5. Conditional probability of fracture as a function of crack length $\left(l/\left(2 \cdot \pi \cdot R\right)\right)$. Sensitivity analysis with and without off-centred cracks for a case with a larger bending over membrane ratio and also excluding weld residual stresses.

As shown above, including or excluding off-centered cracks is of minor importance even in this case (although the difference is somewhat larger than for the baseline case PWR3). To investigate this behaviour even further, we now choose to consider the off-centred position of the crack as a deterministic parameter. In Fig. 8.10.6, fracture probabilities as a function of crack position is given for two different crack lengths (equivalent to 2.5% and 15 of the circumference).
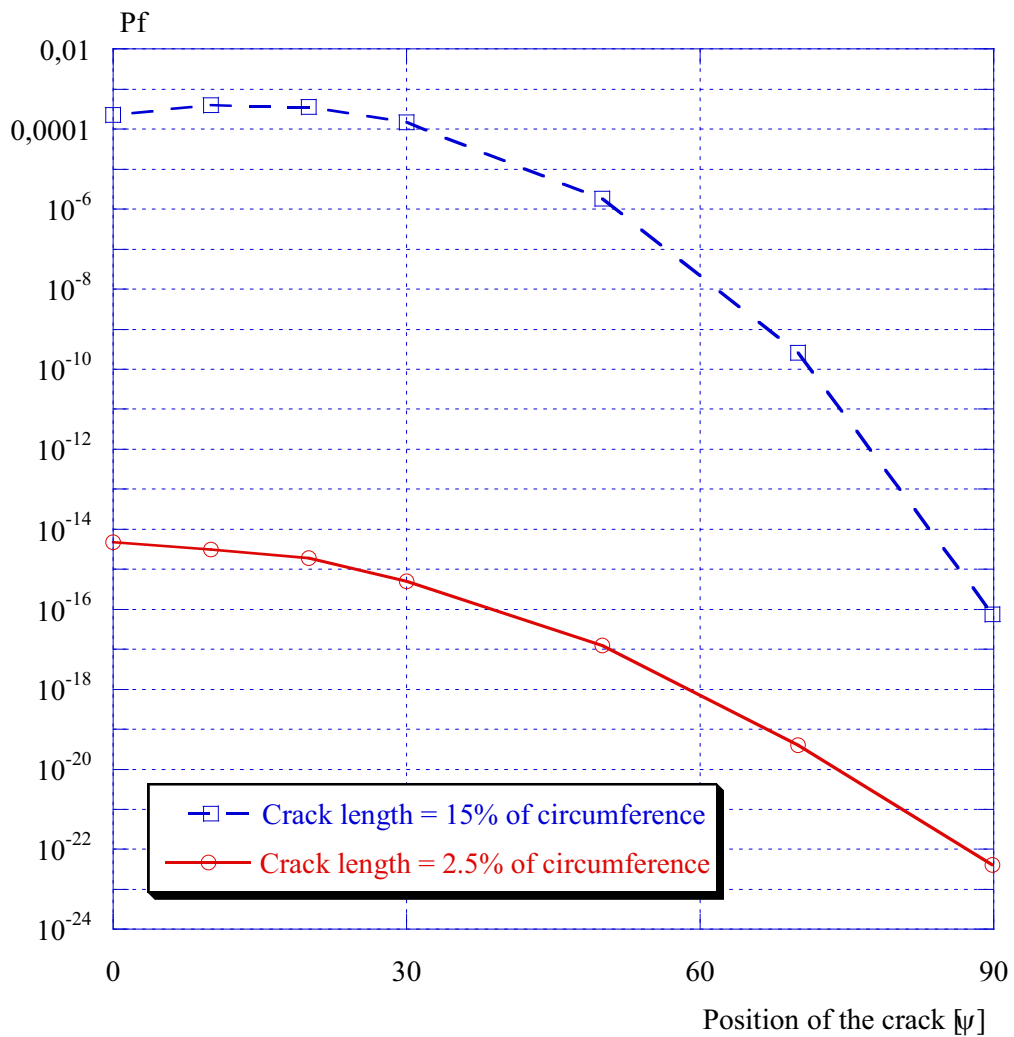
Figure 8.10.6. Conditional probability of fracture as a function of crack position (assuming that the crack position is a deterministic parameter). Sensitivity analysis using two different crack lengths (equivalent to 2.5% and 15 of the circumference) for a case with a larger bending over membrane ratio and also excluding weld residual stresses.

As shown in Fig. 8.10.6, using a predominantly bending load and also having the crack position as a deterministic parameter, the fracture probability is strongly dependent of the chosen position of the crack. This is consistent with the presented stress intensity factor solutions in Appendix A. The figure also explains that the results (fracture probability) is totally dominated by cracks with an angle around 0º (further investigated in section 8.12) when using a uniformly distributed crack position with a mean value of $\psi = 0°$ and min/max-value equal to $\pm 90°$.

Figure 8.10.6 also shows that the maximum fracture probability (using a crack length equal to 15% of the circumference of the pipe) is not located at $\psi = 0°$. This is reasonable since the dominating crack front will have a maximum K_I-value when the crack is at an off-centre position (when using a predominantly bending load).

Finally this shows that including or excluding off-centered cracks is of minor importance, for the considered baseline cases, is a logical result given the conditions of this calculation. A similar conclusion is given in [12], where the ratio of fracture probabilities based on worst-case condition (symmetrically centered crack) to those obtained from random off-center crack angle that is uniformly distributed over the circumference of the pipe varies between 2 and 7, depending on the bending moment applied (see Fig. 8.10.7). Using the results from the present study, and similar conditions as in [12] gives a ratio between 4.3 and 6.4, i.e. a very good agreement.
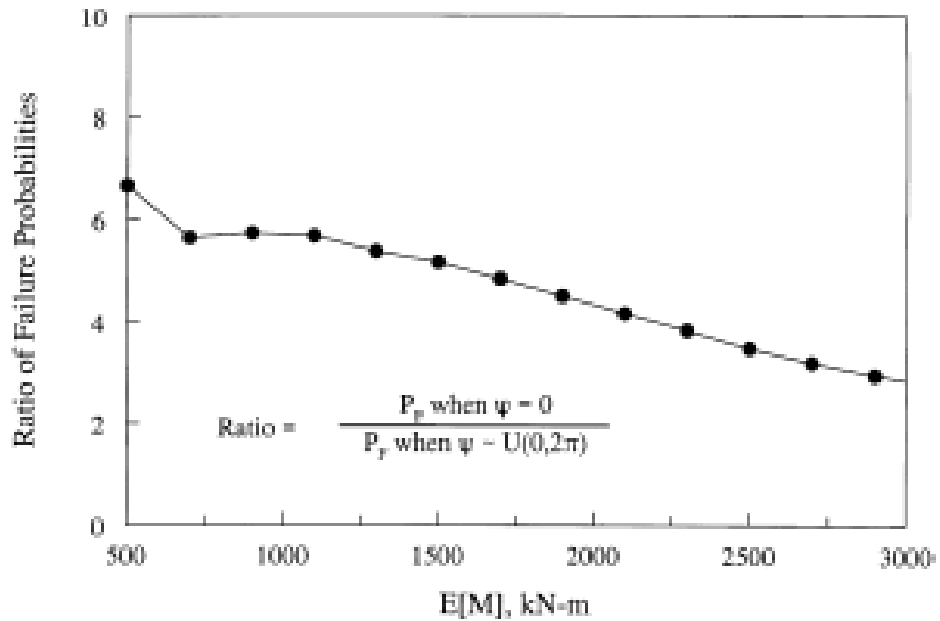
Fig. 9. Ratio of failure probabilities vs. applied moment.

Figure 8.10.7.   The ratio of fracture probabilities based on worst-case condition (symmetrically centered crack) to those obtained from random off-center crack angle that is uniformly distributed over the circumference of the pipe, depending on the bending moment applied [12].

8.11 Sensitivity study – Leak rate calculation using data for fatigue or stress corrosion cracking

As previously stated, LBB is the demonstration that a postulated defect will leak and be detected, before a catastrophic failure. In the present probabilistic approach, there exist an important link between the calculated fracture probabilities and the corresponding leakage flow rate.

In the SQUIRT calculations (see section 7.3), default values are used for most the parameters not related to the geometry of the baseline cases. The main input data are the pipe geometry, postulated crack length, COD (using loads from the normal operation of the plant) and type of cracking mechanism. For the baseline cases we assumed that data for fatigue growth is most relevant (note that no active damage mechanism should be present in the piping segment, if LBB should be considered).

This means that we have used the following values in the SQUIRT calculations (for the baseline case, where we use data for fatigue crack growth):
- Global surface roughness, $\mu_G = 0.0405$
- Local surface roughness, $\mu_L = 0.0088$
- PLC (Vel. Heads/mm), $\eta_L = 6.730$
- Global thickness parameter, $K_G = 1.02$
- Local thickness parameter, $K_L = 1.06$
- Calculations have been made using the improved model for crack morphology parameters (which is dependent of the given COD-values, see section 7.3).

In the sensitivity study in this section, we have used the following values in the SQUIRT calculations (where we use data for stress corrosion crack growth):
- Global surface roughness, $\mu_G = 0.08$
- Local surface roughness, $\mu_L = 0.0047$
- PLC (Vel. Heads/mm), $\eta_L = 28.2$
- Global thickness parameter, $K_G = 1.07$
- Local thickness parameter, $K_L = 1.33$
- Calculations have been made using the improved model for crack morphology parameters (which is dependent of the given COD-values, see section 7.3).

The sensitivity study in this section shows how the resulting fracture probability changes, if one uses data for fatigue or stress corrosion cracking (in the leak rate calculation).
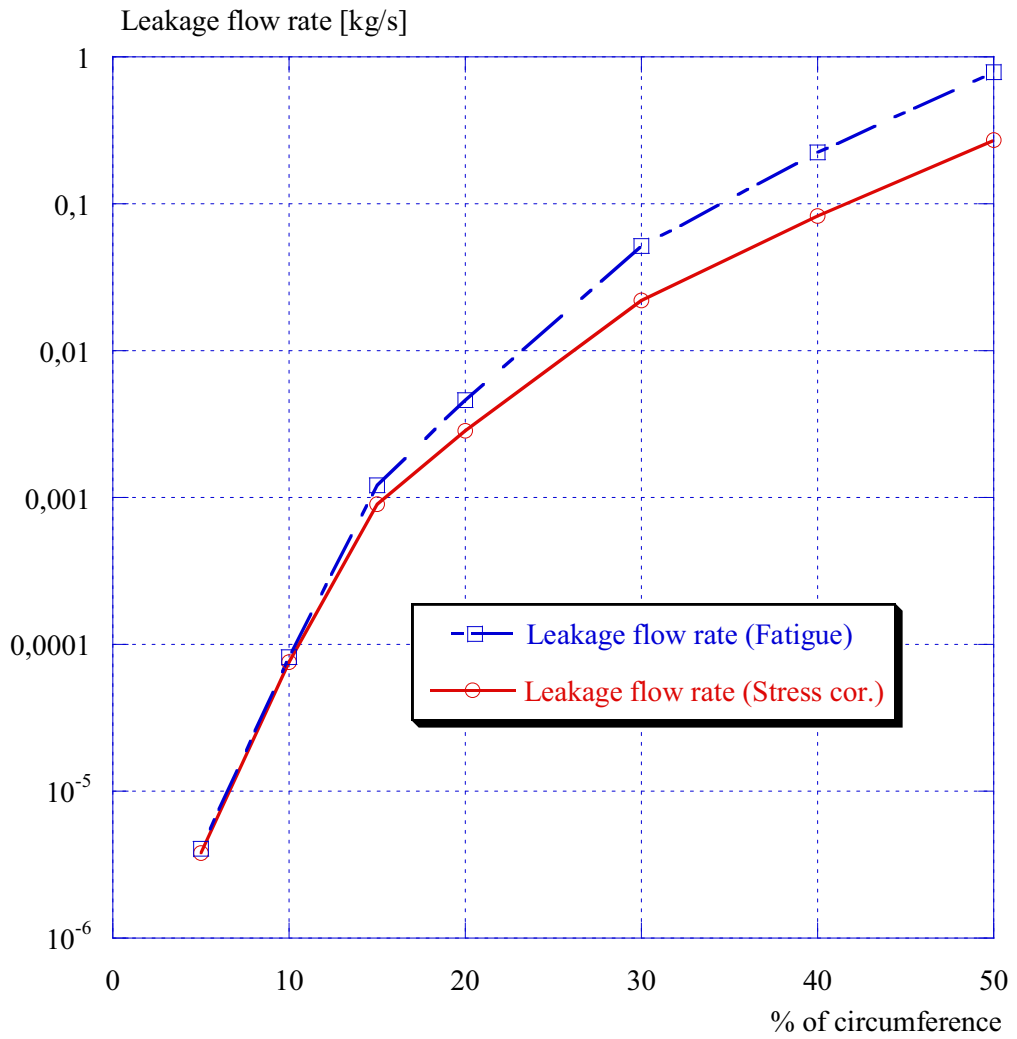
Figure 8.11.1. Leakage flow rate as a function of crack length $\left(l/\left(2\cdot\pi\cdot R\right)\right)$ (BWR1). Sensitivity analysis using data for fatigue or stress corrosion cracking in the leak rate calculation.
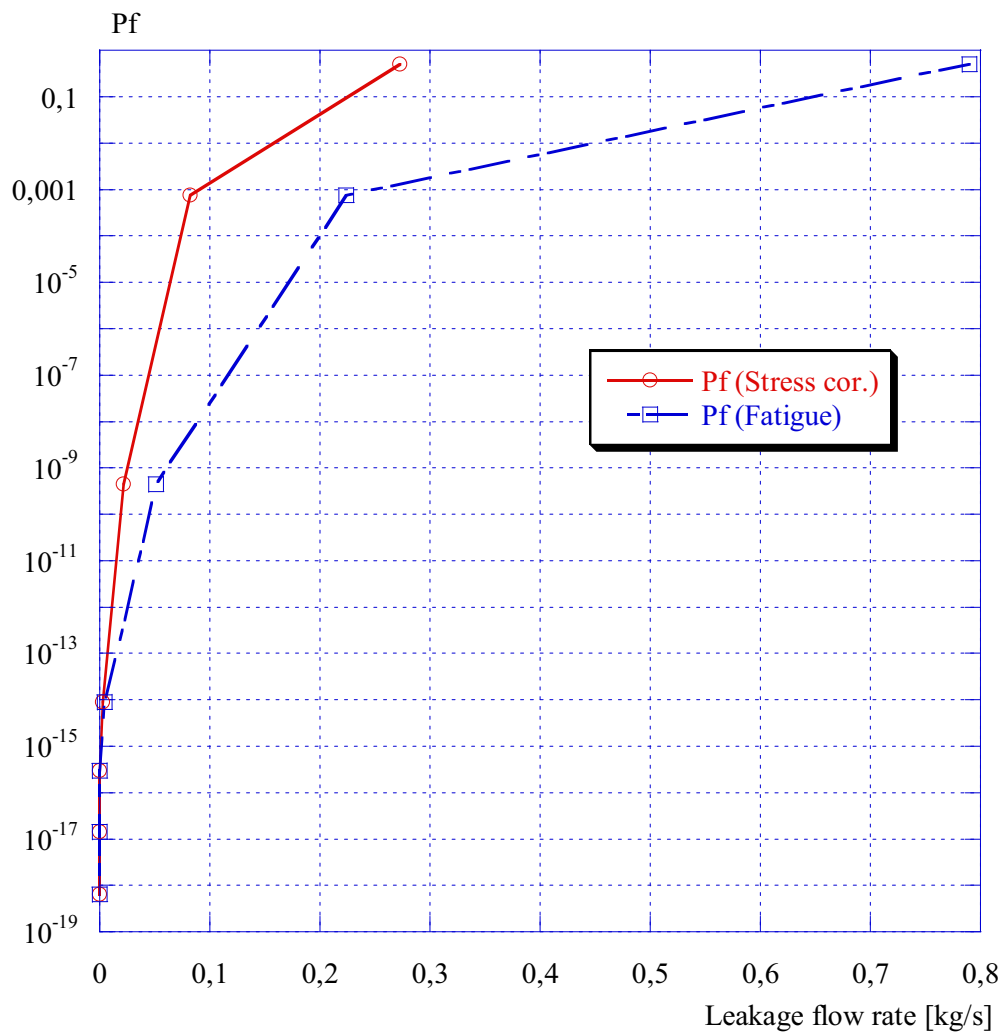
Figure 8.11.2. Conditional probability of fracture as a function of leakage flow rate (BWR1). Sensitivity analysis using data for fatigue or stress corrosion cracking in the leak rate calculation.
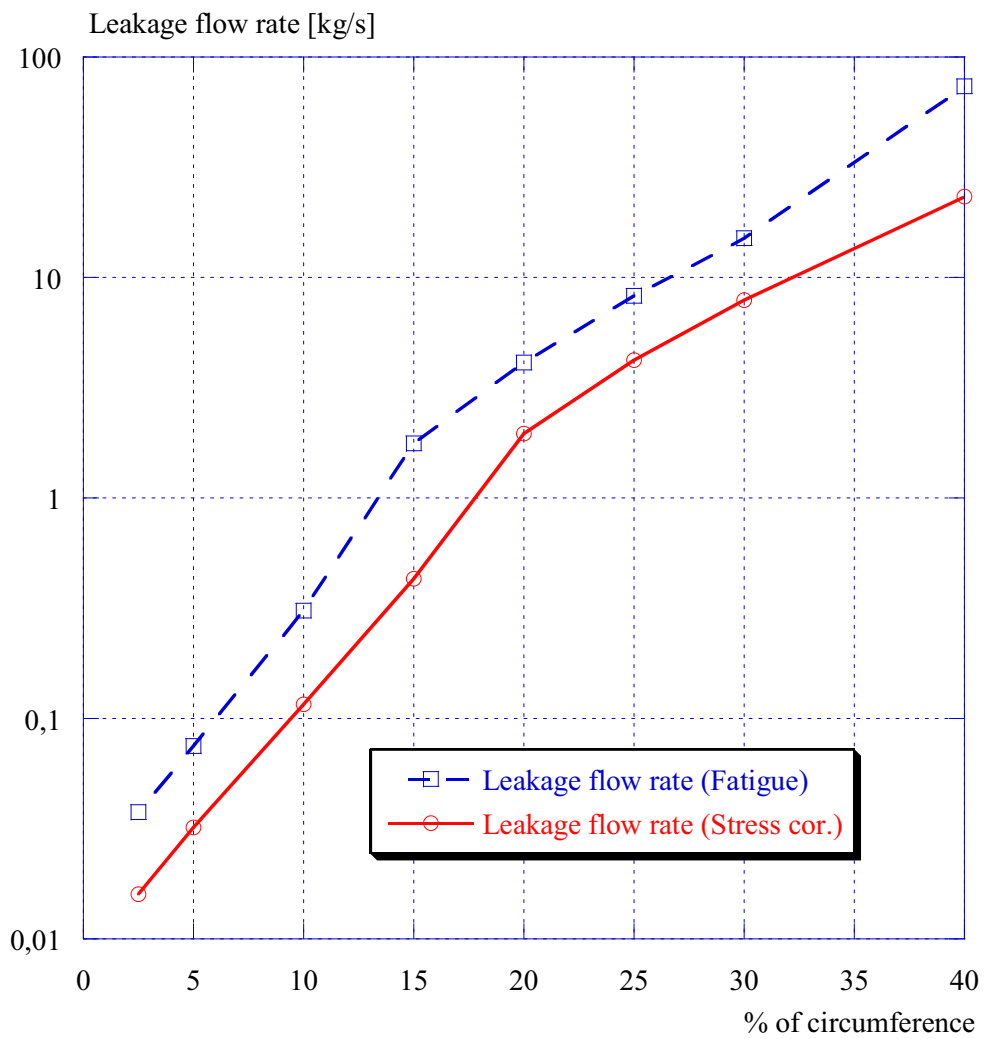
Figure 8.11.3. Leakage flow rate as a function of crack length $\left(l/\left(2\cdot\pi\cdot R\right)\right)$ (PWR3). Sensitivity analysis using data for fatigue or stress corrosion cracking in the leak rate calculation.
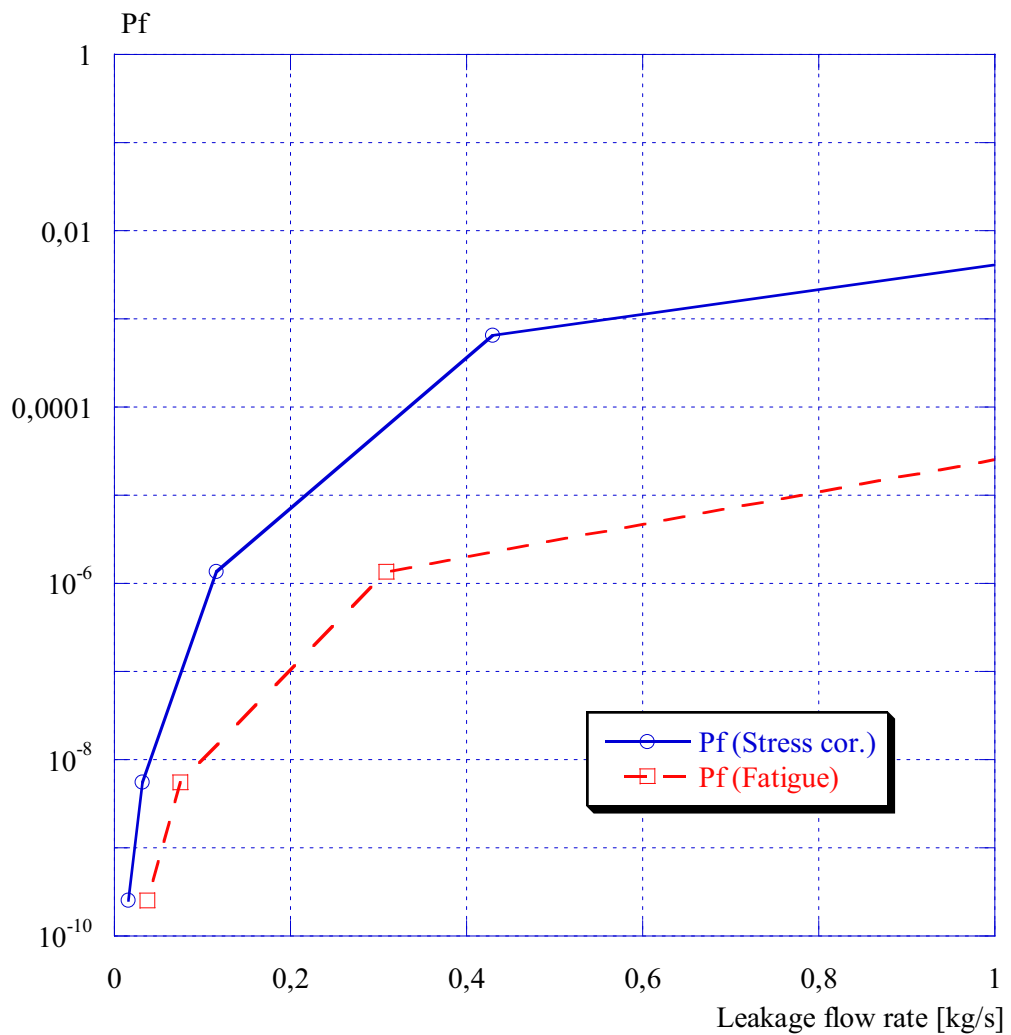
Figure 8.11.4. Conditional probability of fracture as a function of leakage flow rate (PWR3). Sensitivity analysis using data for fatigue or stress corrosion cracking in the leak rate calculation.

As shown above, the chosen cracking mechanism have quite an impact on the resulting fracture probabilities. Also shown, is the fact that P_f (using data for stress corrosion cracking) is larger than P_f (using data for fatigue) at an equivalent leakage flow rate. This has to do with the crack morphology for stress corrosion cracks that restrain the flow more, compared to fatigue cracks, and you therefore need a larger crack (and a larger P_f) to get an equivalent leakage flow rate.

8.12 Sensitivity study – What parameter contributes the most to the calculated fracture probability

In this and the next section a more formal sensitivity analysis is presented. The purpose in this section is to investigate on what parameter that contributes the most to the calculated conditional fracture probability. To answer this, we may use the gradient computation that is readily available in any probability analysis using FORM (see section 3).

However, the simplest approach is to investigate on the relative importance of the basic standard normal random variables that is given in a FORM analysis. These can be given be means of the vector α^* defined as:

$$\alpha^* = \frac{y^*}{\left\| y^* \right\|} \qquad (8.12.1)$$

where y^* denotes the coordinates of the design point in the standard normal space. The ordering of the elements in α^* indicates the relative importance of the random variables in the standard normal space.

Since y^* is the coordinate of the design point (or the most probable point of fracture), then $\left\| y^* \right\|$ is equivalent to the design point β and related to the conditional probability of fracture as given in Eqn. (3.3.5), i.e. $P_f = \Phi(-\beta)$ when using a FORM approximation. This means that there is nonlinear relation between the importance factors given below and how they contribute to the calculated conditional fracture probability. These importance factors should therefore be used to get a qualitative understanding of the different parameters/variables relative importance in a probabilistic analysis. To get a quantitative understanding, a more formal sensitivity analysis should be used; such an analysis is presented in section 8.13 below.

The sensitivity study in this section shows the importance factors, i.e. what parameter that contributes the most to the calculated conditional fracture probability.
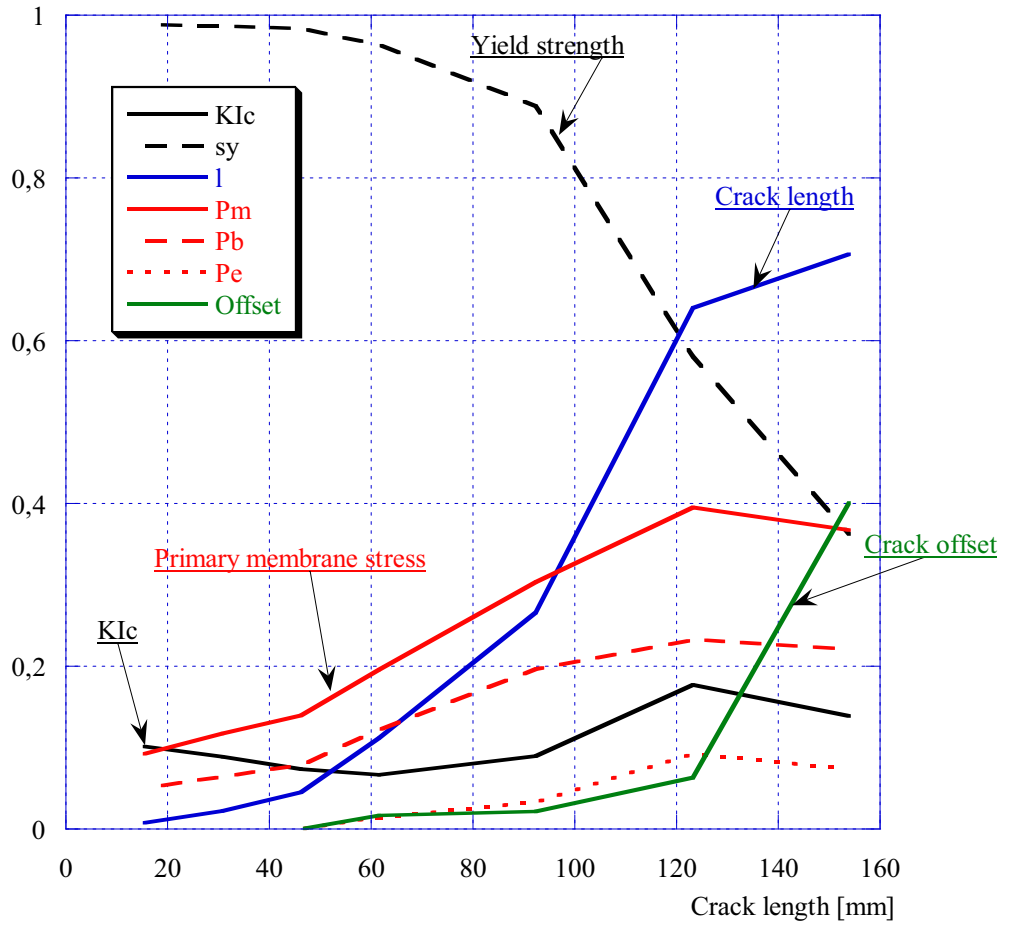
Figure 8.12.1. Importance factors for the baseline case BWR1.
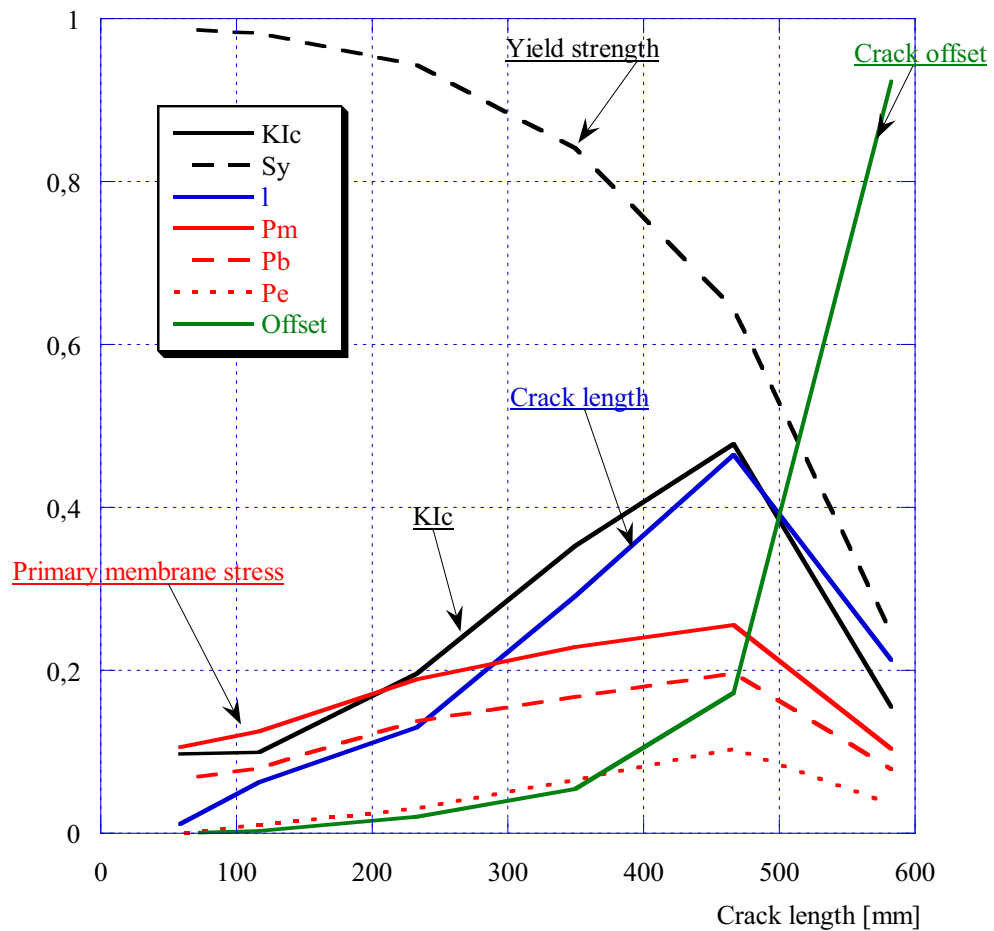
Figure 8.12.2. Importance factors for the baseline case PWR3.

As seen from the figures above, the yield strength dominates the analysis both for small and medium sized cracks (both for BWR1 and PWR3). This is reasonable since the analysis, in this region, is mainly controlled by the limit load. For medium sized crack, the importance of the crack length increases (and also the fracture toughness for the case PWR3). Finally, for very large cracks, the crack offset is more important (dominates the analysis for the case PWR3).

From the sensitivity analysis presented earlier, the following was concluded:

- The case PWR3 is more sensitive to the chosen mean value of fracture toughness than the case BWR1 (see section 8.2). This is verified by the importance factors presented above.
- Both cases are equally sensitive to the chosen mean value of yield strength (see section 8.4). This is verified, for small and medium sized cracks, by the importance factors presented above.
- Including or excluding off-centered cracks is of minor importance for the considered cases. This is verified, for small and medium sized cracks, by the importance factors presented above.
- The only case when the off-centered cracks dominate the analysis is for the case PWR3, if the crack length is larger than 500 mm. Such a large crack (more than 20% of the circumference) will give a leakage flow rate larger than 5 kg/s and would never be accepted in a LBB assessment (please note that the deterministic critical crack length is 509 mm).

100

8.13 Sensitivity study – What parameter change, has the most influence on the calculated fracture probability

In section 8.12, the importance factors were given for the two baseline cases BWR1 and PWR3. The purpose was to show what parameter that contributes the most to the calculated conditional fracture probability. Another aspect of a probabilistic analysis is to define what happens to the calculated conditional fracture probability if we introduce a small change in the input data, i.e. what parameter change has the most influence on the calculated conditional fracture probability.

Of interest is therefore the sensitivity of the reliability index β with respect to parameters θ entering the definition of the limit state function g. The sensitivity of β is given by [18]:

$$\frac{d\beta}{d\theta} = \frac{1}{\|\nabla G\|} \frac{dg}{d\theta} \quad . \tag{8.13.1}$$

When doing a FORM analysis, the probability of failure (fracture) is given as $P_f = \Phi(-\beta)$ and differentiated with respect to θ :

$$\frac{dP_f}{d\theta} = \frac{d}{d\theta}\Phi(-\beta) = \frac{d}{d\theta}\big(1 - \Phi(\beta)\big) = -\frac{d\beta}{d\theta}\frac{d}{d\beta}\Phi(\beta) = -\frac{d\beta}{d\theta}\varphi(\beta) \quad . \tag{8.13.2}$$

The sensitivity of the probability of failure (fracture) P_f with respect to parameters θ is then given by:

$$\frac{dP_f}{d\theta} = -\varphi(\beta)\frac{1}{\|\nabla G\|}\frac{dg}{d\theta} \quad , \tag{8.13.3}$$

where $\|\nabla G\|$ and $dg/d\theta$ is easily computed in any FORM analysis.

The sensitivity study in this section tries to answer the question: What parameter change has the most influence on the calculated conditional fracture probability? We investigate a change in the given mean values and in the given values for the standard deviation. The results are normalised (against the conditional fracture probability) to get a better understanding of the interaction between the calculated sensitivities.
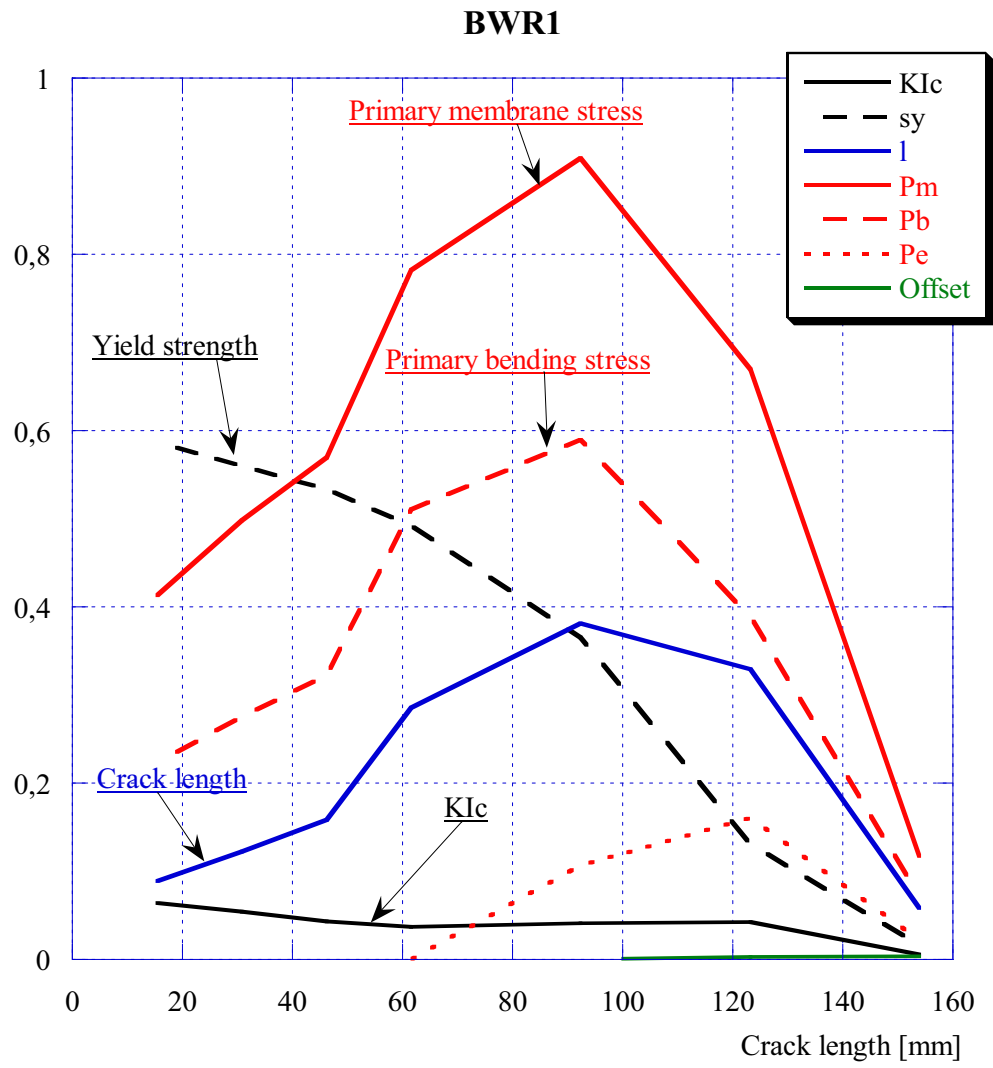
Figure 8.13.1. The normalised sensitivity of the conditional probability of failure (fracture) P_f with respect to the given mean values (for the baseline case BWR1).
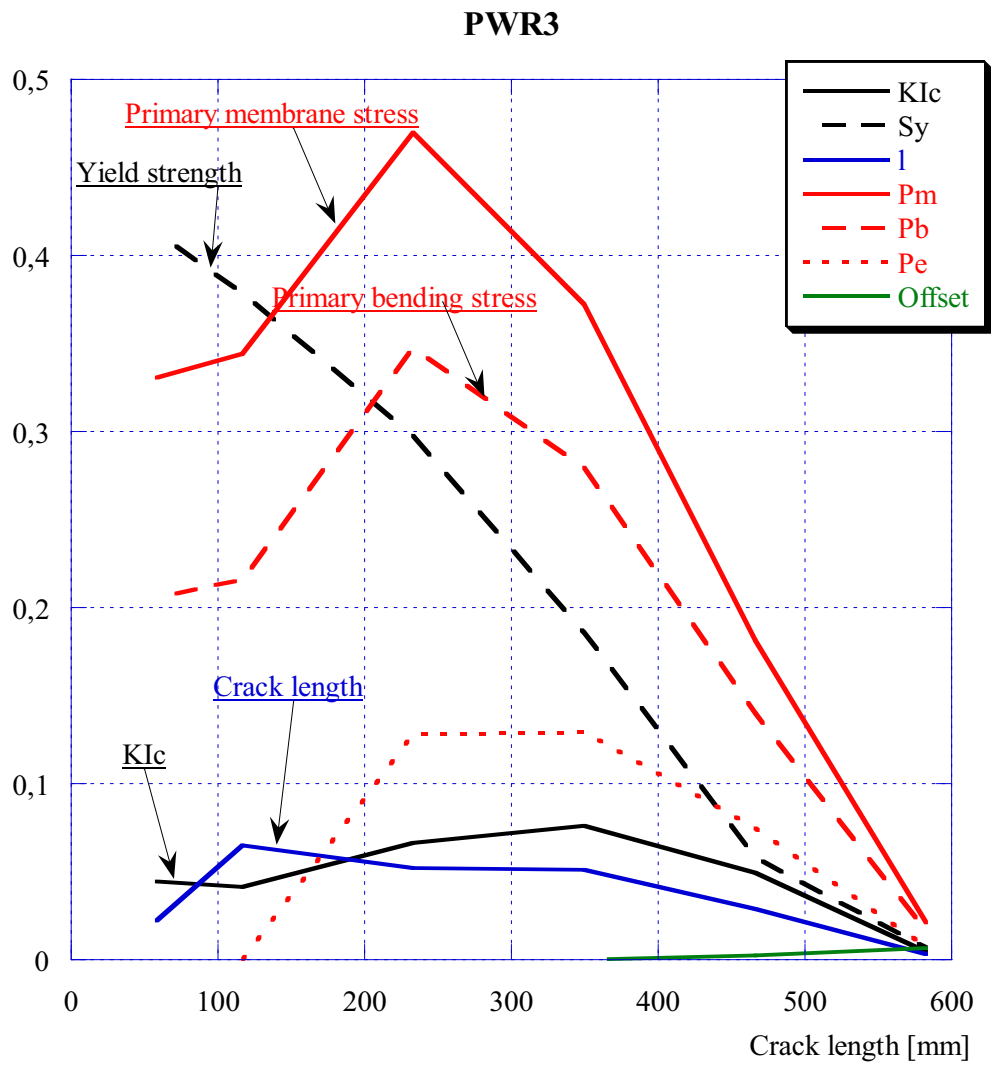
Figure 8.13.2. The normalised sensitivity of the conditional probability of failure (fracture) P_f with respect to the given mean values (for the baseline case PWR3).
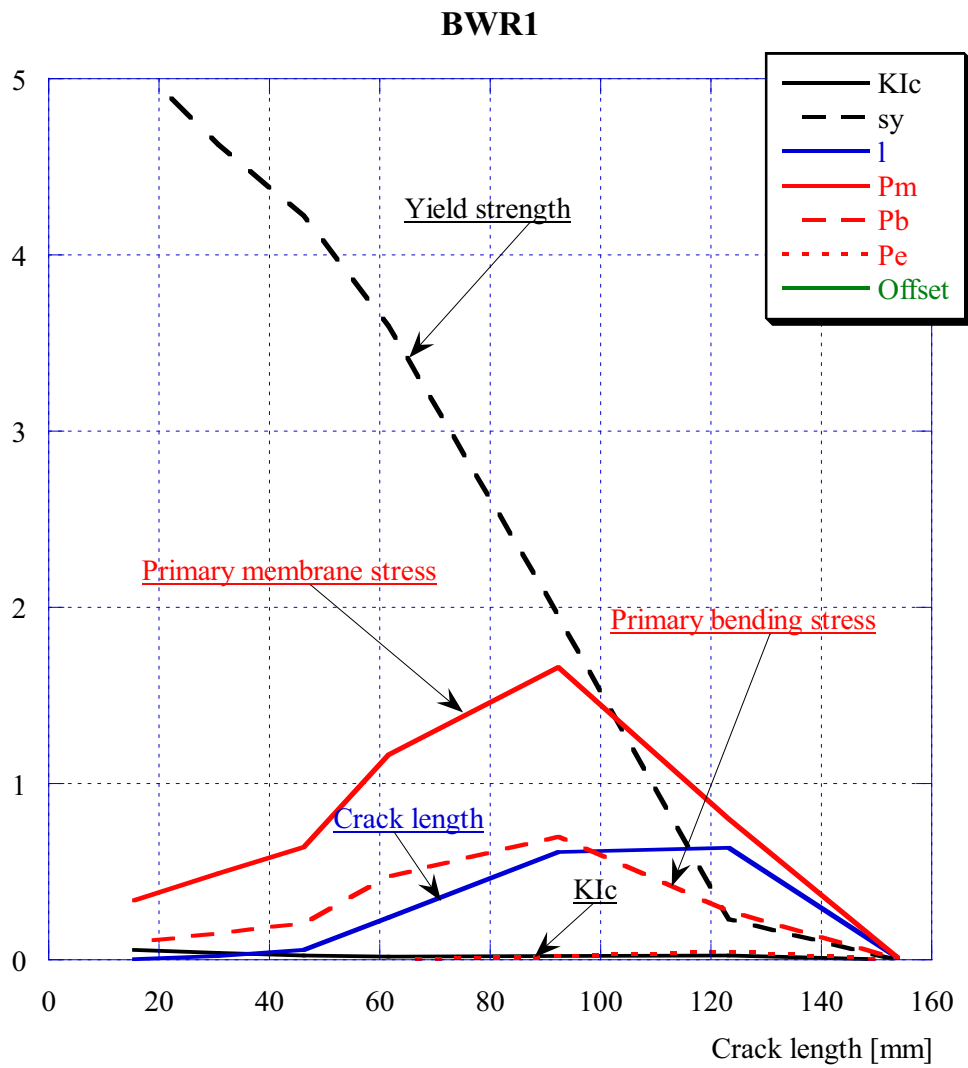
Figure 8.13.3.   The normalised sensitivity of the conditional probability of failure (fracture) P_f with respect to the given values of standard deviation (for the baseline case BWR1).
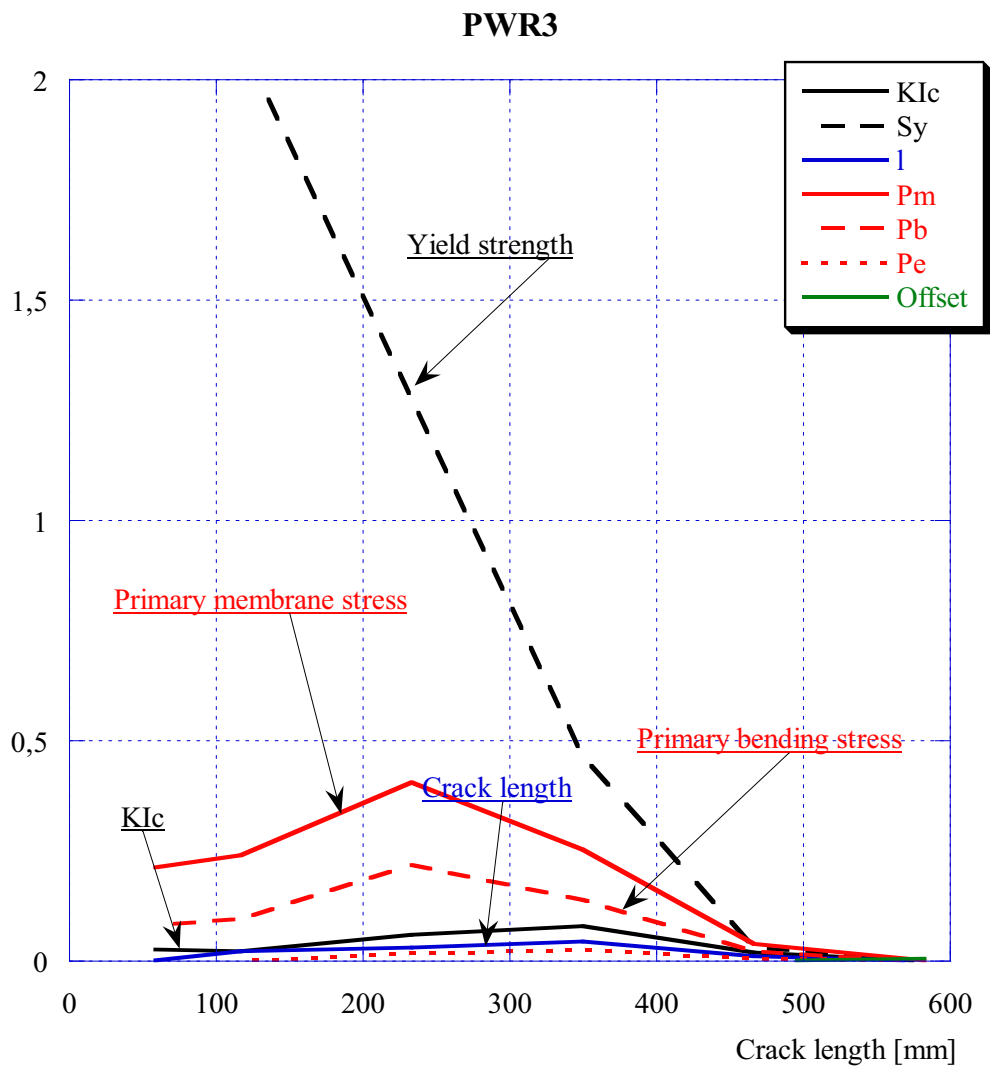
PWR3

Figure 8.13.4. The normalised sensitivity of the conditional probability of failure (fracture) P_f with respect to the given values of standard deviation (for the baseline case PWR3).

As seen from the figures above, the yield strength, primary membrane stress and primary bending stress dominates the analysis using the conditions given in this sensitivity analysis (both for BWR1 and PWR3). This is the case both when changing the given mean values and the given values for the standard deviation. This is reasonable, since the analysis is mainly controlled by the limit load.

From Fig. 8.13.1-8.13.2, one can see that a change of the mean value of the primary membrane stress has the largest impact on the resulting conditional fracture probabilities (when comparing with the mean values of the remaining parameters).

From Fig. 8.13.3-8.13.4, one can see that a change of the standard deviation value of the yield strength has the largest impact on the resulting conditional fracture probabilities (when comparing with the standard deviation values of the remaining parameters).

Finally, from Fig. 8.13.1-8.13.4, one can see that a change of the standard deviation value of the yield strength has the overall largest impact on the resulting conditional fracture probabilities (when comparing with the mean values and standard deviation values of all the parameters). The conclusion is that the chosen value of standard deviation of the yield strength totally dominates the absolute values the calculated conditional fracture probabilities (the analysis, for the chosen baseline cases, is mainly controlled by the limit load).

8.14 Sensitivity study – Comparison with NUREG/CR-6004

There exists an extensive study on probabilistic pipe fracture evaluations for application to leak-rate detection requirements. It is published in a NUREG-report CR-6004 [19] and a comparison between these results and the results from the present study would be of interest.

The probabilistic model in [19] was applied to sixteen nuclear piping systems in BWR and PWR. However, it is quite difficult to make a direct comparison between these results [19] and the results from this study. This has to do with the differences in the underlying deterministic fracture mechanics models (this study uses the R6 method and the so-called LBB.ENG2 method is used in [19]) and also the assumptions regarding loading conditions on the piping systems (this study uses the actual data from the loading specifications including weld residual stresses, in [19] loading data as a percentage of the service level A limits is used).

However, it is possible to make a comparison between the two studies for a case with similar (but not equal) input data and compare the importance factors from the two studies. From this study, we use the results from PWR3 and from [19] we use the design point data given in Appendix F [19]. The importance factors from this study are given in Fig. 8.14.1.
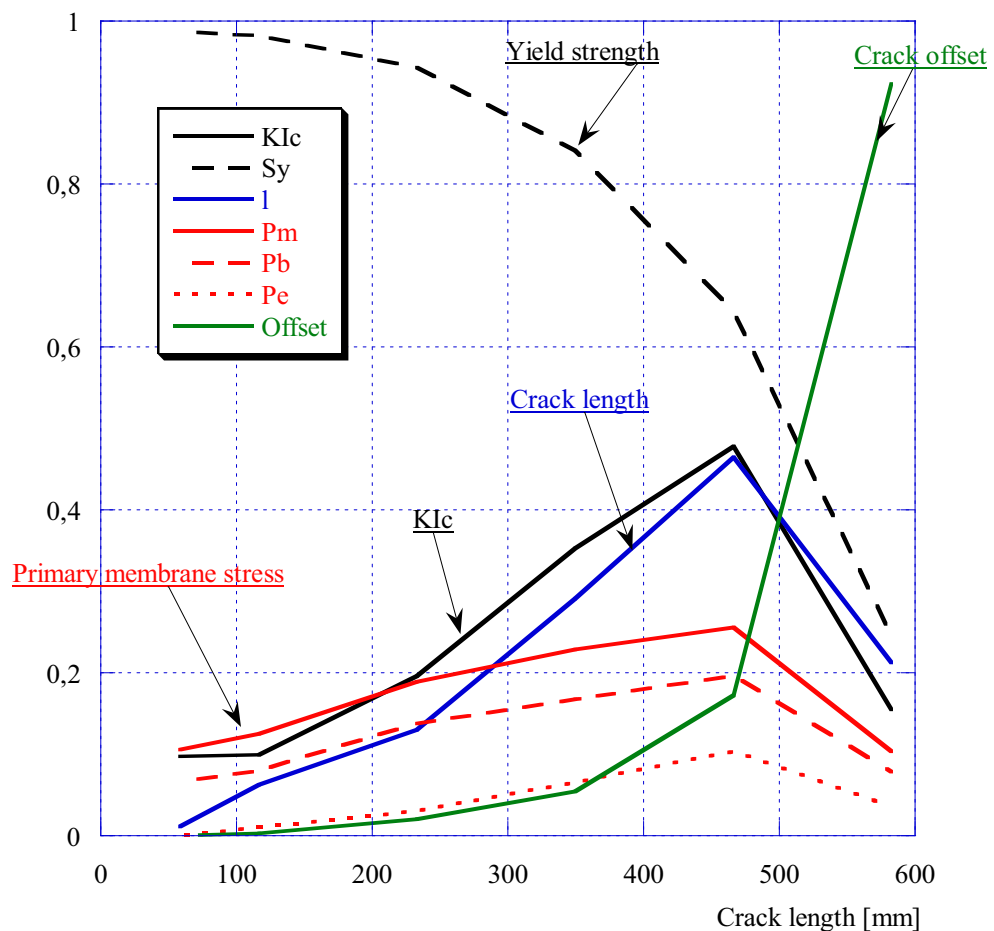
Figure 8.14.1. Importance factors from this study.

Using the importance factors at a specific crack length ($l = 350$ mm) from Fig. 8.14.1, gives comparable conditions as the ones given in [19]. The importance factors from Fig. 8.14.1 (at $l = 350$ mm) is given in Fig. 8.14.2.
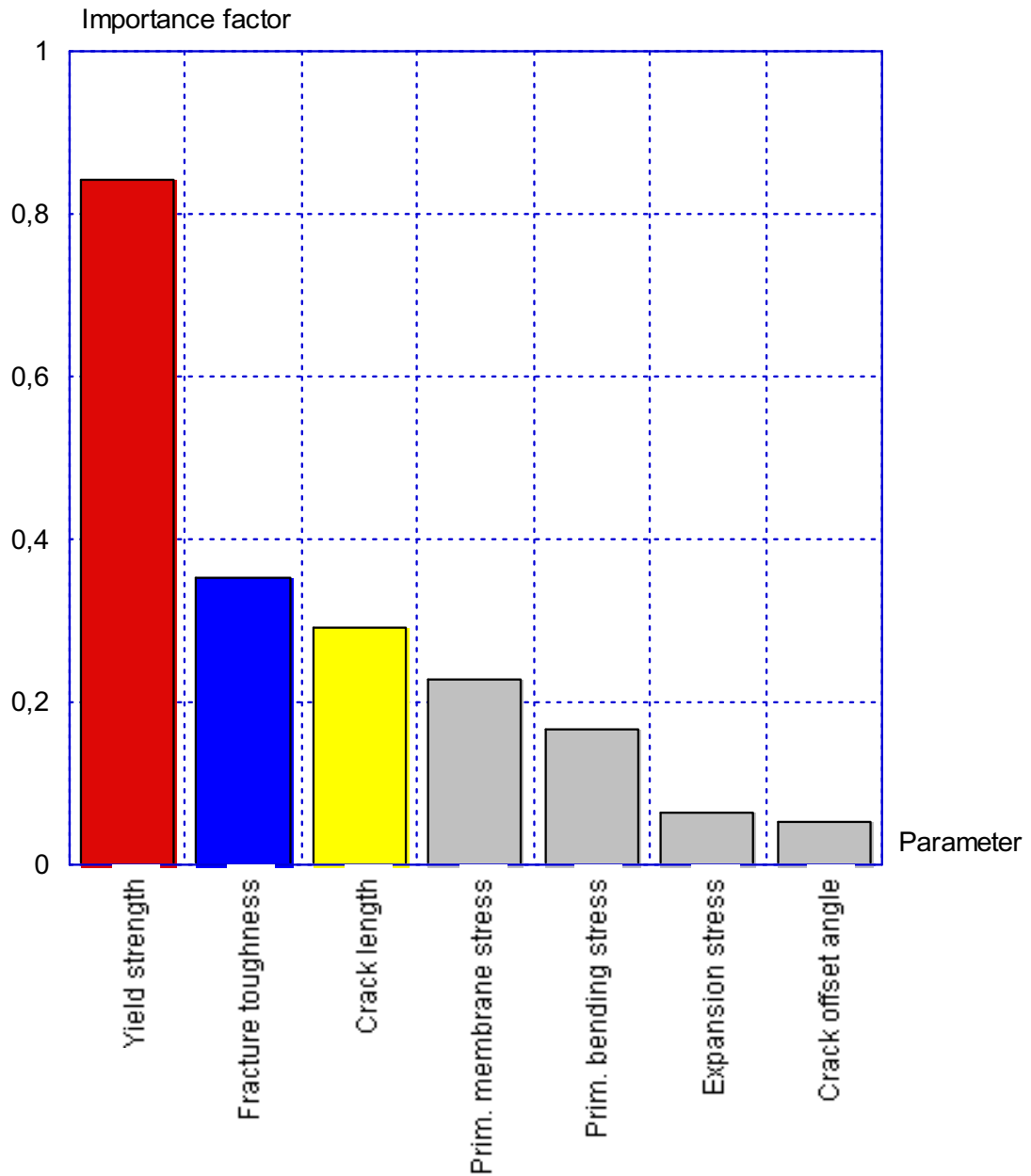
Figure 8.14.2. Importance factors from this study (at $l = 350$ mm).

In Fig. 8.14.2, the importance factor related to yield strength is given in red, fracture toughness in blue and crack length in yellow. The importance factors from [19] are presented in Fig. 8.14.3, using the same colour representation as above.
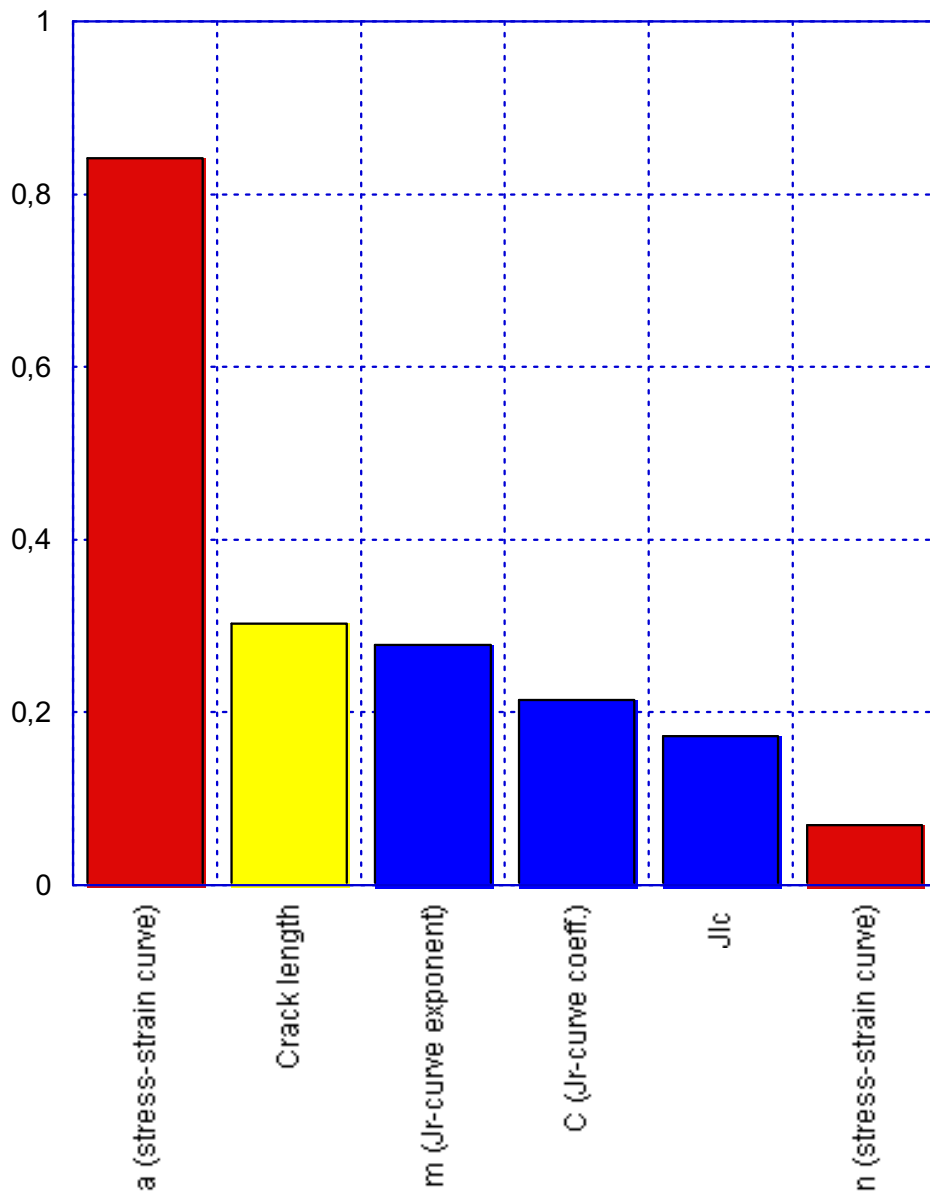
Figure 8.14.3. Importance factors from the example in NUREG-report CR-6004 [19].

From the comparison presented in this section, the following was concluded:

- In both studies, parameters related to the stress-strain curve dominate the analysis.
- In both studies, parameters related to the crack length and fracture toughness are of equal importance.

9 COMPARISON BETWEEN THE DETERMINISTIC GUIDELINES AND PROBABILISTIC APPROACH FOR LBB

An extensive sensitivity study, as presented in section 8, gives an insight on the interaction between the different parameters in an LBB analysis and also how these parameters contribute to the calculated conditional fracture probabilities. However, the probabilistic approach, as defined in this report, can also be used to investigate different deterministic assumptions within the new deterministic guidelines (as given in section 2).

As an example, we investigate the following deterministic assumption: According to the guidelines, it should be a margin between the calculated critical crack size (l_c) and the postulated leakage crack size (l_p) of at least 2.

To be able to check this condition, the following simple assumptions were made:
- The deterministic critical crack size was evaluated using the mean values from the probabilistic analysis.
- The leakage was evaluated at the mean value of the postulated crack length.
- It is then possible to plot the margin l_c / l_p and the conditional fracture probability (P_f) as a function of the leakage flow rate.

The two baseline cases BWR1 (results given in Fig. 9.1-9.2) and PWR3 (results given in Fig. 9.3-9.4) were used in this comparison between the deterministic guidelines and the probabilistic approach for LBB.

Note that the fracture probabilities in this section are equivalent to the conditional probability of fracture, given the existence of a leaking through-thickness crack.
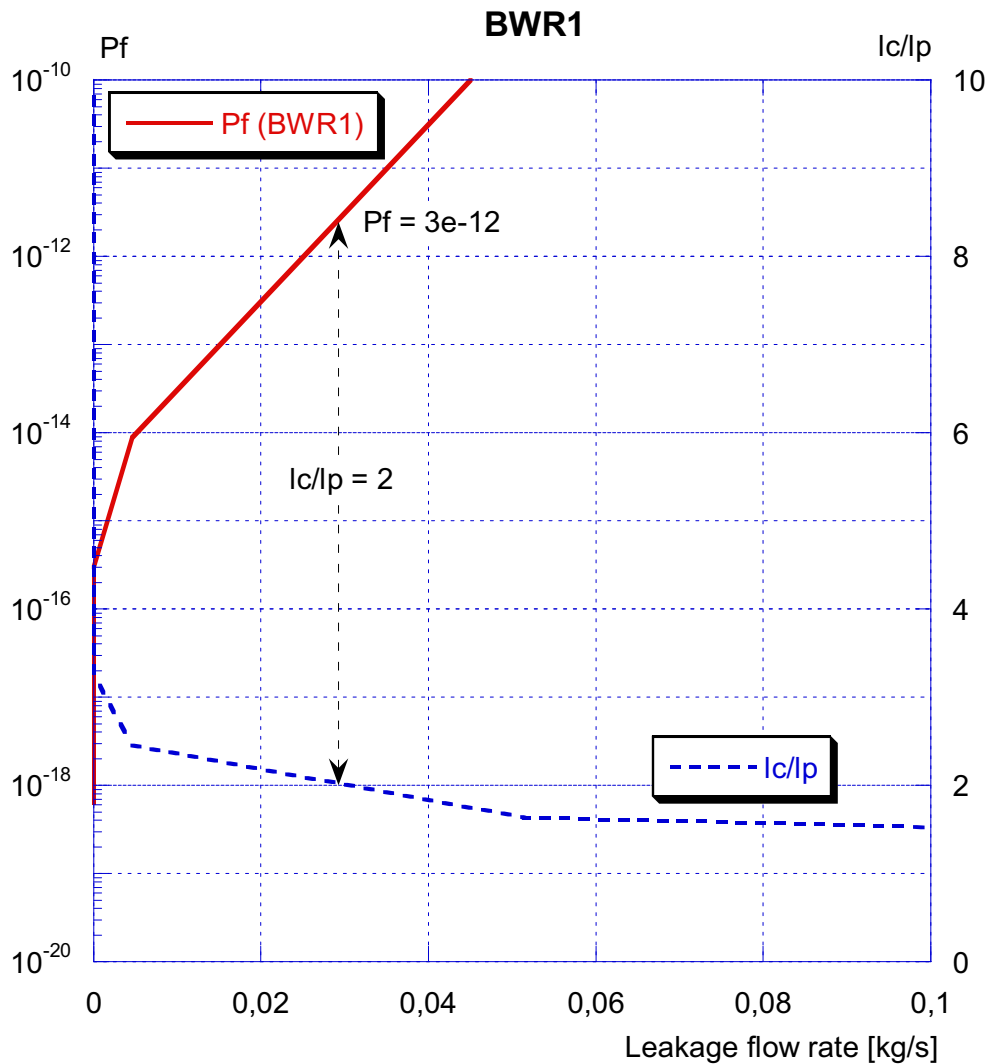
Figure 9.1. Check of the deterministic condition, relating to the margin between the calculated critical crack size and the postulated leakage crack size (for the baseline case BWR1).

As shown in Fig. 9.1 (for the baseline case BWR1), the condition that the margin between the calculated critical crack size and the postulated leakage crack size should be at least 2, is equivalent to a probability of fracture less or equal to $3 \cdot 10^{-12}$ (at a leakage flow rate less or equal to 0.03 kg/s). Please note that, according to the guidelines, you want to have a leakage which is 10 times larger than the detection limit. This means that even if the margin $l_c / l_p = 2$ is equivalent to a small conditional probability of fracture, the corresponding leak flow rate will be difficult to detect if the margin 10 on detectable leak flow rate should be fulfilled.

For a leakage flow rate equal to 10 gpm (equivalent to 0.631 kg/s, which is 10 times larger than the detection limit), the margin l_c/l_p is about 1.05 (which is very small, i.e. there is no margin between the leakage crack size and the critical crack size) and the corresponding conditional probability of fracture is about 0.1 (which is very high). This relation, for the baseline case BWR1, is visualised in Fig. 9.2. These results give another explanation on why the small diameter pipes generally have more difficulty to fulfill the deterministic acceptance criteria.
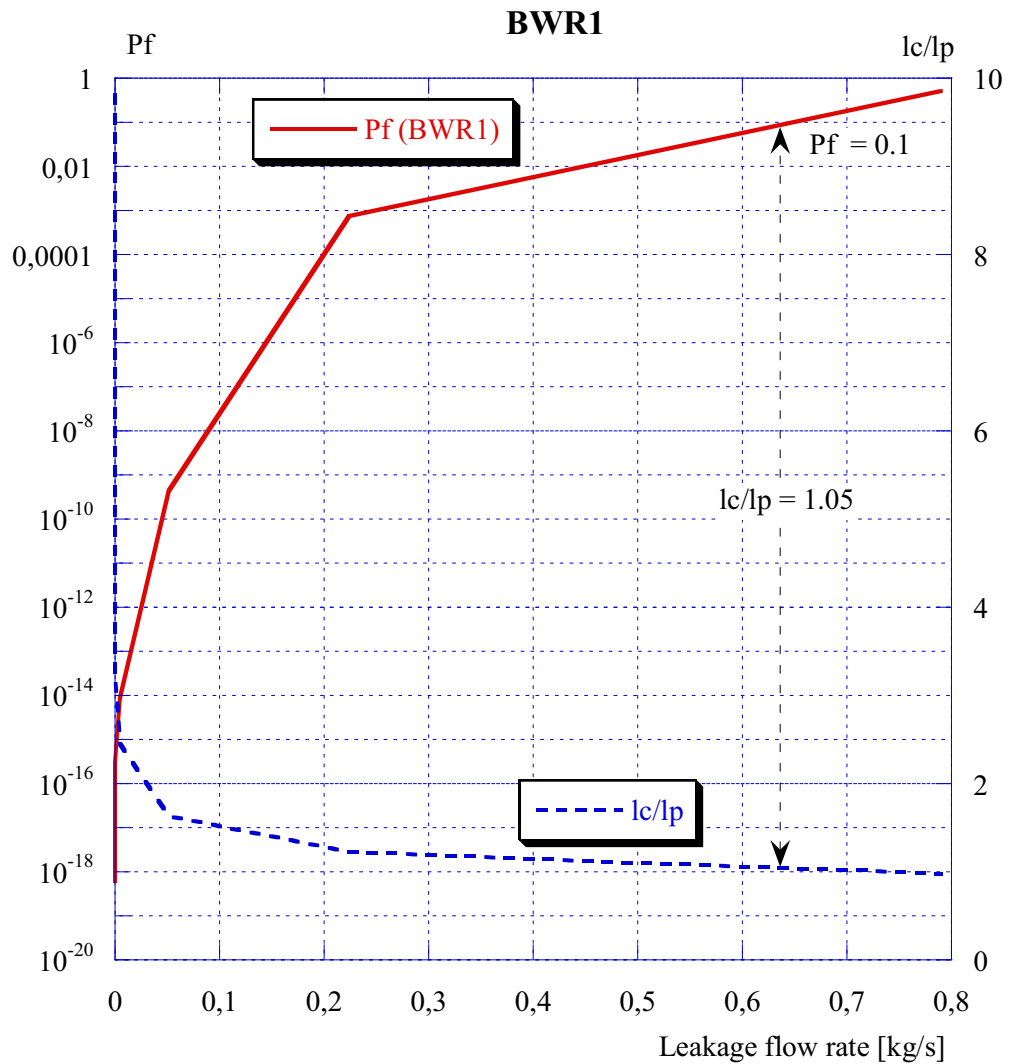
Figure 9.2. Check of the deterministic condition, relating to the margin between the calculated critical crack size and the postulated leakage crack size at a leakage flow rate equal to 10 times the detection limit (for the baseline case BWR1).
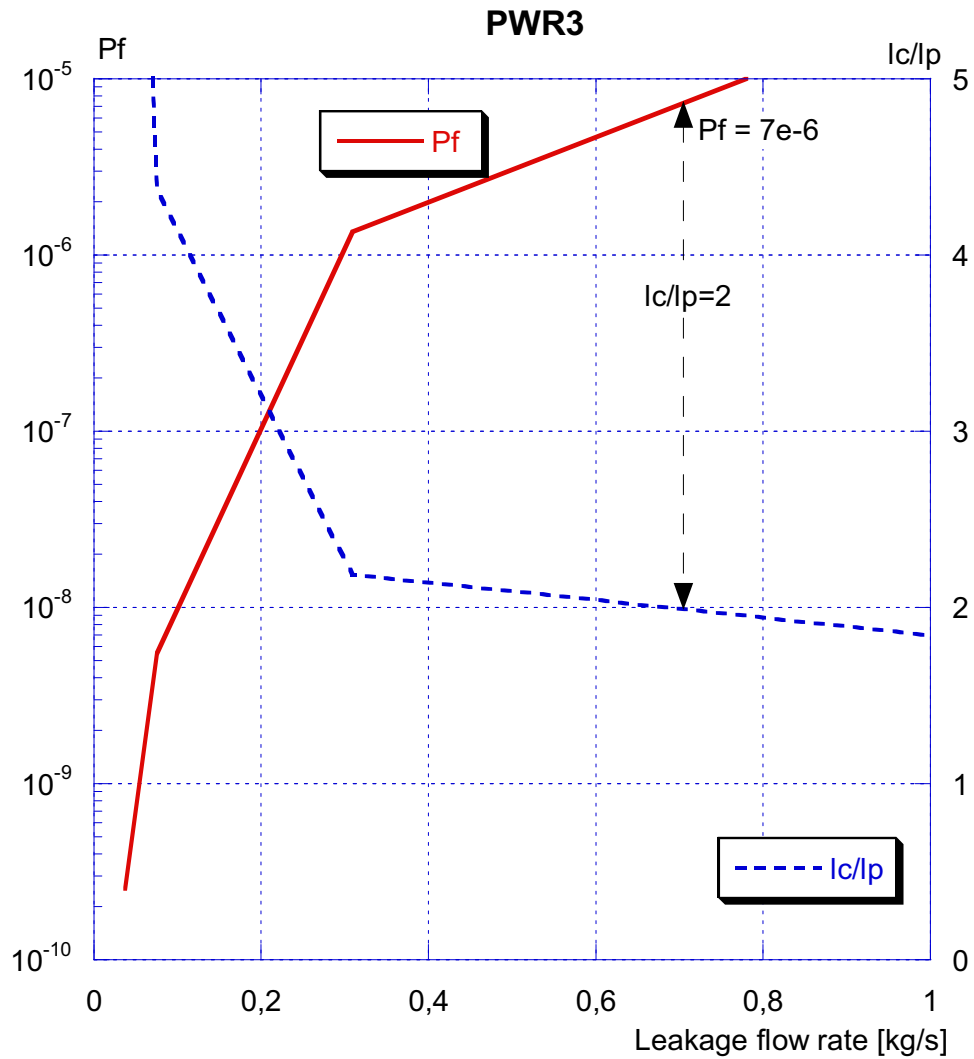
Figure 9.3. Check of the deterministic condition, relating to the margin between the calculated critical crack size and the postulated leakage crack size (for the baseline case PWR3).

As shown in Fig. 9.3 (for the baseline case PWR3), the condition that the margin between the calculated critical crack size and the postulated leakage crack size should be at least 2, is equivalent to a probability of fracture less or equal to $7 \cdot 10^{-6}$ (at a leakage flow rate less or equal to 0.7 kg/s). This leakage is more relevant, if compared to the condition related to the detection limit.

For a leakage flow rate equal to 10 gpm (equivalent to 0.631 kg/s, which is 10 times larger than the detection limit), the margin l_c / l_p is about 2.0 and the corresponding conditional probability of fracture is about $6 \cdot 10^{-6}$. This relation, for the baseline case PWR3, is visualised in Fig. 9.4.
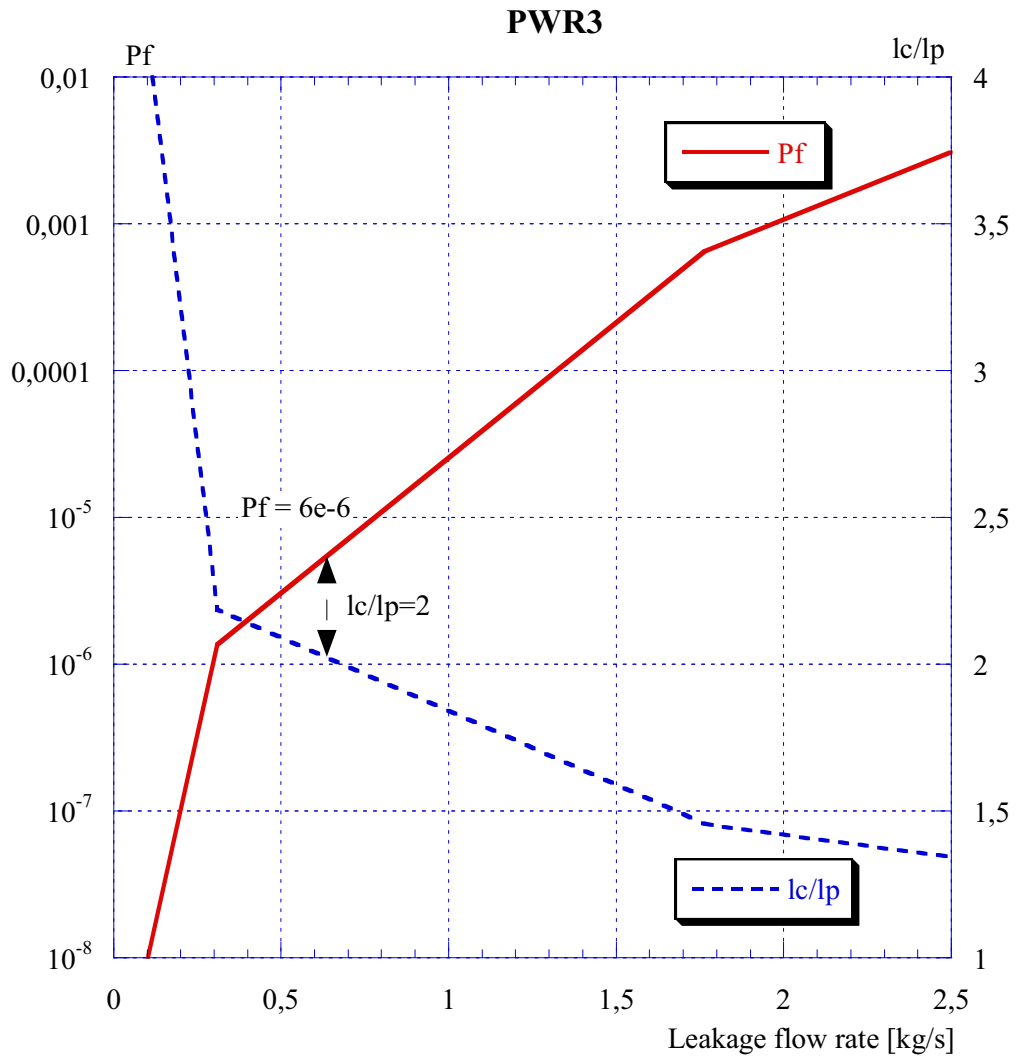
Figure 9.4. Check of the deterministic condition, relating to the margin between the calculated critical crack size and the postulated leakage crack size at a leakage flow rate equal to 10 times the detection limit (for the baseline case PWR3).

Finally, it could be of interest to investigate how a change on the considered condition influences the calculated fracture probabilities and the related leakage flow rates. Such an investigation is presented in table 9.1.

Table 9.1. Check of the deterministic condition, relating to the margin between the calculated critical crack size and the postulated leakage crack size.

Margin	BWR1		PWR3	
	P_f	Leakage flow rate [kg/s]	P_f	Leakage flow rate [kg/s]
1.5	4.9·E-8	0.108	4.5·E-4	1.68
1.8	4.9·E-11	0.0420	3.6·E-5	1.08
2.0	3.4·E-12	0.0305	6.5·E-6	0.680
2.2	2.4·E-13	0.0190	1.3·E-6	0.307
2.5	7.2·E-15	0.00433	6.2·E-7	0.275

Obviously, for the baseline case BWR1, there is a strong influence on the fracture probability when changing the value of margin between the calculated critical crack size and the postulated leakage crack size. Also shown, for the baseline case PWR3, the influence on the fracture probability is not that large. However, there is a strong relation between the calculated fracture probabilities and the related leakage flow rates. This relation is given in table 9.1, and here one can see that the margin 1.5 for the case BWR1, in terms of the corresponding leakage flow rate, is almost equivalent to the margin 2.5 using the case PWR3.

10   CONCLUSIONS

Recently, the Swedish Nuclear Power Inspectorate has developed guidelines on how to demonstrate the existence of Leak Before Break (LBB). The guidelines, mainly based on NUREG/CR-6765, define the steps that must be fulfilled to get a conservative assessment of LBB acceptability. As a complement and also to help identify the key parameters that influence the resulting leakage and failure probabilities, a probabilistic LBB approach has been developed. In this report, the proposed probabilistic LBB approach is defined and implemented into the software ProLBB (using the calculation engine from the software ProSACC). The main conclusions, from the study presented in this report, are summarized below.

-   The probabilistic approach developed in this study was applied to different piping systems in both Boiler Water Reactors (BWR) and Pressurised Water Reactors (PWR). Pipe sizes were selected so that small, medium and large pipes were included in the analysis. Three BWR and three PWR pipes were selected to be the baseline cases. The present study shows that the conditional probability of fracture is in general small for the larger diameter pipes when evaluated as function of leak flow rate. However, when evaluated as function of fraction of crack length around the circumference, then the larger diameter pipes will belong to the ones with the highest conditional fracture probabilities.

-   The total failure probability, corresponding to the product between the leak probability and the conditional fracture probability, will be very small for all pipe geometries when evaluated as function of fraction of crack length around the circumference. This is mainly due to a small leak probability which is consistent with expectations since no active damage mechanism has been assumed. This also means that it can be very conservative to assume the existence of a leaking crack when there is a high confidence of the absence of any active damage mechanism.

-   One of the objectives of the approach was to be able to check the influence of off-centre cracks (i.e. the possibility that cracks occur randomly around the pipe circumference). To satisfy this objective, new stress intensity factor solutions for off-centre cracks were developed.

-   Also to check how off-centre cracks influence crack opening areas, new form factors solutions for COA were developed taking plastic deformation into account. The results shows that using elastic form factors only, gives a maximum error of ~20 % compared to the elastic-plastic finite element analysis when the applied L_r is below ~0.5. For larger L_r-values the error becomes quite large and elastic form factors should not be used for these cases.

-   The influence from an off-center crack position on the conditional probability of fracture is not important when assuming a uniform distribution around the circumference of the crack position. This is because the result is dominated totally by the center crack position. However, if the crack position is treated as a deterministic parameter, the conditional probability of fracture is strongly dependent on the position of the crack, especially for large off-center cracks.

- The weld residual stresses have quite an impact on the resulting fracture probabilities, especially for smaller cracks (this is relevant both for small and large pipes).
    - The difference (with/without the weld residual stresses) would be smaller if only taking the weld residual stresses into account in the calculation of fracture probability and not in the calculation of leakage flow rate (which is incorrect, since both effects should be included in the analysis).
    - The influence from the weld residual stresses on the calculation of leakage flow rate is largest for a thin-walled pipe. This is reasonable, since a local bending stress is used which closes the crack.
    - The influence from the weld residual stresses on the calculation of fracture probability is largest for one of the thick-walled pipes. This is related to the K_I-calculations and the fact that this case is more sensitive to the chosen fracture toughness in the calculation of probability of fracture.

- The conditional fracture probabilities are relatively sensitive to the crack morphology. The conditional fracture probability as function of leak flow rate will be higher for stress corrosion cracks compared to fatigue cracks. This is due to that a stress corrosion crack has a crack morphology which restrains the leak flow rate more compared to a fatigue crack which means that you need a larger crack to obtain an equivalent leak flow rate.

- In the formal sensitivity analyses, it is shown that the standard deviation of the yield strength has the strongest influence on the conditional fracture probability (when comparing with the mean values and standard deviation values of all the parameters included in the analysis). This is reasonable, since the analysis is mainly controlled by the limit load for all crack lengths up to very long cracks.

- This study has given an indication of the relation between the deterministic LBB-criteria (ratio of critical crack length and leakage crack length equal to 2 and margin of 10 on a detectable leak flow rate) and the corresponding conditional fracture probability. As expected, it is easier to fulfil the deterministic LBB-margins for a large diameter pipe compared to a small diameter pipe.

11 ACKNOWLEDGEMENT

12 REFERENCES

[1] BRICKSTAD, B., (2005-11-22), "Rörbrottsskydd och läckage före brott (LBB)", SKI-utredningsrapport, SKI 2005/83, Statens kärnkraftinspektion.

[2] —, (1971), "General Design Criterion 4, Environmental and Missile Design Basis", 10CFR50, Appendix A, US Code of Federal Regulations.

[3] —, (1987), "Leak-Before-Break Evaluation Procedures", Draft Standard Review Plan 3.6.3 (never published in final form), U. S. Nuclear Regulatory Commission.

[4] —, (2004), "SKIFS 2004:2, Statens kärnkraftinspektions föreskrifter om konstruktion och utförande av kärnkraftsreaktorer, Statens kärnkraftinspektions författningssamling.

[5] SCOTT, P. M., OLSON, R. J., and G. M. WILKOWSKI., (2002), "Development of Technical Basis for Leak-Before-Break Evaluation Procedures", Report NUREG/CR-6765, U. S. Nuclear Regulatory Commission.

[6] —, (1973), "Reactor Coolant Pressure Boundary Leakage Detection Systems", Regulatory Guide 1.45, US Atomic Energy Commission.

[7] DILLSTRÖM, P., et. al. (2004), "A combined deterministic and probabilistic procedure for safety assessment of components with cracks – handbook", DNV Research Report 2004/01, Rev. 4-1, Det Norske Veritas AB.

[8] DILLSTRÖM, P., and W. ZANG., (2005), User manual ProSACC Version 1.0, DNV Research Report 2004/02, Det Norske Veritas AB.

[9] RACKWITZ, R., and B. FIESSLER., (1978), "Structural Reliability Under Combined Random Load Sequences", *Journal of Computers and Structures*, V 9, pp 489-494.

[10] DER KIUREGHIAN, A., and T. DAKESSIAN., (1998), "Multiple design points in first and second-order reliability", *Structural Safety*, V 20, pp 37-49.

[11] FIRMATURE, R., and S. RAHMAN., (2000), "Elastic-plastic analysis of off-center cracks in cylindrical structures", *Eng. Fract. Mech.*, Vol. 66, pp. 15-39.

[12] RAHMAN, S., CHEN, G., and R. FIRMATURE., (2000), "Probabilistic analysis of off-center craxcks in cylindrical structures", *Int. J. of Pres. Ves. and Pip.*, Vol. 77, pp. 3-16.

[13] —, (2003), "ABAQUS Users manual", Version 6.3, Hibbit, Karlsson and Sorenson, USA.

[14] DILLSTRÖM, P., ANDERSSON, M., och W. ZANG, (2006-02-05), "Bedömning av svetsegenspänningarnas betydelse för skattning av läckageflöden", Teknisk Rapport 50000570-1, Rev. 0, Inspecta Technology AB.

[15] —, (2003), "SQUIRT: Seepage Quantification of Upsets In Reactor Tubes, User's Manual", Windows Version 1.1, Battelle Informal Report, Battelle, Columbus, Ohio.

[16] HENRY, R. E., and H. K., FAUSKE., (1970), "Two-Phase Critical Flow at Low Qualities, Part I: Experimental", *Nuclear Science and Engineering*, Vol. 41, pp. 79-91.

[17] SCHIMPFKE, T., (2004), "NURBIM, WP-4, Review and benchmarkning of SRMs and associated software, Appendix B, Fatigue benchmark study", NURBIM Report D4 App. B.

[18] DITLEVSEN, O., and H. O. MADSEN., (1996), *Structural reliability methods*, JohnWiley & Sons Ltd, Baffins Lane, Chichester, 372p.

[19]   RAHMAN, S., GHADIALI, N., PAUL, D., and G. WILKOWSKI., (1995), Probabilistic Pipe Fracture Evaluations for Leak-Rate-Detection, Report NUREG/CR-6004 & BMI-2174, U. S. Nuclear Regulatory Commission.

APPENDIX A. STRESS INTENSITY FACTORS FOR OFF-CENTRE CRACKS

In this appendix, new stress intensity factors solutions for off-centre cracks are given using different pipe geometries and material properties.

A1   LOAD APPLICATION

A pure bending moment M is applied at the end surface of the pipe. The moment is projected into two components M_x and M_y (see Fig. A1.1) such that

$$\begin{cases} M_x = M\sin(\psi) \\ M_y = M\cos(\psi) \end{cases}.$$

(A1)
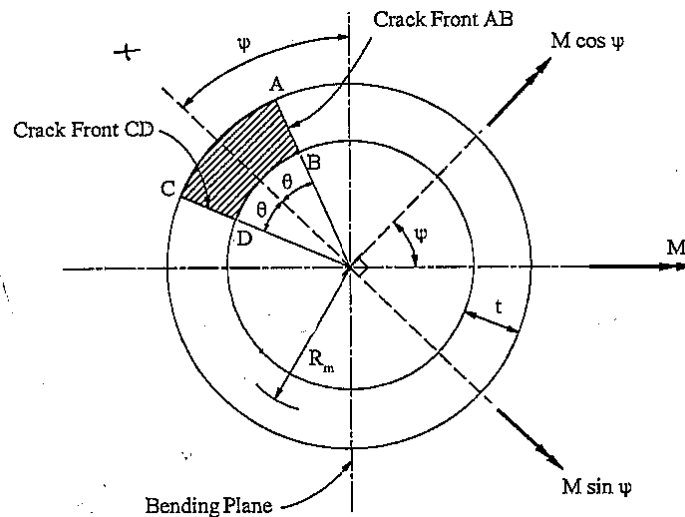
Figure A1.1. Illustration of the geometry and load application for an off-centre crack.

It is observed that both moment components defined in Eqn. (A1) will generate a tensile normal stress at crack front *AB* while the moment component M_x will generate a compressive normal stress at crack front *CD*.

A2   MATERIAL PROPERTIES

Two different materials are considered in the analysis. They represent one typical carbon steel and one typical austenitic stainless steel. The material properties are listed in Table A2.1 and the stress-strain relations are plotted in Fig. A2.1.

Table A2.1. Material properties.

Material	E [GPa]	ν	σ_y [MPa]
Carbon steel - CS	200	0.3	360
Stainless steel - SS	180	0.3	180
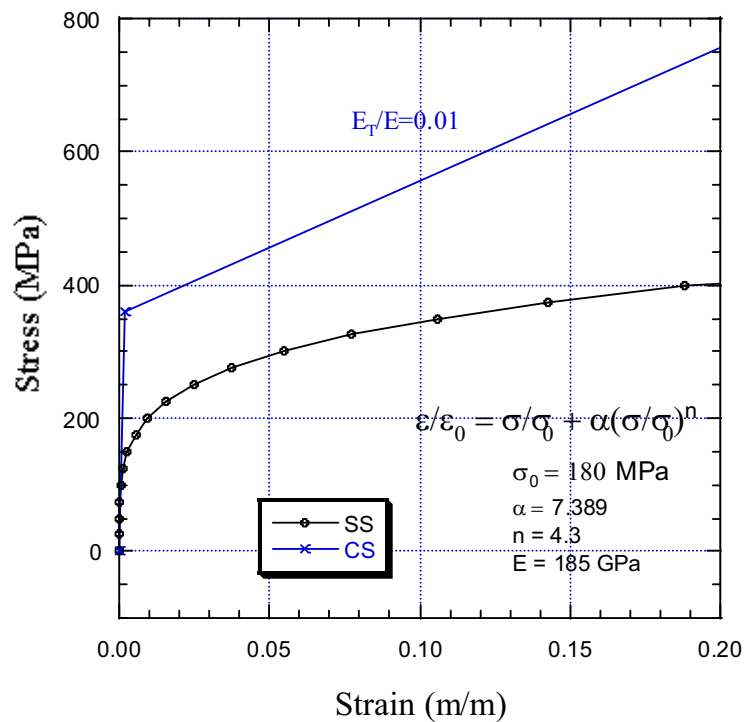
Figure A2.1. Tensile stress-strain curve for Stainless steel - SS and Carbon steel - CS.

A3   DEFINITION OF THE CASES TO BE ANALYSED

In total, 12 cases are considered using different pipe geometries (SKI recommended pipe sizes with an outer diameter between ~100 mm and ~700 mm), crack lengths and material properties. The definitions of the cases are listed in Table A3.1.

Table A3.1. Data for the 12 cases considered in this study.

Case	D_{out} (mm)	t (mm)	R_i/t	Crack length (2θ)	Material
1	114	8.6	5.63	45	CS
2				90	SS
3				135	CS
4				180	SS
5	356	35	4.08	45	CS
6				90	SS
7				135	CS
8				180	SS
9	711	36	8.88	45	CS
10				90	SS
11				135	CS
12				180	SS

Information on the magnitude of the applied bending moment, the plastic limit load parameter L_r and the maximum elastic bending stress are shown in Table A3.2. The result of L_r is for a pipe with a centre crack and the maximum elastic bending stress is calculated for a section without a crack.

Table A3.2. Loading information for the 12 cases considered in this study.

Case	Crack length (2θ)	Material	M_{max} (kN-m)	L_r	σ_b (MPa)
1	45	CS	37.9	1.50	543
2	90	SS	13.7	1.50	196
3	135	CS	17.7	1.50	254
4	180	SS	5.0	1.50	71.2
5	45	CS	1403.3	1.50	543
6	90	SS	506.5	1.50	196
7	135	CS	656.4	1.50	254
8	180	SS	184.0	1.50	71.2
9	45	CS	6660	1.50	543
10	90	SS	2404	1.50	196
11	135	CS	3115	1.50	254
12	180	SS	873.3	1.50	71.2

A4 RESULTS – STRESS INTENSITY FACTORS

The stress intensity factors are calculated using the finite element program ABAQUS, with a sufficiently accurate finite element mesh (example in Fig. A4.0).
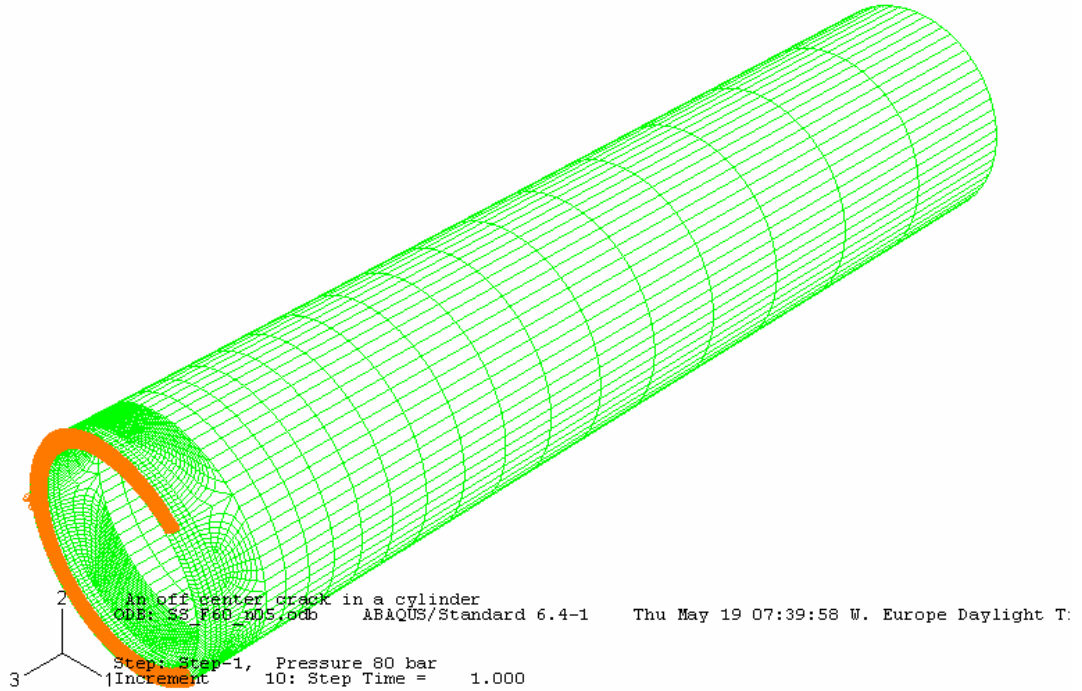
Figure A4.0.   Finite element model used in the calculation of stress intensity factors (example using $2\theta = 90^\circ$ and $\psi = 90^\circ$).

The stress intensity factors are given via the *J*-integral as,

$$K = \sqrt{J} \cdot \sqrt{\frac{E}{1-\upsilon^2}} \; . \tag{A2}$$

In the presentation of the results, the R6 method option 1 is used as an approximate method. The stress intensity factor by the R6 method is calculated as,

$$K_{R6} = \frac{K_{EL}}{f_{R6}(L_r)} \; , \tag{A3}$$

where

$$f_{R6}(L_r) = \left(1 - 0.14 L_r^2\right)\left[0.3 + 0.7\exp\left(-0.65 L_r^6\right)\right] \; , \tag{A4}$$

and

$$K_{EL} = \left[K^0 * \cos(\psi) + K^{90} * \sin(\psi) \right] .$$ (A5)

In Eqn (A5), K^0 is the stress intensity factor of a centre crack ($\psi = 0°$) in a pipe subjected to a bending moment M and K^{90} is the stress intensity factor at crack front AB (defined in Fig. A1.1) for an off centre crack ($\psi = 90°$) subjected to a bending moment M. The comparison is based on the results at the middle point of crack front AB.

Two different alternatives concerning the moment component M_x are used in the approximate evaluation. These two alternatives are defined as,

- Alternative 1: The effect of M_x is included, thus $K^{90} > 0$.

- Alternative 2: The effect of M_x is neglected, thus $K^{90} = 0$.

A4.1 Stress intensity factors for carbon steel

Below, the results for the carbon steel cases 1, 3, 5, 7, 9 and 11 are given as a function of the off-centre crack angle ψ ($\psi = 0°, 30°, 60°, 90°$).

A4.1.1   Results using $\psi = 0^o$

The results for a centre crack ($\psi = 0^o$) in a carbon steel pipe are shown in Figs. A4.1-A4.6.
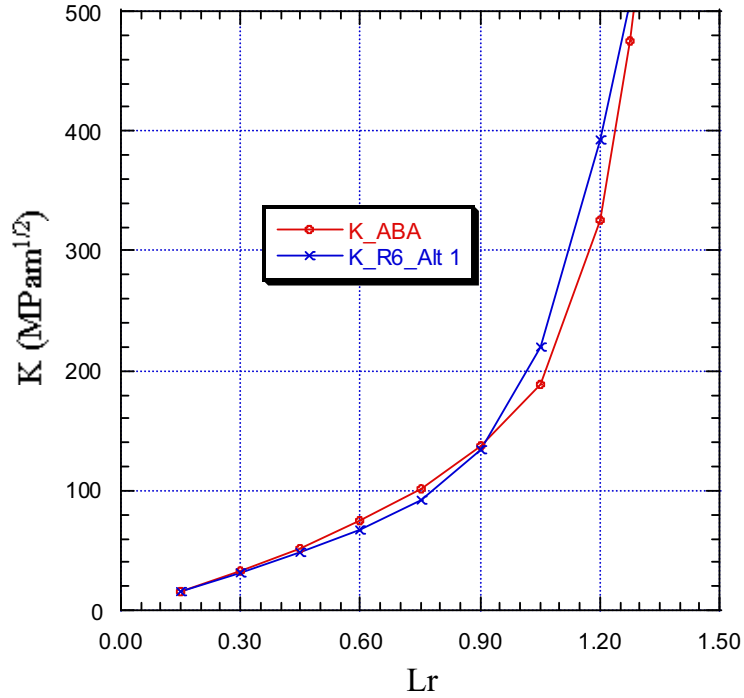
Figure A4.1. Stress intensity factors at the middle point of crack front AB for case 1 ($\psi = 0^o$).
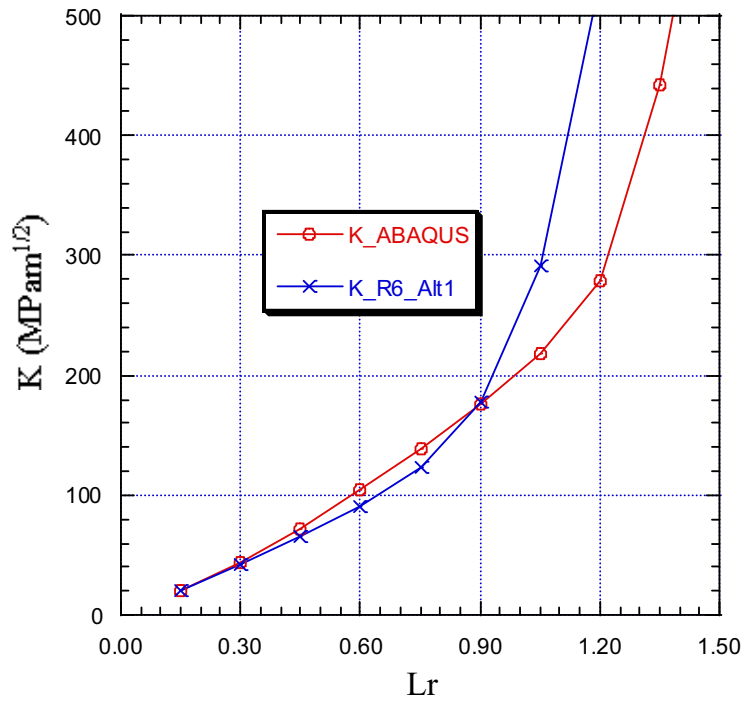
Figure A4.2. Stress intensity factors at the middle point of crack front AB for case 3 ($\psi = 0^o$).
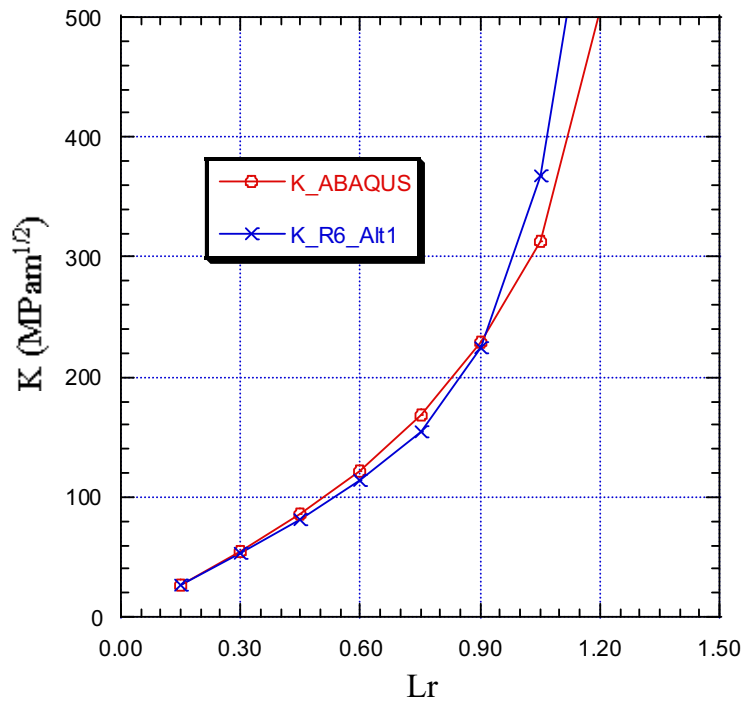
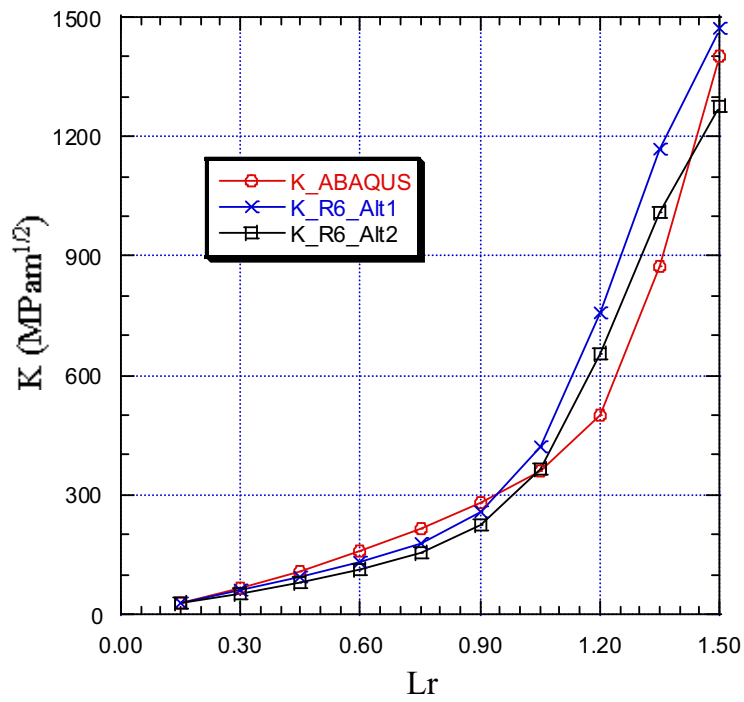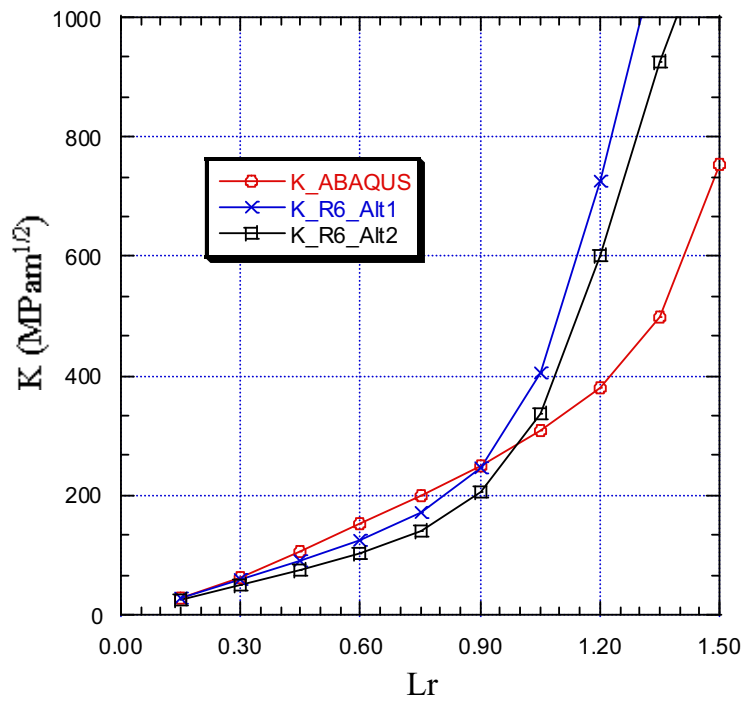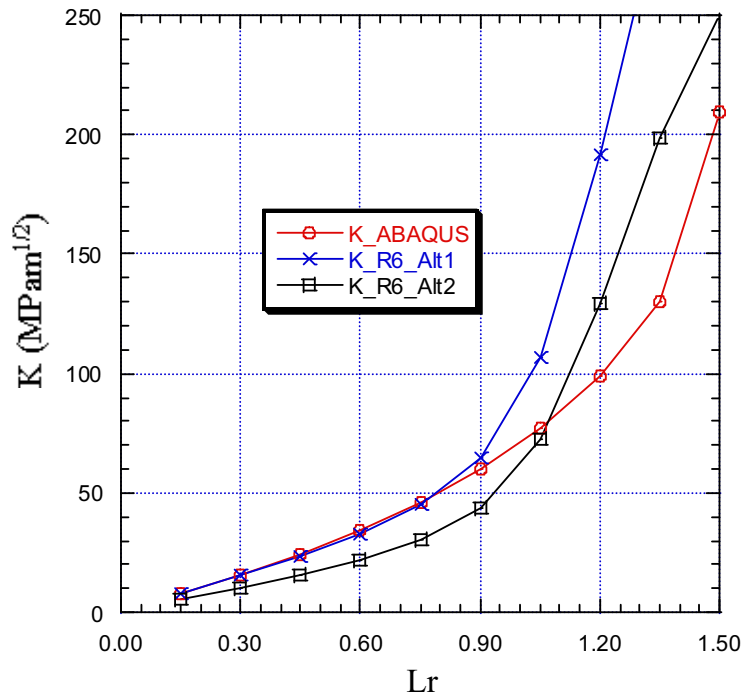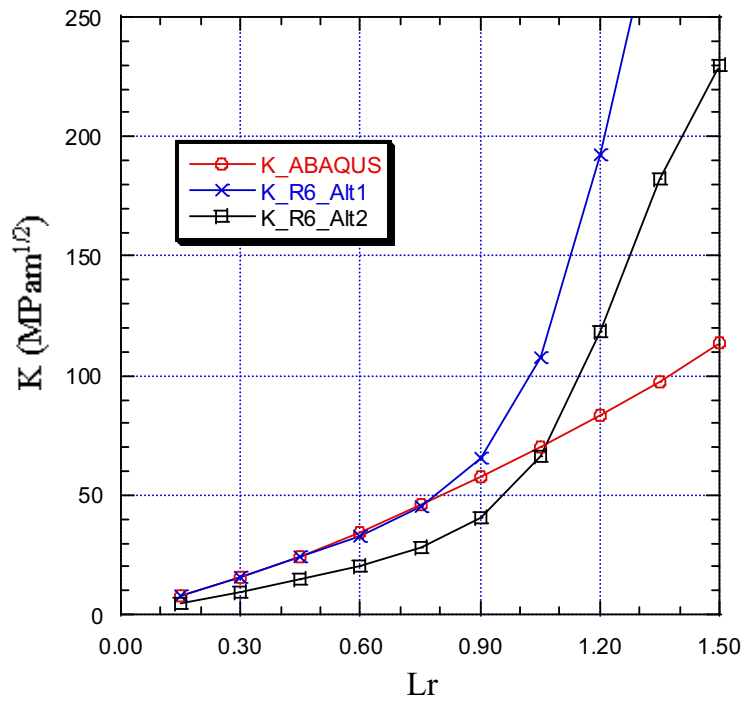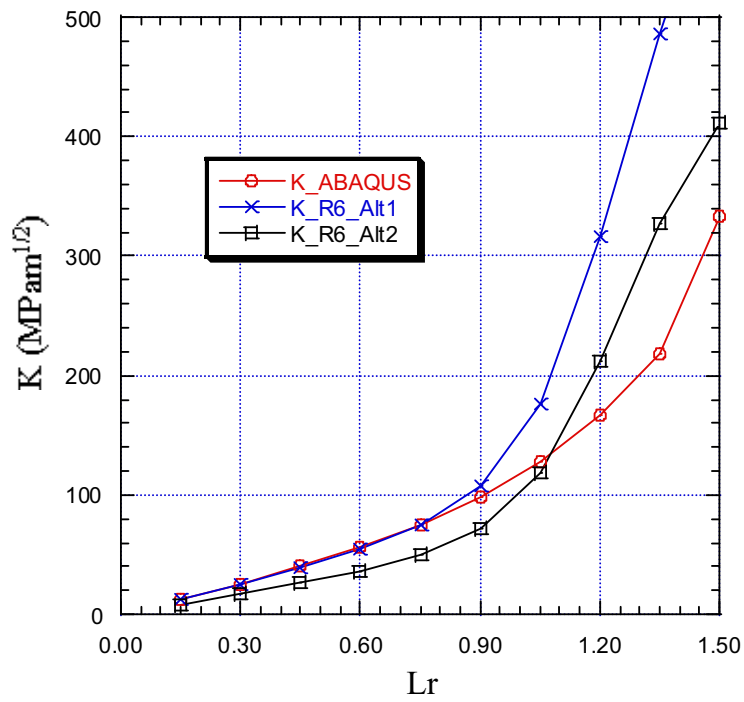Figure A4.3. Stress intensity factors at the middle point of crack front AB for case 5 ($\psi = 0^\circ$).
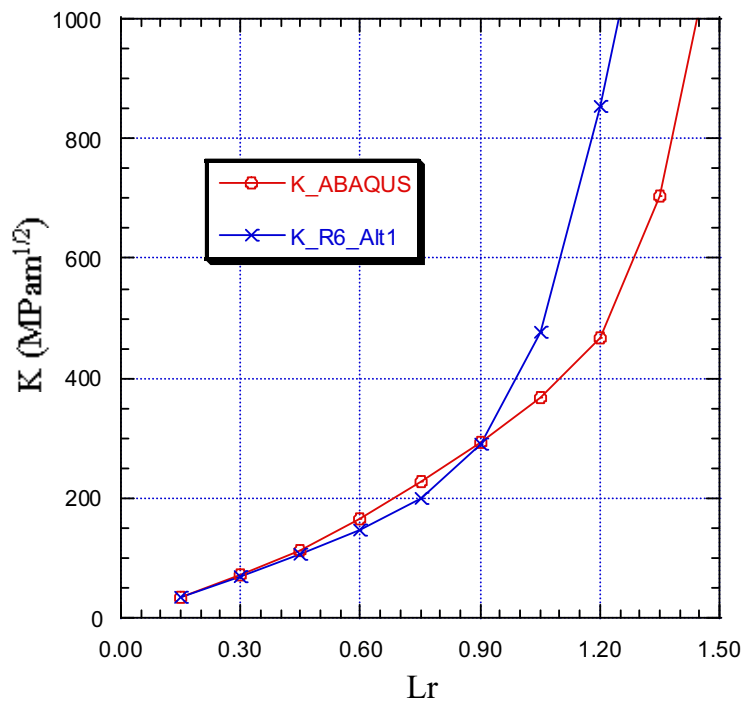
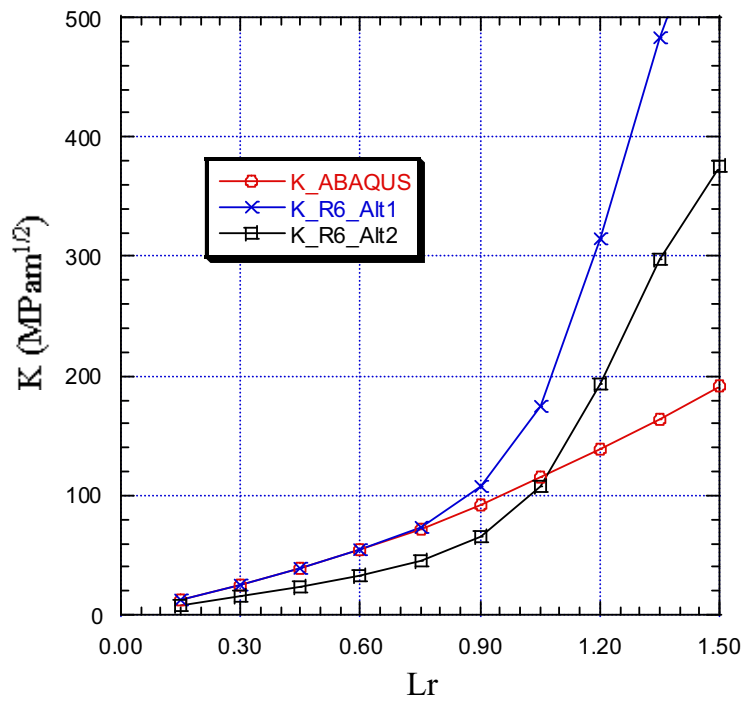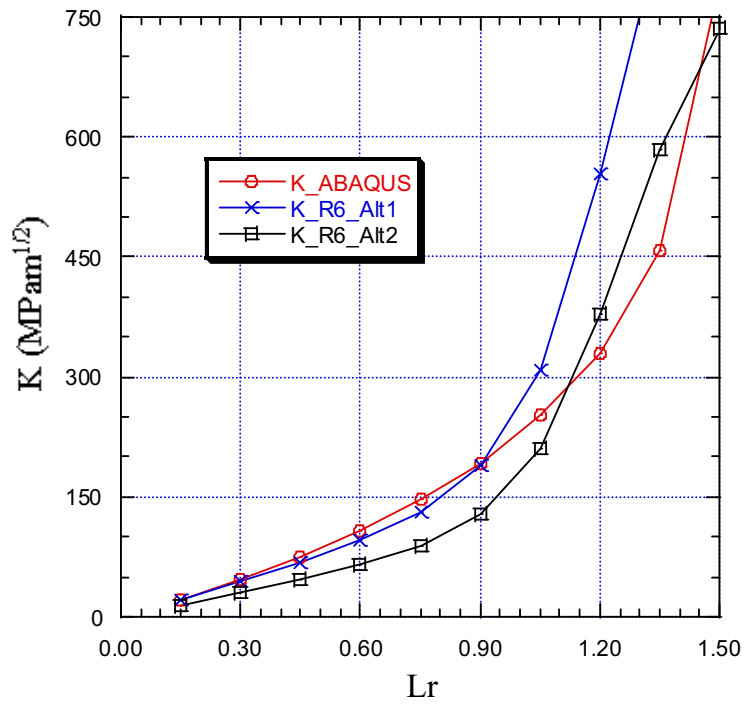Figure A4.4. Stress intensity factors at the middle point of crack front AB for case 7 ($\psi = 0^\circ$).
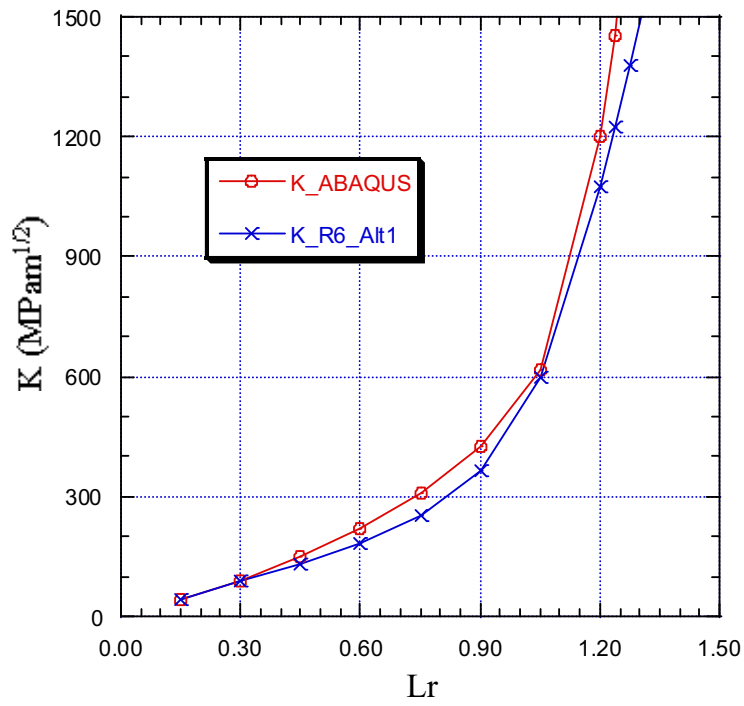
Figure A4.5. Stress intensity factors at the middle point of crack front AB for case 9 ($\psi = 0º$).
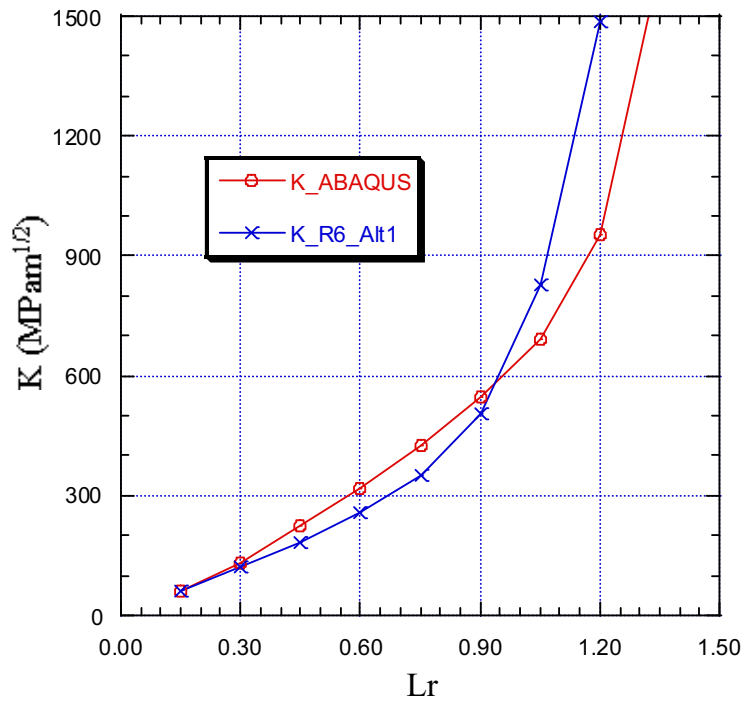
Figure A4.6. Stress intensity factors at the middle point of crack front AB for case 11 ($\psi = 0º$).

A4.1.2 Results using $\psi = 30^\circ$

The results for an off-centre crack ($\psi = 30^\circ$) in a carbon steel pipe are shown in Figs. A4.7-A4.12.
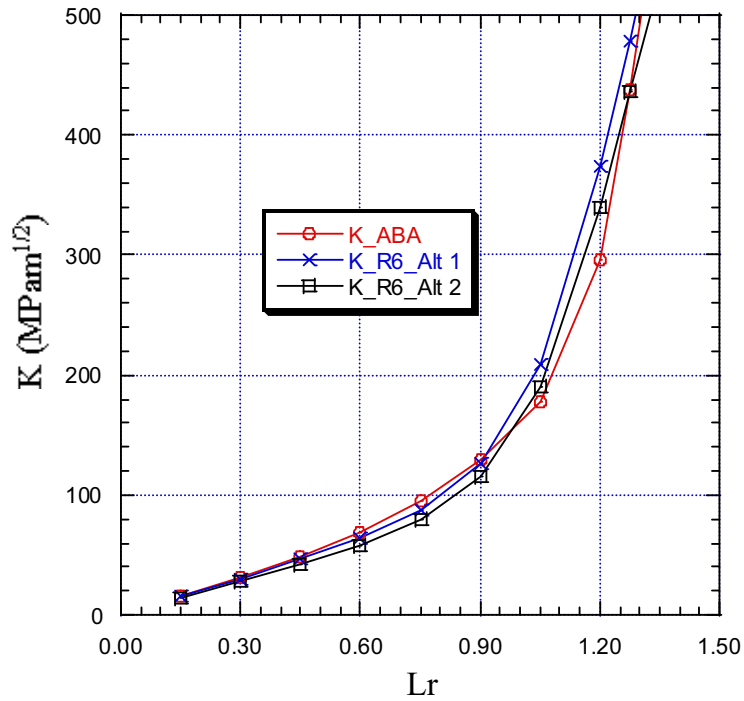
Figure A4.7. Stress intensity factors at the middle point of crack front AB for case 1 ($\psi = 30^\circ$).
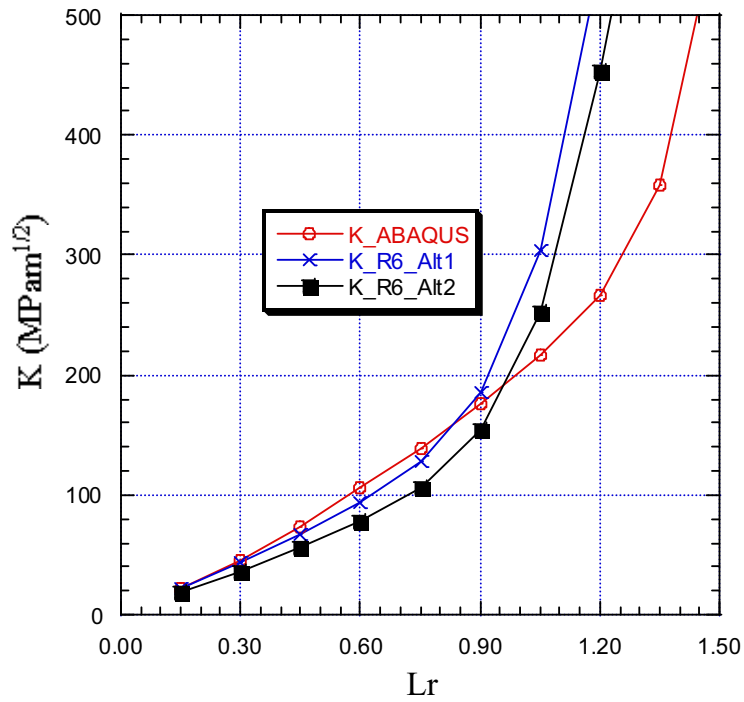
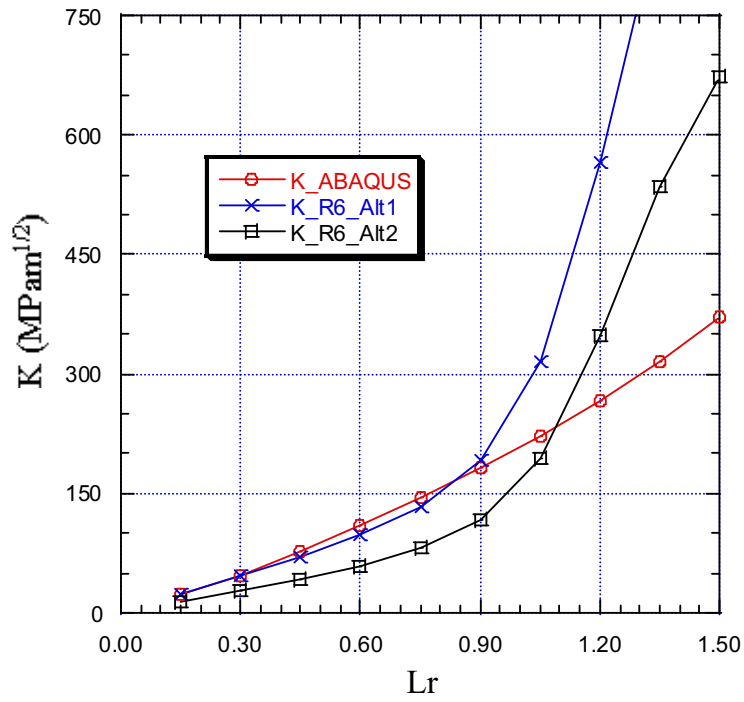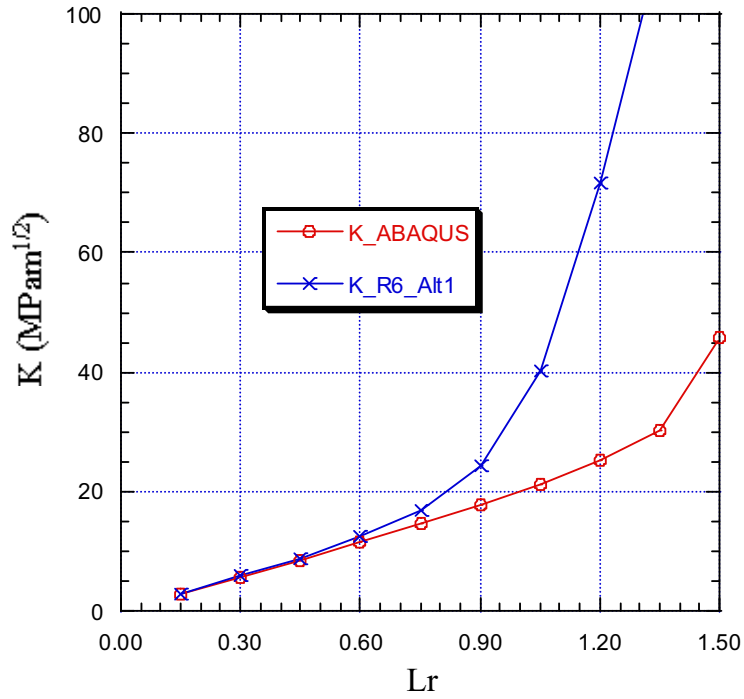Figure A4.8. Stress intensity factors at the middle point of crack front AB for case 3 ($\psi = 30^\circ$).
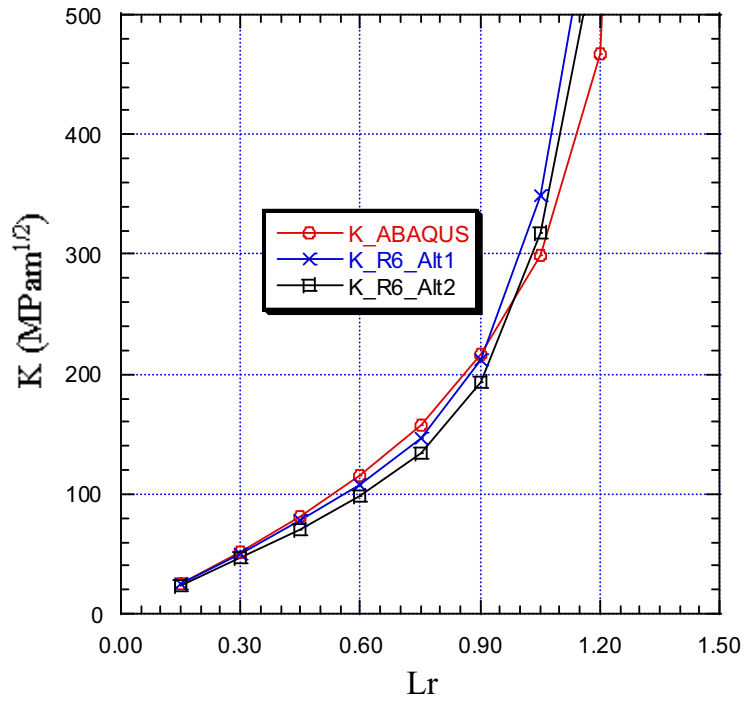
Figure A4.9. Stress intensity factors at the middle point of crack front AB for case 5 ($\psi = 30°$).
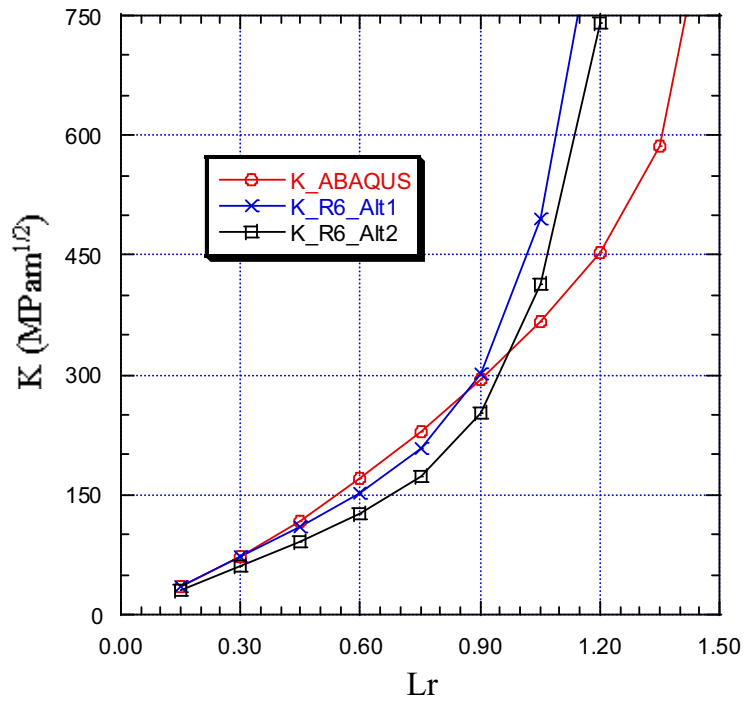
Figure A4.10. Stress intensity factors at the middle point of crack front AB for case 7 ($\psi = 30°$).
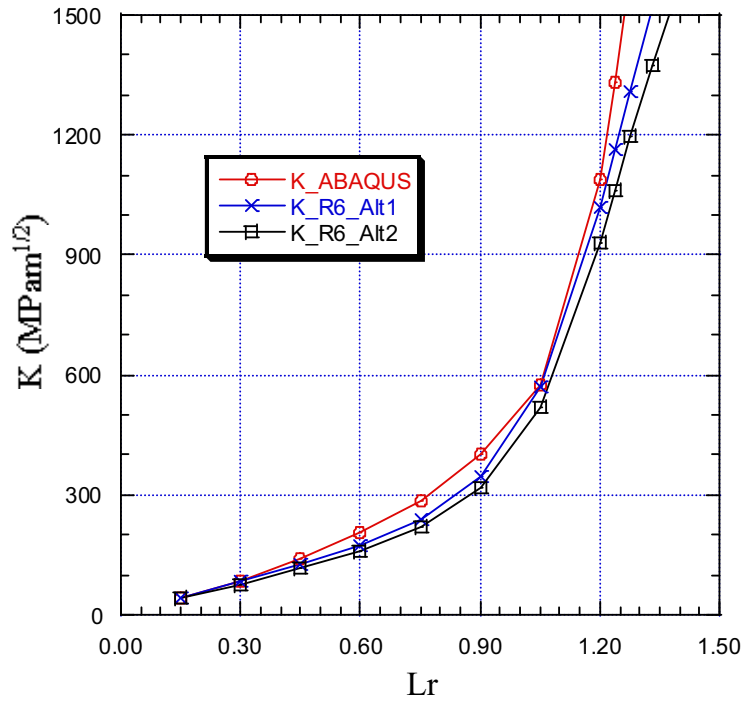
Figure A4.11. Stress intensity factors at the middle point of crack front AB for case 9 (ψ = 30º).
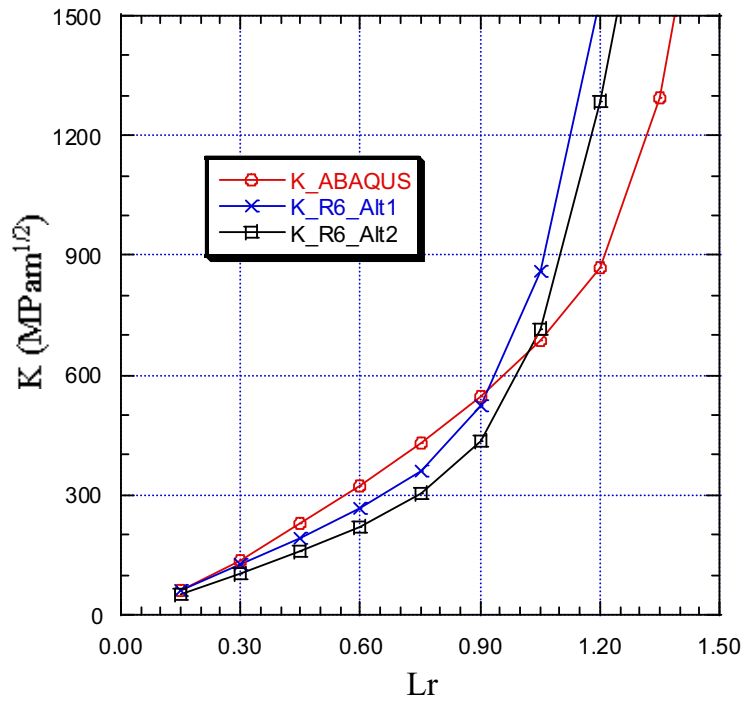
Figure A4.12. Stress intensity factors at the middle point of crack front AB for case 11 (ψ = 30º).

A4.1.3 Results using $\psi = 60^\circ$

The results for an off-centre crack ($\psi = 60^\circ$) in a carbon steel pipe are shown in Figs. A4.13-A4.18.
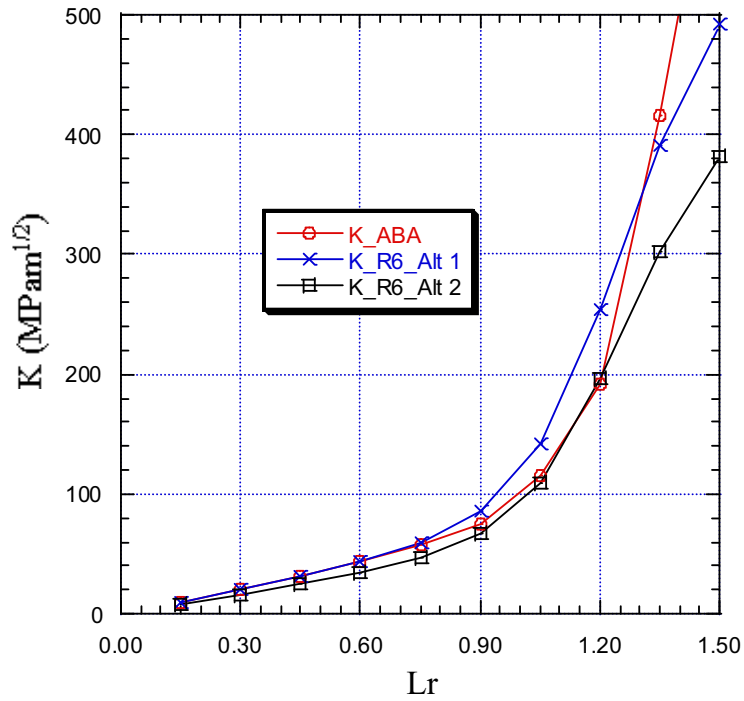
Figure A4.13. Stress intensity factors at the middle point of crack front AB for case 1 ($\psi = 60^\circ$).
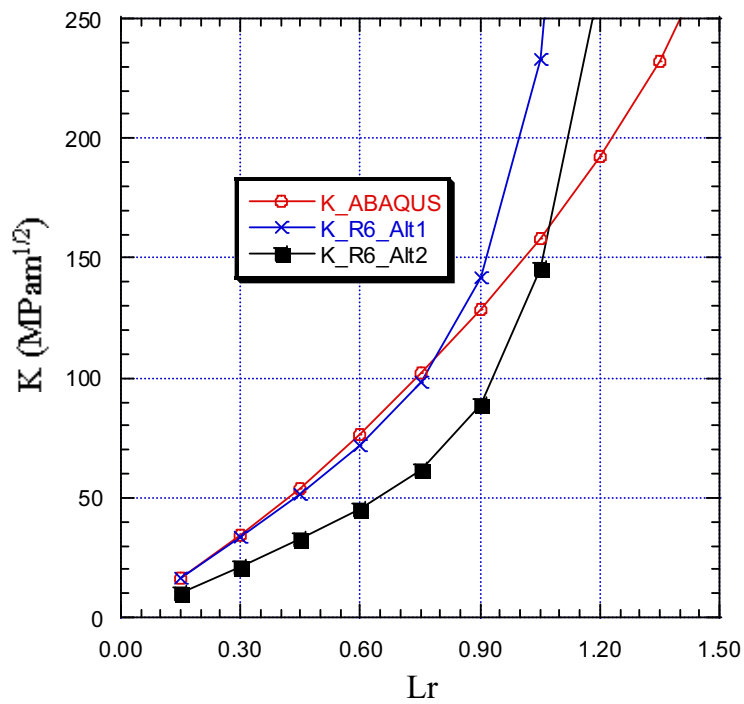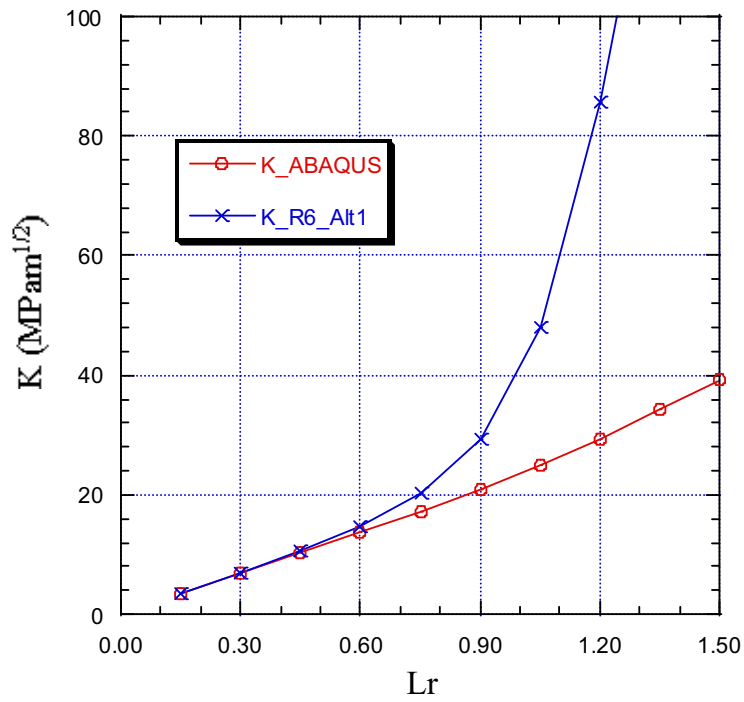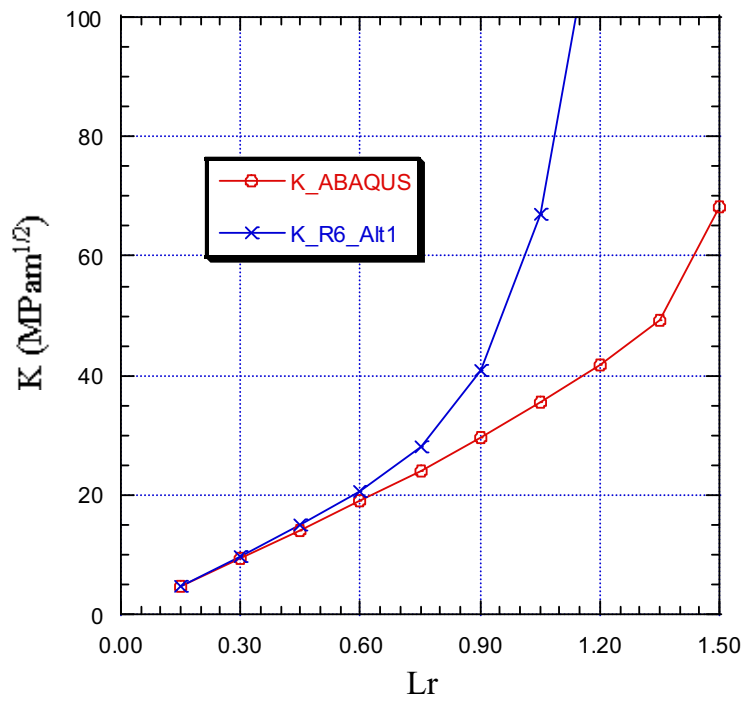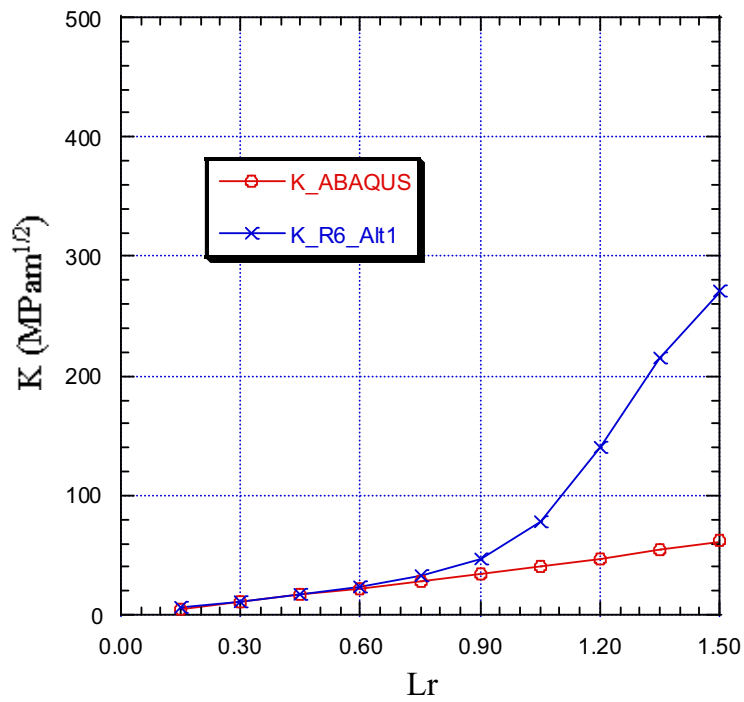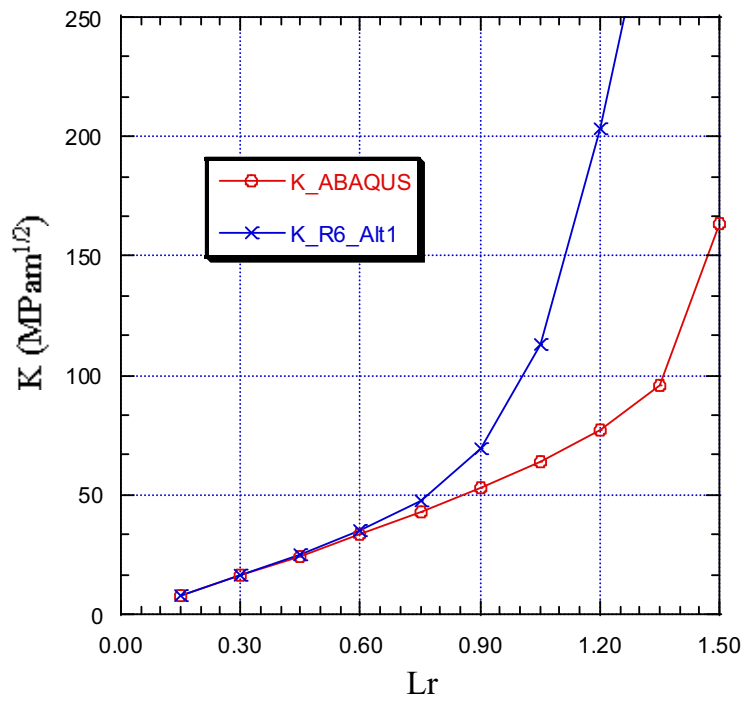

Figure A4.14. Stress intensity factors at the middle point of crack front AB for case 3 ($\psi = 60^\circ$).
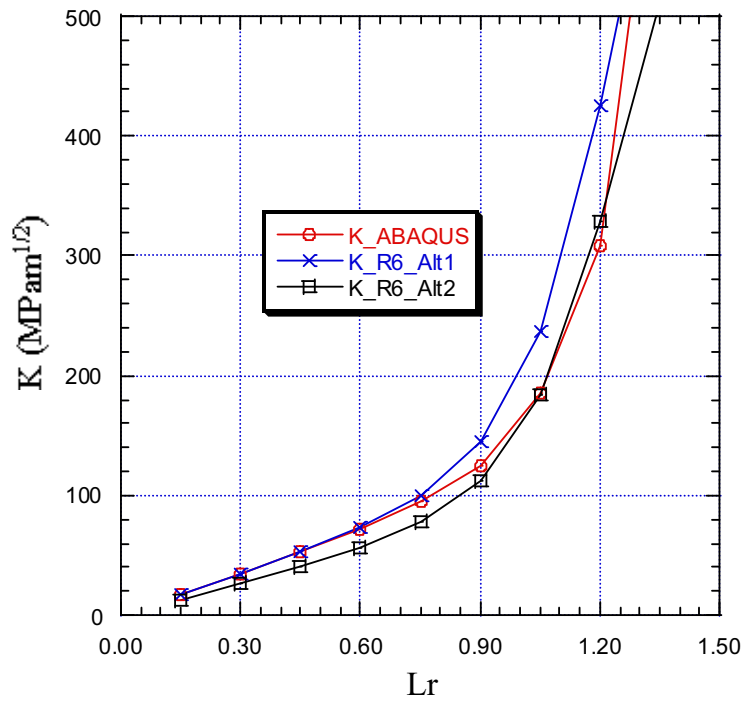
Figure A4.15. Stress intensity factors at the middle point of crack front AB for case 5 (ψ = 60º).
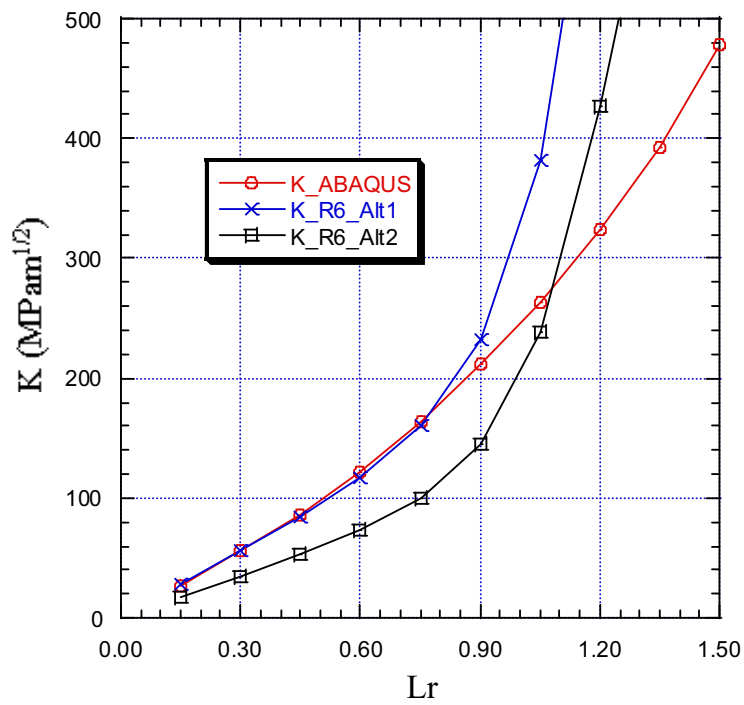
Figure A4.16. Stress intensity factors at the middle point of crack front AB for case 7 (ψ = 60º).
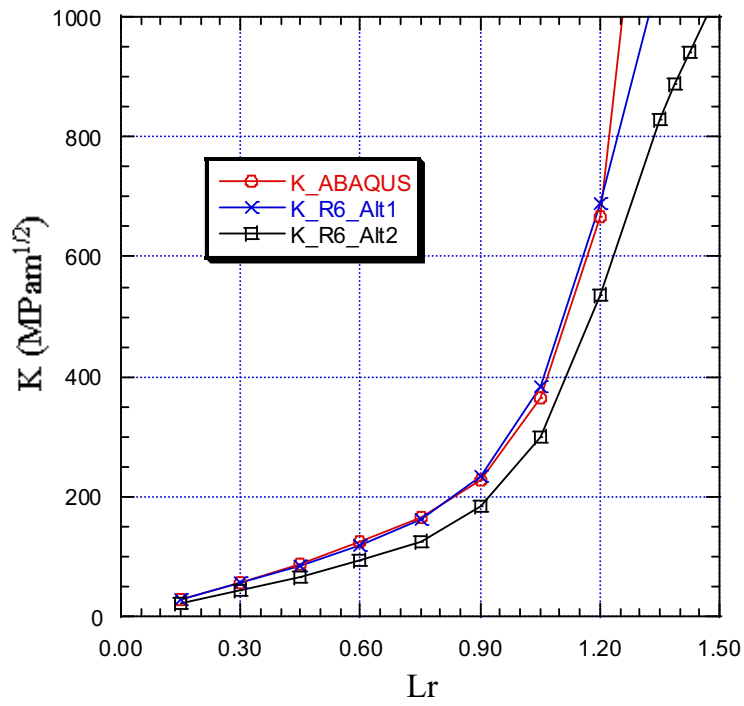
Figure A4.17. Stress intensity factors at the middle point of crack front AB for case 9 ($\psi = 60°$).
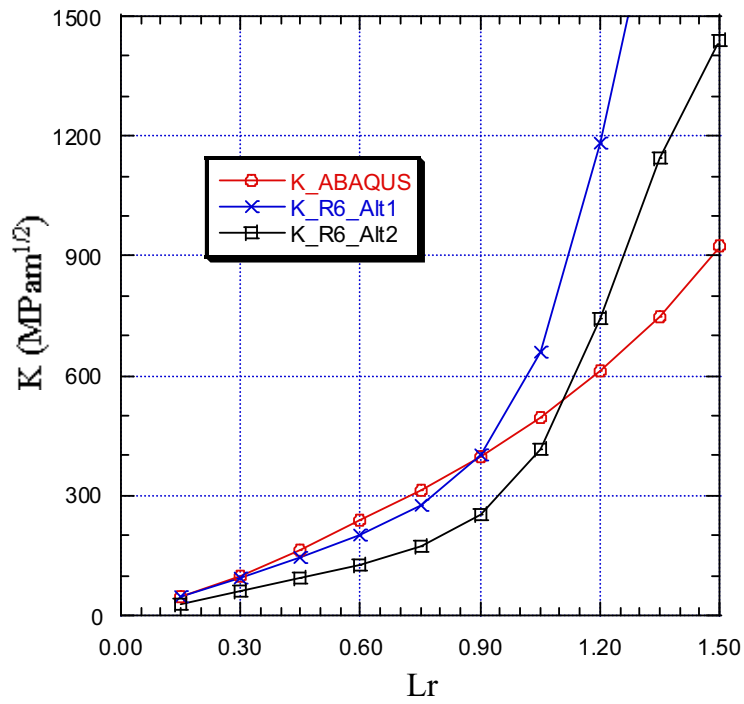
Figure A4.18. Stress intensity factors at the middle point of crack front AB for case 11 ($\psi = 60°$).

Results using $\psi = 90^\circ$

The results for an off-centre crack ($\psi = 90^\circ$) in a carbon steel pipe are shown in Figs. A4.19-A4.24.
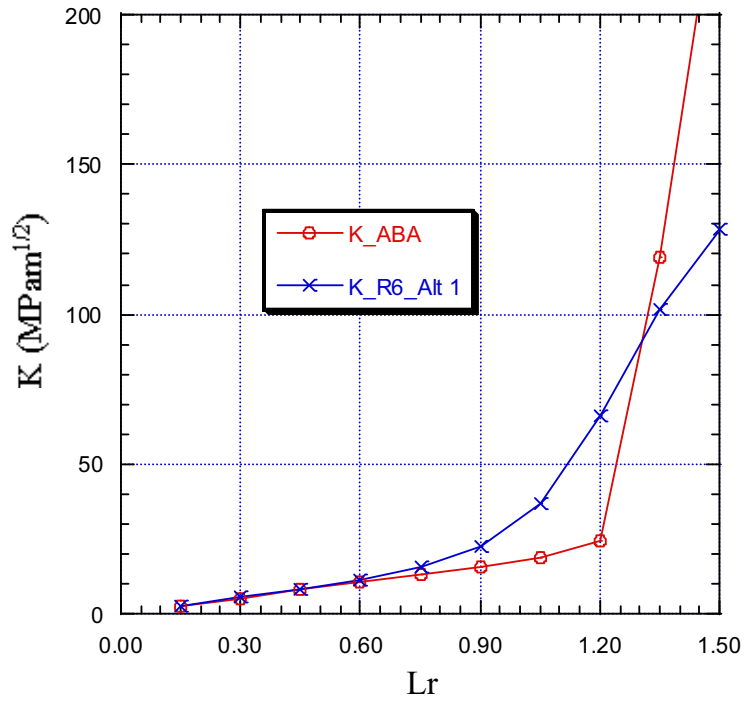
Figure A4.19. Stress intensity factors at the middle point of crack front AB for case 1 ($\psi = 90^\circ$).
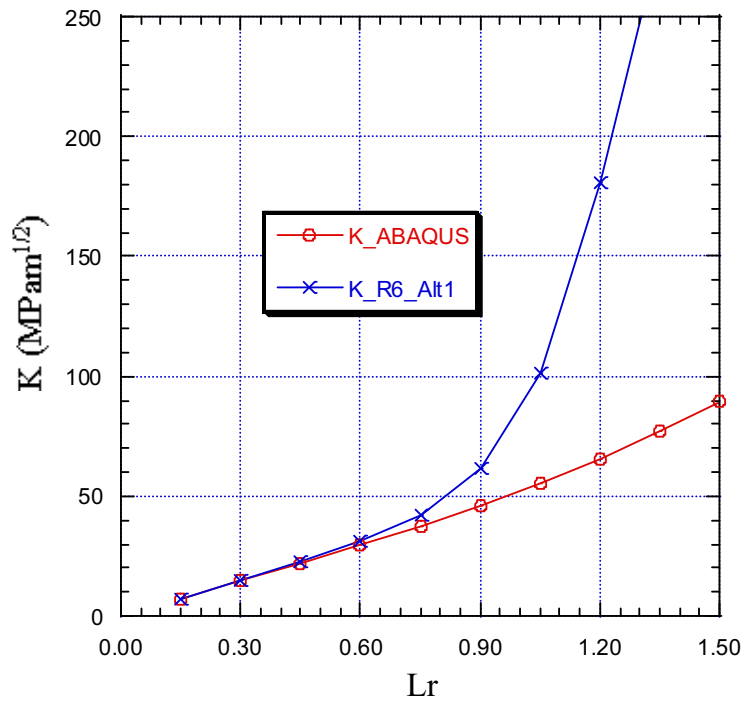
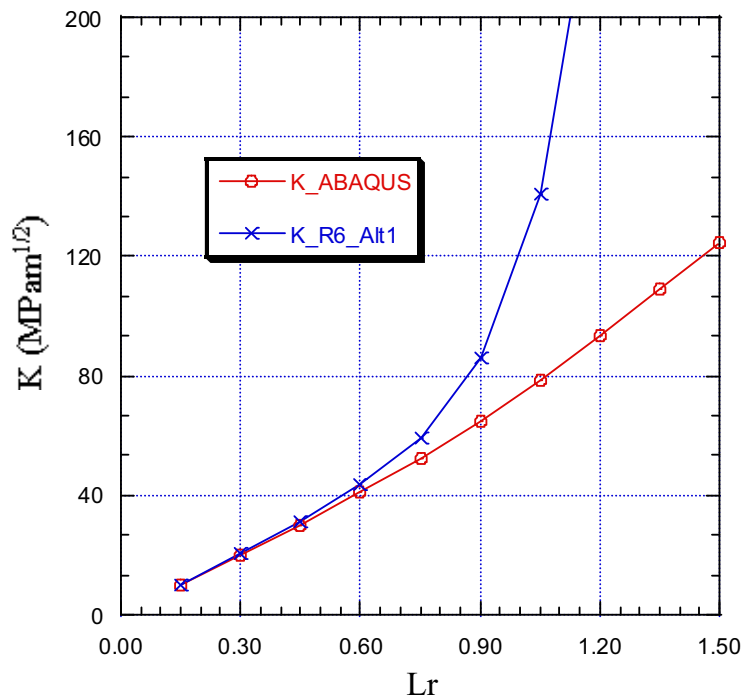Figure A4.20. Stress intensity factors at the middle point of crack front AB for case 3 ($\psi = 90^\circ$).
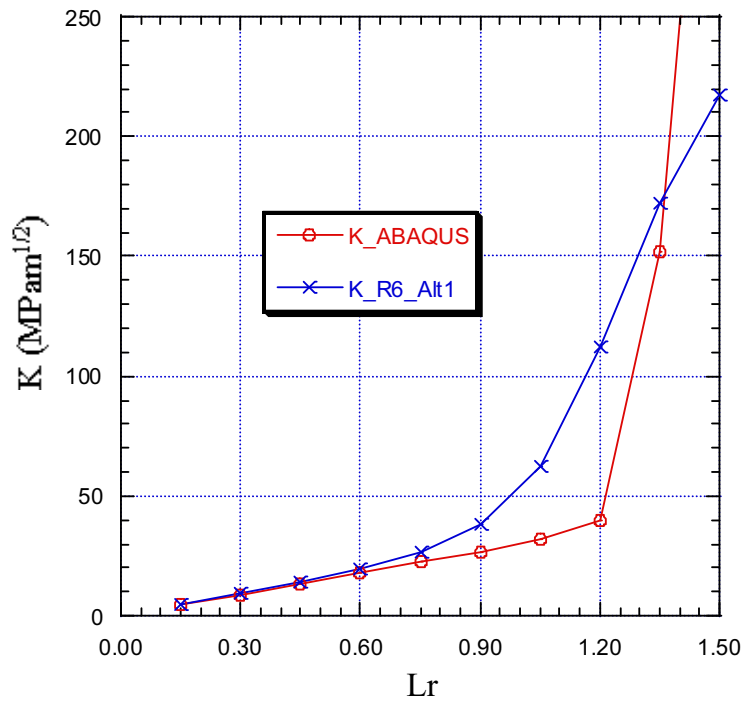
Figure A4.21. Stress intensity factors at the middle point of crack front AB for case 5 (ψ = 90º).
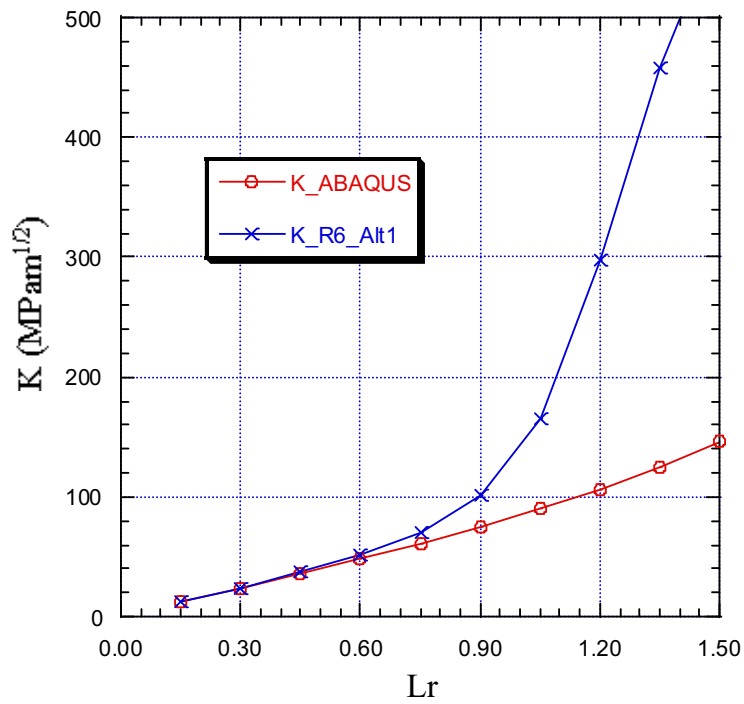
Figure A4.22. Stress intensity factors at the middle point of crack front AB for case 7 (ψ = 90º).
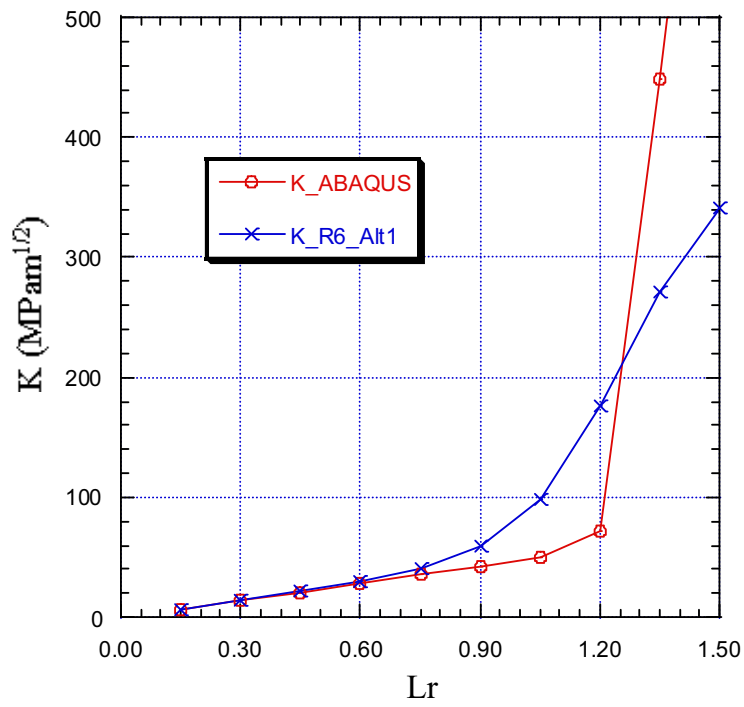
Figure A4.23. Stress intensity factors at the middle point of crack front AB for case 9 ($\psi = 90°$).
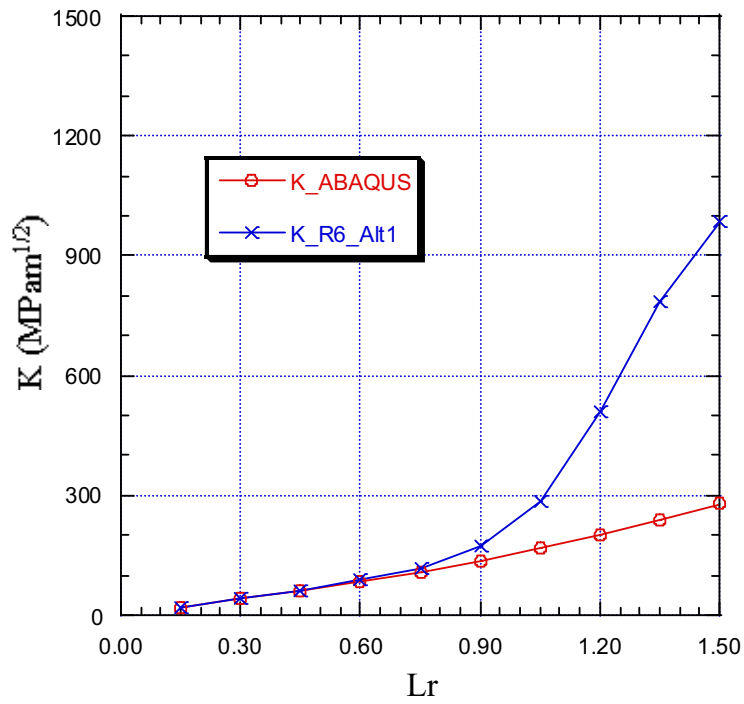
Figure A4.24. Stress intensity factors at the middle point of crack front AB for case 11 ($\psi = 90°$).

A4.2   Stress intensity factors for stainless steel

Below, the results for the stainless steel cases 2, 4, 6, 8, 10 and 12 are given as a function of the off-centre crack angle ψ (ψ = 0º, 30º, 60º, 90º).

A4.2.1   Results using ψ = 0º

The results for a centre crack (ψ = 0º) in a stainless steel pipe are shown in Figs. A4.25-A4.30.
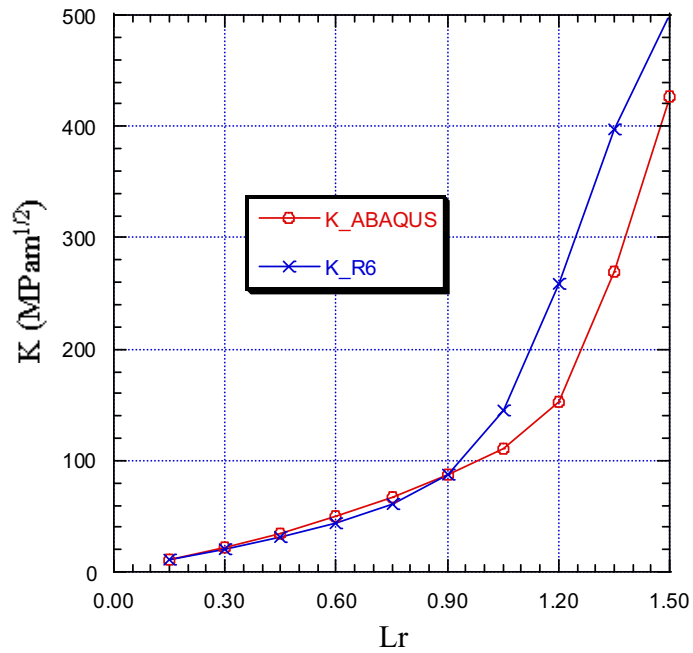
Figure A4.25. Stress intensity factors at the middle point of crack front AB for case 2 (ψ = 0º).
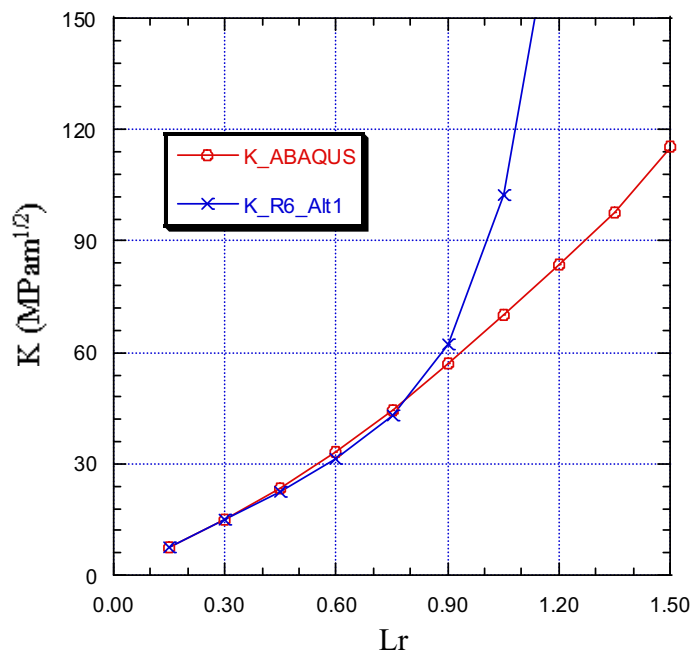
Figure A4.26. Stress intensity factors at the middle point of crack front AB for case 4 (ψ = 0º).
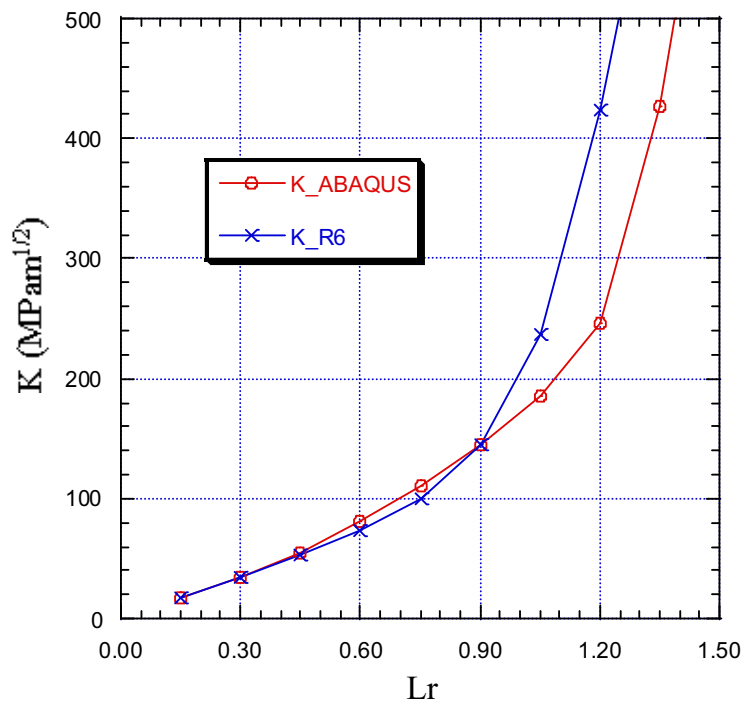
Figure A4.27. Stress intensity factors at the middle point of crack front AB for case 6 ($\psi = 0°$).
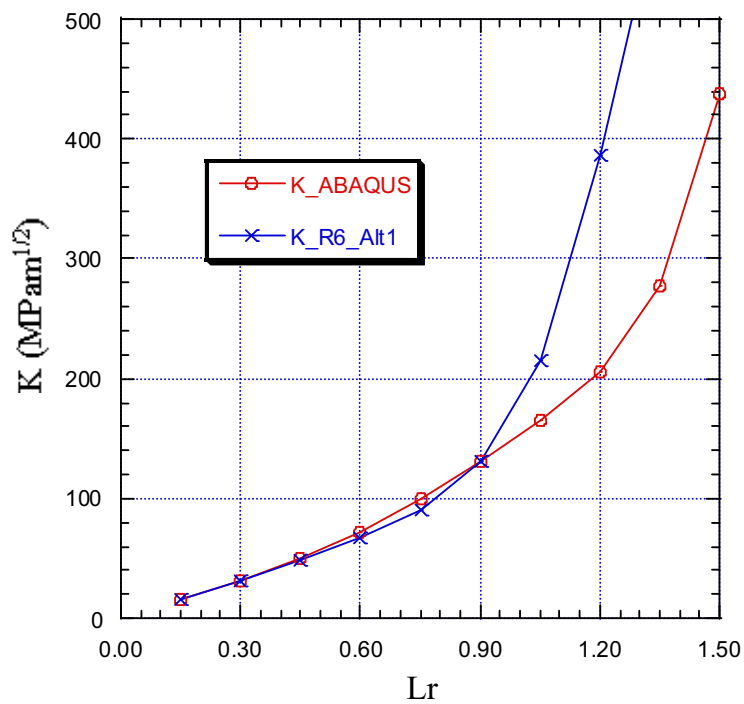
Figure A4.28. Stress intensity factors at the middle point of crack front AB for case 8 ($\psi = 0°$).
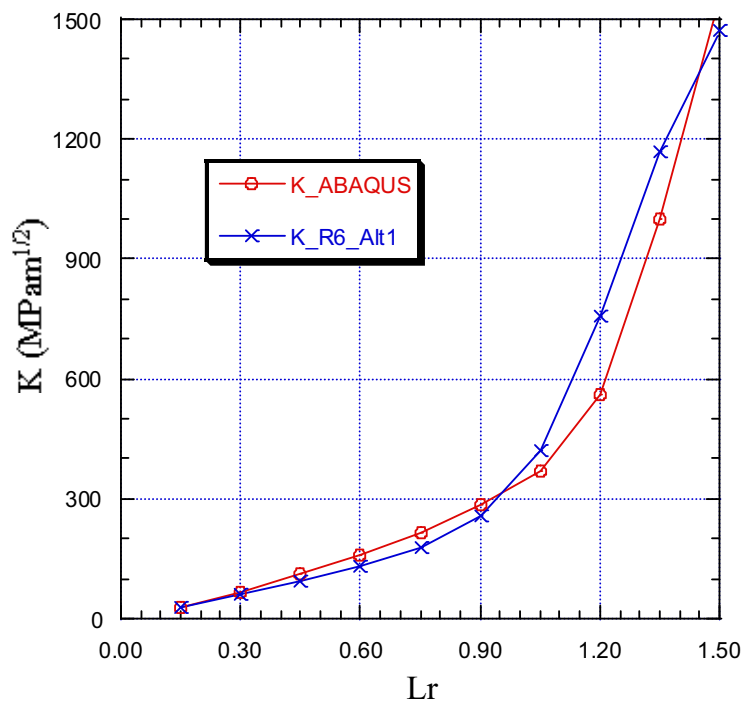
Figure A4.29. Stress intensity factors at the middle point of crack front AB for case 10 (ψ = 0º).
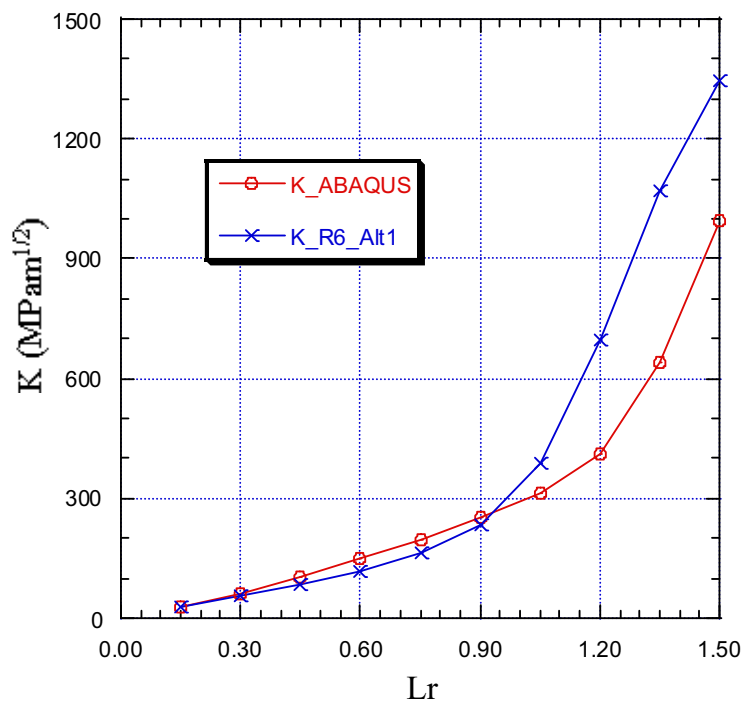
Figure A4.30. Stress intensity factors at the middle point of crack front AB for case 12 (ψ = 0º).

A4.2.2   Results using $\psi = 30^{\circ}$

The results for an off-centre crack ($\psi = 30^{\circ}$) in a stainless steel pipe are shown in Figs. A4.31-A4.36.
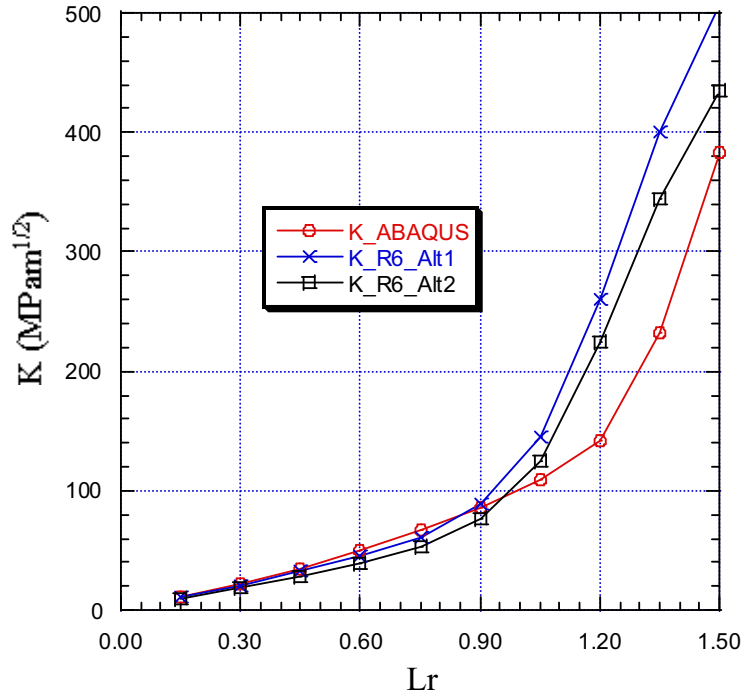
Figure A4.31. Stress intensity factors at the middle point of crack front AB for case 2 ($\psi = 30^{\circ}$).
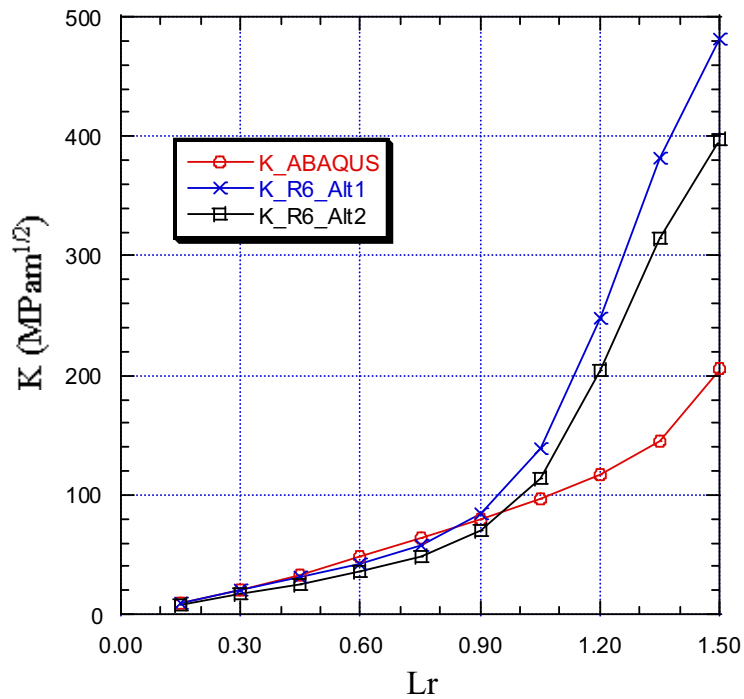
Figure A4.32. Stress intensity factors at the middle point of crack front AB for case 4 ($\psi = 30^{\circ}$).
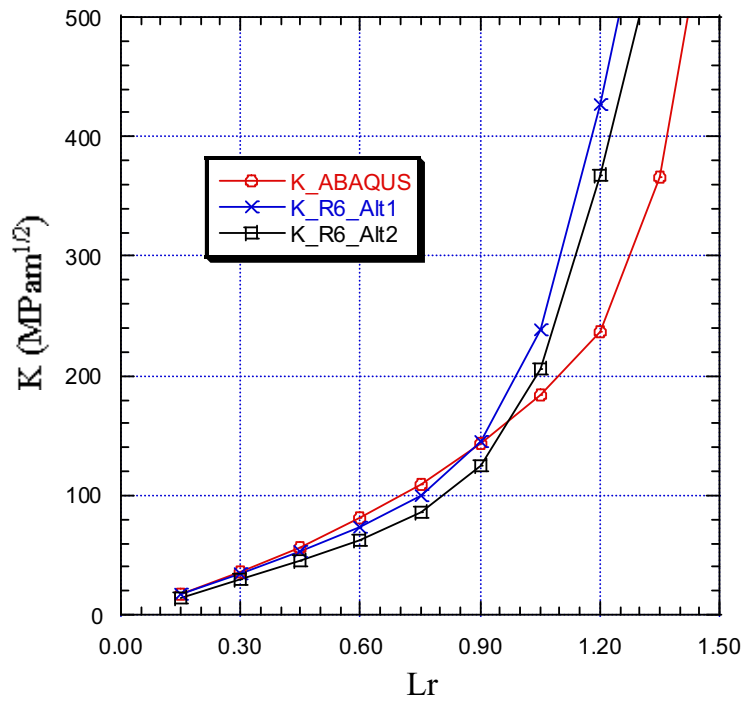
Figure A4.33. Stress intensity factors at the middle point of crack front AB for case 6 ($\psi = 30°$).
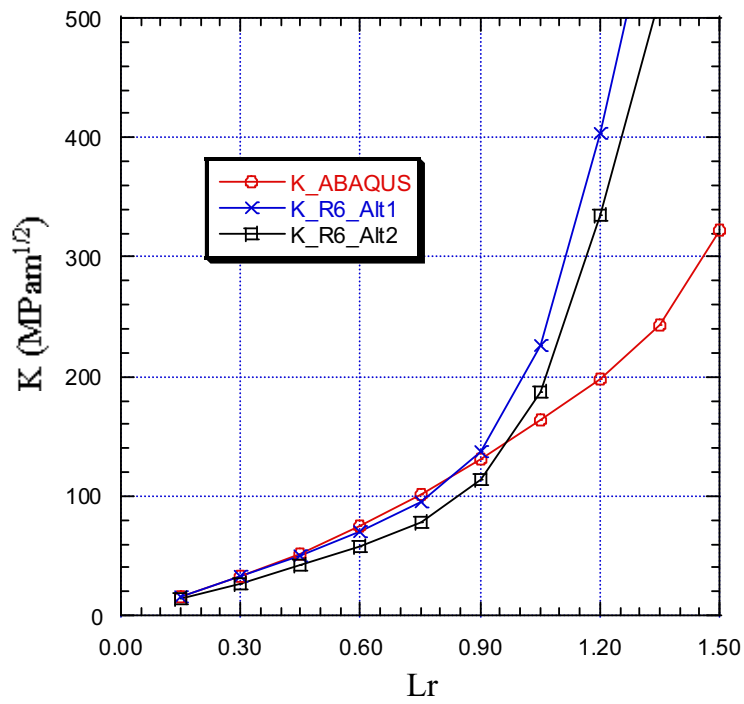
Figure A4.34. Stress intensity factors at the middle point of crack front AB for case 8 ($\psi = 30°$).

Figure A4.35. Stress intensity factors at the middle point of crack front AB for case 10 ($\psi = 30º$).

Figure A4.36. Stress intensity factors at the middle point of crack front AB for case 12 ($\psi = 30º$).

A4.2.3   Results using $\psi = 60^\circ$

The results for an off-centre crack ($\psi = 60^\circ$) in a stainless steel pipe are shown in Figs. A4.37-A4.42.

Figure A4.37. Stress intensity factors at the middle point of crack front AB for case 2 ($\psi = 60^\circ$).

Figure A4.38. Stress intensity factors at the middle point of crack front AB for case 4 ($\psi = 60^\circ$).

Figure A4.39. Stress intensity factors at the middle point of crack front AB for case 6 ($\psi = 60°$).

Figure A4.40. Stress intensity factors at the middle point of crack front AB for case 8 ($\psi = 60°$).

Figure A4.41. Stress intensity factors at the middle point of crack front AB for case 10 ($\psi = 60º$).

Figure A4.42. Stress intensity factors at the middle point of crack front AB for case 12 ($\psi = 60º$).

A4.2.4   Results using $\psi = 90º$

The results for an off-centre crack ($\psi = 90º$) in a stainless steel pipe are shown in Figs. A4.43-A4.48.

Figure A4.43. Stress intensity factors at the middle point of crack front AB for case 2 ($\psi = 90º$).

Figure A4.44. Stress intensity factors at the middle point of crack front AB for case 4 ($\psi = 90º$).

Figure A4.45. Stress intensity factors at the middle point of crack front AB for case 6 (ψ = 90º).

Figure A4.46. Stress intensity factors at the middle point of crack front AB for case 8 (ψ = 90º).

Figure A4.47. Stress intensity factors at the middle point of crack front AB for case 10 ($\psi = 90º$).

Figure A4.48. Stress intensity factors at the middle point of crack front AB for case 12 ($\psi = 90º$).

A4.3   Geometry functions for off-centre cracks

It is noticed that results for R6-Alternative 2 (where the effect of M_x is neglected) are zero for centre cracks and off-centre cracks when $\psi = 90°$. In addition, R6-Alternative 1 (where the effect of M_x is included) will always generate a more accurate result in comparison with the result by R6-Alternative 2. The results using R6-Alternative 2 are below the finite element results (i.e. the results will be un-conservative) when $L_r < 1$. Therefore the elastic results K^{90} are of importance and should be included in the analysis.

The geometry function, f, of the stress intensity factor is defined as,

$$K = \sigma_b \sqrt{\pi a_m} \cdot f\left(2\theta, R_i / t\right) . \tag{A6}$$

In Eqn (A6), σ_b is the maximum global bending stress and a_m is one half the average crack length ($l_m / 2$). The geometry functions for the different cases are listed in Table A4.1.

Table A4.1. Geometry functions for off-centre cracks.

Case	R_i / t	2θ	f^0	f^{90}
1	5.63	45	1.134	0.191
2		90	1.461	0.406
3		135	1.863	0.644
4		180	2.602	0.944
5	4.08	45	1.088	0.185
6		90	1.375	0.389
7		135	1.744	0.607
8		180	2.435	0.881
9	8.88	45	1.226	0.200
10		90	1.693	0.459
11		135	2.090	0.716
12		180	3.019	1.097

The geometry functions in Table A4.1 have been used in the probabilistic calculations presented in this report.

APPENDIX B. CRACK OPENING AREAS FOR OFF-CENTRE CRACKS

Crack opening area (COA) is an important parameter in a LBB analysis. It is commonly known that COA is strongly influenced by plastic deformation. Therefore the use of a correction factor which takes into account the effect of the plastic deformation is necessary.

In this appendix, new crack opening area (COA) form factor solutions for off-centre cracks are given using different pipe geometries and material properties. These form factors can be used to define new correction factor solutions for off-centre cracks.

The load application, material properties and definition of the cases to be analysed are given in Appendix A of this report.

B1   RESULTS – CRACK OPENING AREAS

The crack opening areas (COA) are calculated using the finite element program ABAQUS, with a sufficiently accurate finite element mesh. In the presentation of the results, a comparison is also made between two different approximate methods.

- Method 1:   The crack opening areas are calculated using elastic form factors ($\mathrm{COA_{EL}}$).

- Method 2:   The crack opening areas are calculated using elastic form factors with a correction factor that takes into account the effect of the plastic deformation ($\mathrm{COA_{PL}}$).

The elastic COA is calculated as,

$$\mathrm{COA_{EL}} = \mathrm{COA_{EL}^0} \cdot \cos(\psi) + \mathrm{COA_{EL}^{90}} \cdot \sin(\psi) \ . \tag{B1}$$

In Eqn. (B1), $\mathrm{COA_{EL}^0}$ is the crack opening area of a centre crack ($\psi = 0°$) in a pipe subjected to a bending moment M and $\mathrm{COA_{EL}^{90}}$ is the crack opening area for an off centre crack ($\psi = 90°$) subjected to a bending moment M.

The form factor (COA) is defined as,

$$\mathrm{COA}_k = \frac{\sigma_b \cdot l_k^2}{E} \left(\frac{1}{l_k^2} \int_0^l \mathrm{COD}_k(x)dx \right) = \frac{\sigma_b \cdot l_k^2}{E} D_k \ . \tag{B2}$$

In Eqn. (B2), k is either the inside surface or the outside surface of the pipe. It is obvious that D_k is the average COD divided by l_k under the action of the global bending stress $\sigma_b = E$.

The plastic COA is calculated as,

$$\mathrm{COA_{PL}} = g \cdot \mathrm{COA_{EL}} \ , \tag{B3}$$

where g is a correction factor that takes into account the effect of the plastic deformation (using a primary global bending moment M).

B1.1   Crack opening areas for carbon steel

Below, the results for the carbon steel cases 1, 3, 5, 7, 9 and 11 are given as a function of the off-centre crack angle ψ (ψ = 0º, 30º, 60º, 90º). Results are given both for the inside surface and the outside surface of the pipe.

B1.1.1   Results using ψ = 0º

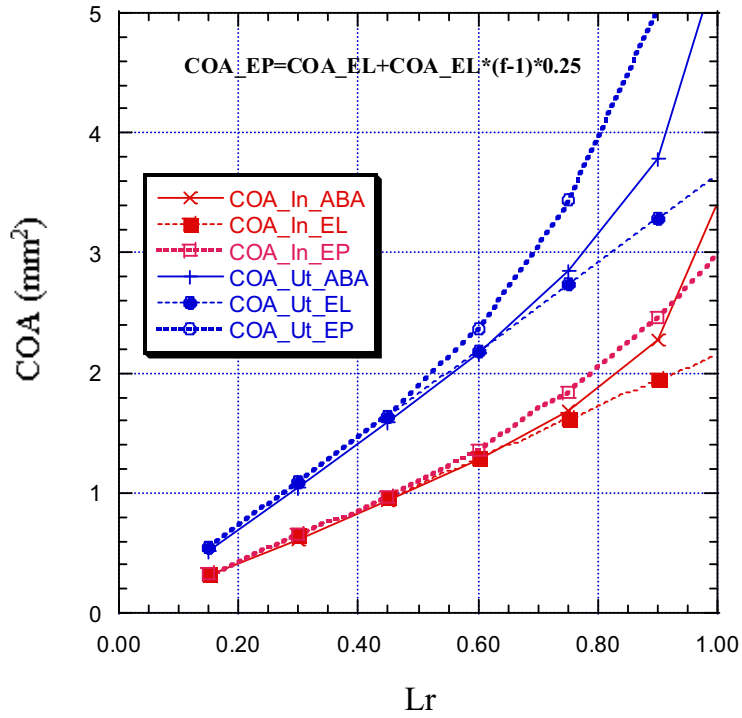The results for a centre crack (ψ = 0º) in a carbon steel pipe are shown in Figs. B1.1-B1.6.
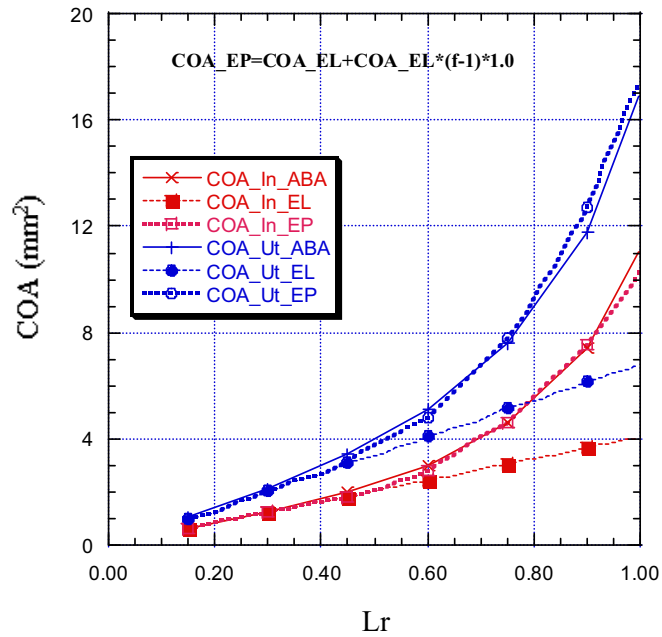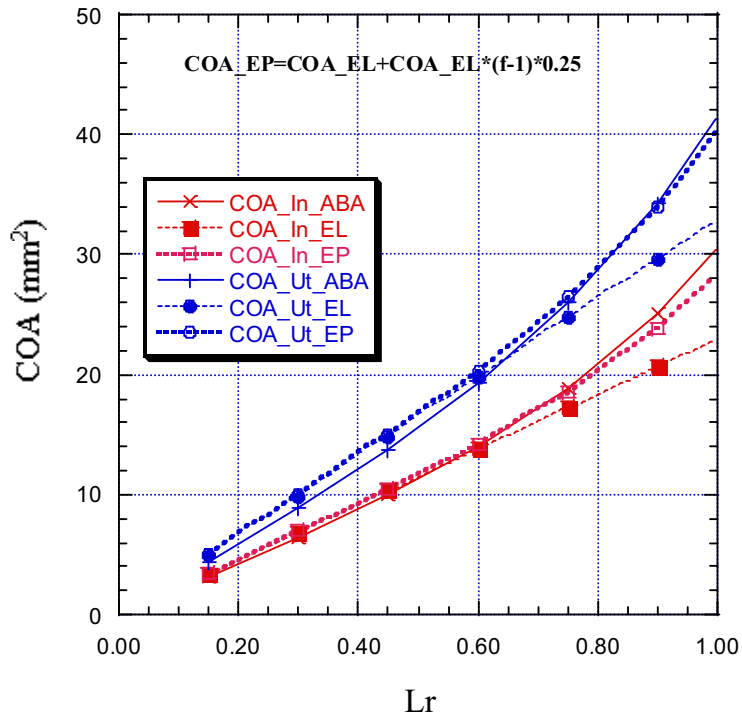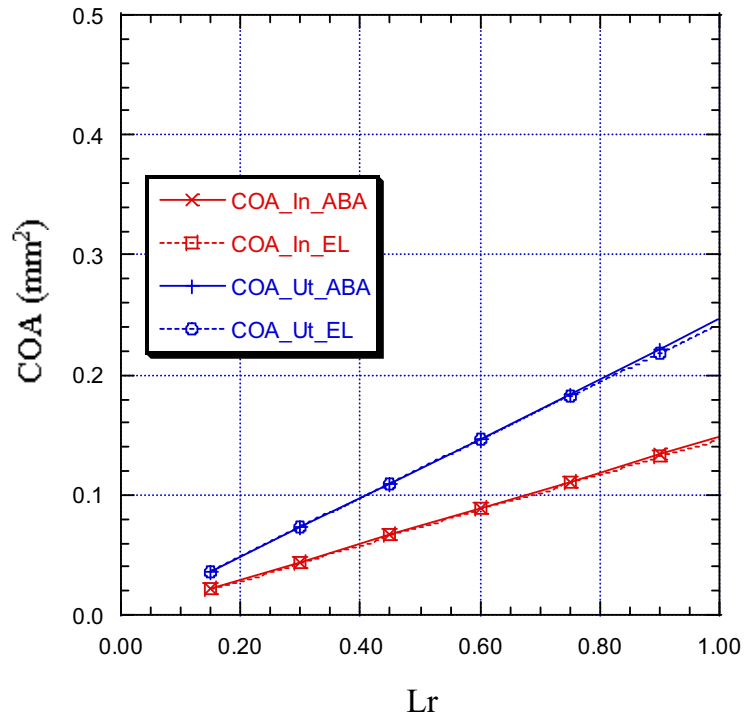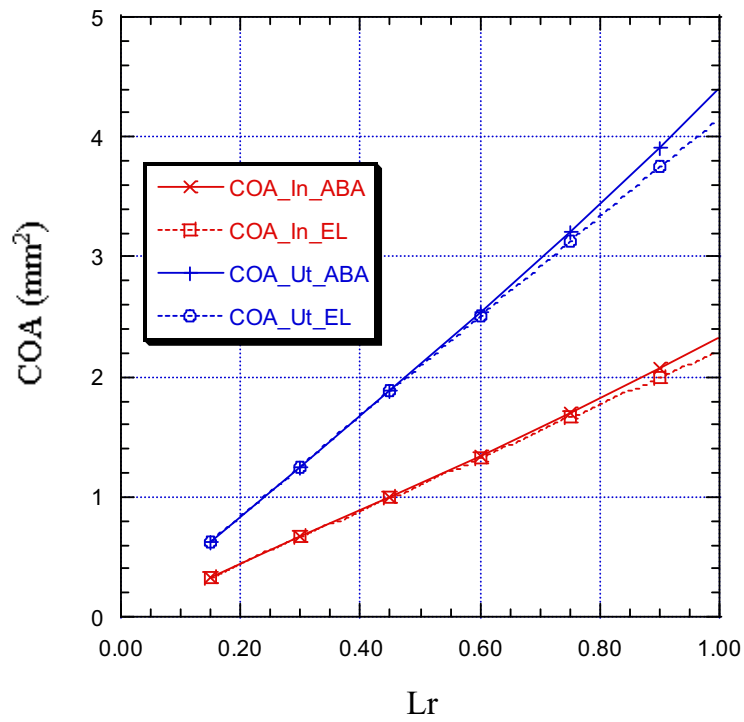

Figure B1.1. Crack opening areas for case 1 (ψ = 0º).
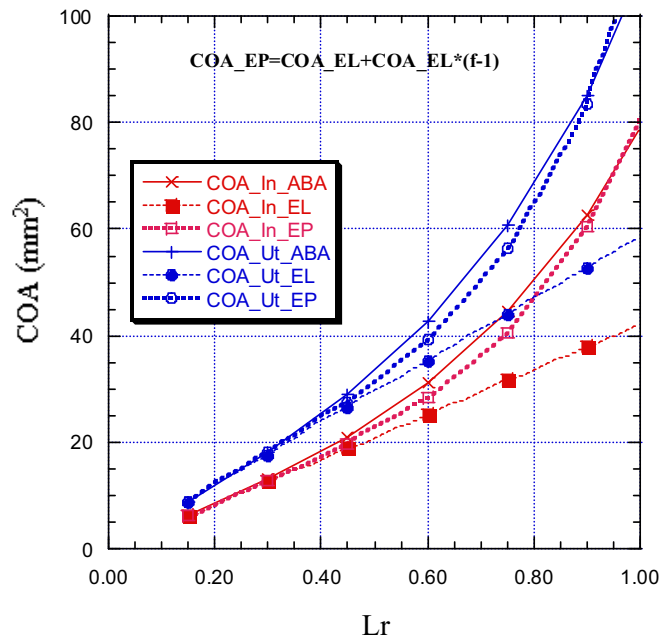
Figure B1.2. Crack opening areas for case 3 (ψ = 0º).
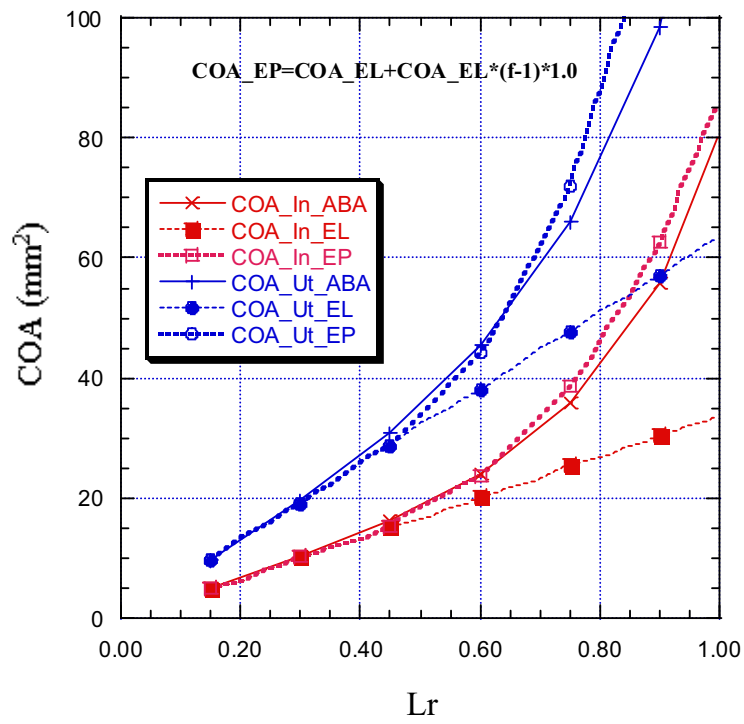
Figure B1.3. Crack opening areas for case 5 ($\psi = 0^\circ$).
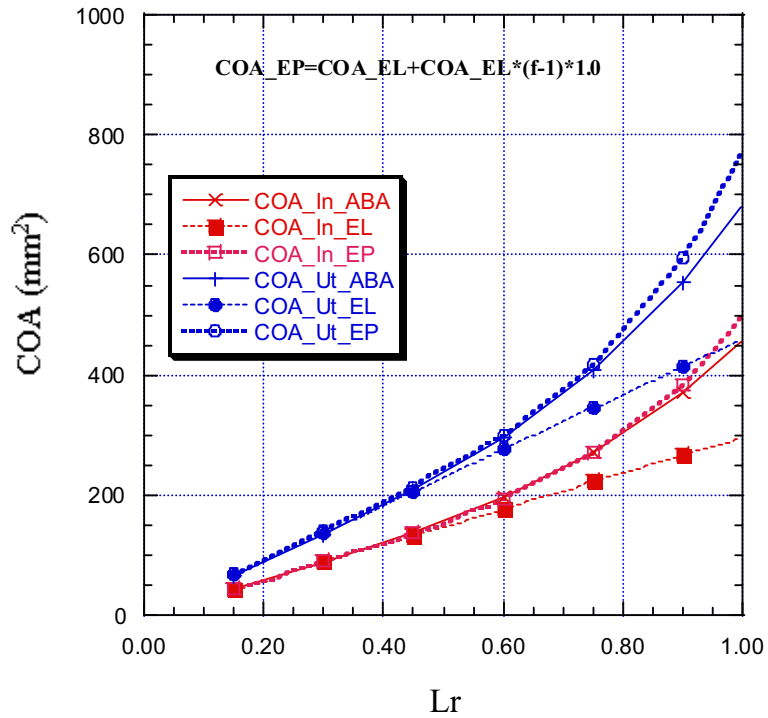
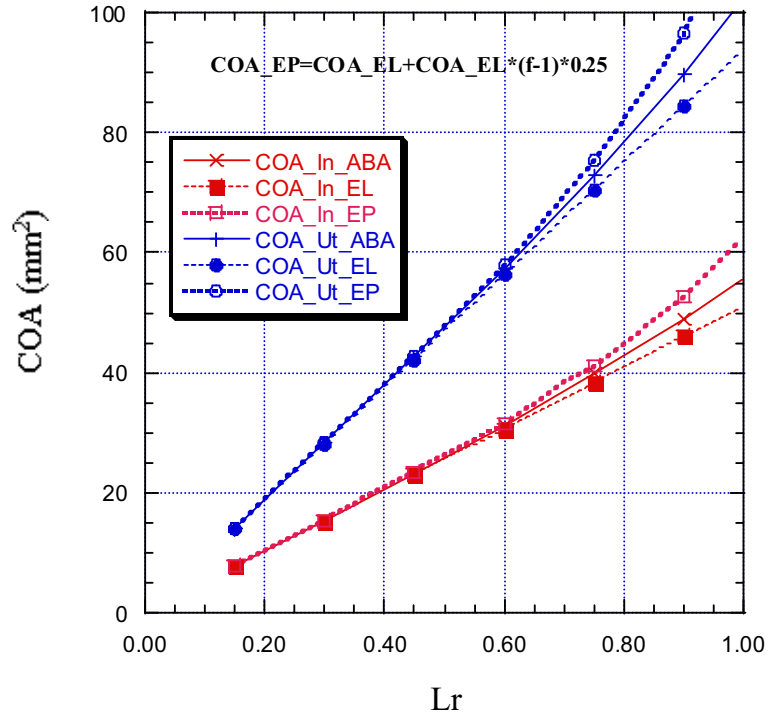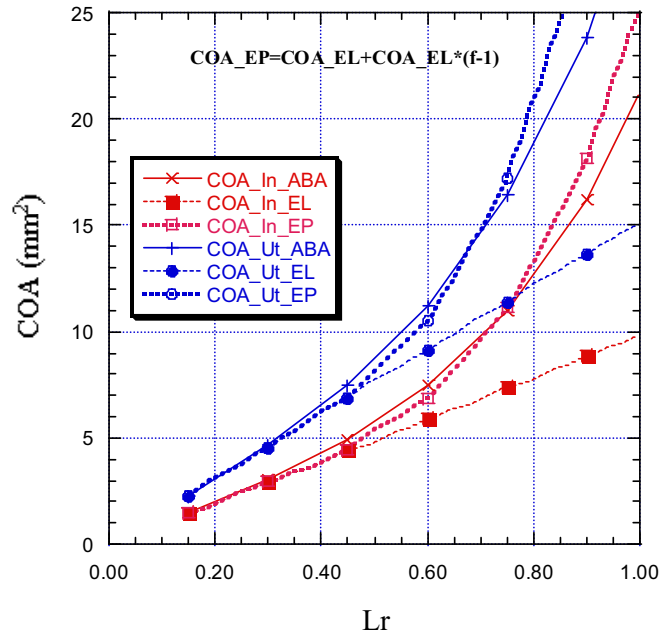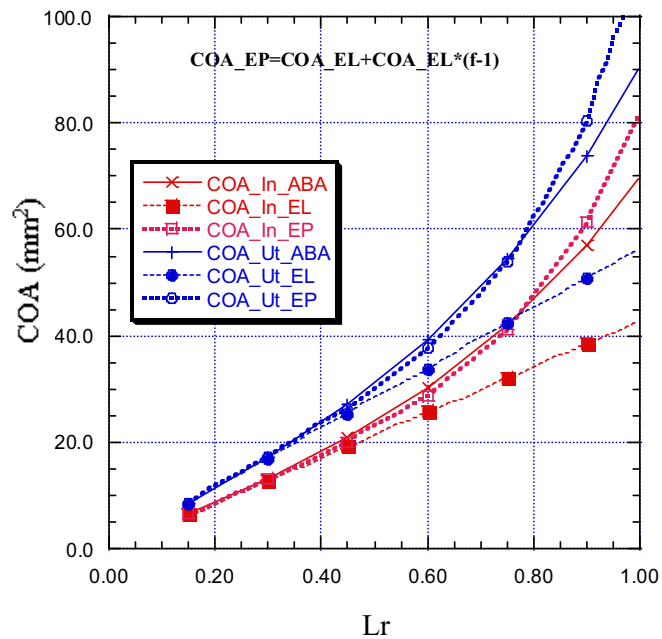Figure B1.4. Crack opening areas for case 7 ($\psi = 0^\circ$).

COA_EP=COA_EL+COA_EL*(f-1)*1.25

Legend:
COA_In_ABA
COA_In_EL
COA_In_EP
COA_Ut_ABA
COA_Ut_EL
COA_Ut_EP
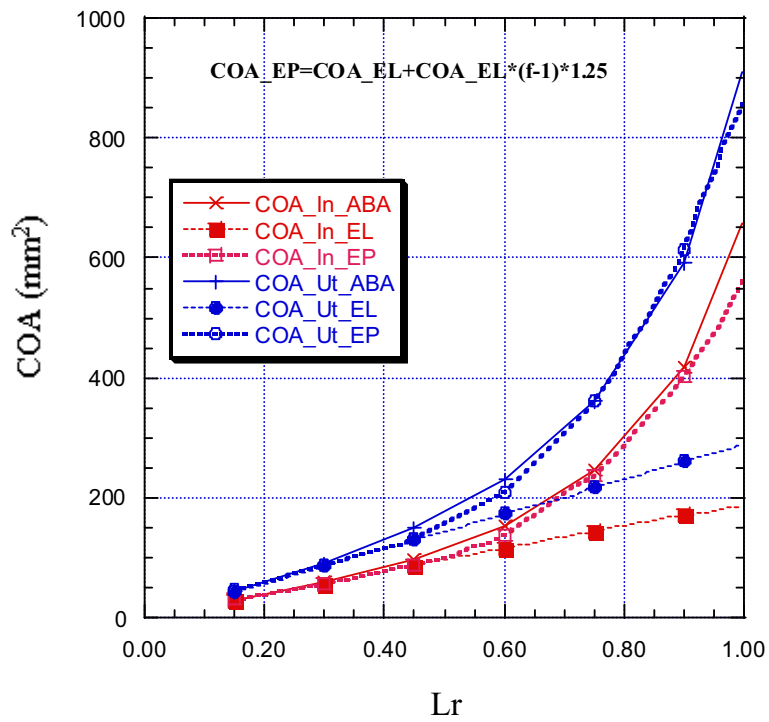
Figure B1.5. Crack opening areas for case 9 ($\psi = 0°$).

COA_EP=COA_EL+COA_EL*(f-1)*1.25

Legend:
COA_In_ABA
COA_In_EL
COA_In_EP
COA_Ut_ABA
COA_Ut_EL
COA_Ut_EP
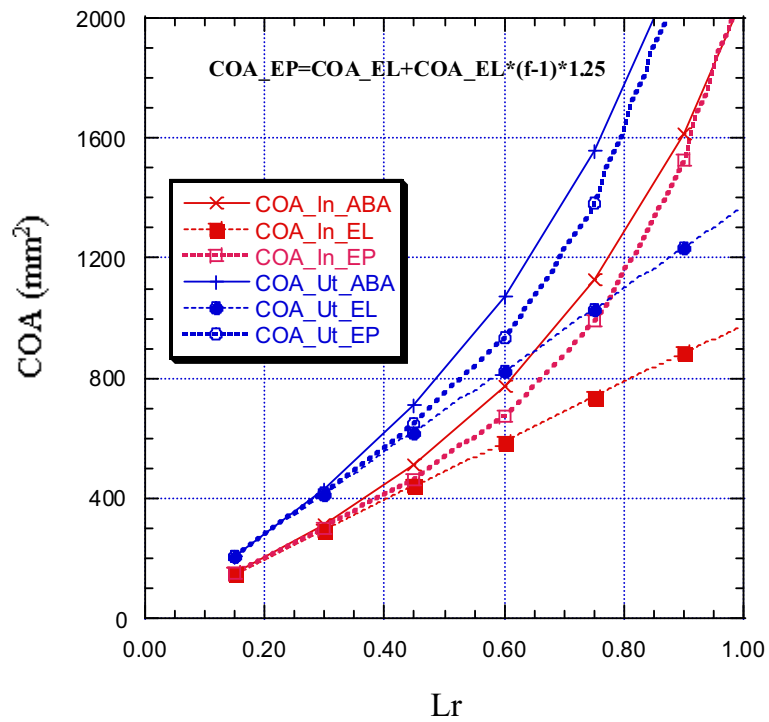
Figure B1.6. Crack opening areas for case 11 ($\psi = 0°$).

B1.1.2   Results using $\psi = 30^\circ$

The results for an off-centre crack ($\psi = 30^\circ$) in a carbon steel pipe are shown in Figs. B1.7-B1.12.
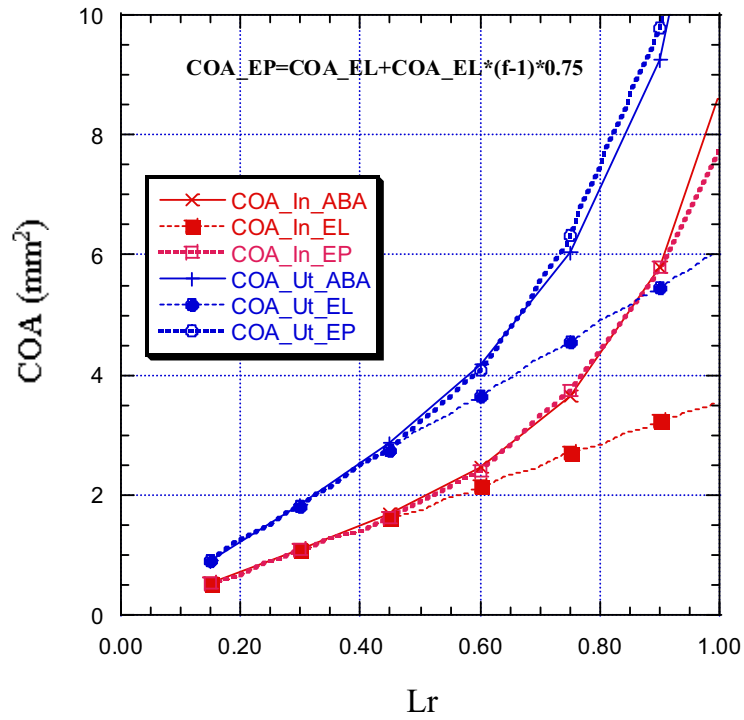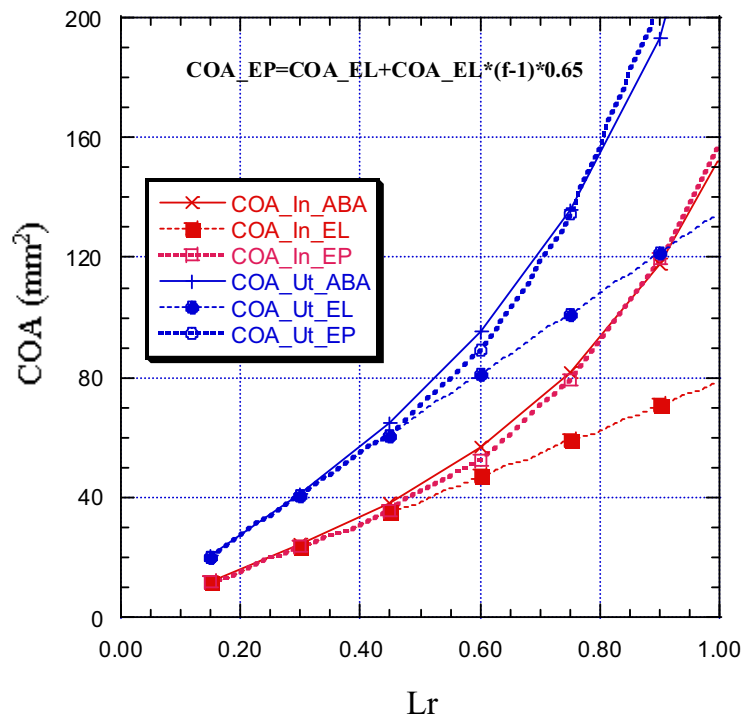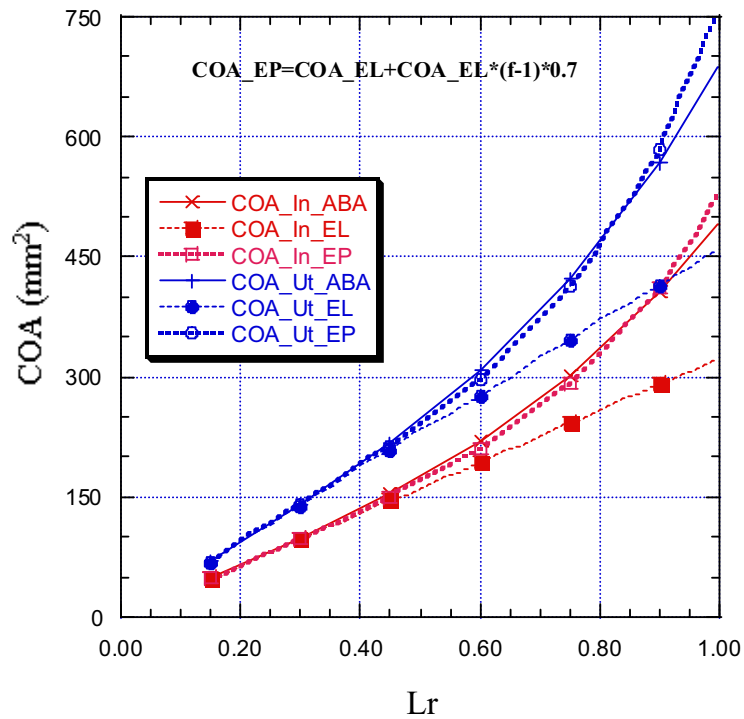

Figure B1.7. Crack opening areas for case 1 ($\psi = 30^\circ$).
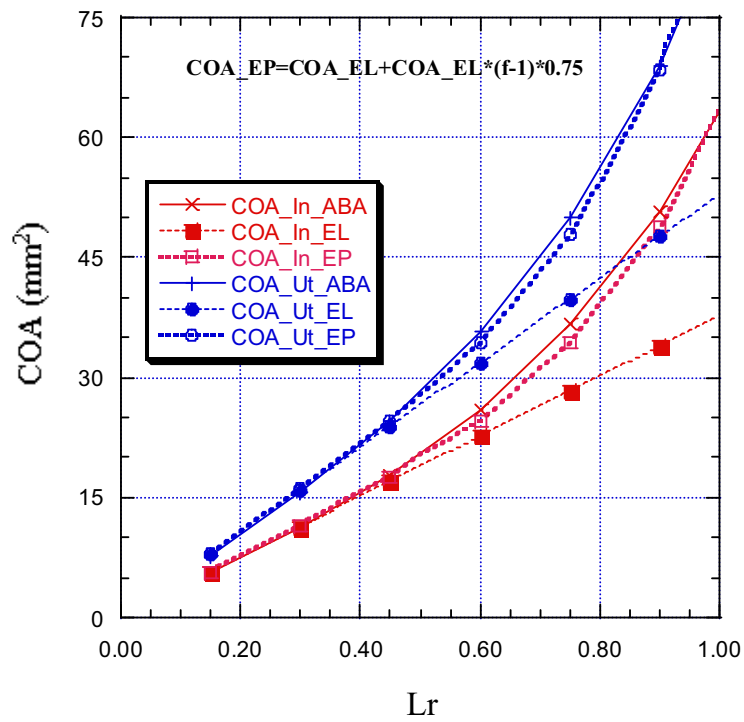
Figure B1.8. Crack opening areas for case 3 ($\psi = 30^\circ$).
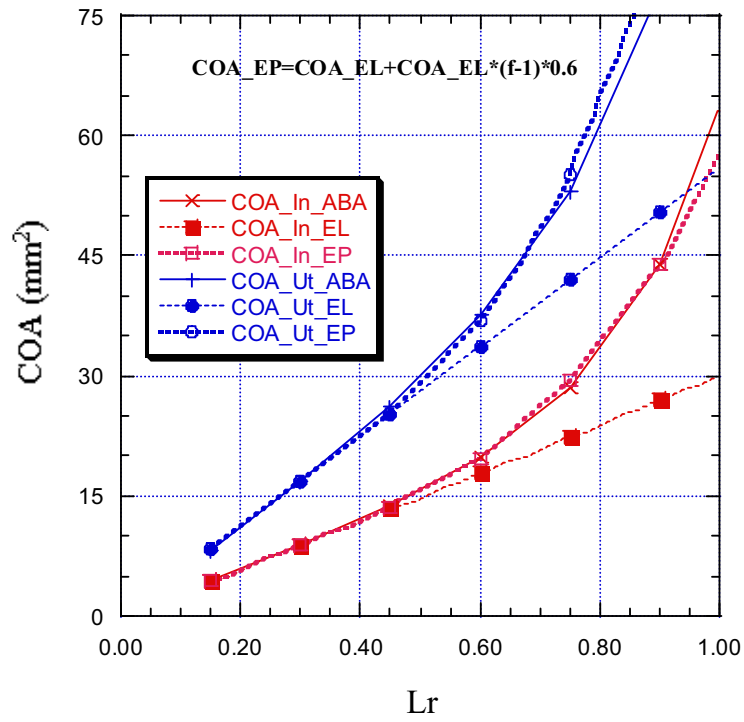
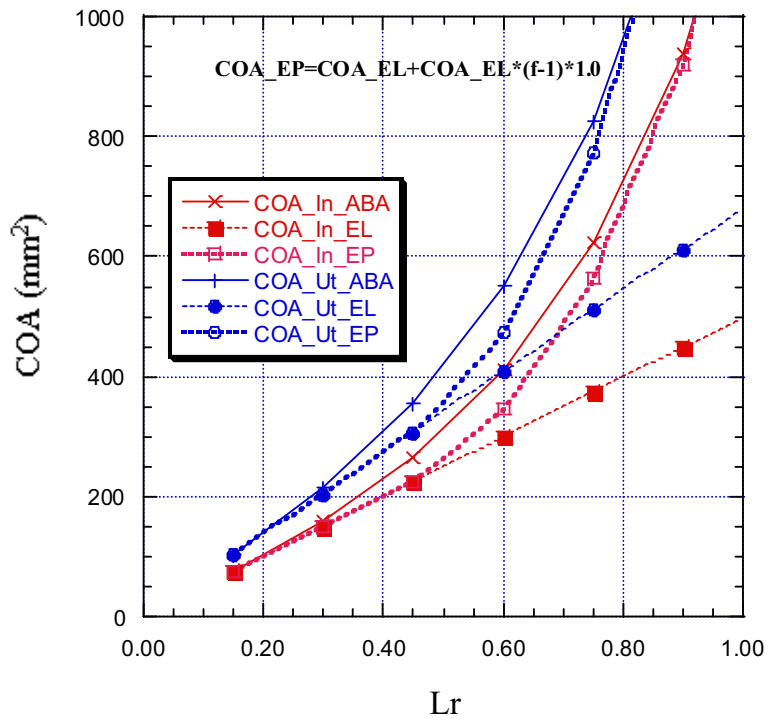Figure B1.9. Crack opening areas for case 5 (ψ = 30º).
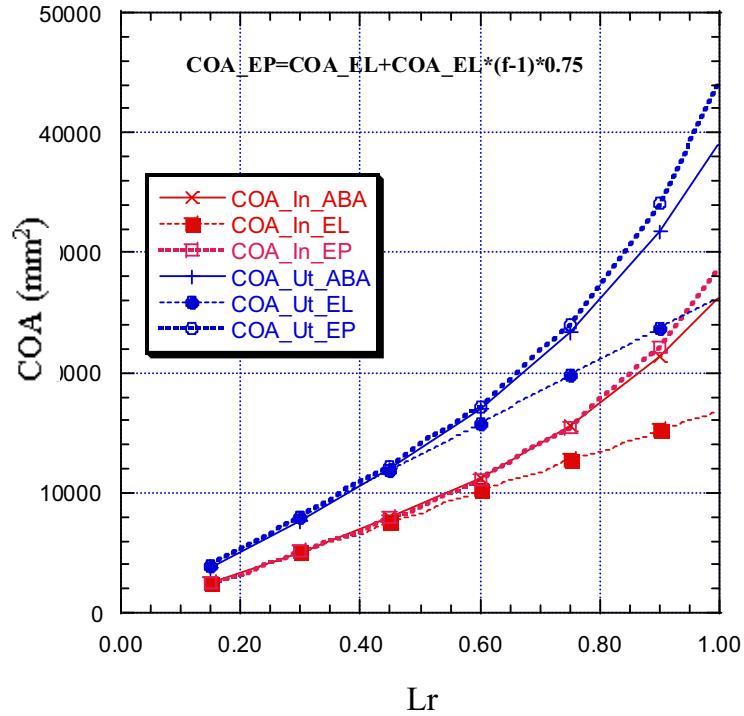
Figure B1.10. Crack opening areas for case 7 (ψ = 30º).
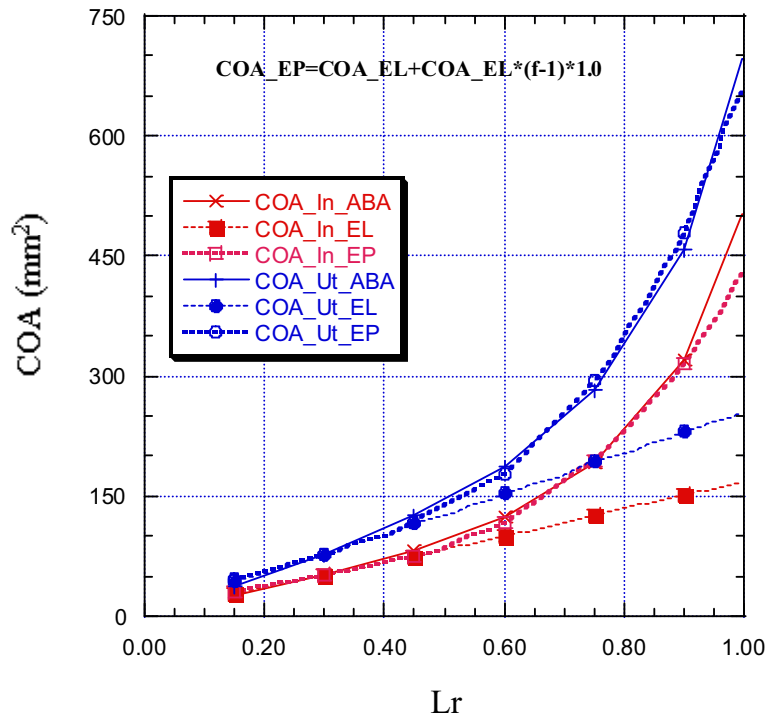
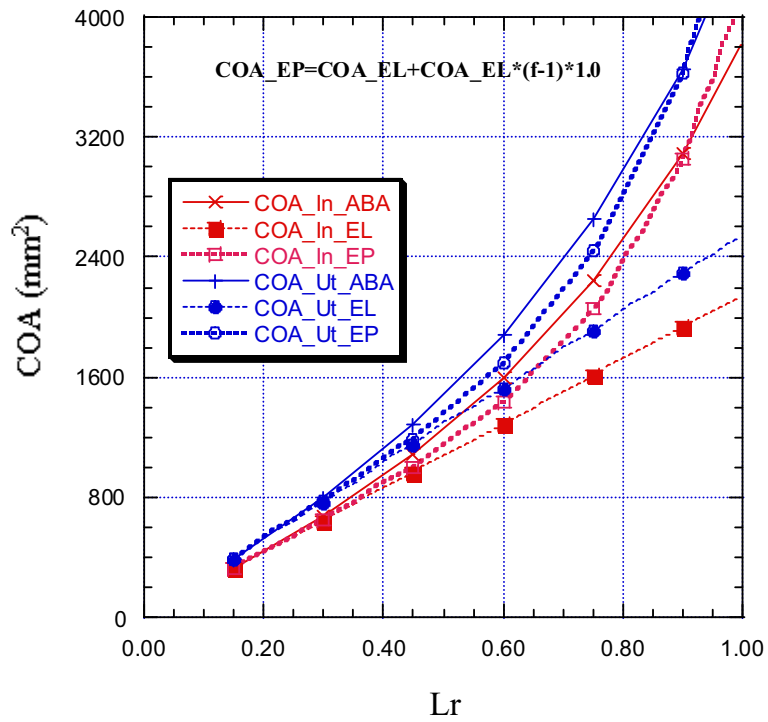Figure B1.11. Crack opening areas for case 9 (ψ = 30º).
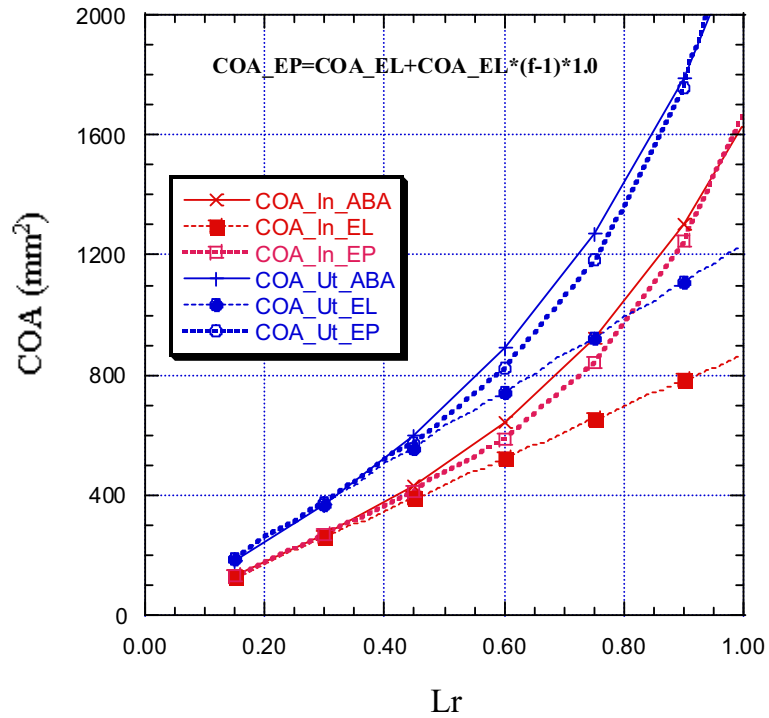
Figure B1.12. Crack opening areas for case 11 (ψ = 30º).

B1.1.3   Results using $\psi = 60^{\circ}$

The results for an off-centre crack ($\psi = 60^{\circ}$) in a carbon steel pipe are shown in Figs. B1.13-B1.18.

Figure B1.13. Crack opening areas for case 1 ($\psi = 60^{\circ}$).

Figure B1.14. Crack opening areas for case 3 ($\psi = 60^{\circ}$).
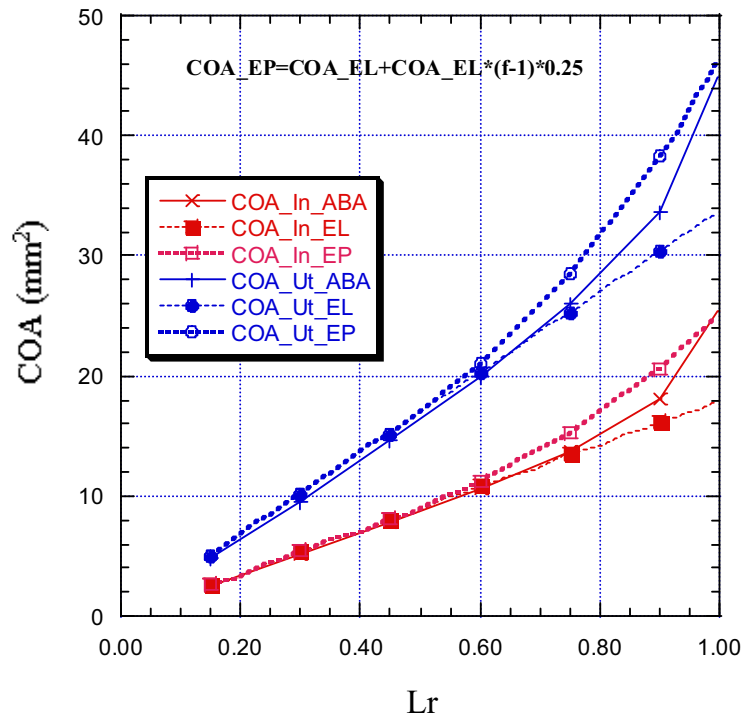
Figure B1.15. Crack opening areas for case 5 ($\psi = 60°$).
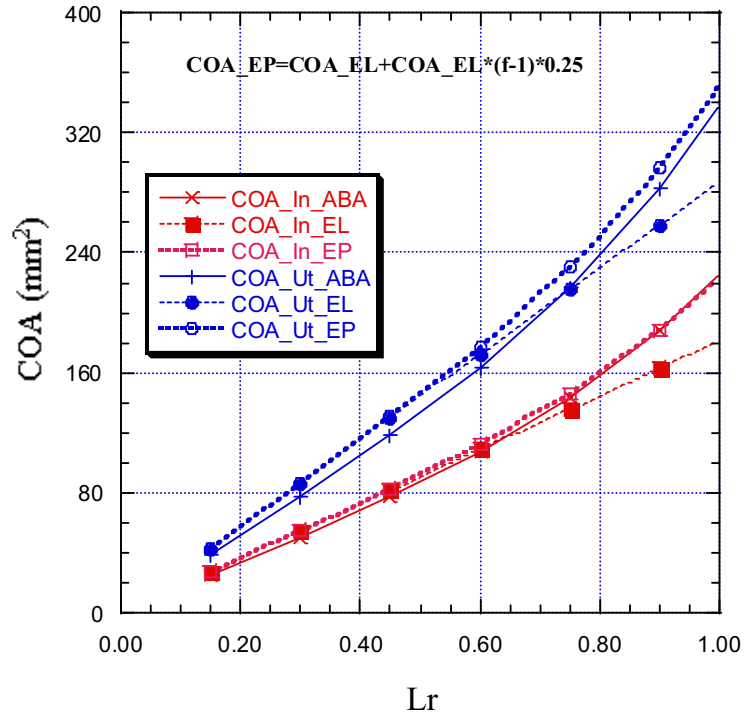
Figure B1.16. Crack opening areas for case 7 ($\psi = 60°$).
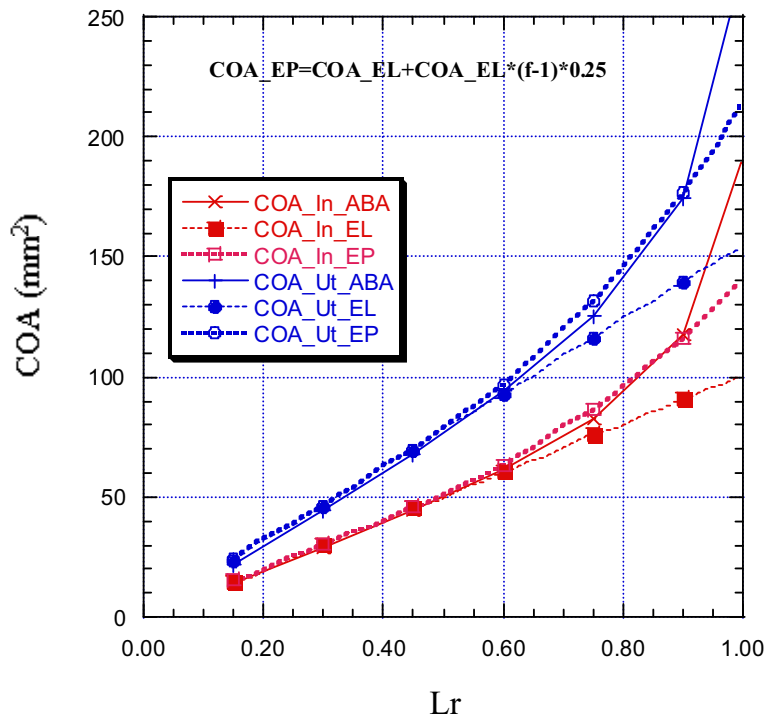
Figure B1.17. Crack opening areas for case 9 ($\psi = 60°$).
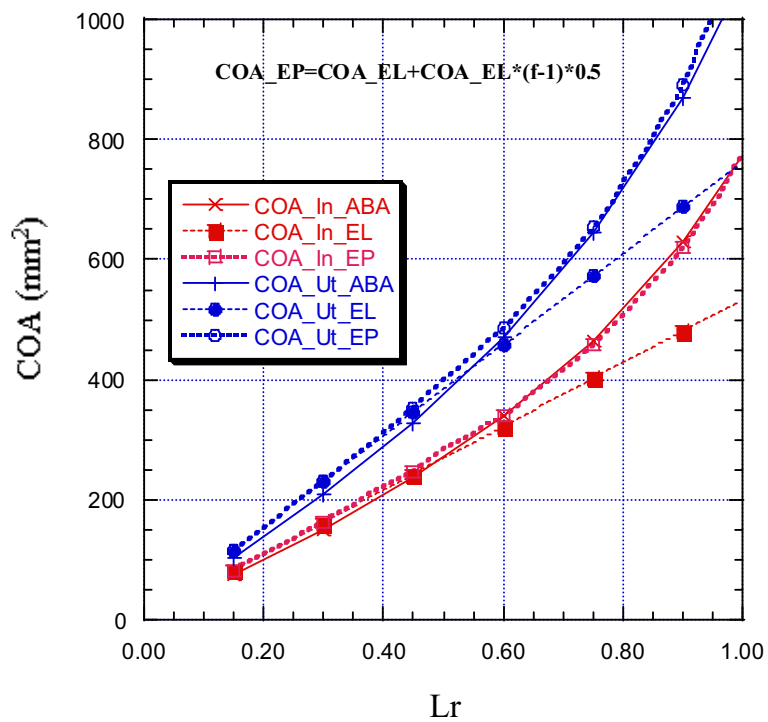
Figure B1.18. Crack opening areas for case 11 ($\psi = 60°$).

B1.1.4   Results using $\psi = 90^\circ$

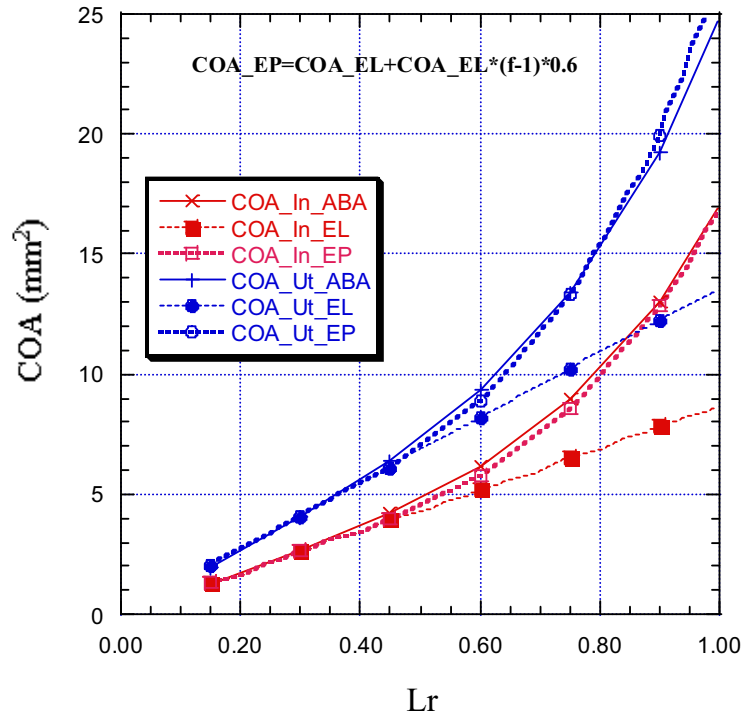The results for an off-centre crack ($\psi = 90^\circ$) in a carbon steel pipe are shown in Figs. B1.19-B1.24.
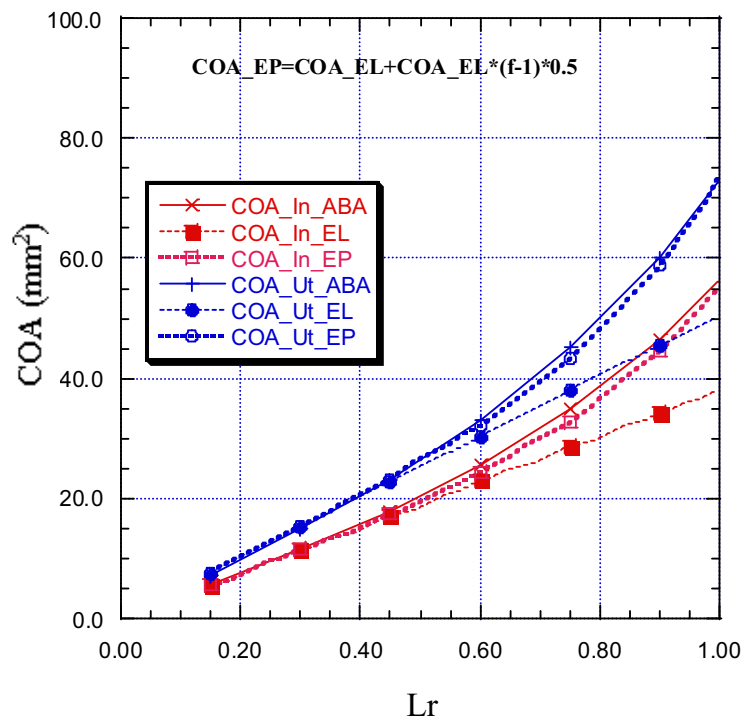

Figure B1.19. Crack opening areas for case 1 ($\psi = 90^\circ$).

Figure B1.20. Crack opening areas for case 3 ($\psi = 90^\circ$).
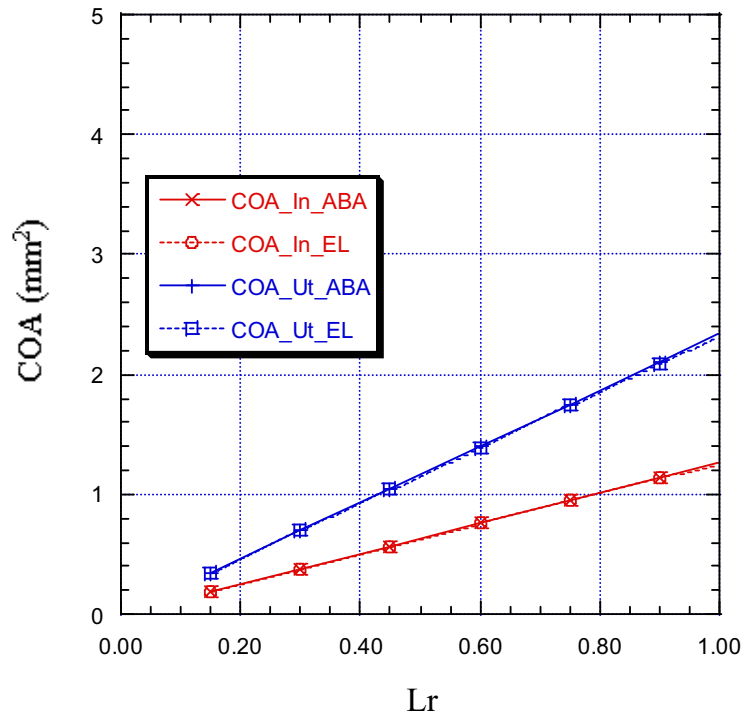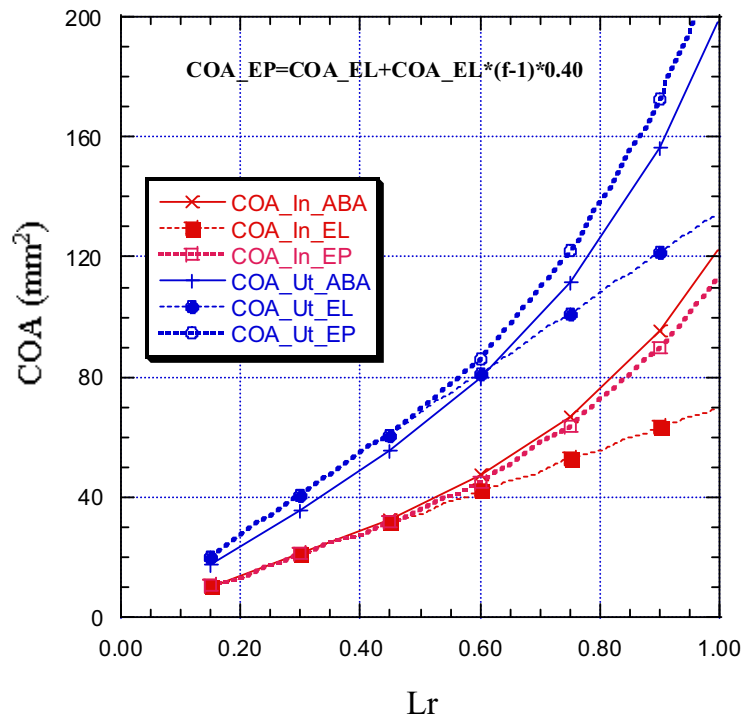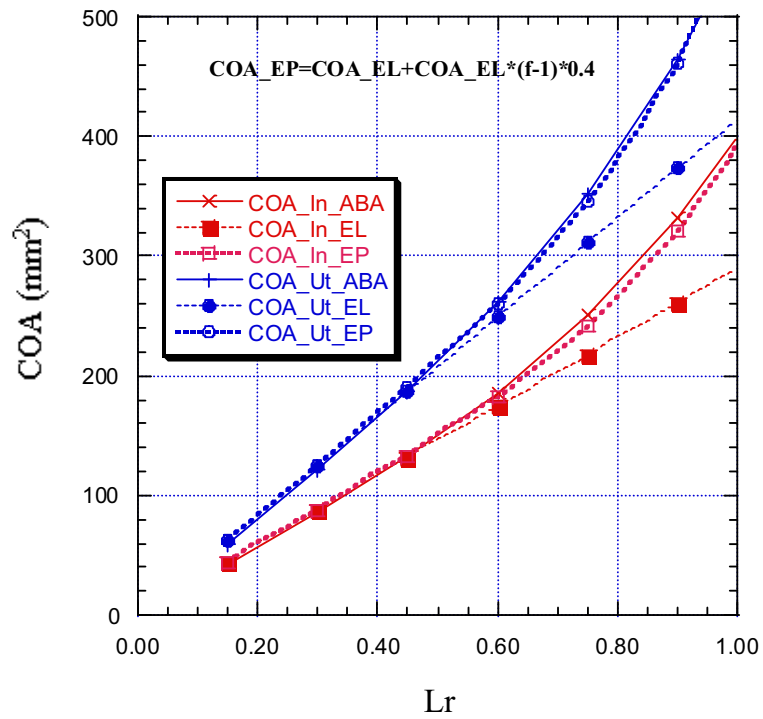
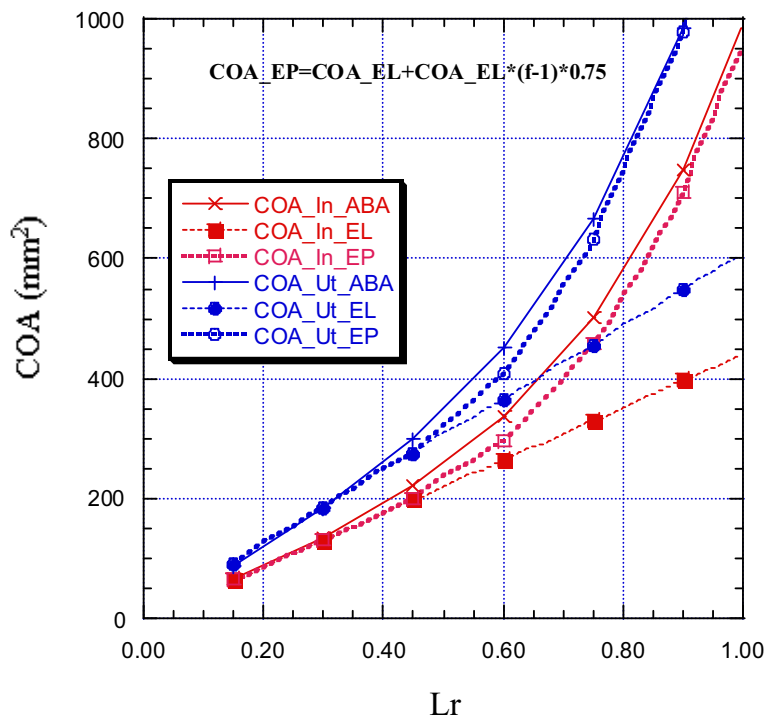Figure B1.21. Crack opening areas for case 5 ($\psi = 90°$).
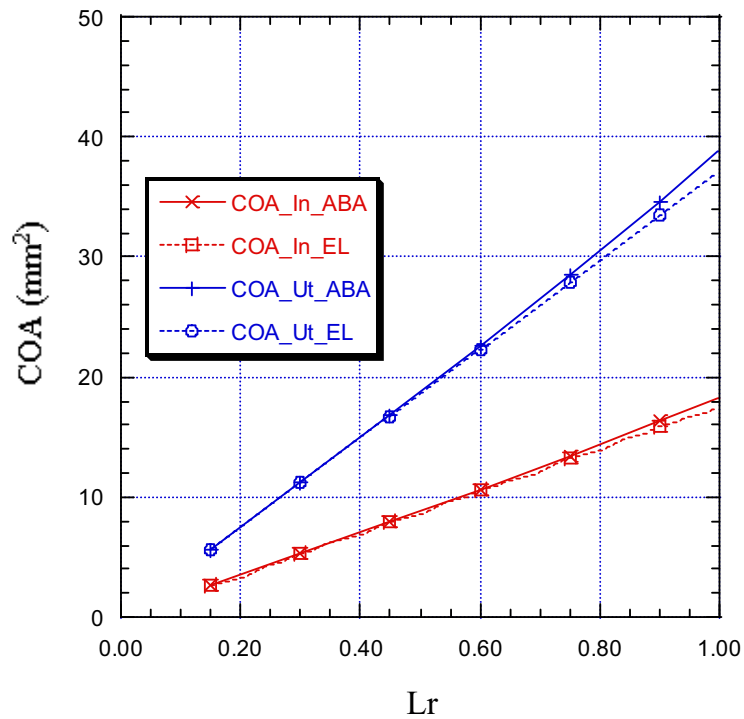
Figure B1.22. Crack opening areas for case 7 ($\psi = 90°$).
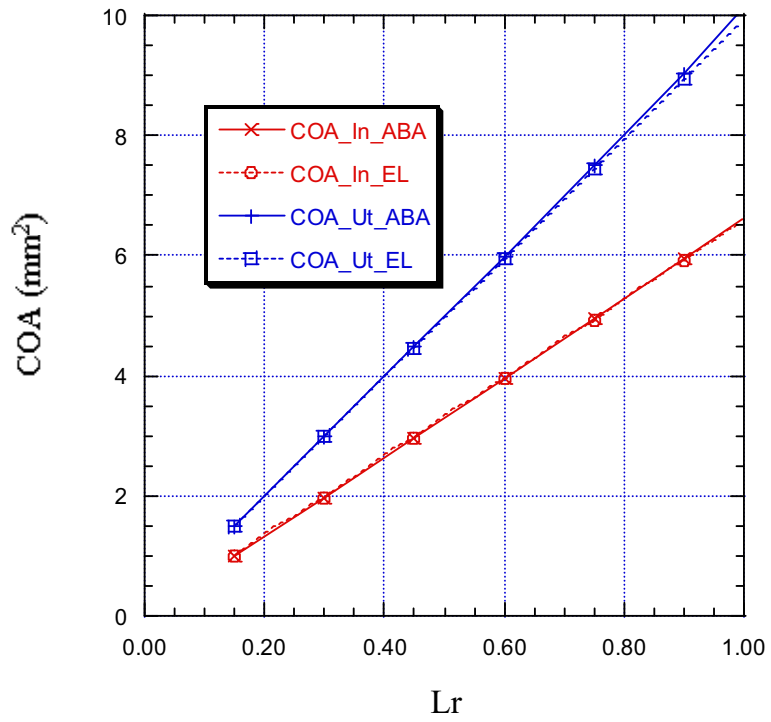
Figure B1.23. Crack opening areas for case 9 ($\psi = 90°$).

Figure B1.24. Crack opening areas for case 11 ($\psi = 90°$).

B1.2   Crack opening areas for stainless steel

Below, the results for the stainless steel cases 2, 4, 6, 8, 10 and 12 are given as a function of the off-centre crack angle ψ (ψ = 0º, 30º, 60º, 90º). Results are given both for the inside surface and the outside surface of the pipe.

B1.2.1   Results using ψ = 0º

The results for a centre crack (ψ = 0º) in a stainless steel pipe are shown in Figs. B1.25-B1.30.

Figure B1.25. Crack opening areas for case 2 (ψ = 0º).

Figure B1.26. Crack opening areas for case 4 (ψ = 0º).

Figure B1.27. Crack opening areas for case 6 ($\psi = 0°$).

Figure B1.28. Crack opening areas for case 8 ($\psi = 0°$).

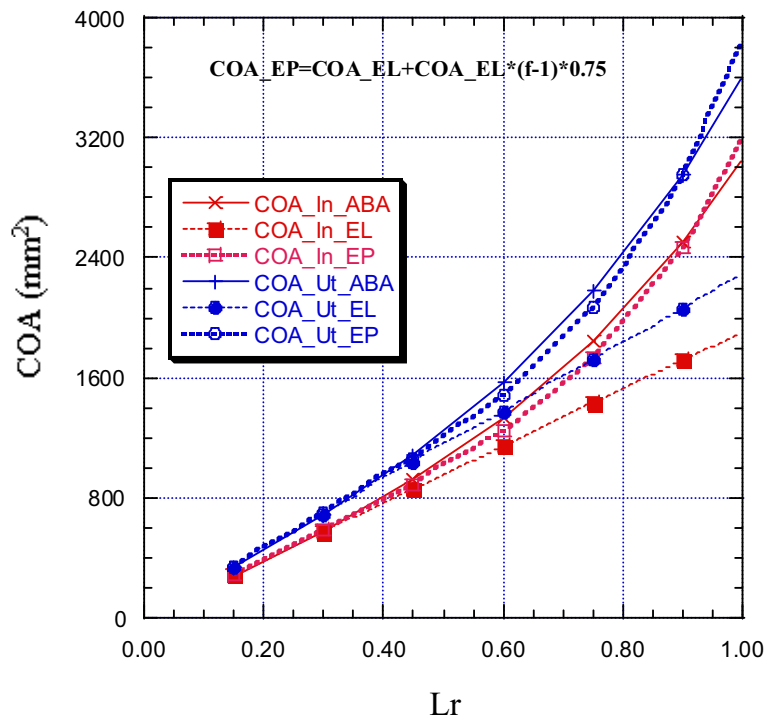Figure B1.29. Crack opening areas for case 10 ($\psi = 0º$).

Figure B1.30. Crack opening areas for case 12 ($\psi = 0º$).

B1.2.2   Results using $\psi = 30^{\circ}$

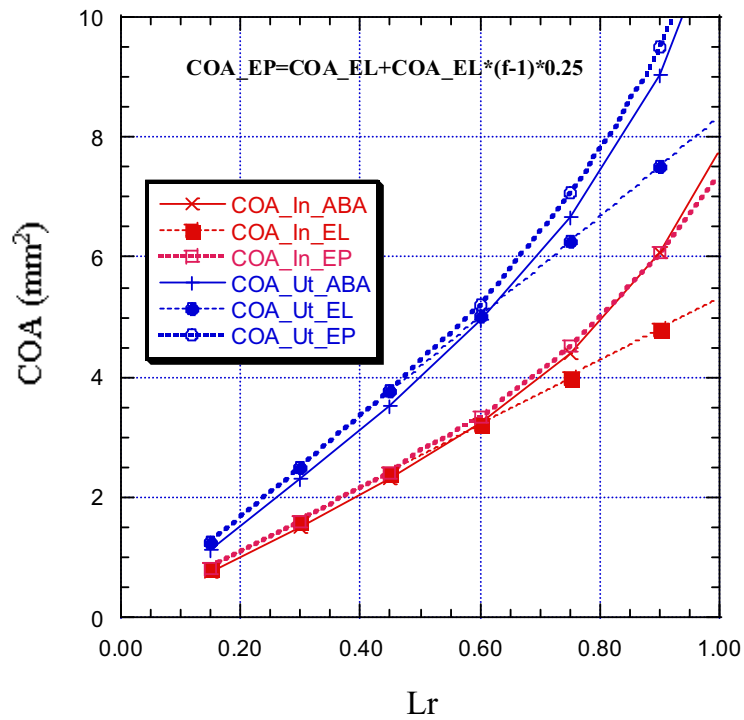The results for an off-centre crack ($\psi = 30^{\circ}$) in a stainless steel pipe are shown in Figs. B1.31-B1.36.

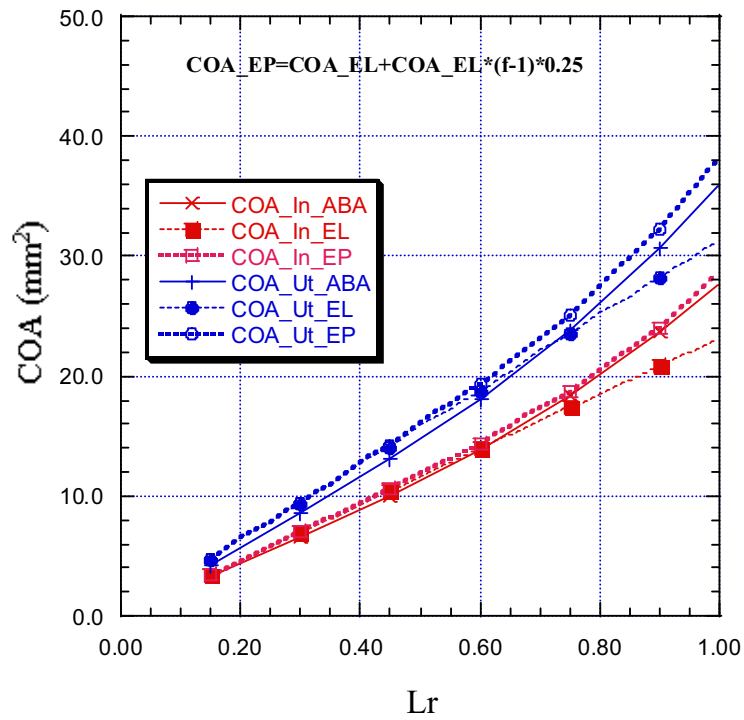Figure B1.31. Crack opening areas for case 2 ($\psi = 30^{\circ}$).

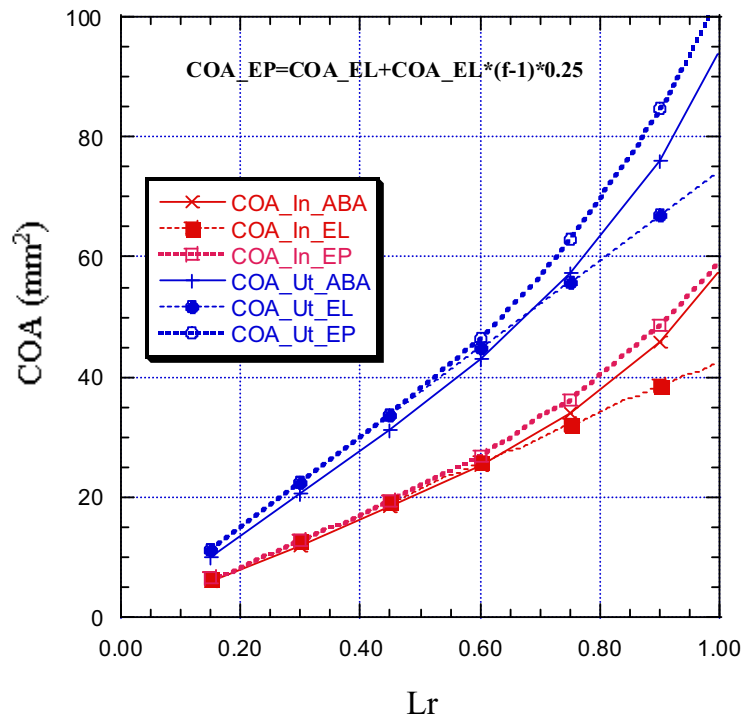Figure B1.32. Crack opening areas for case 4 ($\psi = 30^{\circ}$).

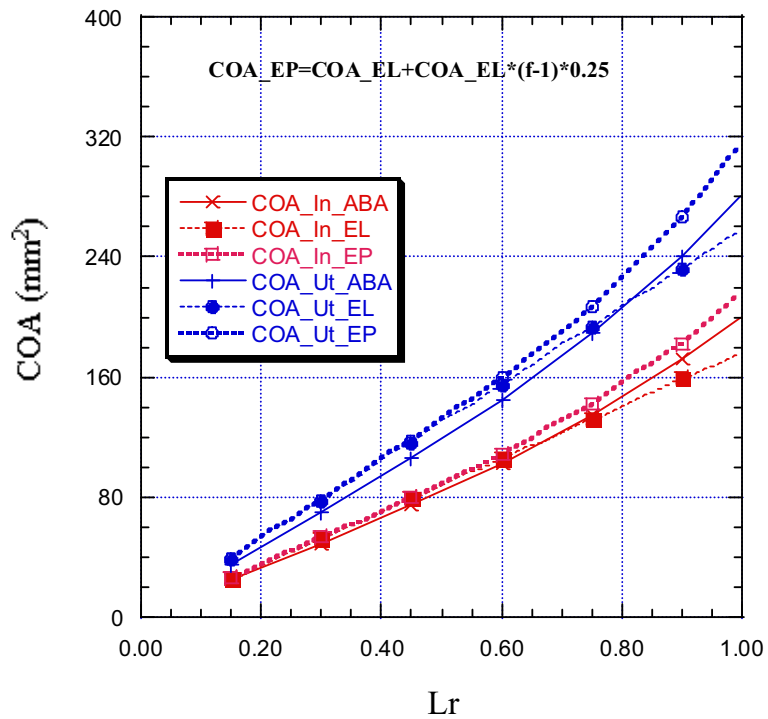Figure B1.33. Crack opening areas for case 6 ($\psi = 30°$).

Figure B1.34. Crack opening areas for case 8 ($\psi = 30°$).

Figure B1.35. Crack opening areas for case 10 ($\psi = 30º$).

Figure B1.36. Crack opening areas for case 12 ($\psi = 30º$).

The results for an off-centre crack ($\psi = 60^o$) in a stainless steel pipe are shown in Figs. B1.37-B1.42.

Figure B1.37. Crack opening areas for case 2 ($\psi = 60^o$).

Figure B1.38. Crack opening areas for case 4 ($\psi = 60^o$).

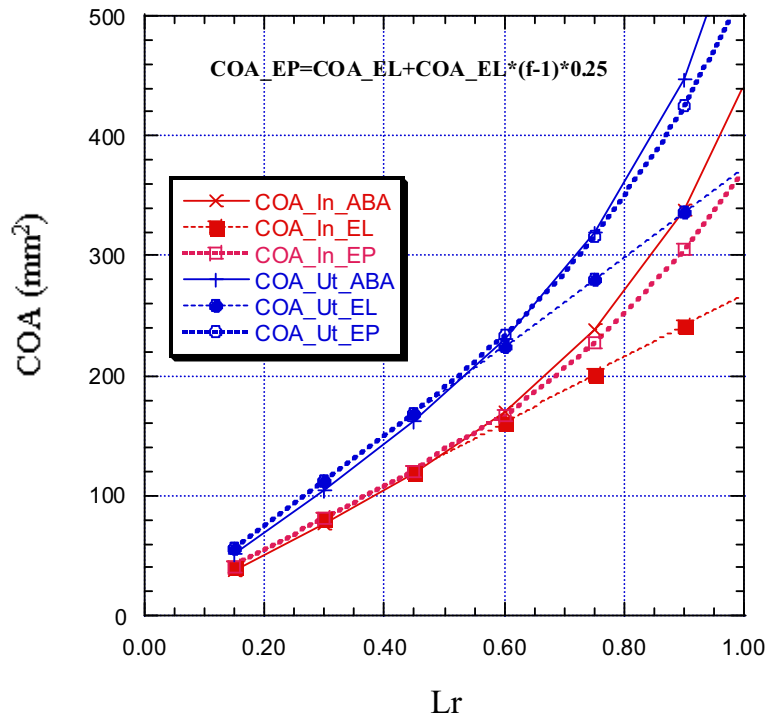Figure B1.39. Crack opening areas for case 6 ($\psi = 60°$).

Figure B1.40. Crack opening areas for case 8 ($\psi = 60°$).

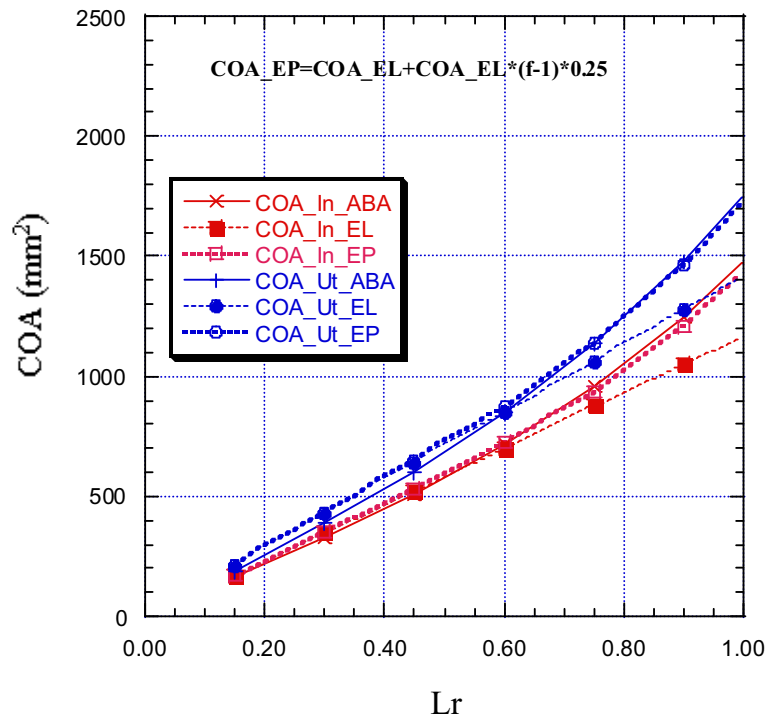**COA_EP=COA_EL+COA_EL*(f-1)*0.25**

Legend:
- COA_In_ABA
- COA_In_EL
- COA_In_EP
- COA_Ut_ABA
- COA_Ut_EL
- COA_Ut_EP

Figure B1.41. Crack opening areas for case 10 ($\psi = 60º$).

COA_EP=COA_EL+COA_EL*(f-1)*0.25

Legend:
- COA_In_ABA
- COA_In_EL
- COA_In_EP
- COA_Ut_ABA
- COA_Ut_EL
- COA_Ut_EP

Figure B1.42. Crack opening areas for case 12 ($\psi = 60º$).

B1.2.4   Results using $\psi = 90^\circ$

The results for an off-centre crack ($\psi = 90^\circ$) in a stainless steel pipe are shown in Figs. B1.43-B1.48.
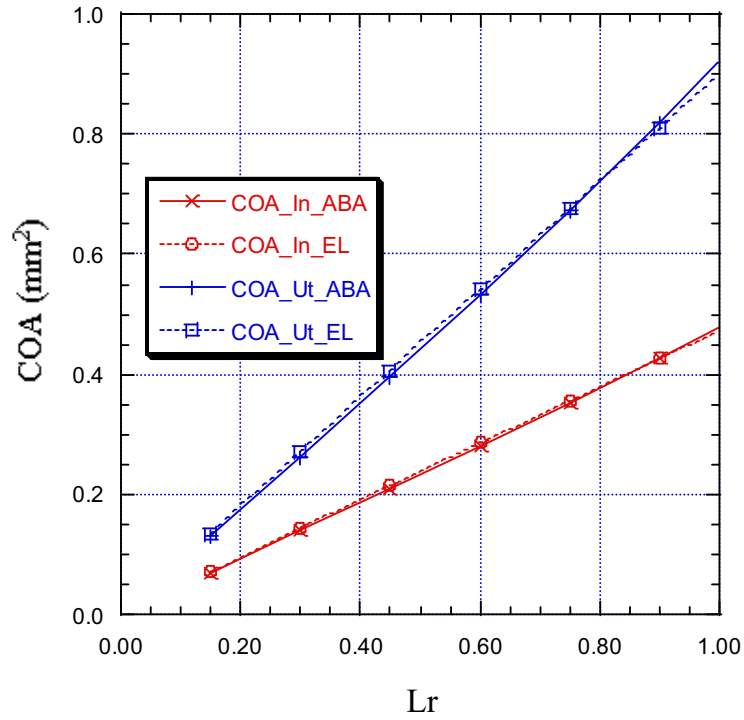

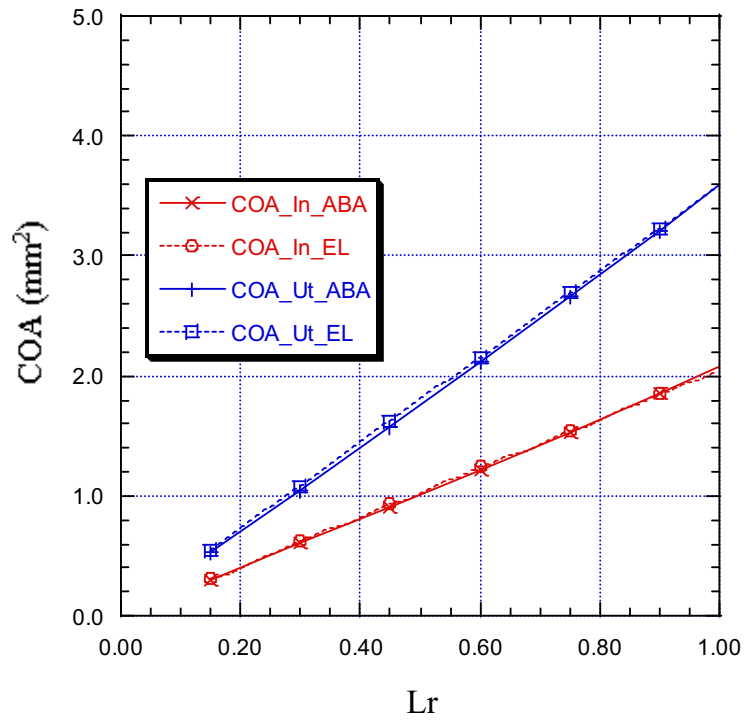Figure B1.43. Crack opening areas for case 2 ($\psi = 90^\circ$).

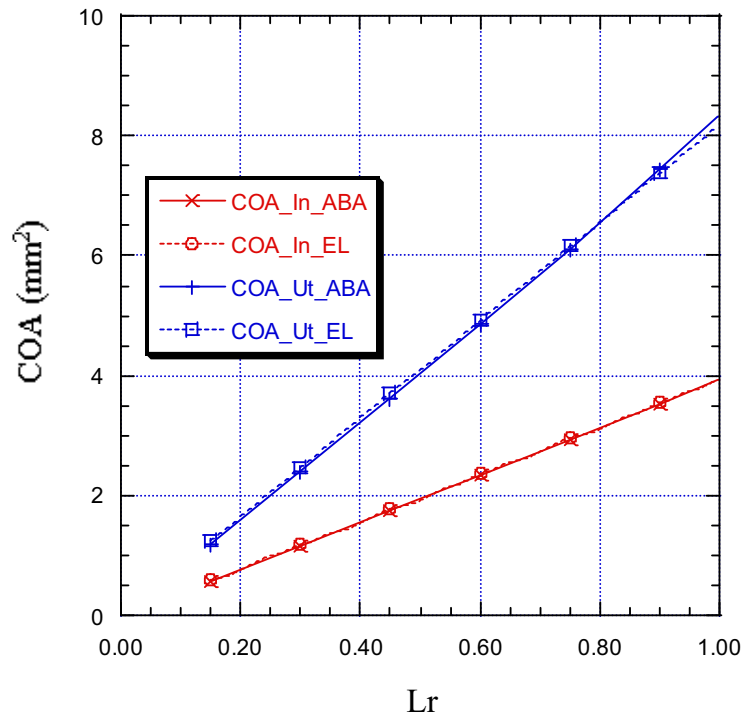Figure B1.44. Crack opening areas for case 4 ($\psi = 90^\circ$).

173

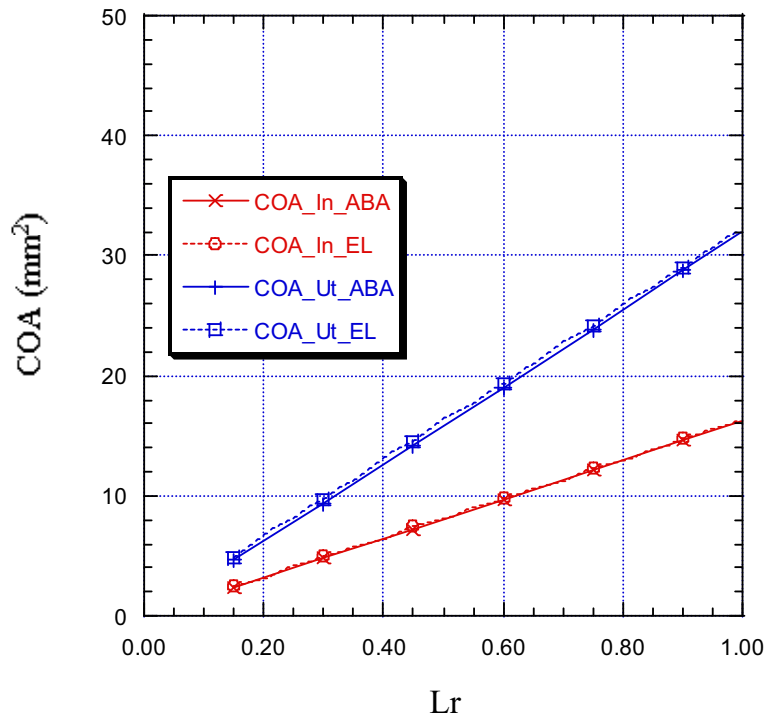Figure B1.45. Crack opening areas for case 6 ($\psi = 90°$).

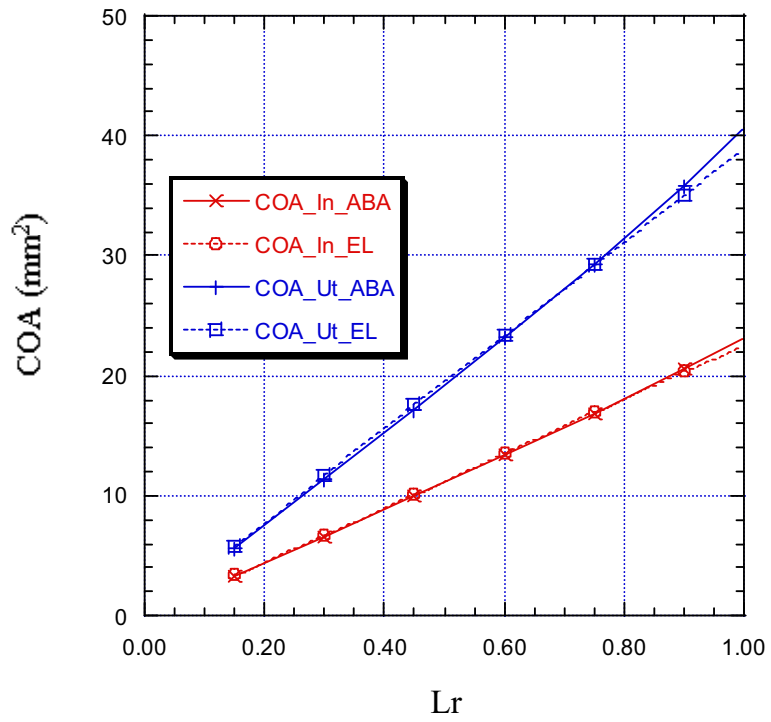Figure B1.46. Crack opening areas for case 8 ($\psi = 90°$).

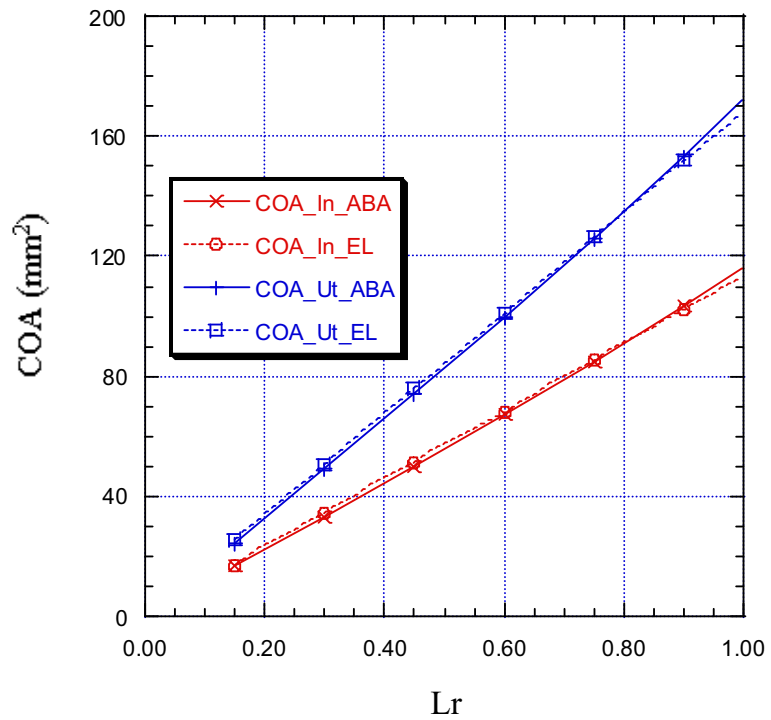Figure B1.47. Crack opening areas for case 10 ($\psi = 90°$).

Figure B1.48. Crack opening areas for case 12 ($\psi = 90°$).

B1.3   COA form factors for off-centre cracks

The form factor (COA) is defined as,

$$\text{COA}_k = \frac{\sigma_b \cdot l_k^2}{E} D_k \ .$$

(B4)

In Eqn. (B4), k is either the inside surface or the outside surface of the pipe. The new COA form factors are listed in Table B1.1. Results using these form factors are presented in section B1.1-B1.2 (Fig. B1.1-B1.48).

Table B1.1. COA form factors for off-centre cracks.

Case	R_i/t	2θ	D_{in}^0	D_{in}^{90}	D_{out}^0	D_{out}^{90}
1	5.63	45	1.557	0.057	1.896	0.067
2		90	2.348	0.113	2.604	0.155
3		135	3.844	0.202	3.843	0.273
4		180	7.050	0.339	6.661	0.425
5	4.08	45	1.487	0.055	1.795	0.066
6		90	2.155	0.108	2.377	0.145
7		135	3.469	0.183	3.423	0.250
8		180	6.108	0.309	5.585	0.391
9	8.88	45	1.679	0.058	2.069	0.070
10		90	2.720	0.123	3.004	0.172
11		135	2.044	0.107	2.306	0.158
12		180	8.061	0.427	7.731	0.513

B1.4   COA plastic correction factors for off-centre cracks

The plastic COA is calculated as,

$$\mathrm{COA_{PL}} = g \cdot \mathrm{COA_{EL}} \ , \tag{B5}$$

where g is a correction factor that takes into account the effect of the plastic deformation. The new plastic correction factors are summarised in Fig. B1.49. Results using these correction factors are presented in section B1.1-B1.2 (Fig. B1.1-B1.48).
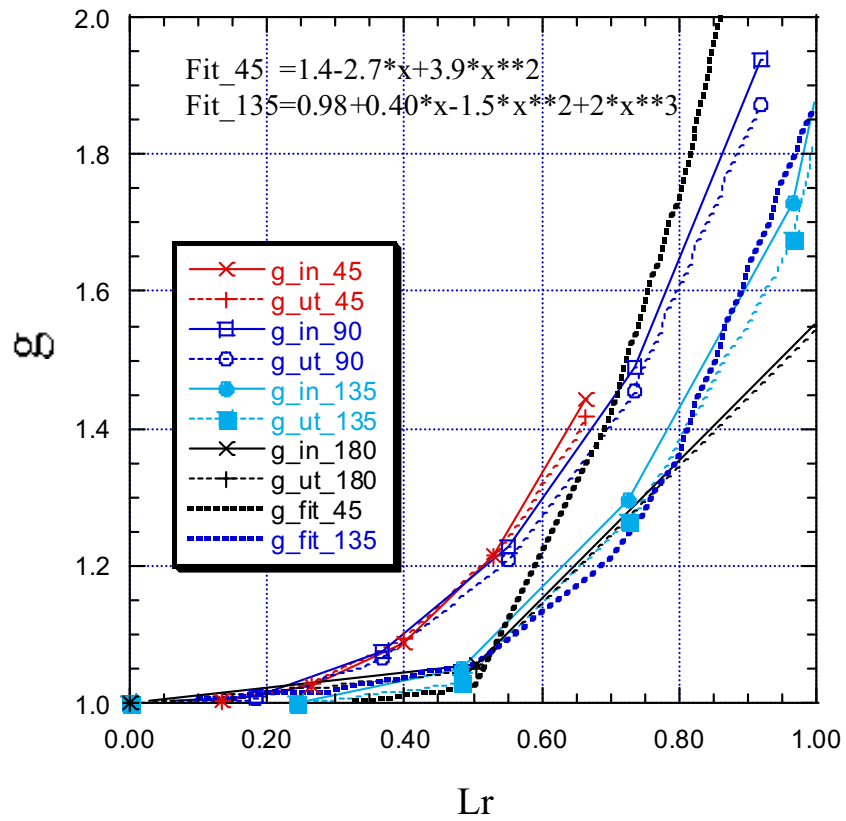

Figure B1.49. COA plastic correction factor.

www.ski.se